Faculty of Engineering and Science

Microwave-assisted Production and Vacuum Distillation for Improved Cold-Flow Properties of Palm Fatty Acid Distillate (PFAD) Biodiesel

Yeong Siew Ping

This thesis is presented for the Degree of
Doctor of Philosophy
of
Curtin University

June 2020

DECLARATION

To the best of my knowledge and belief this thesis contains no material previously published by any other person except where due acknowledgment has been made.

This thesis contains no material which has been accepted for the award of any other degree or diploma in any university.

Signature: …….

Date: ……16 June 2020…….

ACKNOWLEDGEMENT

Firstly, I would like to express my gratitude to my supervisors, Dr. Law Ming Chiat, A/Prof. Stephanie Chan, and A/Prof. Vincent Lee for their patience, motivation and continuous support which helped me in all the time of research and writing of this thesis. In addition, I would also like to thank the chairperson of my thesis committee, A/Prof Jobrun Nandong for his insightful comments to further refine my research work.

My sincere thanks also goes to Dr. You Kok Yeow from UTM Johor who supported me in measuring and analysing the dielectric properties of PFAD feedstock and biodiesel samples, as well as the laboratory officers in my university who assisted me and gave me access to laboratory and research facilities. Without their precious support, it would not be possible to conduct this research.

I would also like to express the deepest gratitude to Malaysian Ministry of Higher Education (MOHE) and Curtin University Malaysia for supporting this research study with Fundamental Research Grant Scheme [FRGS/2/2014/TK06/CURTIN/02/1] and tuition fee waiver throughout the research period.

Last but not least, a very special thanks to my family and friends who have provided me moral and emotional support along the way, with a special mention to Jasly Kong, Kok Ka Yee, Michelle Tiong, Saw Shuey Zi, Room 2 friends, and my other HDR colleagues. It has been a rough journey for me but I am glad to have you all cheering me up and stood by me through the good and bad times.

LIST OF PUBLICATION

Journal Publication

Yeong SP, Law MC, You KY, Chan YS, Lee V C-C. 2019. A coupled electromagnetic-thermal-fluid model for microwave-assisted production of Palm Fatty Acid Distillate biodiesel. *Applied Energy (Vol. 237, p. 457-475).* https://doi.org/10.1016/j.apenergy.2019.01.052

Yeong SP, Law MC, Chan YS. 2020. Investigation of vacuum distillation in improving cold flow properties of Palm Fatty Acid Distillate Biodiesel. *(Submitted to Chemical Engineering Research and Design for review)*

Conference Publication

Yeong SP, Law MC, You KY, Chan YS, Vincent Lee CC. 2017. Dielectric Properties of Palm Fatty Acid Distillate and its Biodiesel under 5.8 and 18 GHz Microwave Frequencies. *Proceedings of One Curtin International Postgraduate Conference (OCPC) 2017.*

Yeong SP, Law MC, Vincent Lee CC, Chan YS. 2017. Modelling batch microwave heating of water. In *IOP Conference Series: Materials Science and Engineering (Vol. 217, No. 1, p. 012035)*. IOP Publishing.

ABSTRACT

The recent development of biodiesel fuel is still hindered by two major factors that affect the cost of biodiesel: costs of feedstock and processing. This sparks worldwide research interests to seek for other measures such as alternative feedstock and green technologies to improve the production efficiency and reduce the biodiesel cost simultaneously. The main aim of this study is to investigate the effectiveness of producing biodiesel via microwave-assisted production and explore the feasibility of improving its cold flow characteristics through vacuum distillation. The production of biodiesel through microwave-assisted esterification of a palm-oil derived product — palm fatty acid distillate (PFAD), is studied experimentally. An optimal biodiesel yield (91.88%) is reported at 15 min of 300 W microwave irradiation, for a 1:9 PFAD to methanol ratio catalyzed by sulphuric acid. The study also reveals that the esterification of PFAD has a second order reaction kinetics under microwave irradiation. The PFAD biodiesel is characterized via GC-FID analysis to determine its ester compositions. Besides, the dielectric properties of PFAD and its biodiesel are also measured for the temperature range of 25–120 °C. At the microwave frequency of 2.45 GHz, the dielectric properties of PFAD and its biodiesel are reported to be 2.78–0.17j and 3.26–0.21j, respectively. Obtaining these values is essential for modelling the microwave-assisted esterification of PFAD. Following the experimental study, a three-dimensional multiphysics model, which includes the effects of electromagnetic propagation, heat transfer, fluid flow, and chemical species conservation, is developed for the first time to model the process of microwave-assisted PFAD esterification. It provides better insights into the changes in the liquid properties as well as the importance of Navier-Stokes equations, vaporization-condensation phenomena of methanol towards a good model prediction. The numerical predictions are found to be in good agreement with the experimental results. Apart from the cost issue, palm-based biodiesel also suffers from poor cold flow properties due to the presence of fatty acid alkyl esters with high melting points. Under cold weather (<16°C), the fuel would crystallize and clog the fuel filter which subsequently cut off the engine fuel supply of a vehicle. Thus, the composition of these high melting point esters in the biodiesel needs to be reduced. In Malaysia, winterization technique is adopted to remove

these esters but the time-consuming process results in low product yield and huge loss of starting materials. In this study, vacuum distillation is proposed as an alternative approach to improve the cold flow properties of PFAD biodiesel. A batch distillation experiment is carried out under vacuum to investigate the distillation performance and its feasibility in removing the high melting point ester (methyl palmitate). The results show that the cold flow properties of the distilled biodiesel have significantly improved by 35–42% (6–8 °C) after removing 13.60 wt.% of total saturated esters. This indicates that vacuum distillation is a feasible approach to improve the cold flow characteristics of PFAD biodiesel. However, the cold flow properties reported are still not satisfactory. It is found that by using vacuum fractional distillation, the composition of methyl palmitate can be further decreased by 27.32%, making the distilled biodiesel to have cold flow quality equivalent to grade C summer biodiesel in temperate climates. At the end of this study, a process design of a vacuum fractional distillation column with its peripherals is carried out and presented. By implementing Fenske-Underwood-Gilliland (FUG) calculations and Kern's method, the operating parameters and sizing of the distillation column and heat exchangers are determined. This preliminary design provides a basis for the integration of vacuum distillation into the industrial biodiesel production and processing facilities in the future.

Keywords: cold flow properties, column design, FUG method, microwave irradiation, multiphysics modelling, PFAD, vacuum distillation

TABLE OF CONTENT

Nomenclature, Symbols, and Abbreviations

A	Frequency factor	1/(M.s)
A_a	Active area	m^2
A_c	Cross sectional area of column	m^2
A_d	Downcomer area	m^2
A_h	Total hole area	m^2
A_h'	Area for a hole	m^2
A_n	Net column area	m^2
A_o	Area for heat transfer across a surface	m^2
A_p	Perforated area	m^2
A_{ap}	Clearance area under downcomer	m^2
A_{cz}	Area of calming zones	m^2
A_{IS}	Peak area of internal standard	m^2
A_{us}	Area of unperforated edge strip	m^2
A_{MeOH}	Frequency factor (vaporisation) of methanol	1/s
AV	Acid value	mg KOH/g
B	Bottom flow rate	kg/s
c_i	Concentration of species *i* at any time	mol/m^3
$c_{i,sat}$	Saturation concentration of species *i*	mol/m^3
c_o	Speed of light in free space	m/s
c_p	Specific heat capacity at constant pressure	J/(kgK)
c_{tot}	Total concentration of all species in the liquid	mol/m^3
C_o	Orifice coefficient	dimensionless

C_{sb}	Souders and Brown factor	m/s
CFPP	Cold filter plugging point	°C
CP	Cloud point	°C
CPO	Crude palm oil	-
d_h	Hole diameter	m
D	Distillate (overhead product) flow rate	kg/s
D_c	Column diameter	m
D_i^m	Mixture-averaged diffusion coefficient for species *i*	m^2/s
E_a	Activation energy	J/mol
E_o	Overall tray efficiency	%
f	Microwave frequency	Hz
F	Feed rate	kg/s
F_t	Correction factor	dimensionless
F_{LV}	Liquid-vapour flow factor	dimensionless
FA	Fatty Acid	-
FAME	Fatty acid methyl ester	-
h_b	Downcomer backup	mm liquid
h_c	Convective coefficient	W/
h_d	Dry plate drop	mm liquid
h_r	Residual loss	mm liquid
h_t	Total pressure drop	mm liquid
h_{ap}	Height of the bottom edge of the apron above plate	$W/(m^2.K)$
h_{dc}	Head loss in downcomer	mm liquid
h_{ow}	Height of liquid crest over downcomer weir	m
h_w	Weir height	m

H_c	Column height	m
H_2O	Water	-
k	Thermal conductivity	W/(m.K)
$k_{c,i}$	Mass transfer coefficient of a species *i*	1/s
k_r	Reaction rate constant	1/(M.s)
K_i	Equilibrium K-value	dimensionless
KOH	Potassium hydroxide	-
l_{cz}	Mean length of calming zone	m
l_c	Column length	m
l_p	Hole pitch	m
l_t	Plate spacing	m
l_w	Weir length	m
l_{us}	Mean length of unperforated edge strips	m
L	Liquid rate	kmol/h
L_m'	Liquid molar flow rate below feed stage	kmol/h
L_w	Liquid mass flow rate	kg/s
L_{wd}	Liquid mass flow rate in downcomer	kg/s
$L_{\max}$	Maximum volumetric liquid rate	m^3/s
m	Mass	kg
m_{IS}	Mass of internal standard	kg
M_i	Molecular weight of a species *i*	kg/mol
MeOH	Methanol	-
N	Number of equilibrium stages	dimensionless

N_c	Number of carbon atoms	dimensionless
N_h	Number of holes	dimensionless
N_r	Number of rectifying stages (top)	dimensionless
N_s	Number of stripping stages (bottom)	dimensionless
N_{act}	Actual number of trays	dimensionless
$N_{\min}$	Minimum number of theoretical stages	dimensionless
P	Pressure	Pa
$P_{i,sat}$	Saturation pressure	mm Hg
P_{FAME}	Methyl palmitate	-
PFAD	Palm fatty acid distillate	-
PP	Pour point	°C
q	Heat load	kW
Q	Volumetric flow rate of vapour	m^3/s
$\dot{Q}_{MW}$	Heat source from microwave electric field	W/m^3
$\dot{Q}_{\Delta H}$	Heat source from enthalpy of esterification reaction	W/m^3
R	Operating reflux ratio	dimensionless
R_m	Minimum reflux ratio	dimensionless
R_U	Universal gas constant	J/(mol.K)
$\dot{R}$	Reaction rate	$mol/(m^3.s)$
t	Time	s
t_1	Cold fluid temperature, inlet	°C
t_2	Cold fluid temperature, outlet	°C
t_P	Plate thickness	m
t_r	Residence time in downcomer	s
T	Temperature	K

T_1	Hot fluid temperature, inlet	°C
T_2	Hot fluid temperature, outlet	°C
U_{FAME}	Unsaturated fatty acid methyl ester	-
u_f	Flooding velocity	m/s
u_h	Minimum design vapour velocity	m/s
u_n	Actual vapour velocity	m/s
U_o	Overall heat transfer coefficient	W/m^2°C
$U_{o,calc}$	Overall heat transfer coefficient (calculated)	W/m^2°C
V	Vapour mass flow rate	kg/s
w_{us}	Width of unperforated edge strip	m
x_i	Mole fraction of a species, *i*	dimensionless
X	Fatty acid conversion	dimensionless
ΔH	Height allowance	m
ΔH_r	Enthalpy of reaction	J/mol
ΔH_{vap}	Heat of evaporation/enthalpy of vaporization	J/mol
ΔS	Entropy	J/K
ΔT_{lm}	Logarithmic mean temperature difference	°C
ΔT_m	Mean temperature difference	°C

Vector Quantities

$\mathbf{D}$	Displacement current density	A/m^2
$\mathbf{E}$	Electric field intensity	V/m
$\mathbf{I}$	Identity matrix	dimensionless
$\mathbf{n}$	Unit normal vector	dimensionless
$\mathbf{u}$	Velocity vector	m/s

Greek Symbols

α_i	Relative volatility of component *i*	dimensionless
γ	Emissivity of a material	dimensionless
ε	Complex permittivity	dimensionless
ε_r	Relative complex permittivity	dimensionless
ε_r'	Dielectric constant	dimensionless
ε_r''	Loss factor	dimensionless
κ	Magnetic permeability	H/m
μ	Dynamic viscosity	Pa.s
μ'	Relative permeability	dimensionless
μ_L	Liquid viscosity of feed	cP
μ_0	Permeability of free space, 1.257×10^{-6}	H/m
ρ	Density	kg/m^3
σ	Stefan-Boltzmann constant, 5.67×10^{-8}	$kg/(K^4.s^3)$
σ_s	Surface tension	dyne/m
ω	Angular frequency	rad/s

Subscripts

B	Bottom
D	Distillate
f	Flooding
HK	Heavy key
L	Liquid
LK	Light key
min	Minimum

MW	Microwave
sat	Saturation
v	Vapour
vap	Vaporization

List of Figures

List of Tables

CHAPTER 1 INTRODUCTION

1.1 Background

1.1.1 What is biodiesel?

Foreseeing the disastrous effects that the depletion of non-renewable fossil fuels could result in the future, researchers and experts worldwide have put in tremendous effort to develop alternative energy production from various renewable energy sources such as solar, wind, tidal, and hydro power. At current stage, it is still difficult to fully replace fossil fuel usage with these renewable energy options. Hence, having an alternative fuel selection which is more environmental friendly than fossil fuels seems to be one of the choices to gradually shift away human dependence from fossil fuels.

This has led to the extensive research towards biofuels — fuels which are produced directly or indirectly from organic materials such as plants and animal waste. Biodiesel, a kind of biofuel, have sparked great interests among scientists and researchers due to its similar performance as diesel fuel. Biodiesel is recognized as a greener burning alternative to the conventional diesel fuel. It is biodegradable, has minimal toxicity and produces lower pollutants emission f. Due to its similarity in fuel properties with the petroleum diesel, biodiesel can be directly used in diesel engine to deliver similar performance, with little or no modifications (Ramadhas et al., 2004; Silitonga et al., 2011). Furthermore, it is also compatible with the conventional diesel to produce stable biodiesel blend. This has made it one of the most promising alternative fuels for the transportation sector (Lin et al., 2011).

The primary source of biodiesel is edible vegetable oils. More than 95% of the biodiesels around the world are produced from this source (Gui et al., 2008). These vegetable oils are yielded from plants such as palm trees, rape plants, and soybean plants. They are able

to absorb carbon dioxide (CO_2) through photosynthesis to such an extent that the amount of oxygen contributed to atmosphere exceeded CO_2 released during combustion, with the fuel yielded from these plants (Atadashi et al., 2011). Hence, biodiesel is considered to be carbon neutral too.

1.1.2 Historical background of biodiesel production

The biodiesel production process (transesterification) was discovered by E. Duffy and J. Patrick in year 1853; which occurred decades before the first functional diesel engine was invented. It was not until 1893 that Rudolf invented the first diesel engine prototype which run on peanut oil. While the first engine test was unsuccessful, Diesel dedicated huge effort to improve the engine and finally succeeded in his third engine test on February 17, 1897 where he demonstrated an efficiency of 27% with the engine under load. Later in the 1920s, the diesel engine was redesigned to run on petrodiesel which were cheaper to produced compared to biofuels. Therefore, the biodiesel infrastructure was not actively developed until oil crisis and greenhouse gas issue in the recent decades (Deutsches Museum, 2019; Lee & Shah, 2012).

The first industrial biodiesel production process using ethanol was only patented in 1977. Two years later, South Africa began researching the transesterification of sunflower oil and subsequently, published a process for fuel-quality, engine-tested biodiesel in 1983. An Australian company, Gaskoks built the first biodiesel pilot plant using this process in 1987. During the 1990s, many European countries also began constructing their own biodiesel plants (Lee & Shah, 2012).

1.1.3 The challenges of biodiesel development

Ever since the 1970's oil crisis, biofuels development has sparked research interests worldwide. It acts as a measure to decrease the socioeconomic shocks of future oil prices, reduce overreliance on fossil fuels and lower the level of harmful emissions to the

environment. Despite all the advantages, biodiesel development in Malaysia has been hindered by challenges such as feedstock selection and biodiesel processing cost.

Palm oil is the major lipid feedstock used for biodiesel production in Malaysia. Palm fruits have the highest average oil yield compared to other oil crops grown for biodiesel feedstock. Palms can provide 5 tons of oil per hectare whereas soybeans or Jatropha only produce approximately 1 ton per hectare (Balat & Balat, 2010). According to Johari et al. (2015), Malaysia has been supplying 40% of the global demand for crude palm oil (CPO). Due to the massive production volume, there have been increasing concerns on the possible negative impacts of palm oil production on the environment such as deforestation, biodiversity loss or pollutions as a result of the large scale expansion of the industry. In addition, there have been debates that the conversion of farmland or crops for palm oil production will lead to the reduction in food supply. This food versus fuel debate has added another challenge to utilize palm oil as a feedstock for the fuel market (Lam et al., 2009).

Biodiesel is not economically competitive with diesel fuel although it has favourable properties to substitute the latter (Canakci & Van Gerpen, 2001). The cost of biodiesel remains the major challenge that suppresses the industrial growth. The two utmost important components of the biodiesel cost are the costs of feedstock and processing (Ma & Hanna, 1999). It is estimated that the cost of raw materials accounts for 60–75% of the total cost of biodiesel fuel (Choo et al., 2007; Karacan & Karacan, 2015). The increasing demand for CPO over the years has led to higher CPO prices. As a result, the biodiesel companies in Malaysia encounter issues such as increased operating costs and low profit margins. In order to reduce the cost to produce biodiesel, it is necessary to make adjustments to either the processing methods, or feedstock selection, or even better, both.

During the physical refining of CPO to produce refined bleached deodorized palm oil with low percentage of free fatty acid (FFA), a lower value by-product known as palm fatty acid distillate (PFAD) is produced at the deodorization stage. Although its FFA content is very high, this oil has similar fatty acid composition as the refined palm oil. Hence, PFAD could potentially serve as an alternative feedstock for biodiesel production.

On the other hand, the technology selected for the processing method of biodiesel could have a significant impact on the cost of biodiesel production as it involves the use of time, labour, and energy to generate biodiesel from raw feedstock. The biodiesel plants in Malaysia currently still practise the conventional heating and mechanical stirring method for biodiesel processing. In order to lower the production cost of biodiesel, it is inevitable for the biodiesel industry players to transition to greener technologies such as microwave irradiation which promotes efficient energy usage and short processing time.

Apart from using refined edible vegetable oils for biodiesel production, researchers have been looking into the possibilities of using inedible or waste vegetable oils to reduce the feedstock cost. However, using alternative feedstock with lower quality leads to another issue. The biodiesel produced usually has poor cold flow properties. For instance, given the presence of a substantial amount of high melting point saturated long chain fatty acid esters in the fuel, palm biodiesel has poorer cold flow properties compare to the conventional diesel fuel (Edith et al., 2012). Hence, the cold flow quality of palm-based biodiesel must be improved in order to increase its market and economic value.

The fatty acid profile of a biodiesel corresponds to its feedstock. The five common fatty acids present in a biodiesel feedstock are C_{16} and C_{18} fatty acids, namely, palmitic (C16:0), stearic (C18:0), oleic (C18:1), linoleic (C18:2) and linolenic (C18:3) acids. Palmitic and stearic acids are saturated fatty acids with no double bond. According to the information collected by Cermak et al. (2012), these esters possess high melting points, which are 62.9^{o}C and 70.1^{o}C, respectively. Once they are converted into their corresponding methyl esters, their melting points reduce to 28.5^{o}C and 37.7^{o}C, which are still unfavourable for export grade biodiesel, as these indicate that fuel which mainly comprised of these esters would crystallize in cold climate and clog the fuel systems of vehicles.

To produce export grade biodiesel and consequently increase Malaysia's position in the global biofuels market, improving biodiesel cold flow properties is inevitably a technical challenge which has to be tackled. It is a difficult task as its improvement usually results in lower ignition quality (ease of fuel ignition in diesel engine) and lower oxidation stability of the biodiesel. This is due to the removal of saturated esters which have better

ignition quality and oxidation resistance but contribute to poor cold flow properties (Edith et al., 2012). Nonetheless, to the author's best knowledge, the possibility for cold flow properties of PFAD biodiesel to be improved to export grade level has not yet been studied. The current method used in Malaysia for cold flow improvement is winterization technology, which allows the removal of poor cold flow components that crystallized in the biodiesel fuel as a result of freezing. However, this method has some undesired drawbacks such as being time-consuming and causing huge loss of starting materials during the process. Thus, other than improving the processing method for biodiesel production, searching an alternative processing method to improve the cold flow properties of biodiesel is also a reasonable option for expanding the economic potential of PFAD biodiesel, or even for other biodiesel fuels which comprised of similar constituents of esters as well.

To summarize, two of the main issues of biodiesel development in Malaysia are related to the cost of processing and feedstocks, as well as the inferior low-temperature operability of palm-based biodiesel. The first problem could be minimized with the introduction of energy-efficient technology (e.g. microwave) and a low-cost alternative feedstock (PFAD) while the second issue could be investigated with the use of alternative method (e.g. vacuum distillation) to replace the time-consuming winterization process.

1.2 Objectives

The main aim of this study is to investigate the effectiveness of producing PFAD biodiesel via microwave-assisted production and explore the feasibility of improving its cold flow behaviour through vacuum distillation technologies. The objectives of this study are as follows:

i. identify the reaction kinetics of microwave-assisted PFAD esterification,
ii. determine the complex permittivity values of PFAD and its biodiesel by using open-ended co-axial probe method,
iii. develop a numerical model for the microwave-assisted esterification of PFAD,

iv. investigate the possibility of vacuum distillation in enhancing the cold flow properties of PFAD biodiesel, and
v. generate a preliminary design of industrial scale vacuum distillation column for improving the cold flow behaviour of PFAD biodiesel using FUG method.

1.3 Novelty, contribution and significance

For the first time, a three-dimensional multiphysics model which couples the physics of electromagnetic propagation, heat transfer, fluid flow, and chemical species conservation, is developed to model the microwave-assisted esterification of PFAD feedstock. This model gives a further insight into the physics behind the chemical reaction. Apart from that, the model is also capable to generate temperature profile of the reaction with good prediction at reaction temperature above the boiling point of methanol. This is made possible by taking the phase change effect (i.e. vaporization of methanol) of reactant into consideration. This model serves as a basis to evaluate optimized reactor design for power-modulated microwave reactor (i.e. microwave power level is user-controllable) as well as the effects of the thermophysical parameters of chemical species on the reaction.

Apart from that, this project also provides significance in studying the feasibility of using vacuum distillation technology to improve the cold flow properties of a second generation biofuel, PFAD biodiesel. Instead of separating the esters from impurities or other components that might be present in the biodiesel (e.g. glycerol, alcohol, glycerides) as studied by other researchers, the author aims to separate the major saturated ester (methyl palmitate) from the rest of the esters present in PFAD biodiesel in this study. By removing the specified saturated ester which solidify at higher temperature, the cold flow properties of the PFAD biodiesel will be substantially improved.

The preliminary design of an industrial scale distillation column for the vacuum distillation of PFAD biodiesel which may be useful for the process design and control of second generation biodiesel production is proposed in this work. This column has the chance to be part of the equipment in an extended production line which can be integrated into a palm oil refining facility to produce biodiesel. In addition, both dielectric constant

and dielectric loss measurement of PFAD feedstock and biodiesel, which are important inputs for the numerical model, are also identified in this work. Furthermore, this project also explores the potential of microwave technology in enhancing the reaction rate of PFAD biodiesel production. The reaction kinetics of microwave-assisted PFAD esterification under pulsed microwave irradiation is identified.

1.4 Dissertation structure

This thesis has been structured and presented in the following 9 chapters.

Chapter 1 briefly presents the main challenges in the biodiesel industry and suggested an approach to achieve the objectives of this study in an effort to tackle the challenges.

Chapter 2 reviews the existing experimental work on enhancing biodiesel production rate and improving the cold flow properties of biodiesel, along with the numerical work in developing multiphysics models for biodiesel production, which finally leads to the identification of research gaps, forming the objectives of this current study;

Chapter 3 outlines the research methodology for the experimental work and data analysis of microwave-assisted esterification of PFAD;

Chapter 4 discusses the experimental results for microwave-assisted esterification of PFAD. This includes the identification of the reaction kinetics of the process, and the measurement of dielectric properties of the PFAD biodiesel produced;

Chapter 5 outlines the research methodology in developing a three-dimensional multiphysics numerical model of the microwave-assisted PFAD esterification.

Chapter 6 discusses the numerical study of the microwave-assisted PFAD esterification. The numerical results are verified with the experimental results, and the effects of microwave on the biodiesel production are also discussed;

Chapter 7 presents the research methodology for the vacuum distillation experimental setup and numerical design of the distillation column. The analytical techniques required to identify the cold flow properties of PFAD biodiesel are also included;

Chapter 8 summarizes the experimental results of the vacuum distillation. A preliminary design of the vacuum distillation column is also shown and validated with the calculation from a computational software;

Chapter 9 presents the conclusion for the current study and provides recommendations for future work in several aspects.

CHAPTER 2 LITERATURE REVIEW

This chapter reviews the existing literature studies on the enhancement of biodiesel production process in order to improve the economic feasibility of biodiesel and hopefully replace diesel fuel in the future. Researchers have proposed several approaches and study their possibilities in order to tackle the aforementioned issues. Some of the greener methods to produce biodiesel which are of interest in this research work are described here in more detail. Due to the nature of the feedstock, the biodiesel produced in Malaysia is not suitable for export purpose without further process. A new idea is raised in this project to improve the biodiesel quality, particularly its cold flow properties.

2.1 Biofuel and its evolution

Biofuels are defined as fuels that are harvested from biomass resources, or their processing and conversion derivatives, for transportation purpose. Biomass refers to any organic matter that is available on a renewable or recurring basis. This includes all plants and plant derived materials, such as crops, trees, algae, animal waste, and municipal residues (Wright et al., 2009). Examples of biofuels are corn ethanol, cellulosic ethanol, algae diesel, and biodiesel (Lee & Shah, 2012). Unlike other types of green energy resources, biofuels usually exist in liquid state which are essential for transportation usage (Alalwan et al., 2019).

The annual energy consumption for the non-OECD (Organization for Economic Cooperation and Development) region in year 2040 is predicted to be 739 quadrillion BTU, which is more than double compare to the year 1990 (recorded at 356 quadrillion BTU). Non-OECD countries include India, China, Africa, Middle East, Brazil, Russia,

other parts of Asia, as well as non-OECD parts of Europe and Americas. The recorded and projected figures of the energy consumption of each region from year 1990 to 2040 are shown in Figure 2.1. Asia is projected to experience the largest increase in energy use among non-OECD nations, from 200 quadrillion BTU in year 2015 to 303 quadrillion BTU in year 2040, which is a whopping 51.5% increase in energy demand within 25 years' time.

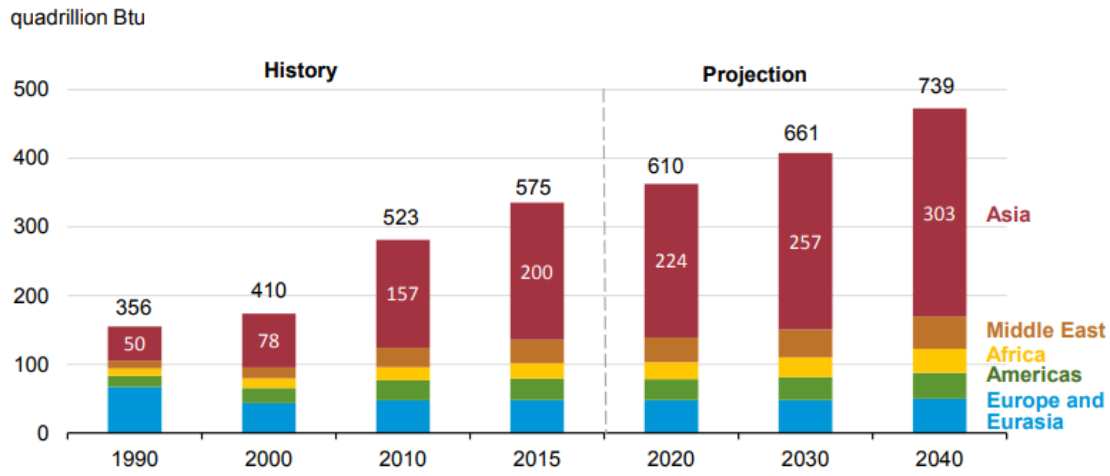

Figure 2.1 IEO 2018 Reference Case: Non-OECD Energy Consumption by Region (Capuano, 2018)

Generally, biofuels, which includes biodiesel, bioethanol, and biogas, are classified into four generations based on the type of the feedstock used. The benefits and limitations of each generation of biofuels are shown in Table 2.1. The first generation biofuels such as bioethanol and biodiesel are produced from edible biomass which are available in abundance. Bioethanol is produced from the fermentation of feedstocks that contain fermentable sugars or carbohydrates, such as sugarcane, corn, whey, barley, and potato (Lee & Lavoie, 2013). On the other hand, first generation biodiesel is produced from edible oil crops such as soybean, canola, corn, and palm. Using edible crops for biofuel production has raise concerns regarding the risks of food competition due to the limited availability of cultivation area (Singh et al., 2020).

Table 2.1 Types of Biofuels [adapted from Alalwan et al. (2019); Aro (2016); Fokaides and Christoforou (2016); Lee and Shah (2012); Sikarwar et al. (2017); Singh et al. (2020)]

Biofuel Generation	**Feedstock**	**Benefit**	**Limitation**
First generation	Edible biomass	• Established technology • Easy conversion procedure	• Food versus fuel debate • High production cost
Second generation	Non-edible oils, agricultural residues, industrial waste, lignocellulosic biomass	• Higher net energy yield (less energy input for crop production & harvesting) • No food vs fuel debate • More sustainable than first generation • More cost competitive	• Cost issue in commercializing • Lower crop yields • Under active R&D
Third generation	Algal biomass	• High growth rate • Low cost, high-energy and renewable • Wider fuel application (diesel, petrol, jet fuel)	• Still in early development stage • Costly to scale • Extensive downstream processing
Fourth generation	Genetically modified microorganisms	• Higher production rate • Low structural complexity • Improved hydrogen-to-carbon yield • Create artificial carbon sink to minimize carbon emission	• Still in very early stage of research • Concerns over disposal of genetically modified residue • Costly to scale

The second generation of biofuels are produced in a more sustainable way such that the net carbon emission of combusting the fuels is neutral or negative. The feedstock includes a wide array of different feedstocks, ranging from non-edible oils, lignocellulosic biomass, agricultural and forest residues, to industrial wastes. They are usually produced via physical (e.g. briquetting, pelletizing, fiber extraction), thermochemical (e.g. pyrolysis, gasification, liquefactions, and direct combustion), and biochemical (e.g. fermentation) technologies, after preparing the biomass feedstock via a pre-treatment stage to facilitate the conversion processes (Fokaides & Christoforou, 2016). For instance, a pre-treatment step is required to isolate cellulose from lignocellulosic biomass before conducting hydrolysis and subsequently fermentation to convert the sugars to bioethanol (Lee & Lavoie, 2013). However, the lack of active technologies for the commercial exploitation of waste generated during the biofuel production limits the development of the fuel of this generation.

Third generation of biofuels refer to algal-based fuels. Based on their size and morphology, algae are classified into macro-algae (e.g. kelp) and micro-algae. In contrast to lignocellulosic biomass, algal biomass has a very distinctive growth yield. Species like Chlorella are targeted due to their high lipid content and high productivity. Microalgae can be used to produce several biofuels such as bio-oil, bioethanol and biodiesel via biochemical (e.g. transesterification, anaerobic digestion, fermentation, photobiological hydrogen production) or thermochemical processes (e.g. pyrolysis). However, the development of microalgae fuel is still very limited due to economic reasons. For instance, the current dewatering technologies to separate microalgae from culture media are too expensive compare to other low-cost feedstock sources and are hard to scale. The requirement of large water volumes for industrial scale algae cultivation is also an issue for countries with temperate climate as the temperature is below 0 °C during a significant part of the year. Extensive research is undergoing to improve both the metabolic production and the separation process in bio-oil production, while keeping the production cost affordable (Alalwan et al., 2019; Aro, 2016; Lee & Lavoie, 2013).

The fourth generation biofuels are synthesised from genetically modified algae to create an artificial carbon sink and enhance the desired hydrogen-to-carbon yields (Alalwan et al., 2019; Sikarwar et al., 2017). The main benefit of producing engineered microalgae biofuels is the simplification of process steps from solar to fuel. However, there are several bottlenecks that have to be overcome to produce fourth generation biofuels. The main obstacles include the lack of understanding of algal growth, metabolism and biofuels production, development of cellular tolerance, disturbance in native metabolism of feedstock due to altered metabolic network, insufficient research in foreign genes-regulated enzymes for optimal biofuel production, and disposal issue of genetically-modified residue from biofuel extraction (Abdullah et al., 2019; Lü et al., 2011).

With the ever growing global demand for energy, producing sustainable and affordable energy has turned into a major concern to the world, as many industrialized and developing nations are economically hurting from escalating costs of energy and petroleum-based transportation fuels (Lee & Shah, 2012). Biodiesel is one of the alternative biofuels that can replace petroleum diesel fuel one day and address these issues. The advantages and disadvantages of biodiesel are shown in Table 2.2.

Table 2.2 Advantages and disadvantages of biodiesel in comparison to petroleum diesel (Moser, 2009)

Advantage	Disadvantage
• Inherent lubricity • Low toxicity • Derive from renewable source • Superior flash point • Excellent biodegradability • Negligible sulphur content • Lower exhaust emissions	• High feedstock cost • Inferior storage and oxidative stability • Lower volumetric energy content • Inferior low-temperature operability • Higher NO_x exhaust emissions

Just like biofuel, biodiesel can be classified into four generations based on the type of feedstocks. Biodiesel produced from edible oils is termed as first generation, non-edible

oils as second generation, and microalgae is classified as the third generation feedstock whereas the fourth generation feedstock is genetically modified microalgae. The edible crops used as the feedstock for first generation biodiesel include soybean, canola, rapeseed, coconut, palm, corn, olive, etc. They are largely available and can be converted into biodiesel via comparatively easy procedure (e.g. transesterification). Due to risks of environmental condition adaptation, high feedstock cost, food supply issue and impact on croplands, biodiversity, these drawbacks constrain the users to seek alternatives for biodiesel feedstock.

Hence, researchers have turned their interests to inexpensive non-edible oils such as Jatropha, mahua, Karanja, Neem, rubber seed, Jojoba, waste cooking oil, etc. These oils are more environmental friendly and cheaper to use but the yields of plants are lower compared to the first generation oil crops. Fortunately, these non-edible crops (e.g. Jatropha, Jojoba) are more weather resistant and can be cultivated on marginal lands instead of farming lands (Singh et al., 2020). However, growing non-edible crops still require land, which may conflict with agriculture land use. While second-generation feedstocks do not compete with the food cycle, more processing steps are required to improve the quality of the feedstocks. For instance, oils with high FFA content or other undesired impurities require a pre-treatment step to prepare the oil properties before the conversion processes could be carried out. Additionally, the biodiesel also has comparatively low performance in cold temperatures (Alalwan et al., 2019). Hence, more efforts need to be done to develop the cost-effectiveness of this generation of biodiesel and finally bring them forward to commercialization.

Third generation biodiesel can mitigate the food and land-use issues associated with first and second generation biodiesel. Microalgae is a very promising choice of biodiesel feedstock because they have rapid growth rates, the ability to grow in a wide range of conditions, and potential for higher yield rates (Lee & Shah, 2012). The yield of oil per unit area of microalgae can be 15-300 times higher than traditional crops (Mahlia et al., 2020). Some microalgae species possess high triacylglycerol content of 30–60%, or even up to 80% of their total dry biomass, which are higher than the first-generation crops.

However, there are production difficulties such as scaling up of culture and investing in stress control strategies for lipid production which hinder the commercialization of these microalgae species (Alalwan et al., 2019).

To the author's best knowledge, publications related to biodiesel production from fourth generation feedstock are not available in literature yet.

2.2 Biodiesel feedstock selection

Feedstock selection is the utmost important consideration for reducing biodiesel production cost as the feedstock supply and price alone covers more than 75% of the overall biodiesel production cost, as shown in Figure 2.2. Feedstock selection according to the local climate, soil condition and agricultural practice of each country is vital to reduce the cost of biodiesel production (Silitonga et al., 2011).

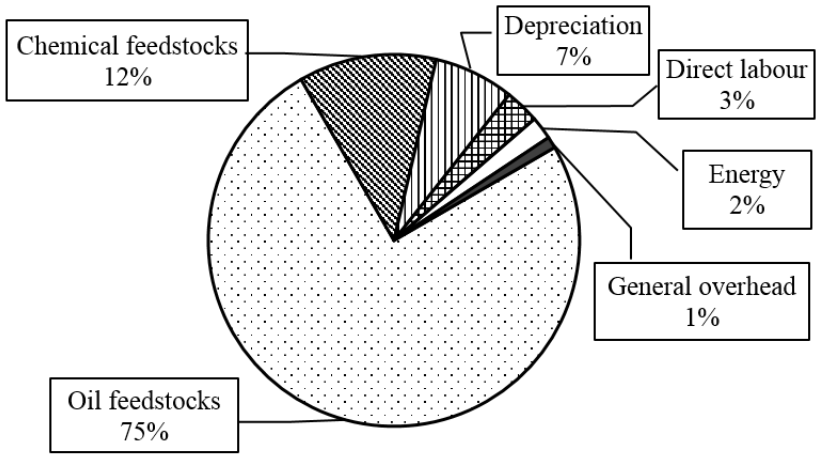

Figure 2.2 General cost breakdown for biodiesel production

Palm is an important raw material in Southeast Asian countries such as Malaysia and Indonesia, which have a surplus production of palm oil (Altaie et al., 2015). In Malaysia, palm oil is the most abundant and widely available source for biodiesel production.

Producing biodiesel from palm oil in Malaysia pose distinct advantages as it requires less manual labour for harvesting and the yield of vegetable oil per hectare is generally higher than other oil crops such as rapeseed and soybean. However, producing biodiesel from palm oil sparks several controversial issues notably the fuel versus food debate as well as the clearance of indigenous rainforests (Lim & Teong, 2010).

Judging from Table 2.1, developing a second generation biodiesel could help reduce the disputes arising from producing biodiesel using edible refined palm oil while lowering the cost of biodiesel. Several feedstocks for second generation biodiesel which can be used to produce commercialized biodiesel production in the near future are available in Malaysia. This includes PFAD (Soltani et al., 2016), Jatropha oil (Mofijur et al., 2012), and waste cooking oil (Motasemi & Ani, 2011).

The development of biodiesel production from Jatropha oil in Malaysia is still in its infancy stage as compared to the palm oil biodiesel industry. Being a non-edible oil feedstock, Jatropha oil will not spur the food versus fuel dispute. However, as Jatropha oil contains up to 34 wt.% of saturated fatty acids, it is expected that Jatropha oil will show inferior cold flow behaviour as well (Tiwari et al., 2007). The fatty acid composition of Jatropha oil is shown in Table 2.3.

Table 2.3 Fatty acid composition of Jatropha oil (Adebowale & Adedire, 2006)

Symbol	**Compound Name**	**Composition (wt.%)**
C16:0	Palmitic Acid	11.3
C18:0	Stearic Acid	17.0
C20:0	Arachidic Acid	4.7
C18:1	Oleic Acid	12.8
C18:2	Linoleic Acid	47.3

Jatropha, also known as *Jarak Pagar* in Malaysia, can grow well in Malaysia weather (Mofijur et al., 2012). In fact, the plant is drought resistant and needs minimal care to survive in harsh conditions. This enables the utilization of marginal lands for its plantation. Furthermore, the plantation cost of Jatropha crops can be significantly reduced as it does

not require much fertilizer and water (Lim & Teong, 2010). In spite of all these advantages, the yield of Jatropha oil is reported at 1.5 – 2 tonnes per hectare, which is lower than palm oil that yield 5 tonnes per hectare. In other words, the planting area required would be much higher to produce similar amount of oil feedstock.

The second feedstock option is waste cooking oil. Converting waste cooking oil into biodiesel could reduce water pollution as people usually discard the waste oil into the drains or rivers. Despite the relatively cheaper cost when compared to palm oil, the production process of biodiesel using waste cooking oil will be very challenging due to the presence of impurities. A wider range of process parameters would have to be considered to produce high quality biodiesel that meets the biodiesel standards. In addition, this feedstock may induce more corrosion problems to the pipelines, requiring tougher cleaning procedures and maintenance (Lim & Teong, 2010).

Biodiesel could be produced in a sustainable way under biorefinery concept by using low quality oil streams from oil refinery or other waste oil feedstocks (Tabatabaei et al., 2019). During the physical refining of CPO to produce refined bleached and deodorized (RBD) palm oil with low percentage of FFA, PFAD is produced at the fatty acid stripping and deodorization stage. PFAD is generated at an operating condition of high temperature heating ranging about 240-260°C, under vacuum of 0.27 – 0.67 kPa and direct steam injection of about 2.5 – 4.0 wt.% in the palm oil refining process (Leong, 1992; Sroynak et al., 2013). PFAD has similar cold flow properties as palm oil due to their similarity in fatty acid composition as shown in Table 2.4.

Table 2.4 Major fatty acid composition for palm oil and PFAD

Oil	**C14:0**	**C16:0**	**C18:0**	**C18:1**	**C18:2**
Palm (Gunstone et al., 2007)	1.1	44.1	4.4	39.0	10.6
PFAD (Lokman et al., 2014)	1.93	45.68	4.25	40.19	7.90

Cold flow properties indicate the low-temperature operation ability of a fuel in cold weather. This includes cloud point (CP), cold filter plugging point (CFPP), and pour point

(PP). Cloud point is the temperature at which crystals of solidified biodiesel first become visible, turning the fuel cloudy. CFPP measures the lowest temperature at which a sample fuel could pass through a 45-micron filter. Meanwhile, pour point is the lowest temperature where the liquid fuel is observed to flow. The average CP and PP of PFAD are reported as 13.2 °C and 12 °C respectively (Lokman et al., 2014). The CFPP of PFAD has not been measured but it can be reasonably assumed to be within the CP and PP. In comparison, the CP and PP of palm biodiesel are 21 °C and 19.7 °C respectively (Verma et al., 2016). Hence, we can deduce that PFAD is not only a cheaper alternative but also has better cold flow properties compared to palm oil for biodiesel production. In addition, it does not inflict food competition with human since PFAD is usually sold for non-food applications (Cheah et al., 2010).

In order to evaluate the feasibility of the most suitable second generation feedstock in substituting palm oil, it is important to investigate the cost of these feedstock first. Table 2.5 listed the prices of crude oil and biodiesel produced from palm oil and the other three second generation feedstocks. Palm oil is more expensive than the rest of the second generation feedstocks (waste cooking oil and PFAD). The cost for producing crude Jatropha oil is currently not available in literature yet.

As shown in Table 2.5, Malaysia Palm Oil Board (MPOB) reported that the average export price of RBD palm oil in year 2018 was about USD 570.50 per tonne. Instead of using the edible palm oil (first generation biofuel) to produce biodiesel, PFAD is an alternative palm-based feedstock that can be adopted to produce biodiesel (Abdul Kapor et al., 2017). Being a lower value by-product, PFAD is currently traded at a discount to RBD palm oil at approximately USD 100 per tonne. The price difference between PFAD and RBD palm oil is about the same as in early year 2010 (Cheah et al., 2010). This shows the potential of consistent cost saving by using PFAD feedstock. In comparison with using refined vegetable oil feedstock, utilizing PFAD feedstock could save 20–30% in production cost via the conventional processing route (Zahan & Kano, 2018). Although PFAD feedstock is still relatively expensive when compare to waste cooking oil, its consistent quality makes it a better choice for simpler biodiesel production. Using waste

cooking oil for biodiesel production would incur additional cost and effort to remove the undesired impurities which may vary every single batch, increasing the difficulties of pre-treating waste cooking oil.

Table 2.5 Price comparison of biodiesel from different feedstock [adapted from (Lim & Teong, 2010)]

Feedstock	**Price of crude vegetable oil (USD/tonnes)**	**Price of B100 biodiesel (USD/tonnes)**
Palm oil	610[a], 570.50[d*]	720 – 750
Waste cooking oil[b]	360	600
Jatropha[c]	N/A	400 – 500
PFAD [d]	476	N/A

Source: [a] Kingsman; [b] Rice; [c] Goldman Sachs; [d] MPOB (2018);
**RBD palm oil is assumed to be the feedstock of palm oil biodiesel according to information given by Mekhilef et al. (2011); Shahbazi et al. (2012)*

In order for the biodiesel to remain economically competitive with petroleum-derived diesel, not only should the feedstock be available at the lowest price possible, but also exist in abundance. Although using Jatropha oil has the potential to keep the biodiesel cost at the cheapest rate, the price benchmark or market mechanism for Jatropha oil has yet to be established. This lays uncertainty to the revenue stream, causing reluctance in industrial companies to invest in Jatropha oil at a larger scale. Therefore, Jatropha is still regarded as a supplementary feedstock in Malaysia instead of being an alternative (Lim & Teong, 2010). By year 2018, the total area of oil palm plantation in Malaysia has increased to 5.85 million hectares as compared to 4.85 million hectares in year 2010. The amount of PFAD that Malaysia produced in year 2018 was 1.16 million tonnes, which is twice more than the export volume of biodiesel (0.5 million tonnes) recorded. Thus, considering the availability of abundant feedstock supply, selecting PFAD would still be the most viable option to produce second generation biodiesel in Malaysia.

2.3 Chemical reaction of biodiesel production

Biodiesel which consists of long-chain mono-alkyl esters is the product of either the transesterification of triglycerides, or the esterification of free fatty acids, with low molecular weight alcohols such as methanol. The esters produced are also known as fatty acid methyl esters (FAME) or biodiesel. Catalysts are usually added to the process to enhance the reaction rate.

The three stepwise transesterification and one-step esterification reactions are shown in Equations (2.1) and (2.2), as follows:

Transesterification of triglycerides:

$$\begin{aligned} \text{Triglycerides} + CH_3OH &\leftrightarrow \text{FAME} + \text{Diglycerides} \\ \text{Diglycerides} + CH_3OH &\leftrightarrow \text{FAME} + \text{Monoglycerides} \\ \text{Monoglycerides} + CH_3OH &\leftrightarrow \text{FAME} + \text{Glycerol} \end{aligned} \tag{2.1}$$

Esterification of FFA:

$$\underset{\text{FFA}}{R-COOH} + \underset{\text{Methanol}}{CH_3OH} \leftrightarrow \underset{\text{FAME}}{R-COOCH_3} + H_2O \tag{2.2}$$

During the transesterification reaction, three alcohol molecules liberate the long-chain fatty acids from the glycerine backbone by bonding with the carboxyl group carbons in the triglyceride molecule (Lee & Shah, 2012). The triglycerides are converted into alkyl esters and glycerol during the transesterification reaction. After the reaction completes, FAME can be separated easily from the glycerol as both are immiscible. Stoichiometric alcohol-to-oil molar ratio is not used in biodiesel production as transesterification is a reversible reaction. Thus, increasing the alcohol-to-oil ratio by adding excess methanol shifts the reaction equilibrium in favour of producing FAME. In industrial processes, an alcohol-to-oil molar ratio of 6:1 is usually implemented for transesterification (Stavarache et al., 2003).

The production process can be operated either in batch or continuous mode and it is usually base-catalyzed or acid-catalyzed. The base-catalyzed transesterification of triglycerides is the most popular method implemented in the biodiesel industry to produce biodiesel from vegetable oil. This is because base catalyst is more active than the acid catalyst and adopting this method also poses fewer corrosion problems in the equipment (Perego & Ricci, 2012).

To produce biodiesel via transesterification, there is a strict requirement that applies on the oil feedstock quality. The feedstock must not contain more than 1% FFA. FFAs are long-chain carboxylic acids that have broken free from triglycerides, typically from the thermal degradation of triglycerides due to prolonged exposure to heat (Lee & Shah, 2012). These FFAs will directly react with the base catalyst to form soap, which is certainly not desirable for biodiesel production. This makes it difficult to separate the FAME from the glycerol after reaction and reduces the ester yield at the same time (Canakci & Van Gerpen, 2001). Hence, oil feedstock with higher FFA content should be pre-treated first via esterification reaction to reduce its FFA amount to below 1% such that saponification can be avoided (Aranda et al., 2008).

Since FFA reacts with base catalyst, esterification is usually acid-catalyzed. For instance, Phoo et al. (2014) who investigate the potential of a native plant in Asia (Indian milkweed seed oil) as an alternative feedstock, carried out acid-catalyzed esterification to pre-treat the oil which has a 27.5 wt.% FFA content. FFAs were esterified to form FAMEs and water until the FFA amount decreased to below 1%. After the pre-treatment, the mixture which now consists of unreacted compounds (triglycerides), biodiesel would be washed to remove the acid catalyst, excess methanol and water. Subsequently, the remaining triglycerides in the oil feedstock were converted to FAME via alkali-catalyzed transesterification. After that, FAME is further purified by washing off the homogeneous catalyst and other trace amount of contaminants (Banavali et al., 2010).

Most of the alternative feedstocks are of lower quality in which they contain high amount of FFA (>1%). This indirectly translates to higher production cost as pre-treatment is a necessity before the triglycerides in the oil can be transesterified into biodiesel. Thus,

having a two-step process (acid-catalyzed esterification pre-treatment & base-catalyzed transesterification) while using an alternative feedstock may not be an effective way to reduce the biodiesel production cost, considering the additional wastewater production and the processing time required.

Interestingly, from the literatures, it is observed that not all alternative feedstocks are subjected to the two-step biodiesel production process. To be exact, there is an alternative feedstock that researchers specifically do not apply this method with — PFAD. In contrast to the edible vegetable oils and even the other alternative feedstocks, PFAD has a comparatively high amount of FFA content which can be around 85 – 93% (Lokman et al., 2014; Yadav et al., 2010). Due to its high fatty acid content (>80%), researchers usually employed acid-catalyzed esterification to convert PFAD into biodiesel instead of using the conventional base-catalyzed transesterification or the two-step process (Cho et al., 2012; Chongkhong et al., 2007; Kim et al., 2011; Soltani et al., 2016). In fact, acid-catalyzed transesterification can occur simultaneously during esterification to convert the remaining triglycerides in the PFAD feedstock into FAME. Acid catalyst that is commonly used for the reaction is sulphuric acid (H_2SO_4).

2.4 Factors affecting biodiesel production reaction

The yield of biodiesel is affected by some critical parameters in the reaction as listed below (Atabani et al., 2012; Leung et al., 2010; Liu et al., 2008; Motasemi & Ani, 2012; Murugesan et al., 2009; Nomanbhay & Ong, 2017; Tabatabaei et al., 2019):

i. FFA and moisture content of feedstock
ii. Reaction time
iii. Alcohol-to-oil molar ratio and type of alcohol used
iv. Reaction temperature
v. Catalyst type and concentration
vi. Mixing speed

2.4.1 FFA and moisture content of feedstock

The FFA content and water concentration of feedstock could have detrimental effects in the yield and quality of biodiesel, depending on the production techniques used. For instance, to obtain best yield for beef tallow which is processed via base-catalysed transesterification, the FFA and water content of the feedstock should be <0.5% and <0.06%, respectively (Ma et al., 1998). They also reported that the presence of moisture has more negative effect on the transesterification that the presence of FFA does.

In general, oil feedstock with high FFA contents (>1%) should be pre-treated first or neutralize with higher concentration of base catalysts to avoid reduction in the yield of biodiesel. A 2.2% reduction in biodiesel yield is reported with an increase of FFA content from 0% to 4% in the waste cooking oil feedstock (Bouaid et al., 2016). However, for PFAD feedstock which contains >80% of FFA, base-catalyzed transesterification is not a suitable method to be used regardless how high the concentration of base catalyst is, because the FFAs in abundance will react and deactivate the base catalyst, causing soap formation and terrible yield.

Although moisture content is generally unfavourable, a study carried out by Liu et al. (2008) shows that the base-catalyzed transesterification rate of soybean oil to biodiesel is enhanced with the rising water content in methanol. The biodiesel yield is increased from 80% to 95% when the water content in methanol is in excess of 2.03%. This interesting observation is only possible due to the use of calcium oxide catalyst which generates more methoxide anions that has high catalytic activity in transesterification reactions. Thus, the reaction rate is accelerated and the biodiesel yield is improved. Nonetheless, if higher water content (>2.8 wt.%) is added, the yield would still decrease as the converted biodiesel would hydrolyse and become fatty acids to react with the base catalyst, resulting in soap formation.

2.4.2 Reaction time

Adewale et al. (2017) who investigated enzyme-catalyzed esterification of crude tall oil report that reaction time is one of the most contributing factors to the biodiesel yield. In

general, the yield of biodiesel increases with longer reaction time. The reaction time required for biodiesel production very much depend on the types of reactants and catalyst used as well as the production method applied. Normally, the yield will reach a maximum at an optimal reaction time and then remains relatively constant with a further increase in the reaction time. Alamu et al. (2007) studied the reaction time for base-catalyzed transesterification of palm kernel oil from 30–120 min. They observe a plateau of yield at 96% after 90 min. Once the maximum yield is achieved, it would be meaningless and no longer cost effective to increase the reaction time. Furthermore, there are findings which show that excess reaction time will result in lower product yield due to the backward reaction of transesterification which make the esters to hydrolyse into soap-forming FFAs (Eevera et al., 2009; Ma et al., 1998).

2.4.3 Alcohol-to-oil molar ratio and type of alcohol used

Another important variable affecting the yield of ester is the molar ratio of alcohol to vegetable oil. High molar ratio of alcohol to vegetable oil would interfere with separation of glycerin due to an increase in the glycerin solubility in biodiesel and alcohol. This is troublesome as the glycerin would drive the equilibrium of the reaction back to the left, thus lowering the yield of esters (Murugesan et al., 2009). Therefore, an appropriate alcohol-to-oil molar ratio must be determined to avoid yield loss and uneconomic alcohol recycling process. In line with that, Encinar et al. (2002) studied the transesterification reaction of Cynara oil with ethanol at alcohol-to-oil molar ratios from 3:1 to 15:1. The ester yields increased as the molar ratio increased up to 12:1 with the optimal results reported for molar ratios between 9:1 and 12:1. For molar ratios less than 6:1, the reaction was found to be incomplete whereas at 15:1 molar ratio, the yield decreased due to dissolved glycerin in the biodiesel phase, making the separation of glycerin difficult. Considering that the ester yields obtained using molar ratios higher that 9:1 did not increase considerably to compensate the cost of using additional consumption of alcohol, Encinar et al. (2002) recommended an optimal alcohol-to-oil molar ratio of 9:1 for biodiesel production. On the other hand, Liu et al. (2008) reported an optimal alcohol-to-

oil molar ratio of 12:1 for the transesterification of soybean oil with methanol and heterogeneous calcium oxide catalyst.

The types of alcohol which are most commonly used for biodiesel production are methanol and ethanol. Methanol is advantageous over other alcohols, mainly due to its affordable cost as well as physical and chemical characteristics. For instance, it can react quickly with triglycerides and dissolve very well in sodium hydroxide (Tabatabaei et al., 2019). Methanol is the more favourable type of alcohol as emulsions formed after the reaction would break down quickly to form a glycerol rich layer and methyl ester rich layer. On the other hand, emulsions formed after reacting oil with ethanol are more stable but making the separation and purification of esters more complicated (Murugesan et al., 2009). However, the low boiling point of methanol raises concerns over possible explosion risk associated with the colourless and odourless methanol vapours (Leung et al., 2010). Care should be taken while handling the chemicals during biodiesel production.

2.4.4 Catalyst type and concentration

Catalysts are used to shorten the reaction time. They are used depending on the type and quality of the feedstock. Base catalyst dominates the current biodiesel production methods due to its excellent performance in improving the rate of transesterification. For instance, the reaction rate of base-catalyzed transesterification is about 4000 times faster than acid-catalyzed transesterification. It has been reported that acid-catalyzed reaction is slow (3–48h). Furthermore, high purity and yield of biodiesel product can be achieved in a short time (30-60 min) using base catalyst (Nomanbhay & Ong, 2017; Singh et al., 2020). However, to use base catalyst, this puts a strict requirement on the quality of the feedstock (e.g. FFA <1%).

Apart from the acid and base catalysts, biodiesel reaction can be catalyzed with enzymes as well. In contrast to the chemical catalysts, enzymatic catalysts attracted research interests as they can prevent soap formation, which translates into easy product separation. In other words, the purification process of biodiesel is simpler. The enzymatic catalysts are also suitable to be applied to low cost feedstock with high FFA and water (Tabatabaei

et al., 2019). However, enzymatic catalysts incur higher cost and result in longer reaction time (Leung et al., 2010; Nomanbhay & Ong, 2017).

Alkali and acid catalysts can be further categorized into liquid (homogeneous) and solid (heterogeneous) catalysts. Homogeneous catalysts are used in the conventional transesterification process. Although large amount of water is required for wet washing of biodiesel produced via homogeneous transesterification process, the technology is commercialize worldwide due to its relatively lower energy use, high conversion efficiency, and cost effective reactants and catalysts (Motasemi & Ani, 2012). Recently, researchers have gained huge interests in developing green heterogeneous catalysts as they can be rapidly separated from the products by filtration, which reduces the downstream processing cost. In addition, solid catalysts are also recyclable and can be reused for multiple times. In contrast to homogeneous acid catalysts, solid acid catalysts also offer other advantages such as the elimination of corrosion and environmental problems (Leung et al., 2010). However, reaction catalyzed with solid catalyst proceeds at a slower rate because the reaction mixture constitutes of a three-phase system (oil-methanol-catalyst) which inhibits the reaction due to diffusion resistance between the phases (Chen et al., 2012; Liu et al., 2008). The advantages and disadvantages of the various types of catalysts used in biodiesel production are shown in Table 2.6.

Table 2.6 Advantages and disadvantages of different types of catalysts in biodiesel production [adapted from (Nomanbhay & Ong, 2017; Tabatabaei et al., 2019)]

Type of Catalyst	**Advantages**	**Disadvantages**
Homogeneous base catalyst	• Rapid reaction rate • Mild reaction conditions (less energy intensive) • Relatively cheap and widely available	• Sensitive to FFA content in oil • Decrease in biodiesel yield due to soap formation • Generate huge amount of wastewater in downstream processing
Heterogeneous base catalyst	• Mild reaction conditions (less energy intensive) • Can be separated easily after reaction	• Poisoning of catalyst when exposed to the surrounding air • Sensitive to FFA content in oil • Decrease in biodiesel yield due to soap formation

Type of Catalyst	Advantages	Disadvantages
	• High possibility to reuse and regenerate	• Leaching of catalyst active sites may lead to product contamination
Homogeneous acid catalyst	• Insensitive to FFAs and water content in feedstock • Perform simultaneous esterification and transesterification • Preferable method for cheaper feedstock • Mild reaction conditions (less energy intensive)	• Very slow reaction rate • Cause corrosion problems on equipment • Separation of catalyst from product is problematic
Heterogeneous acid catalyst	• Insensitive to FFAs and water content in feedstock • Perform simultaneous esterification and transesterification • Preferable method for cheaper feedstock • Can be separated easily after reaction • High possibility to reuse and regenerate	• Complicated catalyst synthesis process • Higher overall production cost • Energy intensive reaction condition (high temperature, high molar ratio & long reaction time) • Leaching of catalyst active sites may lead to product contamination
Enzymes	• Not affected by water content in feedstock • Simple glycerol recovery and produce high grade glycerol • Low reaction temperature (20–50 °C) • Low environmental impact (wastewater treatment not required)	• Low to moderately-high reaction rate • Relatively high cost of catalysts if enzymes cannot be recovered and reused • Possible enzyme inhibition by alcohols

Encinar et al. (2002) studied the effects of catalyst type and catalyst concentration on the transesterification reaction of Cynara oil. They have tested two homogeneous catalysts (sodium hydroxide and potassium hydroxide) with their concentration vary in the range

0.25–1.5 wt.%. The overall performance of sodium hydroxide (NaOH) catalyst is found to be better than KOH catalyst. The optimal yields are achieved at a catalyst concentration of 1.0 wt.%. Hence, using higher catalyst concentration does not always give high biodiesel yield. Stavarache et al. (2003) discovered that adding large amount of catalyst does not lead to an increase in the biodiesel yield. In fact, some of the catalyst react with the oil, causing soap formation that results in the separation difficulties of esters from the reaction mixture (Leung et al., 2010). The soap becomes a phase transfer catalyst which increases the solubility of the FAME in the glycerol phase. Thus, a significant amount of the FAME remains in the glycerol after phase separation, causing the product yield to decrease further. In addition, high catalyst concentration also results in another issue: forming emulsions while washing the esters. During washing process, the soap that form in the esters phase would accumulate at the interfacial region between the immiscible esters phase and water phase. The soap molecules would trap esters inside, thus causing greater loss in biodiesel yield when the soap molecules are removed from the esters together with the water (Stavarache et al., 2005). This is similar to the findings reported by Encinar et al. (2002). At higher concentration, reduction of yield is reported. For refined oil with FFA contents of <1%, the addition of an excessive amount of base catalyst gives rise to the formation of emulsion, which hinders the glycerin separation, causing a fraction of the esters to be lost during the separation and purification process.

2.4.5 Reaction temperature

Reaction temperature has been generally reported as a significant variable for speeding up the reaction rate and reducing the reaction time by facilitating mass transfer (Leung et al., 2010). According to Freedman et al. (1984), the reaction rate of biodiesel production from various vegetable oils, such as cottonseed, peanut, soybean, and sunflower, are four-time faster when conducted at temperature ≥60 °C compare to at 32 °C. At elevated temperature, the solubility of oil in alcohol improves. The high temperature also increases the molecular activity in the reaction mixture, thus resulting in better diffusion and higher probability of molecular collisions, which enhances the reaction rate (Roy et al., 2014).

An increase in the reaction temperature also makes the breaking of bonds of triglycerides and methyl combinations into FAMEs easier (Wei et al., 2013).

However, the increase in temperature beyond certain limits can have adverse effects on the reactants or products (e.g. degradation, vaporization) and being less cost-effective. It is noteworthy that for non-enzymatic biodiesel production, the temperature near to alcohol boiling point is the optimum temperature (Tabatabaei et al., 2019). Beyond this temperature, both mass transfer and yield of transesterification reaction drop due to loss of alcohol through vaporization. Liu et al. (2008) reported that the reaction rate of transesterification using solid base catalyst is accelerated with increasing temperatures up until an optimum reaction temperature is reached at 65 °C (i. e. boiling point of methanol). At higher temperature, not only does methanol is lost through vaporization, the boiling methanol also forms a large number of bubbles in the reaction mixture which inhibit the reaction on the three-phase interface (oil-methanol-solid catalyst).

2.4.6 Mixing speed

Mixing performance is another crucial parameter in optimizing biodiesel production process as it can greatly influence the mixing degree between immiscible alcohol-oil phase, the mass transfer, and thus affecting the rate of conversion. A direct relation was reported between increasing rotation speed (200–800 rpm) and improved biodiesel yield (Z.-H. Li et al., 2013). According to Roy et al. (2014), the stirrer speed considerably controls the mass transfer kinetics with respect to the economic production of biodiesel from the transesterification of Jatropha oil. It has been revealed that the influence of stirring rate on the control of biodiesel production is the highest during the initial stages of reaction when the alcohol and oil are still immiscible with each other. As the reaction proceeds, the significance of agitation drops as the reaction mixture gradually becomes a homogeneous phase with an increase in the mass fraction of esters that increase the solubility of methanol in the oil and esters. It is reported that the oil, methanol and FAME mixture becomes a homogeneous phase when the FAME content increases to 70% (Zhou et al., 2006). Nonetheless, excess mixing can reduce the economic feasibility of biodiesel

production process as this increases the equipment and operation complexities which results in higher capital and energy requirement, as well as reduces the yield of ester conversion by making less alcohol available for reaction due to vaporization and/or bubble formation (Tabatabaei et al., 2019).

2.5 Process intensification for biodiesel production

To date, scientists and researchers have been contributing vast amount of ideas and great effort into improving the conventional biodiesel production process. Apart from finding the new green and cost-effective catalyst in an effort to keep the biodiesel cost more affordable, some choose to switch their focus to improve from other aspects, which is the heat and mass transfer of fluid within the process. The typical process treatments in biodiesel conversion and utilization technologies could be categorized in Table 2.7.

Table 2.7 Typical Biodiesel Production Process

Process	Description
Feedstock Preparation and Pre-treatments	Pre-treatment processing usually takes place in the pre-screening of feedstock, where unfavourable materials are removed or converted (e.g. FFA).
Chemical Reactions	Triglycerides or free fatty acids are converted to alkyl esters via transesterification or esterification reaction. Addition of suitable catalysts accelerates the reaction. Glycerin or water are generated during the reaction.
Heat and Mass Transfer Enhancement	Efficient control of heat and mass transfer to and from the reactants is crucially important to enhance the reaction rate. This includes the usage of the conventional heating and mechanical stirring method, and the deployment of green technologies such as microwave and ultrasound.
Downstream Processing of Biodiesel Products	The principal product of biomass processing using vegetable oil and animal fat is biodiesel (FAME). This principal product can be used for direct end use after purification, as an alternative fuel that replace petroleum diesel. Crude glycerin is generated as a by-

Process	Description
	product from the transesterification process. It is a value product which enhance the profitability of the biodiesel production process.
Product Purification and Separation	Purify the biodiesel product by separating other undesired reactants or products from the fuel product. The unfavourable products are further processed to recover useful materials for future usage. For instance, the separation of methanol and salts from crude glycerin that was produced by the transesterification process. Methanol that is recovered can be reused again for biodiesel production.

During the pre-treatment, filtering process is employed to remove dirt and other particulate matters from the oil when necessary. In addition, water must be removed from the oil as well because it will hydrolyse the triglycerides to form free fatty acids and glycerin. Typically, feedstock that is acceptable for processing without pre-treatment has less than 1% FFA content. To deal with the FFAs, acid-catalyzed esterification is performed to convert them into biodiesel (Leung et al., 2010). Alternatively, neutralize the FFAs by turning them into soap and then remove the soap from the oil. After the pre-treatment, the oil is sent to a reactor for biodiesel production. With efficient mass and heat transfer enhancement, biodiesel is obtained with excellent conversion. Upon completion of the process, the reaction mixture is subjected to gravity separation or centrifugation to induce phase separation. After that, the biodiesel goes through a neutralization and purification process whereby the other undesired compounds such as catalyst, soap and unreacted triglycerides are removed by using dry or wet washing methods. Wet washing is a water and energy intensive process whereby 2-120 L of wastewater is generated for treating every 100 L of biodiesel that are neutralized by acids. Lastly, the biodiesel is dried and stored as the final product. The costly treatment of generated wastewater and drying the final product increase the downstream processing cost of biodiesel production. In contrast, dry washing biodiesel using absorbents is a more environmental friendly

option but the use of absorbents and additional equipment may not be economical under certain industrial circumstances (Lee & Shah, 2012; Tabatabaei et al., 2019).

Most of the commercial biodiesel are produced via base or acid-catalyzed transesterification of vegetable oils and animal fats in stirred tank reactors. According to Qiu et al. (2010), there are several challenges related to this conventional process which consequently result in high alcohol-to-oil molar ratio, catalyst concentration, and long reaction time. As transesterification itself is a reversible reaction, hence there is an upper limit to the biodiesel conversion without any product removal. In order to overcome this, the alcohol-to-oil molar ratio has to be increased. Meanwhile, the limited mass transfer between oils and alcohol which are immiscible in nature negatively affects the reaction rate. To solve this issue, mechanical stirring mechanism is adopted.

During the conventional biodiesel production process, heat is transferred via thermal convection and conduction, from the wall surface of the reaction vessel, to the internal reaction mixture. As a result, a large amount of energy from the heat source is lost to the environment through the conduction of materials and convection currents, making this method relatively slow and inefficient (Motasemi & Ani, 2012). Furthermore, the heating effect of conventional method also highly depends on the thermal properties of the surface materials in order to transfer heat to the internal sample volume, which results in non-uniform sample temperatures and higher thermal gradients (Gude et al., 2013). Additionally, the reaction mixture has to be mechanically stirred to enhance the heat transfer in order to increase the reaction rate between the feedstock and alcohol for biodiesel production. The current biodiesel production reactions suffer from mass transfer limitation due to the limited miscibility of alcohol and oil (Boffito et al., 2014). They will form a two-phase solution instead of a homogeneous solution. Hence, mechanical mixing is applied in the conventional method to improve the reaction rate. Kalva et al. (2008) reported that the typical reaction time to achieve at least 95% biodiesel yield for base-catalyzed transesterification at about 50^{o}C is around 2 hours using mechanical agitator.

There has been substantial searching for more efficient biodiesel production methods to enhance the mass and heat transfer of fluids. This has led to the integration of green

technologies such as microwave and ultrasound into the current biodiesel production method to further accelerate the reaction, which is also referred to as process intensification. Process intensification is the development of methods and/or equipment to provide higher yields with improved benefits compared to existing conventional procedures. It is a strategy for making significant reductions of chemical plant size through size shrinkage of individual pieces of equipment or reduction of the number of unit operations involved so as to reach a given production objective. Process intensification could also lead to other desirable effects such as increase in production capacity, decrease in energy consumption or even a cut in waste or by-product formation (Stankiewicz & Moulijn, 2000). The goal of process intensification is to develop substantially smaller, cleaner, and energy-efficient technologies for the industries.

Many researchers explored and put in a lot of effort to integrate several types of intensification technologies into the current biodiesel production process. Tabatabaei et al. (2019) has comprehensively reviewed 18 types of chemical reactors used for biodiesel production and classified them into five categories of reactor: (i) rotating reactors; (ii) simultaneous reaction-separation reactors; (iii) plug-flow reactors; (iv) microwave reactors; and (v) cavitational reactors. Among the five categories of reactors, various new reactor designs have been proposed and researched for the rotating reactors and plug-flow reactors. It is found that the investigations on reactors from these two categories are mostly carried out to study the effects of mechanical configurations or internal geometries of the reactor design towards the enhancement of mass transfer in the chemical reaction. Meanwhile intensification methods which are under the simultaneous reaction-separation category include reactive distillation, and membrane separation. Both methods could be used to combine the reaction as well as the downstream separation and purification process for biodiesel production. The reactor technologies that have been reviewed and are of interest in this work are the microwave and cavitational reactors. Another type of process intensification technology for biodiesel production – the supercritical solvent method would be discussed as well.

2.5.1 Supercritical solvent method & co-solvent

The production process of biodiesel is usually performed catalytically. Alternatively, it can be performed non-catalytically by using supercritical methanol. Supercritical methanol is superior to catalytic methods as no catalyst is needed and the reaction time is relatively shorter (Tan et al., 2009). The absence of catalyst indicates that the elimination of complicated separation and purification process of biodiesel. In addition, the supercritical method has a higher adaptability with alternative feedstock which has higher FFA and water content as there is no risk of saponification without the addition of catalyst. The supercritical method is expensive as it requires higher energy input to operate at/above the critical temperature and pressure of solvents (Nomanbhay & Ong, 2017).

When a fluid is subjected to temperatures and pressures in excess of its critical point, a distinct liquid and vapour phase no longer exist. Beyond the critical temperature and pressure, a single-phase fluid exists due to the significant drop in the solubility parameter and dielectric constant of fluid (Tan et al., 2009). This is referred to as the supercritical fluid phase. The critical point of methanol is found to be 239.6 °C and 8.1 MPa (Wei et al., 2013). In the supercritical methanol method, the temperature and pressure are maintained above the critical point of methanol, thus the alcohol becomes more soluble in oil. This approach can solve the immiscibility issue associated with the two-phase nature of methanol/triglycerides mixture by forming a homogenous solution, whereby the reaction is completed in a very short time (Han et al., 2005; Leung et al., 2010).

The biodiesel production via supercritical methanol without catalyst requires temperatures of 350–400 °C and pressures of 45–65 MPa (Han et al., 2005). However, this is impractical as esters will thermally decompose at high temperature. Román-Figueroa et al. (2016) who study the transesterification of castor oil using supercritical methanol observes an 80.9% of thermal decomposition of esters at 350 °C and 43 MPa. The maximum yield (96.5%) is achieved at 300 °C, 21 MPa and 90 min. On the other hand, Tan et al. (2009) investigate the non-catalytic biodiesel production from palm oil by using supercritical methanol at a methanol-to-oil ratio of 30 ffor 20 min. The reaction temperature is 360 °C at 22 MPa pressure. Their results show that the reaction time is

reduced to 20 min by using non-catalytic supercritical methanol technology, compare to the 1-hour reaction time required for catalytic methods to produce more than 70% yield. Subsequently, Tan et al. (2010) carry out an optimization study on the non-catalytic supercritical methanol reaction using refined palm oil feedstock. The optimum conditions for achieving 81.5% yield are 16 min reaction time, 372 °C reaction temperature and a methanol-to-oil molar ratio of 40. The optimum pressure is not reported but the pressure range they studied is between 15–25 MPa.

The main parameters influencing the supercritical reaction are temperature, pressure, methanol-to-oil molar ratio, reaction time and agitation speed. The effect of pressure is said to be lower than that of temperature and reaction time in general (Shin et al., 2012). When the reaction is carried out in a batch reactor at optimal agitation speed of 200–500rpm, the operating pressure range can be reduced from 30-35 MPa to 18-21 MPa (Román-Figueroa et al., 2016).

In addition, co-solvent such as supercritical carbon dioxide can be added to the reaction mixture in order to reduce the reaction temperature and increase the mutual solubility between methanol and vegetable oil under supercritical conditions (Han et al., 2005). The critical temperature and critical pressure for carbon dioxide is 31.1 °C and 7.4 MPa, respectively. Han et al. (2005) reported a significant decrease in the severity of the conditions required for supercritical reaction with the addition of CO_2 in the reaction system. For instance, the optimal reaction temperature to achieve the same yield is reduced by 50 °C, from 330 °C to 280 °C, with the addition of CO_2. They obtained a 98% ester yield from soybean oil in 10 min with an optimal reaction temperature of 280 °C, methanol-to-oil ratio of 24, and CO_2-to-methanol ratio of 0.1 at 14.3 MPa reaction pressure. Maçaira et al. (2011) also employed a similar approach for the continuous transesterification of biodiesel in a fixed bed reactor to get optimal yield (88%) at reaction conditions of 200 °C, 25 MPa and 2 min. The observed reaction rate is 20 time faster than the conventional biodiesel production process.

Although many researchers have shown the feasibility of supercritical methanol technology, the over-production of glycerol by-product could not be avoided as it leads

to uneconomical biodiesel processing. Thus, a non-catalytic biodiesel production process using supercritical methyl acetate has been proposed. Rather than glycerol, triacetin (glycerol triacetate) is produced along with esters during the reaction. The triacetin has no adverse effects on the main fuel characteristics and using it as an additive can improve the cold flow properties of biodiesel (Niza et al., 2013). Thus, ideally no separation step is needed after the reaction when a 100% biodiesel yield is obtained. Niza et al. (2011) reported that the optimum conditions to achieve 71.9% biodiesel yield for the transesterification reaction of Jatropha oil using supercritical methyl acetate are 400 °C reaction temperature, and a methyl acetate-to-oil molar ratio of 50 in 32 min reaction time. The reaction pressure was maintained above the critical pressure of methyl acetate (4.6 MPa).

Due to the requirement of high reaction temperature (400 °C) in the supercritical methyl acetate method, the thermal stability of the major ester components (methyl oleate and methyl linoleate) as well as triacetin are investigated (Niza et al., 2013). The results revealed that thermal decomposition phenomena occur for both esters at the tested temperature range from 330 °C to 420 °C, but at a different rate. The thermal stability of methyl linoleate significantly decreases as temperature increases from 330 °C to 420 °C while the methyl oleate is still relatively stable at <360 °C (>80% ester recovery). Similar thermal degradation behaviour was also observed for triacetin whereby the recovery is already less than 40% at 330 °C. Hence, the use of supercritical methyl acetate method for biodiesel production is still not a feasible method yet compare to supercritical methanol. The thermal stability study of esters conducted by Imahara et al. (2008) revealed that decomposition occur dominantly at temperature >350 °C over a prolonged period of reaction time. To achieve thermal stabilization for high quality biodiesel production, they recommend the reaction temperature to be < 300 °C (preferably 270 °C) with a supercritical pressure higher than 8.09 MPa (for supercritical methanol case).

Nonetheless, instead of adding methyl acetate directly, adding acetic acid to supercritical methanol can reduce the amount of glycerol content that is produced, by converting them into triacetin. Wei et al. (2013) reported a 97.83% yield of esters from soybean oil after

90 min of supercritical transesterification with carbon dioxide at 20 MPa, 280 °C, at a methanol-to-oil ratio of 60, and an acetic acid-to-oil ratio of 3. The glycerol by-product is reduced by 30.2%.

2.5.2 Cavitation

For two-phase liquids such as oil-methanol that are immiscible in each other, the use of cavitation generally results in improved emulsification and smaller droplet size. This increases the surface area at which alcohol, catalyst, and oil interact with each other and therefore intensify the mass transfer and reaction rate (Chipurici et al., 2019; Tabatabaei et al., 2019). Acoustic energy or flow energy are used in cavitational reactors to intensify chemical processes through cavitation phenomenon. The formation of cavities as well as their subsequent growth and violent collapses, release huge amount of energy over a very small area, leading to large energy densities (Chuah et al., 2017). In other words, localised hot spots under extreme temperature and pressure are formed. This also generates very fine emulsions that improve reaction rate when the disruption and mixing caused by cavitational collapse occur near or at the interface of two liquids. Apart from accelerating the reaction rate, this phenomenon reduces the amount of catalyst required and shorten the reaction time from hours to minutes (Oliveira et al., 2018). In contrast to the number of cavitation bubbles, the size of cavitation bubble, which relates to the energy released when bubble collapse, has an inverse relationship with the ultrasonic frequency. (Tabatabaei et al., 2019). To maximize the process intensification effect in any cavitational reaction, parameters which increase the maximum size and life of the cavities must be optimized (Gogate, 2008).

The cavitational reactors can be classified into sonochemical (ultrasonic) reactors and hydrodynamic cavitation reactors. The ultrasonic reactors can be further categorized into ultrasonic horn and ultrasonic bath. Ultrasonic horn is an immersion type of transducer which directly produce very high pressure intensities close to the horn. The pressure intensity decreases exponentially with increasing distance from the horn. The second sonochemical design, ultrasonic bath (cleaner) consists of single or multiple ultrasonic

transducers encompassing the bottom of the reactor. The active ultrasonication zone is limited to a vertical plane on top of the transducers where the highest intensity is found at the centre of the transducer(s) (Gogate, 2008). Compared to ultrasonic bath which is low cost and widely available, ultrasonic probe has some disadvantages such as scale up complexity, erosion and particle shedding on the horn tip surface and low cavitation efficiency due to the concentrated acoustic intensity distribution (Oliveira et al., 2018; Tabatabaei et al., 2019).

In most cases, the ultrasonic reactors operate in the frequency range 20–50 kHz with output power typically over 200 W. Ultrasound is used for the first time to produce FAME on a laboratory scale by Stavarache et al. (2003). Later, the same team applied for a patent to use ultrasound irradiation for biodiesel production (Maeda et al., 2005). Stavarache et al. (2003) studied the effect of low frequency ultrasounds (28 and 40 kHz) on the transesterification reaction of vegetable oil and compare with mechanical stirring. The reaction which is performed under 40 kHz ultrasonic irradiation in ultrasound bath completes the fastest (20 min), followed by 28 kHz (40 min), and lastly mechanical stirring (60 min). They do not fully understand the differences behind the formation and collapse of cavitation bubbles at 28 and 40 kHz which lead to the difference in reaction time. Two years later, Stavarache et al. (2005) also reported the same findings, concluding that low frequency ultrasonic irradiation is useful for transesterification reactions. The optimal frequency is observed at 40 kHz with 400W power. At higher frequencies, the formation and collapse of cavitation bubbles are not strong enough, causing poor mixing between the two immiscible layers (alcohol and oil). Emulsification does not occur; therefore, the reaction rate is not accelerated as desired.

Ho et al. (2015) carried out ultrasound-assisted transesterification of refined palm oil (RPO) and CPO using heterogeneous palm oil mill fly ash supported calcium oxide catalyst. They introduced ultrasound of 20 kHz (max. power 700 W) in a pulse mode (10s on and 7s off) via an ultrasonic horn to prevent instantaneously temperature spikes and generate sudden impacts for better cavitation. The reaction temperature is fixed at 45 °C. Their experiments show that the reaction time is reduced from 360 min under

conventional mixing to 30 min with 60% ultrasonic amplitude (yield >97%). It is reported that further increment in the amplitude does not improve the biodiesel yield. This could be due to the small reactor volume (250 mL) where ultrasound at 60% amplitude is more than sufficient to enhance the mass transfer. In addition, the size of bubbles form at high ultrasound amplitude are larger and they inhibit the transfer of acoustic energy through the liquid phase (Kumar et al., 2010).

Stavarache et al. (2007) investigated the base-catalyzed transesterification of commercial edible oil and RBD palm oil in ultrasonic continuous flow reactors at 38–40 °C reaction temperature. A 45 kHz 600W power push-pull ultrasonic transducer (similar to ultrasonic horn) is used to provide the ultrasonic irradiation. The effects of the reactor's volume and the residence time on the yield are studied. Their results reveal that the yield decreases with increased reactor volume, as the ultrasounds power and bubbles density diminished, leading to a low mass transfer between the reactants. To obtain the highest yield, they recommend using a small reactor in continuous mode with shorter residence time. It is noteworthy that for RBD palm oil which partially solidified at room temperature, the oil-to-alcohol molar ratio and residence time required for ultrasonic irradiation have to be increased from 1:6 to 1:7.5 and 10 min to 20 min to achieve similar yields as commercial edible oil. Thus, low quality feedstocks are comparatively not suitable for ultrasonication.

Nonetheless, Deshmane et al. (2008) studied ultrasound-assisted esterification of PFAD, a low quality feedstock with high FFA in an ultrasonic bath. They discover that ultrasound significantly enhances the reaction rate after the system has reached about 30% of FAME conversion. At this stage, the liquid mixture starts to form two layers (ester-rich layer and excess methanol layer) and the progress of the reaction highly depends on the mass transfer between the two phases. Ultrasound eliminates the mass transfer resistance and reduces reaction time required from 300 minutes (conventional method) to 150 minutes in order to achieve FAME conversion around 95% at 40 °C. They use a fixed ultrasound power output rate (22 kHz frequency at 120 W) during the experiment, which may not be the optimum power output for mass transfer enhancement. Compared to the results

obtained by Stavarache et al. (2007), it can be seen that reaction time required is relatively longer for low quality feedstock.

Apart from the power output rate and type of feedstock, alcohol-to-oil molar ratio also plays an important role for optimal ultrasound-assisted biodiesel production. The reaction is usually carried out with excessive amount of alcohol instead of at its stoichiometric alcohol-to-oil molar ratio in order to drive the reaction to the right and to prevent reverse reaction. However, if the molar ratio used is too high, it reduces the beneficial effect ultrasound may bring. Kalva et al. (2008) reported that the optimum alcohol-to-oil ratio for transesterification of soybean oil under 20 kHz ultrasonication is 12:1. Further increase in the ratio reduces the biodiesel yield due to lower intensity of microturbulence generated by the cavitation bubbles in the reaction medium.

Hydrodynamic cavitation is an alternative method to create large scale emulsification through cavitation phenomena that combined with intense turbulent mixing. Unlike acoustic cavitation, hydrodynamic cavitation is generated via pressure variations when the fluid passes through a constriction channel such as orifice plates at high velocity by using Venturi type devices or pumps (Chipurici et al., 2019; Tabatabaei et al., 2019). The simplicity of hydrodynamic cavitation reactors with respect to the design, structure, operation and maintenance makes them a promising process intensification technology. Unlike ultrasonic reactors, hydrodynamic cavitation reactors are easy to scale up and they face less erosion problems because the cavitation takes place at the shear layer in bulk (Shah et al., 1999). The intense turbulent mixing and the subsequent uniform cavitation throughout the reactor allow efficient chemical reaction at milder conditions of pressure and temperature. Furthermore, the energy input per unit volume of reagents required by hydrodynamic cavitation can be up to 10 times lower than that of ultrasound cavitation (Gogate, 2008; Shah et al., 1999).

Pal et al. (2010) studied the biodiesel conversion through a hydrodynamic cavitation system which consists of a feed tank, a pump, an orifice, and control valves. The process achieved 80% yield within 30 min residence time with a reduction of energy consumption by more than half when compared to the conventional mixing method. Same process

approach is also implemented by Gole et al. (2013) who pre-treated and transesterified non-edible Nagchampa oil. In the process, a 92% conversion of biodiesel is achieved within 20 min treatment of pre-esterified oil with 1 wt.% KOH and 1:6 oil-to-alcohol ratio. Furthermore, Joshi et al. (2017) reported that the use of hydrodynamic mixer (high-speed homogenizer, 12,000 rpm) for the heterogeneous catalyzed-transesterification reaction of soybean and waste cooking oils reduces the reaction time from 120–180 min to 30 min with same yields of biodiesel.

Compared with mechanical stirring, hydrodynamic and ultrasonic mixers have lower requirements for catalyst and shorter reaction times (10–60 min) (Tabatabaei et al., 2019). However, the limitation of ultrasound is its low effective heating transfer ability (Gole & Gogate, 2013). Hydrodynamic cavitation is a better mixing technique than acoustic cavitation, allowing better mixing for immiscible liquids as well as easier scale up process regardless of the geometric characteristics of reactor. Kelkar et al. (2008) reported that that hydrodynamic cavitation is more energy efficient than acoustic cavitation (ultrasound). Despite the many advantages of hydrodynamic cavitation, it should be noted that pressure drop beyond the optimum condition could lead to choked cavitation phenomenon in which the downstream is completely filled with a cavity cloud which escape from the liquid without collapsing, and consequently reduced the micro turbulence intensity and the ester conversion (Maddikeri et al., 2014). Furthermore, great amount of energy loss associated with the fluid pumping process and the cost of pumping are also issues that have to be tackled of for the economical implementation of hydrodynamic cavitation (Dindar, 2016).

2.5.3 Microwave heating

A more recent approach to process intensification of biodiesel production is the use of microwave heating as it delivers better heat transfer than conventional heating (Chipurici et al., 2019). This helps improve the cost effectiveness of the chemical process by reducing reaction time and energy requirement. Microwave is an electromagnetic wave in the wavelength ranging from 0.01 to 1 m which corresponds to frequency range of 0.3

to 300 GHz. The typical bands approved for industrial applications are 915 MHz and 2.45 GHz. In order to avoid interference with telecommunications and cellular phone frequencies, all microwave reactors for chemical synthesis as well as domestic microwave ovens operate at 2.45 GHz frequency, which corresponds to a wavelength of 12.25 cm (Motasemi & Ani, 2012).

Microwave comprises of electric and magnetic field which lay perpendicular to each other. According to Fernández et al. (2011), there are four ways to categorize materials that interact with the electric field component of the microwave field, namely (i) insulator, (ii) conductor, (iii) absorber, and (iv) mixed absorber. The insulator refers to material that are transparent to microwave, which let microwave penetrates without incurring any losses. In contrast, microwave cannot pass through the conductor and tend to reflect or bounce back. Absorber, which is also referred to as 'dielectric', absorbs microwave radiation and heats up. Thus, microwave heating is also known as dielectric heating. Meanwhile, the mixed absorber is a composite or multi-phase material which consists of different phases with low and high dielectric loss respectively. This makes it advantageous to utilize the selective heating mechanism, one of the most significant characteristics of microwave processing. The component with high dielectric loss absorbs the microwave and passes the generated heat to the low dielectrics loss component without wasting much energy. For instance, methanol which has high dielectric loss absorbs microwave energy and heats up oil feedstock with low dielectric loss.

Conventional heating is a non-selective mode of heating that strongly depends on efficient stirring to facilitate heat distribution (Díaz-Ortiz et al., 2019). Unlike conventional heating where energy is wasted to heat the vessel wall to subsequently heat up the reagents inside through conduction and convection, microwave energy can directly penetrate the vessel wall without heating it and directly increase the temperature of the reaction mixture (Gude et al., 2013). Hence, microwave dielectric heating is not restricted by the thermal conductivity of the vessel. It is a non-contact energy source which provides rapid heating and cooling as well as selective heating of polar components. A reaction which may take hours to complete can therefore be shortened into minutes. As a result, yield is improved,

unwanted side reactions are minimized and less by-products are formed, resulting in a simplified downstream process that decreases the overall time taken for product separation (Muley & Boldor, 2013; Patil et al., 2012). It also reduces the equipment size required (Gude et al., 2013). This makes it an energy, time and workspace saving technique for biodiesel production.

The thermal effects of microwave can be summarized as inverted temperature gradients, overheating (superheating), hot-spots and inhomogeneity, and selective heating (Díaz-Ortiz et al., 2019). Some researchers that investigate microwave technology in other fields claim that 'non-thermal microwave effects' (i.e. influence of electromagnetic radiation) exist and that purely thermal microwave effects, which fundamentally based on Arrhenius phenomena, is insufficient to explain the reaction rate enhancement (Díaz-Ortiz et al., 2019; Nomanbhay & Ong, 2017). This issue remains a controversial topic among the researchers. The 'non-thermal microwave effects' are difficult to prove as the conversion of electromagnetic energy into kinetic energy is slower than the conversion of kinetic energy into thermal energy plus it is difficult to isolate experimentally thermal heating from other possible effects of microwave radiation (Rodríguez et al., 2015). Mazubert et al. (2014) rebutted the claims regarding the presence of non-thermal microwave effects. For homogeneous-catalyzed reactions, they suggest that the effect may seem to exist due to the poor temperature measurements using infrared sensors, where higher biodiesel yield is observed due to higher values of actual temperature during reaction and the reactants could possibly be superheated too. Nonetheless, it is accepted that in most cases, the observed 'non-thermal effects' enhancements in microwave-heated reactions are the results of purely thermal/kinetic effects (Rodríguez et al., 2015).

Ever since the first publication on microwave-assisted organic synthesis by Gedye et al. (1986), microwave heating technology has been extended to various fields such as medicinal chemistry, materials science, biochemistry, and green chemistry (Rodríguez et al., 2015). Currently, the superior benefits of microwave irradiation for biodiesel synthesis has been reported by several researchers. The study conducted by Duz et al. (2011) proves that microwave irradiation has superior benefits over the conventional heating method in

biodiesel production. The reaction time is reduced from 2 hours to 6 min under microwave irradiation. On top of that, the biodiesel yield obtained is 4.1% higher compare to the conventional method. Apart from enhancing reaction rate and producing higher yield with less energy usage, microwave-assisted transesterification also produces less by-product, which leads to a simplified and time-saving downstream process (Gude et al., 2013; Patil et al., 2012).

On the other hand, Lokman et al. (2014) also reported that the use of microwave heating in biodiesel production helps reduce the amount of solvent and energy required to complete the reaction at a lower temperature in a short time. El Sherbiny et al. (2010) also reported that the reaction time needed to produced 97.4% of biodiesel from microwave-assisted transesterification of Jatropha oil reduces from 60 minutes (conventional reflux) to less than 2 minutes. In their experiments, a scientific microwave oven is used to maintain the reaction temperature at 65 °C. However, there is no extra specifications given for the microwave oven. This makes it harder to compare the results with other microwave-assisted experiments.

A microwave reactor consists of a magnetron equipped with controls (the duty cycle) that transfer the electromagnetic energy through waveguide into a reactor vessel, enclosed within a metallic cavity (Leonelli & Veronesi, 2015). The reactor vessel can be constructed from microwave-transparent materials such as PTFE, quartz, or silicon carbide, which allow the volumetric heating of reactants within the vessel (Tabatabaei et al., 2019). Researchers have utilized several types of microwave reactors during their investigation of microwave-assisted biodiesel production, which can be categorized to function in either mono-mode (single mode) or multimode; and controlled either through microwave power level or temperature feedback. In a mono-mode oven, a standing wave pattern is created as shown in Figure 2.3.

The interference of electric fields with the same amplitude but different oscillation creates an arrangement of nodes with zero microwave energy intensity and a collection of antinodes with maximum amount of microwave energy. The sample vessel is placed right at the antinodal position of the standing wave pattern (as depicted in Figure 2.4), which

results in high heating rate (Rana & Rana, 2014). However, only one vessel can be inserted in the mono-mode oven at a time.

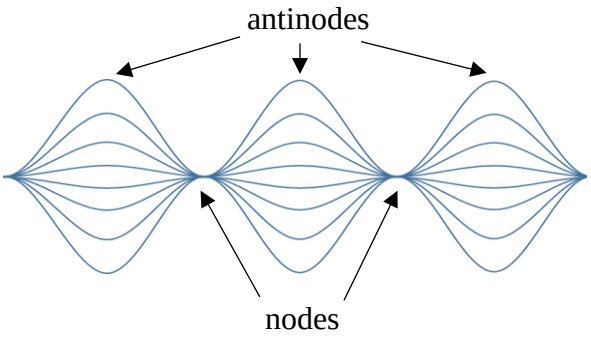

Figure 2.3 Standing wave pattern [adapted from Rana and Rana (2014)]

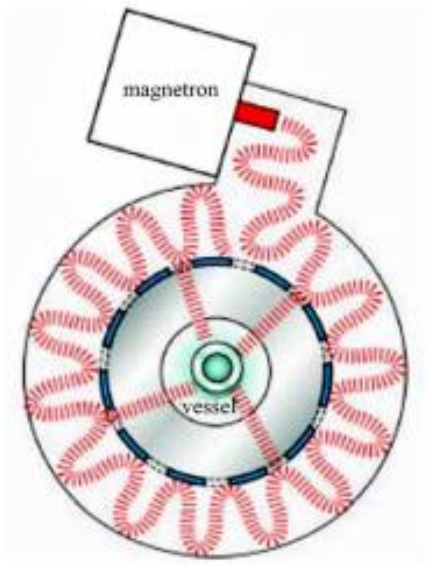

Figure 2.4 Heating mechanism in mono-mode microwave reactor [Reprinted permission obtained as shown in Appendix C, Rana and Rana (2014)]

In multimode reactors such as domestic ovens, the microwave that enters the cavity is reflected by the metal walls and the load over the cavity. In most equipment, a mode stirrer is installed (as shown in Figure 2.5) to disperse the microwave irradiation and ensure better field distribution such that the area of effective heating increases (Gude et al., 2013). Thus, it is possible to accommodate multiple samples in a multimode microwave reactor

simultaneously, making parallel synthesis possible. Nonetheless, the chaotic wave dispersion also results in the absence of temperature uniformity within the cavity, which creates hot-spots and cold-spots within the samples.

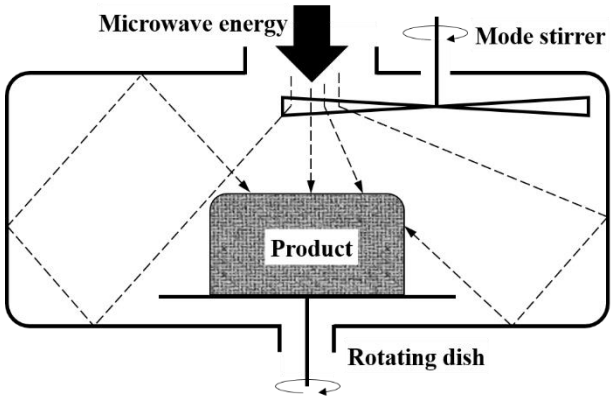

Figure 2.5 Schematic of a multimode microwave reactor [adapted from Rana and Rana (2014)

Apart from the microwave functioning modes, the way microwave reactor is controlled during its operation may also play a part in affecting the results obtained by different researchers. Some researchers use microwave reactors that are controlled via temperature feedback while some use microwave ovens that are controlled at fixed power levels. In the former form of microwave reactors, samples will be heated to a temperature level which is kept constant but the microwave irradiation is inconsistent over time. Meanwhile, samples in the latter microwave oven controlled using power level scales experience uniform cyclic dielectric heating but subject to varying temperature over time. For instance, Mazubert et al. (2014) uses a mono-mode microwave reactor equipped with a 2-bladed PTFE impeller (as shown in Figure 2.6) for their experiment to produce waste cooking oil biodiesel using two step approach (esterification followed by transesterification). The maximum microwave power is 300W and the power is automatically adjusted to the desired temperature by using optical fibre for temperature monitoring.

Putting the reactor design aside, variables which could affect the yield performance of the microwave-assisted esterification process are microwave frequency, power level, initial temperature and the dielectric properties of the reacting materials (Filho et al., 2016). While the former three variables are controllable by user, dielectric properties are material specific. Therefore, investigating the frequency and/or temperature-dependent dielectric properties of PFAD and its biodiesel will aid in predicting not only the temperature profiles for the reactions, but also the heating rates, the distribution of electrical field, as well as understanding the mechanism of microwave dielectric heating on the feedstock (Muley & Boldor, 2013; Terigar et al., 2010).

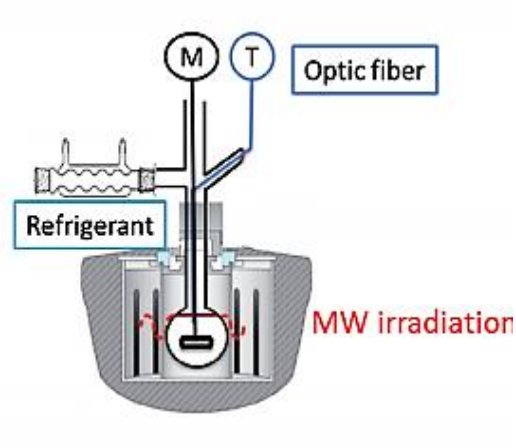

Figure 2.6 Schematic of mono-mode microwave reactor (CEM Discover SP model) with impeller and temperature control mechanism [Reprinted permission obtained as shown in Appendix C, Mazubert et al. (2014)]

During the research on biodiesel production of waste cooking oil using sulphuric acid catalyst, Patil et al. (2012) reported that the energy consumption required for microwave heating (288 kJ) is more than 90% lower than that for the conventional heating (3150 kJ). They also noted that 6 min of 800W microwave heating is sufficient to produce comparable biodiesel yields as to 105 min of conventional heating. This large discrepancy in reaction time is attributed to the limitations of conventional heating in which higher amount of heat energy is lost to the ambient while increasing the reaction temperature from the surface of the reaction vessel.

Interestingly, apart from comparing the effectiveness of microwave heating with respect to the conventional heating method, Patil et al. (2010) has conducted a side investigation on the effect of controlling the power dissipation of a domestic microwave oven towards biodiesel yields. Five different microwave power levels (20%, 40%, 60%, 80% and 100% of 800W) are tested. They observe that the biodiesel yield achieved under 1 min of 40% microwave power dissipation is similar to that obtained using 15 min conventional heating, with 23 times lower amount of energy required. Their results suggest that proper power dissipation control could further reduce the energy requirements. Regrettably, they have not discussed this part of their results in much detail. Nevertheless, several clues could be found from the graph they plotted. When the power dissipation level increases from 20% (160W) to 40% (320W), a huge spike is observed in their biodiesel yield, where the conversion obtained in 1 min reaction time increases sharply from below 40% to 80%. However, the conversion rate is not linearly proportional to the power dissipation levels. The biodiesel yield achieved with further increment in the power dissipation level (60%, 80% & 100%) only increase gradually (<10% in total). This points out that the energy requirements of microwave heating could be enhanced by finding the optimum microwave power level for a specific chemical reaction. However, these results are hard to compare with the results obtained by other researchers without knowing the actual power efficiency and the other specifications of the power equipment they used in detail. For instance, Kim et al. (2011) discovered that pulsed microwave irradiation (instantaneous power output in cyclic manner) is a more effective method to enhance esterification than continuous microwave irradiation at the same power level. However, this difference in microwave power application is not commonly mentioned in papers.

There are several studies which focus on the microwave-assisted esterification of PFAD. Lokman, Rashid, and Taufiq-Yap (2015) investigated the performance of a solid acid catalyst in microwave-assisted esterification of PFAD. The microwave oven they used is pulse-width modulated, or in other words, repeating instantaneous strong microwave energy is used to control the temperature at desired level. The optimum conditions reported is 12:1 alcohol-to-oil molar ratio, 3 wt.% of catalyst, 75 °C and 15 min to produce 96% yield. When compared to the study conducted by Lokman, Rashid, Taufiq-Yap, et

al. (2015) using conventional reflux technique (optimal parametric conditions for 95% yield: 10:1 alcohol-to-oil molar ratio, 2.5 wt.% catalyst, 75 ℃ and 120 min), the results show that the reaction time was shorten but the amount of reactants required slightly increased. With temperature-controlled microwave irradiation at 800W power, the reaction time required has drastically reduced by 87.5%. The rise in the amount of reactants is most probably due to the type of catalyst used. This can be justified by an experimental study conducted by Lokman et al. (2014) earlier. They achieved a higher yield (99.5%) from PFAD at an optimum alcohol-to-oil molar ratio of 9:1 at 55 ℃ with 15 min of microwave irradiation when only 1 wt.% of H_2SO_4 catalyst is needed.

Despite the advantage of dielectric heating, one of the major obstacles that prevents the scale-up and commercial usage of microwave in chemistry is the small penetration depth microwave has in various reactive media. For example, the penetration depth of microwave in methanol at 2.45 GHz frequency only increases from 0.76 cm at 20 ℃ to 1.4 cm at 60 ℃ (Mazubert et al., 2014). To put it briefly, the effectiveness of microwave heating is largely constrained by the thickness of the sample material. Another problem associated with microwave reactors is the difficulty of power and temperature control which results in low process reproducibility (Tabatabaei et al., 2019). Hence, the effort to scale up microwave production from laboratory to industrial scale has not been proved feasible in the biodiesel industry so far.

Sharma et al. (2019) who studied the microwave-assisted transesterification of waste cotton-seed cooking oil have attempted a scale-up study whereby the reaction volume is increased ten-fold from 50 ml to 500 ml. They reported that the reaction time required to achieve >90% yield under 180 W microwave irradiation is increased from 10 min to 20 min. In order to reduce the reaction time required for 500 ml size, the power input needs to be increased. It is observed that using 450 W can reduce the reaction time required by 5 min to achieve 90% yield. Nonetheless, the team also reported that the effect of power output increment on reaction time might differ depending on the catalyst used.

To eliminate mass-transfer resistances which occur in biodiesel production processes that are carried out at reaction temperature lower than the boiling point of solvents, either

mixing or heating systems must provide significantly high amounts of energy, which is economically unfavourable (Tabatabaei et al., 2019). Therefore, both mixing and heating systems can be applied together to simultaneously cope with mass transfer limitation in the biodiesel synthesis process as well as to simplify the separation process of catalysts, products, and reactants. The various advantages of using microwave heating for process intensification also lead to the coupling of this technology with the other intensification methods (e.g. ultrasound).

Microwave and ultrasound are energy saving techniques which promote faster and more selective reactions. Since microwave improves heat transfer and ultrasound improves mass transfer, the combination of both methods can be immensely beneficial for the biodiesel production process. However, the research in this area is still in its infant stage (Gude et al., 2013). As they are of different nature, each must be fine-tuned by its specific parameters to avoid possible hazards after combination (Cravotto & Cintas, 2007). Nevertheless, such combination is possible and safe. Martinez-Guerra and Gude (2014a) conducted a study on the transesterification of waste vegetable oil with sodium hydroxide under three different power configurations: microwave, ultrasound and simultaneous microwave-ultrasound irradiations. The reactor is shown in Figure 2.7.

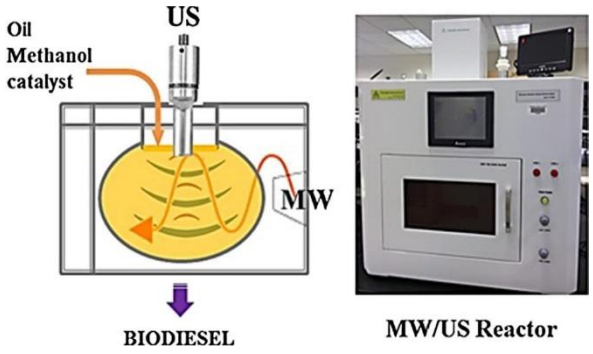

Figure 2.7 Schematic of the microwave/ultrasound unit [Reprinted permission obtained as shown in Appendix C, Martinez-Guerra and Gude (2014a)]

The biodiesel yield obtained using the simultaneous microwave-ultrasound irradiations is higher (97.6%) compared to individual microwave (87.1%) or ultrasound (89.8%)

irradiation. They discover that the optimum process conditions for the experiment are 6:1 methanol/oil molar ratio, 0.75 wt.% NaOH catalyst, 2 minutes of reaction time at a combined power output rate of 200W (100/100 microwave/ultrasound). Using the same parametric condition but with different catalyst (barium oxide), Martinez-Guerra and Gude (2014b) reported that simultaneous microwave-ultrasound irradiations also gives higher yield (~93.5%) when compared to individual microwave (91%) and ultrasound (83.5%) irradiations. Therefore, it is certain that simultaneous microwave-ultrasound irradiations result in a synergistic effect that significantly enhances reaction rate by eliminating mass and heat transfer related limitations, regardless of the type of catalyst used. Higher yields are observed under the combined irradiations as compared to the individual microwave and ultrasound irradiation approaches.

In addition, Ma et al. (2015) directly transesterified Chlorella vulgaris microalgae in a coupled microwave-ultrasound apparatus as shown in Figure 2.8 in the presence of a heterogeneous base catalyst. The ultrasound frequency is set at 40kHz and the microwave irradiation is temperature-regulated. A biodiesel yield of 93.07% is obtained under the optimum conditions of 12 wt.% catalyst, 8:1 methanol-to-oil molar ratio, 60 °C, 45 min). The yield performance of algal biodiesel is reported to be better than the individual use of ultrasound (63.49%) or microwave (58.12%) irradiation.

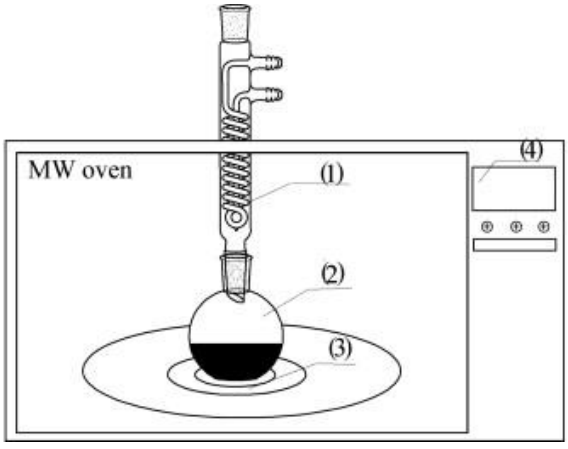

Figure 2.8 Schematic of ultrasound-microwave synergistic extraction apparatus: (1) reflux condenser; (2) reaction flask; (3) ultrasound contactor; (4) control panel [Reprinted permission obtained as shown in Appendix C, Ma et al. (2015)]

Ardebili et al. (2015) also conducted an investigation on the effect of simultaneous microwave-ultrasound irradiations on CPO transesterification. The microwave irradiation is generated at 900W power and the ultrasound irradiation is 25 kHz with 100W power. Instead of the power level, they study the irradiation time for both microwave and ultrasound. Using response surface analysis, the optimum parameters for a 97.53% yield are found to be 7:3.1 methanol/oil molar ratio at 58.4 °C with 1.09% KOH catalyst concentration, subjected to only 2 minutes of microwave and ultrasound irradiations. This performance is significant as compared to the conventional method which requires about 1 hour.

Apart from the combined setup where microwave and ultrasound are placed in a single reactor, researchers also tested another configuration, which is the sequential approach. The reaction mixture is first irradiated in a microwave reactor and moved to an ultrasound reactor or vice versa. Gole and Gogate (2013) pre-treats high FFA Nagchampa oil using sequential microwave-ultrasound technique and compare the yield with that of using individual microwave or ultrasound approach. The results reveal that the optimum molar ratio required for esterification is reduced from 3:1 (microwave) or 4:1 (ultrasound) for individual approaches, to 2:1 in sequential approach, which is more economical. The equipment they used is a modified domestic microwave oven reactor with 108W output power (160W rated power) and a 20 kHz ultrasonic horn that is rated at 120W but only dissipates 39W in exact. Although they have provided more details on the power specifications, their scope of study only limited to molar ratio and catalyst concentration for the pre-treatment of Nagchampa oil. They have not evaluated the effects of the power output and microwave irradiation time on the chemical reaction.

Ardebili et al. (2014) also conducted an experimental study on castor oil transesterification using sequential approach. Their results show that the optimized microwave and ultrasound power are 350 W and 80W respectively, at 2 min and 4 min irradiation time to achieve 94.78% FAME conversion. Furthermore, Hsiao et al. (2010) also employ sequential ultrasound and microwave irradiation method for the base-catalyzed transesterification of soybean oil. An optimum yield of 97.7% is reported at 1:6

oil-to-methanol ratio, 1 wt.% of catalyst, 1 min ultrasonic mixing, 2 min microwave irradiation, and a reaction temperature of 60 °C. The method is found to be quite successful due to the relatively lower energy requirements and operation temperature, as well as elimination of mechanical stirring and cooling systems.

Looking at the experimental data obtained by the researchers, it is reasonable to deduce that simultaneous microwave-ultrasound irradiation do provide greater improvement to the reaction rate compare to the individual approaches, regardless of the configuration (combined setup/sequential approach) used. They give similar effects towards biodiesel production by reducing the reaction time required to less than 5 minutes. Nonetheless, the application of simultaneous microwave-ultrasound irradiation is still relatively new in the research field of biodiesel industry due to concerns such as cost issues (capital and operational costs) and designs of reactors. It is reported that the capital cost for sequential approach of microwave-ultrasound coupling is about 17.8% higher in comparison to conventional method but considerable savings could be achieved with methanol requirements (34%), utility (2%) as well as processing times (Gole & Gogate, 2013). Certain aspects such as the properties of the reaction contents, microwave and ultrasound frequencies have to be taken into considerations as well for the designs of the reactors (Gude, 2015).

Interestingly, there are no studies which investigate the biodiesel synthesis by coupling microwave heating with hydrodynamic cavitation despite its advantages over ultrasound irradiation. On the other hand, there have been some studies on the integration of microwave heating with supercritical heating. For instance, Patil P. et al. carried out the direct conversion of both dry and wet algal biomass into biodiesel with a non-catalytic transesterification method under microwave-mediated supercritical ethanol conditions (Patil, Reddy, Muppaneni, Ponnusamy, et al., 2013; Patil, Reddy, Muppaneni, Schaub, et al., 2013). Conducting microwave heating under supercritical condition is inefficient by nature as dielectric constant of fluid decreases with increasing temperature at a constant pressure (Tan et al., 2009). In other words, the advantage of using microwave dielectric heating will diminish. To improve the heating rate, passive heating elements such as

silicon carbide has been added into the reaction medium (Patil, Reddy, Muppaneni, Ponnusamy, et al., 2013). However, the maximum yield reported in both studies are only about 31%. Although increasing the reaction pressure can increase the dielectric constant of fluid, the degree of increment is comparatively lower than increasing the temperature as observed from the dielectric constant values reported by Franck and Deul (1978) at various pressures. Hence, to make full use of the microwave heating technology, the reaction conditions should be mild.

2.5.4 Selection of production method to be studied

Several process intensification technologies for biodiesel production have been discussed in this subchapter. In spite of the numerous advantages, the high operational and equipment costs to produce biodiesel under non-catalytic supercritical conditions are inevitable obstacles that hindered the development of the technology (Nomanbhay & Ong, 2017). A general comparison between the heating methods that are generally used or studied (conventional heating, supercritical heating, microwave heating) are shown in Table 2.8.

Table 2.8 Comparison between three types of heating methods for biodiesel production [adapted from (Nomanbhay & Ong, 2017)]

Characteristic/ Parameter	**Conventional heating**	**Supercritical heating**	**Microwave heating**
Reaction time	1–2 h (long)	< 1 h (short)	0.05–1 h (very short)
Temperature	40–100 °C	250–400°C	40–100°C
Pressure	Atmospheric	35–60 MPa	Atmospheric*
Catalyst required	Yes	No	Yes/No
Heat losses	High	Moderate	Low
Process efficiency	Low	Moderate	High
Catalyst & soap removal	Yes	No	Yes

Characteristic/ Parameter	Conventional heating	Supercritical heating	Microwave heating
Advantages	Simple to operate	Short reaction time, easy product separation	Rapid heating rate, cleaner products, energy efficient
Disadvantages	High energy requirement, saponified products, inefficient heating	High capital costs, pressure vessel safety issue, energy intensive	May be inefficient with feedstock containing solids, non-uniform heating

*Reactions at higher temperature and pressure without catalysts are possible

At mild reaction condition, microwave heating is the most suitable green technology to enhance heat transfer of biodiesel production. Meanwhile, ultrasonication and hydrodynamic cavitation are great for improving mass transfer. Chipurici et al. (2019) studied and compared the effects of ultrasonic, hydrodynamic cavitation and microwave irradiation on the base-catalyzed transesterification of sunflower oil. To achieve a 96.5% ester conversion, it is found that the ultrasound system is the most energy efficient (<220 J/ml), followed by the microwave reactor (660 J/ml). As opposed to the usual findings, the hydrodynamic cavitation system tested performs the worst among the three methods and could not achieve the required yield.

In contrast, Maddikeri et al. (2014) reported that higher yield is obtained using the hydrodynamic cavitation-based approach as compared to the ultrasound-based approach. Nonetheless, Chipurici et al. (2019) specified that the data may not be used directly to predict energy requirements for larger scale installations. A closer look on the parametric condition used for the microwave reactor also rises another concern as a mono-mode microwave reactor is used. Thus, the result is not comparable with multi-mode microwave oven. Furthermore, in order to compare with the ultrasound systems, the reaction temperature is kept at a low temperature (40 °C) which is not the best setting for efficient microwave irradiation. Contrary to their findings, Martinez-Guerra and Gude (2014b)

reported that the biodiesel yield for microwave irradiation (91 wt.%) is better than ultrasound cavitation (83.5 wt.%) under the optimal conditions. On the other hand, Chuah et al. (2017) reckon the use of hydrodynamic cavitation for biodiesel production in terms of yield efficiency, followed by microwave, ultrasound, and lastly mechanical stirring. Hence, it is a little hard to justify which process intensification technology is the best. The respective studies related to the several process intensification technologies are summarised in Table 2.9.

The advantages and limitations of the respective technologies that have been discussed in subchapter 2.5 are listed in Table 2.10. To get the most benefits in heat and mass transfer enhancement, it is undeniable that the integration of two process intensification technologies (e.g. microwave and ultrasound) can substantially optimize the heat and mass transfer of biodiesel production in the future. However, in order to gain a better insights of the synergistic effect of the simultaneous microwave and ultrasound approach, it is important to understand the underlying physics of the individual technologies first. The numerical studies regarding the microwave heating of biodiesel production are still in an early stage. Thus, in this work the focus would be on microwave heating. The numerical modelling related to microwave heating will be discussed in the subchapter 2.7.

Table 2.9 Literature studied for several process intensification technologies in biodiesel production

Technology	Feedstock	Tested parameter[a]	Optimal Value	Yield	Findings/Comments	References
Supercritical methanol	Purified palm oil	Temperature Time Methanol/oil ratio	372 °C 16 min 40	81.5%	Biodiesel yield is highly dependent on reaction temperature.	(Tan et al., 2010)
Supercritical methanol	Purified palm oil	Temperature Time Methanol/oil ratio	360 °C 20 min 30	72%	Reaction time reduced but require higher methanol-to-oil molar ratio and reaction temperature.	(Tan et al., 2009)
Supercritical methanol	Jatropha oil	Temperature Time Methanol/oil ratio	358 °C 27 min 44	89.4%	Higher yield can be obtained using supercritical methanol compare to supercritical methyl acetate.	(Niza et al., 2011)
Supercritical methanol + co-solvent CO_2	Soybean oil	Temperature Time Methanol/oil ratio CO2/methanol ratio	280 °C 10 min 24 0.1	98%	Addition of CO_2 co-solvent reduce the operating temperature, pressure & molar ratio of methanol-to-oil molar ratio of supercritical method.	(Han et al., 2005)
Supercritical methanol + co-solvent CO_2 & acetic acid	Soybean oil	Temperature Time Methanol/oil ratio Acetic acid/oil ratio	280 °C 90 min 60 3	97.83%	Addition of co-solvent (acetic acid) reduce glycerol by-product by 30% in comparison with supercritical methanol method.	(Wei et al., 2013)
Supercritical methyl acetate	Jatropha oil	Temperature Time Methyl acetate/oil ratio	400 °C 32 min 50	71.9%	The parametric condition is less favourable compare to supercritical methanol but the glycerol by-product can be utilised as an	(Niza et al., 2011)

Technology	Feedstock	Tested parameter[a]	Optimal Value	Yield	Findings/Comments	References
					additive for biodiesel and no glycerol separation is required.	
Ultrasonic bath	Neat vegetable oil (25 °C)*	Time Methanol/oil ratio Ultrasound frequency	20 min 6 40 kHz (400W)	98%	Ultrasonic irradiation reduce reaction time from 60 min (mechanical stirring) to 20 min and improve 18% yield.	(Stavarache et al., 2003)
Ultrasonic horn	RPO, CPO (45 °C)*	Time Methanol/oil ratio Ultrasound amplitude	30 min 9 60% (20 kHz, 700W) pulsed	98.18%, 97.04%	Increasing ultrasound amplitude increase the size of cavitation bubbles that collapse to induce stable emulsions. However, larger bubbles formed at high ultrasound amplitude (> 60%) which inhibits the transmission of acoustic energy through the liquid phase.	(Ho et al., 2015)
Ultrasonic horn	Jatropha oil	Time Methanol/oil ratio Ultrasound amplitude	15 min 9 50% (24 kHz, 200W) pulsed	98.53%	Ultrasound reduces the reaction time from the 3–6 h (conventional) to 15 min and reduce catalyst loading with improved chemical activity.	(Kumar et al., 2010)
Ultrasonic horn	RBD palm oil	Time Methanol/oil ratio	20 min 7.5	>90%	The performance of ultrasound-assisted transesterification decrease when lower quality feedstock is	(Stavarache et al., 2007)

Technology	Feedstock	Tested parameter[a]	Optimal Value	Yield	Findings/Comments	References
	(45 kHz, 600W)*				used. The reaction under ultrasound irradiation is mainly influenced by reaction time and alcohol-to-oil molar ratio.	
Ultrasonic bath	PFAD (22 KHz, 120W)*	Temperature Time Methanol/oil ratio	40 °C 150 min 7	>90%	Reaction time required for PFAD esterification under ultrasound irradiation is relatively longer than transesterification of refined oil.	(Deshmane et al., 2008)
Ultrasonic bath	Nagchampa oil (20 kHz, 120W)*	Temperature Time Methanol/oil ratio	40 °C 40 min 6	92.5%	The reaction time is reduced from 90 min (conventional) to 40 min with cavitation.	(Gole & Gogate, 2013)
Hydrodynamic cavitation	Nagchampa oil	Time Methanol/oil ratio	20 min 6	92.1%	The reaction time is 50% shorter than using ultrasonic bath.	(Gole et al., 2013)
Hydrodynamic cavitation	Thumba oil	Time	30 min	80%	The energy consumption is reduced by >50% when compared to conventional mixing.	(Pal et al., 2010)
Microwave (temp-controlled)	Safflower seed oil (300W, 60 °C)*	Time Methanol/oil ratio	6 min 10	98.4%	Microwave heating has reduced reaction time from 120 min (conventional) to 6 min.	(Duz et al., 2011)

Technology	Feedstock	Tested parameter[a]	Optimal Value	Yield	Findings/Comments	References
Microwave (temp-controlled)	Jatropha oil (65 °C)*	Time Methanol/oil ratio	2 min 7.5	97.4%	Reduce reaction time from 60 min (conventional) to 2 min.	(El Sherbiny et al., 2010)
Microwave (power-controlled)	Waste cooking oil (800W)*	Time Methanol/oil ratio	6 min 9	92%	Microwave heating reduce >90% energy to achieve the same yield as conventional method.	(Patil et al., 2012)
Microwave (power-controlled)	*Camelina Sativa* oil (800W)*	Time Methanol/oil ratio	1 min 9	98%	Microwave heating consumes <10% of energy to achieve the same yield as conventional method.	(Patil et al., 2010)
Microwave (temp-controlled)	PFAD (70 °C)*	Time Methanol/oil ratio	15 min 12	96%	Regardless of the feedstock quality, microwave enhances the reaction rate. Reaction time is reduced from 120 min (conventional) to 15 min.	(Lokman, Rashid, & Taufiq-Yap, 2015)
Microwave (temp-controlled)	PFAD	Temperature Time Methanol/oil ratio	55 °C 15 min 9	99%	Reaction temperature did not significantly affect the rate of microwave-assisted esterification. Reaction time is substantially reduced to achieve the same yield as conventional method.	(Lokman et al., 2014)

Technology	Feedstock	Tested parameter[a]	Optimal Value	Yield	Findings/Comments	References
Microwave	Waste cotton-seed cooking oil (180 W, 50 °C)*	Time Methanol/oil ratio	9.6 min 7	96.44%	Scale-up study reveals that the reaction time required increased (10 min → 20 min) when the reaction volume increased (50ml → 500ml). Increase microwave power input (180W → 450W) can compensate the time required for larger volume size.	(Sharma et al., 2019)
Microwave (power-controlled) + ultrasonic horn	Waste vegetable oil	Time Methanol/oil ratio Microwave power Ultrasound power	2 min 6 100W 100W	97.6%	Yield improved by 7.8 – 10.5% compare to individual microwave and ultrasound irradiations. Microwave is efficient at lower power output and at short reaction times whereas ultrasound improves yield at prolonged reaction times.	(Martinez-Guerra & Gude, 2014a)
Microwave (power-controlled) + ultrasonic horn	Waste vegetable oil	Time Methanol/oil ratio Microwave power Ultrasound power	2 min 6 100W 100W	93.5%	Yield for simultaneous microwave and ultrasound irradiation is higher than using microwave (91%) or ultrasound (83.5%) individually. The lower yield for ultrasound could be attribute to its inability to raise the reaction temperature.	(Martinez-Guerra & Gude, 2014b)
Microwave (temp-	Palm oil	Temperature Time	58.4 °C ~2.2 min	97.53%	Reaction time is reduced from 1 hour (conventional) to 2.2 min.	(Ardebili et al., 2015)

Technology	Feedstock	Tested parameter[a]	Optimal Value	Yield	Findings/Comments	References
controlled) + ultrasonic horn		Methanol/oil ratio	7.3			
Microwave (temp-controlled) + ultrasonic horn	Soybean oil	Temperature Methanol/oil ratio Microwave time Ultrasound time	60 °C 6 2 min 1 min	97.7%	Study used closed microwave irradiation instead of open microwave irradiation. Pressure build up might occur.	(Hsiao et al., 2010)
Microwave (temp-controlled) + ultrasonic bath	Microalgae (60 °C)*	Time Methanol/oil ratio	45 min 8	93.07%	The yield of micro algal biodiesel is substantially increased in comparison to ultrasound (63.49%) and microwave (58.12%) irradiation.	(Ma et al., 2015)
Supercritical ethanol + microwave (ramp, power-controlled)	Dry algal biomass	Time Ethanol/oil ratio	20 min 12	~30%	Yield is comparatively lower than using other intensification technologies.	(Patil, Reddy, Muppaneni, Ponnusamy, et al., 2013)
Supercritical ethanol + microwave (ramp, power-controlled)	Wet algal biomass	Time Ethanol/oil ratio	25 min 9	~31%	Yield is comparatively lower than using other intensification technologies.	(Patil, Reddy, Muppaneni, Schaub, et al., 2013)

* Fixed parameters; [a] Parameter related to catalyst type & concentration is not included.

Table 2.10 Advantages and disadvantages of several process intensification technologies

Technology	Advantages	Disadvantages
Supercritical methanol	- Suitable for high FFA and water content feedstock - Non-catalytic, no saponification - Easy separation step - Increase solubility of oil in methanol	- Expensive, higher energy input - Higher pressure and temperature - Over-production of glycerol by-product - Risk of thermal degradation
Supercritical methanol + co-solvent	- Generally lower temperature and pressure than supercritical methanol method - Generation of useful by-products - Reduced methanol-to-oil molar ratio	- High pressure and temperature - Products separation step is still required - Risk of thermal degradation - Expensive, high energy input
Ultrasonic bath	- Low cost and easy to acquire - Reduce energy cost - Reduce reaction time - Improve mass transfer	- Distribute dispersed and non-homogeneous acoustic intensity - Mechanical agitation is usually required
Ultrasonic horn	- High power output capability (concentrate energy distribution) - Reduce energy cost - Reduce reaction time - Improve mass transfer	- Horn tip easily corrodes - Distribute acoustic intensity in a concentrated and non-homogeneous manner
Hydrodynamic cavitation	- More energy efficient than ultrasound - Easier to scale up - Less erosion problems - Improve mass transfer	- Substantial energy loss in fluid pumping process - Pressure drop may lead to choked flow which reduce yield
Microwave	- Rapid heating rate - Energy efficient - Reduce reaction time - Improve heat transfer - Cleaner products	- Non-uniform heating - Hard to scale up (batch)

Technology	Advantages	Disadvantages
Microwave + supercritical ethanol	- Reduce energy cost - Eco-friendly technology - Improve heat transfer	- Low yield - Risk of thermal degraded products - High pressure and temperature
Microwave + ultrasound	- Improve heat and mass transfer - Higher yield due to synergistic effect between microwave and ultrasound - More energy efficient than using only microwave or ultrasound	- Scale up issue (e.g. microwave) - More complicated setup - Higher capital cost

2.6 Reaction kinetics of biodiesel production

The rate of a chemical reaction can be modelled based on Arrhenius equation:

$$k_r = Ae^{\frac{-E_a}{R_U T}} \tag{2.3}$$

where k_r is reaction rate constant, A is frequency factor, E_a is activation energy, R_U is universal gas constant (8.314 J K^{-1} mol^{-1}), and T is the absolute temperature (K). The reaction rate constant is temperature dependent. According to Gude et al. (2013), there are two possible ways to increase the reaction rate. First, increase the frequency factor which is the molecular mobility that depends on the vibrating frequency of molecules at the reaction interface. This is made possible with the microwave effects of dipolar polarization and ionic conduction mechanisms. Second, decrease the activation energy which is given in terms of enthalpy and entropy ($E_a = \Delta H - T\Delta S$). In microwave-assisted reactions, the quick and random dipolar movement and molecular level microwave interactions result in higher entropy generation, which increases the value of the second term in Equation (2.3).

For a pseudo 1st order reaction, k_r can be determined experimentally using Equation (2.4) as follows:

$$\ln\left(\frac{[\mathrm{FA}]}{[\mathrm{FA}]_0}\right) = \ln(1 - X) = -k_r t \tag{2.4}$$

where [FA] is the concentration of FA, $[\mathrm{FA}]_0$ is the initial concentration of FA at $t = 0$, and X is the conversion of FA at any time t. Plot of $-\ln(1 - X)$ against t gives k_r as the slope (Parkar et al., 2012).

The reaction kinetics for the conversion of oil feedstock into biodiesel have been investigated by numerous researchers. Most of the reaction kinetics were reported to be of the first order, especially for transesterification (Talebian-Kiakalaieh et al., 2013), while some reactions were reported to be of the second order. Lieu et al. (2016) reported that the microwave-assisted esterification of FFA derived from *Ceiba pentandra* seed oil followed the second-order reaction kinetics. Mazubert et al. (2014) reported that under second-order reaction order, the activation energy and frequency factor for the esterification of 39% FFA waste cooking oil in the microwave-heated reactor is 45.4 kJ/mol and 7.0×10^7 L/mol/min, which is lower when compared with the values for conventionally-heated reactor at 56.1 kJ/mol and 4.2×10^9 L/mol/min respectively.

Nonetheless, this does not necessarily suggest that all esterification reactions would be of the second order. Mohammad Fauzi et al. (2014), who investigated the esterification of oleic acid in the presence of magnetic ionic liquid, reported that the reaction followed a pseudo-first order reaction kinetics. Zhang et al. (2018) also reported the same reaction kinetics in their experimental study on the esterification of oleic acid. Meanwhile, Ye et al. (2016) investigated the transesterification of palm oil using calcium oxide catalyst. Their results reported that by using microwave heating, the overall reaction order of the process increased from one (conventional heating) to three.

Similarly, the reaction kinetics of PFAD esterification were also investigated under different operating conditions. Aranda et al. (2008) reported that the esterification of PFAD followed first order kinetics. Chabukswar et al. (2013) investigated the kinetics of PFAD esterification with several acid catalysts including sulphuric acid using the conventional heating and stirring method. They assumed first-order reaction kinetics for

the process and reported that the E_A and A for esterification of PFAD with H_2SO_4 catalyst were 30.1 kJ/mol and $1.2x10^4$ $(m^3/kmol)^2$ /min, respectively. Saimon et al. (2020) reported that the PFAD esterification under conventional method followed first-order reaction kinetics with E_A = 28.8 kJ/mol and A = 8.124×10^5 min^{-1}. However, some researchers reported that the esterification rate of PFAD might be of the second order. For instance, Metre and Nath (2015) conducted PFAD esterification experiments, catalyzed with super phosphoric acid, by using the conventional heating and stirring method. Their results showed that a second-order kinetic model can better describe the experimental data than a pseudo-first-order model. Meanwhile, Hong et al. (2012) studied the reaction kinetics of PFAD esterification at high temperature (230–290°C) and moderate pressure (0.81 MPa). They initially assumed that each component in the system operates under first-order reaction kinetics but their results showed that the assumption of PFAD esterification reaction rate based on the first-order reaction kinetics could not provide sufficient accuracy. Instead, they derived their own equations from the mass balance of the reactants, by taking into account the effects of evaporation of methanol and water, to better model the reaction kinetics. Therefore, it is reasonable to deduce that the esterification of PFAD under microwave irradiation might operate under different reaction order kinetics, which is worth investigating.

2.7 Numerical modelling of microwave heating

Numerical modelling helps to provide further understanding of the underlying physics behind microwave irradiations towards biodiesel production. Although there are countless experimental approaches in literature that studied microwave-assisted biodiesel production, there is a lack of a detailed and multi-physics-based modelling approach to investigate and analyse the behaviour of such process.

Salvi et al. (2011) stated that the modelling of microwave heating is governed by Maxwell's equations as follows:

$$\nabla \times \left(\frac{1}{\mu'} \nabla \times \mathbf{E} \right) - \frac{\omega^2}{c} \left(\varepsilon_r' - j\varepsilon_r'' \right) \mathbf{E} = 0 \tag{2.5}$$

where μ' is relative permeability of a material, $\vec{\mathbf{E}}$ is electric field intensity inside the MW cavity (V/m), ω is angular frequency ($= 2\pi f$) of the microwave operating frequency (f =2.45 GHz), c is the speed of light in free space (3×10^8 m/s), ε_r' is the dielectric constant of a material, and ε_r'' is the relative dielectric loss of a material. Dielectric constant measures the ability of a material to store electrical energy whereas dielectric loss indicates the ability of a material to dissipate the electrical energy as heat energy to heat up the dielectric material. It should be noted that the dielectric constant depends strongly on temperature.

After obtaining the electric field intensity from Equation (2.5) and the material properties, the volumetric power $\dot{Q}_{MW}$ dissipated from the electric component of microwaves can be determined as follows (Salvi et al., 2011):

$$\dot{Q}_{MW} = 2\pi f \varepsilon_0 \varepsilon_r'' \left| \vec{\mathbf{E}} \right|^2 \tag{2.6}$$

where ε_0 is the free space permittivity (8.854×10^{-12} F/m).

Loss tangent, $\tan \delta$ is the ratio of loss factor to dielectric constant. It determines the attenuation of microwave power in material which resulted in heating. A high loss tangent indicates a high susceptibility to microwave energy (Navarro et al., 2019).

$$\tan \delta = \frac{\varepsilon_r''}{\varepsilon_r'} \tag{2.7}$$

The penetration depth, D_p (m) is the distance at which the microwave power drops to e^{-1} from its value at the surface of the dielectric material. It is expressed as (Mehdizadeh, 2015):

$$D_p = \frac{c}{\pi f \sqrt{2\varepsilon_r' \left(\sqrt{1 + \tan^2 \delta} - 1 \right)}} \tag{2.8}$$

Small penetration depth of microwave in the reaction mixture is a major hindrance to the scale-up and commercialization of microwave in biodiesel production. For example, at 2.45 GHz, the penetration depth of microwave in methanol is only 0.76 cm at 20 °C. However, as temperature increases, the penetration depth rises to 1.4 cm at 60 °C (Mazubert et al., 2014).

There are many studies on the numerical studies of microwave heating but most of them are done on solid samples that are relevant to the food industry (Campañone & Zaritzky, 2010). There have been a few studies that numerically modelled the microwave heating of liquids. The modelling is more complex as there is a coupling of electromagnetism with fluid flow and convective heat transfer for liquid samples. For instance, Sabliov et al. (2007) developed a model using ANSYS Multiphysics. The model couples a high frequency electromagnetic wave, heat transfer, and fluid flow to simulate the microwave heating of water, without any chemical reaction involved. A similar investigation is also conducted by Yeong et al. (2017). In addition, Lee et al. (2020) modelled the heating and boiling phenomena of water under microwave irradiation using OpenFOAM. As the heating time increases, the temperature in the sample becomes non-uniform rapidly, but with a decreasing rate due to the intensification of natural convection. During the initial phase of the boiling process, no vapour bubble is formed in the water sample and the water can be deduced as superheated. The nucleation of vapour bubbles at a later stage removes most of the superheat in the water and prevent its accumulation mainly by enhancing heat transfer to the liquid free surface. It is found that the free surface evaporation dominates about 90% of the overall evaporation process during the boiling stage.

Ratanadecho et al. (2002) studied both numerically and experimentally the microwave heating for liquid layers using a self-built microwave reactor with rectangular wave guide. They developed a mathematical model using two-dimensional heat and momentum equations to describe the unsteady temperature and fluid flow fields. Their results revealed that the liquid heating strongly depends on the dielectric properties of the components. This is also in agreement with the study conducted by Navarrete et al. (2012)

which implied that measurement of dielectric properties is essential for the development of an accurate numerical model. Traditionally, most of the previous studies on the microwave heating of a reaction solution assumed the dielectric properties to be a constant or a simple function of the volume fractions of the components (Nakamura et al., 2005). However, the calculated temperature distributions might be quite different from the measured results. For instance, Wu et al. (2013) described the dielectric properties of the reaction solution using a bivariate function, which depends on the liquid temperature and species concentration. They studied the microwave-assisted esterification of biodiesel numerically by using Maxwell's equations, Fourier's law and the chemical reaction kinetics equation. The chemical reaction was described by the rate change of water concentration using second-order kinetics. They reported that by using the new method to determine the dielectric properties, their simulated temperature profile under 18 s of microwave irradiation showed better agreement with the experimental results compared to the traditional method. Nevertheless, the temperature validation was too short (only 18 s) and there was no validation for the biodiesel production.

Navarrete et al. (2012) developed a three-dimensional model using the COMSOL Multiphysics software to predict the evaporation phenomena of water from the treated material (*Lavandin super*) under microwave heating. The treated material was modelled as a lumped porous media. The microwave distribution was calculated by using Maxwell's equation and the heat transfer of the treated material was modelled by using the Fourier's law. A heat source term was added to the heat conduction equation to accommodate the heat source provided by the microwave. Only the rate of change of water (due to evaporation) in the time domain was calculated, and the spatial effect of water evaporation was ignored. In addition, the model also assumed that the evaporation of water would consume all the heat generated from the microwave. Their results suggested that apart from the heat source, the heat loss from the reactor to the surrounding should also be taken into consideration to predict the temperature profile more accurately.

In contrast, Salvi et al. (2011) who developed a numerical model to simulate the temperature profiles of fluids using the COMSOL Multiphysics software used a slightly

different approach. In their study, Newtonian and non-Newtonian liquids were numerically modelled for a continuous flow microwave reactor. The single phase Navier-Stokes equations were used to model the system and a convection term was included in the Fourier's energy balance equation. An apparent specific heat method was employed to incorporate the phase change phenomenon that occurred at the boiling point of the liquid. No heat loss calculations were included. It was reported that although the average temperature values they obtained through the numerical model were generally lower than that obtained through experiments, the values for both were in a fairly good agreement.

On the other hand, Navarro et al. (2019) studied the radial microwave heating of liquid samples (water and ethanol) in a cylindrical vessel both numerically and experimentally at 2.45 GHz frequency. Their numerical model was based on spectral methods and solved for the Maxwell's equations, coupled with heat and momentum equations. They first solved the Maxwell's equations to determine the resulting electric field and used it as a source term in the heat transfer equations, which was then coupled with the fluid flow equations. The dielectric properties of the liquid samples were temperature dependent where the values were predicted using the empirical equations provided by Liao et al. (2001).

To date, there is only one literature study which investigated the modelling of microwave-assisted esterification for biodiesel production. Ye et al. (2019) developed a model to describe the biodiesel synthesis in a continuous flow microwave-assisted screw propeller system as shown in Figure 2.9. Maxwell's equations, Navier-Stokes equation, heat energy, and chemical reaction kinetics equations are intercoupled for the multiphysics calculation of the microwave-assisted esterification reaction of oleic acid. In their model, the stirring process of the rotating screw propeller system was computed by employing a step-by-step algorithm based on implicit functions, level set methods and Arbitrary Lagrangian-Eulerian machinery. They focused on analysing the effects of rotation speed, material composition, pitch and blade widths of the screw propeller as well as inlet velocities towards the temperature distribution in the reactor. The change in temperature at the outlet

of the reactor is modelled from room temperature up to 45 °C during the 250 s reaction time of oleic acid esterification.

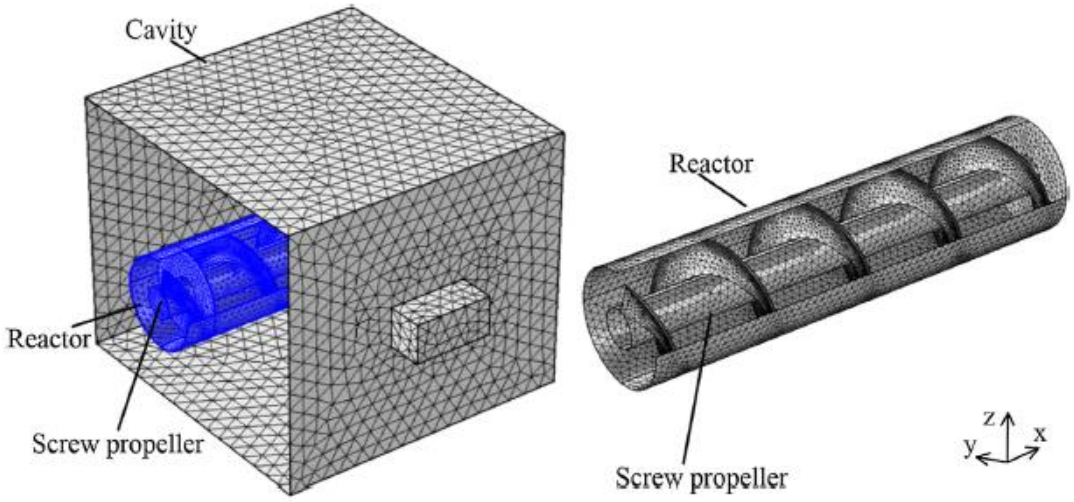

Figure 2.9 General geometry of the microwave reactor with screw propeller model [Reprinted permission obtained as shown in Appendix C, Ye et al. (2019)]

2.8 Biodiesel standards

Biodiesel is a renewable alternative fuel for diesel engines as it is produced from plant oils or animal fats, which meets the specifications of American Standard Specification for Biodiesel (ASTM D-6751). Although ASTM D-6751 provides the original specifications for 100% pure biodiesel (B100), there are other objective fuel standards and specifications for biodiesel fuel blends. For instance, ASTM D975-19a for biodiesel blends up to 5% (B5) for on- and off-road diesel vehicles; ASTM D7467-19 for biodiesel fuel blends from 6 to 20% (B6-B20); and ASTM D396-19 for residential heating and boiler applications (Lee & Shah, 2012). Apart from the ASTM D-6751 standard, another major biodiesel standard that have been followed worldwide is the European Standard for Biodiesel (EN 14214). Motasemi and Ani (2012) has listed down the biodiesel specification parameter limits regulated by ASTM 6751-02 and EN 14214 standards for pure biodiesel fuel. There was no clear specification on the cloud point requirement of biodiesel. It depends very much on the country specification or clients' needs. A search in the Europe EN 14214

standard document shows that CFPP for biodiesel used in temperate climates could be categorized into six grades, where the maximum CFPP is reduced in 5 °C interval from grade A to F, as shown in Table 2.11. For instance, the CFPP for summer biodiesel in Europe is required to be grade C (max. -5 °C) while winter biodiesel should have a grade E CFPP (max. -15 °C). An even stricter grading requirement is enforced for FAME fuels used in Arctic climates where the maximum CFPP must be below -20 °C at grade A.

Table 2.11 CFPP grades for temperate climates (British Standards Institution, 2014)

Property	Unit	Grade					
		A	B	C	D	E	F
CFPP	°C, max	+5	0	-5	-10	-15	-20

2.9 Cold flow behaviour of biodiesel

The cold flow properties of biodiesels can be specified by three temperature measures: cloud point, cold filter plugging point, and pour point.

2.9.1 The cold flow properties

Cloud point (CP) is the highest temperature at which visible crystals formed and a cloudy suspension is visually observed in the fuel; cold filter plugging point (CFPP) is the lowest temperature where 20mL of fuel can safely pass through a filter within a minute, whereas pour point (PP) is the lowest temperature when the fuel can still flow as it becomes gel-like (Dunn & Moser, 2010). Although PP and CP have been widely used to estimate the behaviour of diesel fuels at cold temperature, they cannot predict the performance of diesel fuel in the diesel engine accurately. CFPP is therefore introduced since fuel filter plugging usually occurs after reaching CP and before reaching PP (Edith et al., 2012).

The palm oil biodiesel produced in Malaysia suffers from poor cold flow properties due to its high percentage of saturated palmitic acid methyl ester (C16:0) or methyl palmitate, which can be up to 48%. For instance, Serrano et al. (2014) observed that the CFPP for

palm oil biodiesel was 13 °C while the CFPP of rapeseed oil biodiesel is much lower at −14 °C. Palm oil biodiesel has a CP of 15-18°C, CFPP of 12-16°C and PP of 12-13°C (Dunn & Moser, 2010; Edith et al., 2012; Lv et al., 2013). This clearly implies that palm oil biodiesel is only fitted to be used in tropical countries without causing any operability issues. At temperature beyond CFPP, the biodiesel would solidify and therefore, clogging the fuel filter and restricting fuel flow to the vehicle engine. This would drastically affect the engine performance and cause engine start-up problems in temperate countries.

To optimize the cold flow properties of biodiesel, the desirable attributes of its esters are short, unsaturated and branched carbon chains. However, these would result in poor ignition quality and oxidation stability of the fuel. Thus, the cold flow properties of biodiesel should be improved while taking good oxidation stability and sufficient ignition quality into considerations. Ignition quality which measures the relative ease for the fuel to ignite in an internal combustion engine could be determined by their cetane number. A high cetane number indicates a good ignition quality. Biodiesel typically exhibits better ignition quality than petroleum diesel due to the presence of greater quantities of straight hydrocarbon chains in the esters (Edith et al., 2012). However, the oxidation stability of biodiesel is worse than petroleum diesel. In the presence of oxygen in the ambient air, biodiesel quality will deteriorate during long term storage.

The cold flow behaviour of biodiesel is affected by two factors:

(1) the fatty acid composition of its parent oil, and
(2) the presence of minor components such as monoglycerides and steryl glycosides.

The effect of the minor components on the cold flow of biodiesel was discussed in detail by Dunn (2009). Usually, researchers study on ways to improve the cold flow behaviour of biodiesel fuels via former approach, by affecting the fatty acid composition of the esters.

There are three types of fatty acids which can be found in any oil or fat: saturated, mono-unsaturated, and poly-unsaturated fatty acids. Saturated fatty acids have zero double bond in their carbon chain while mono-unsaturated fatty acids have only one double bond in their carbon chain. As for poly-unsaturated fatty acids, there are either two or three double

bonds in their carbon chain. Studies show that unsaturated fatty acids improve esters cold flow, while saturated fatty acids increase cetane number, oxidation stability and lubricity of the esters. Varying composition of these three types of fatty acids in various feedstocks would result in different cold flow properties. Biodiesel with high amount of saturated fatty acids esters that crystallize at high temperature would exhibits worse cold flow and has higher cloud points (Edith et al., 2012; Imahara et al., 2006). Hence, saturated feedstocks such as palm oil tends to crystallize more rapidly at low temperature (Altaie et al., 2015).

2.9.2 Existing method for cold flow improvement

Several techniques have been employed to enhance the cold flow properties of fatty acid methyl esters (FAMEs). Edith et al. (2012) have reviewed several methods that can be applied for cold flow properties improvement of biodiesel, which include winterization, blending with petroleum diesel, transesterification with branched chain alcohol, use of chemical additives, genetic modification, and alternative feedstock.

The most widely used method to improve cold flow properties of biodiesel is through blending with petroleum diesel. Verma et al. (2016) studied the biodiesel blending and cold flow improver methods to improve cold flow properties of palm biodiesel. They suggest that the blending of biodiesel is a simple and effective method to improve the cold flow behaviour of biodiesel. For instance, the CP and PP of palm biodiesel are reported to improve from 21 ℃ to 8.9 ℃ and 19.7 ℃ to 6.2 ℃ after blending 20% of biodiesel into diesel (B20). However, blending requires larger proportion of blending agent (diesel) which is not economically feasible for the development of alternative fuel.

Apart from blending with diesel, the most economically and technically favoured method of improving the cold flow of biodiesel is by using chemical additives, which is also known as cold flow improvers. The conventional additives used for petroleum diesel are mostly polymeric materials which are able to co-crystallize with the hydrocarbon chain of the fuel and subsequently suppress the nucleation and growth of wax crystals to a certain extent. Dunn et al. (1996) studied the effects of 12 commercial cold flow improver

additives for diesel fuels on soybean biodiesel. They reported that those additives do not improve the CP of both the biodiesel and its blend with petroleum diesel. It is suspected that the additives only started to take effect after crystal nucleation occurred. They also restate that the effort should be focus on reducing the CP of biodiesel in order to improve the cold flow behaviour of biodiesel. Furthermore, other fuels such as kerosene and ethanol can also be added to biodiesel to improve its cold flow. Ethanol has been reported to be a good cold flow improver for palm biodiesel. By adding 20% ethanol, the CP and PP of palm biodiesel is improved from 21 °C to 7.30 °C and 19.7 °C to 4.1 °C respectively (Verma et al., 2016). However, higher blends of ethanol are discouraged as ethanol reduced the flash and fire point of biodiesel.

The current cold flow improving method that is applied in the biodiesel plants in Malaysia is winterization. MPOB has applied winterization technology for producing 100% pure palm biodiesel (B100) with CFPP ranging from 0 to -21 °C. By year 2008, three commercial winter-grade biodiesel plants have been established in Malaysia (Choo et al., 2008). During the process, biodiesel is cooled to a temperature between its cloud point and pour point. Any wax crystals that form are then fractionated until no crystals appear when the biodiesel is held at the specific temperature for minimum three hours. However, winterization is time-consuming and results in one-fifth loss of starting materials, not to mention the low product yield (about 25%) too (Edith et al., 2012). Hence, there is a need to look for other alternatives to improve the cold flow properties of palm biodiesel.

2.10 Alternative method to modify ester composition

Apart from using winterization, another possible alternative to alter the CFPP of 100% pure biodiesel is via distillation. Distillation separates a mixture of components physically by heating the mixture to the boiling point of the more volatile component. It can remove those saturated methyl esters with unfavourable high melting points and low boiling points from biodiesel. Distillation is a unit operation used for the separation of liquid mixtures in processing plants. In general, this process is the cheapest and best method for separating liquid mixtures into its components according to their relative volatility, which

is a measure of the ease of separation. As shown in Figure 2.10, a conventional batch distillation column consists of a column, a condenser, and a reboiler. Feed is initially placed in the reboiler to boil. Light key components which have lower boiling points would vaporize into the column section, and subsequently reach the condenser. The vapour which goes through the condenser is then either collected as distillate or returned to the column as reflux, while bottom product is discharged or left in the reboiler.

Batch distillation offers great flexibility in design and operation, making it a common solvent recovery technology utilized in processing industries such as pharmaceutical, food and specialty chemical industries. It is typically used where the separation only needs to be operated intermittently (e.g. in pilot-plant operations) and the materials to be separated are produced in small quantities. Multicomponent mixtures can be separated in a batch distillation column too (Kister, 1992; Talebian-Kiakalaieh et al., 2013).

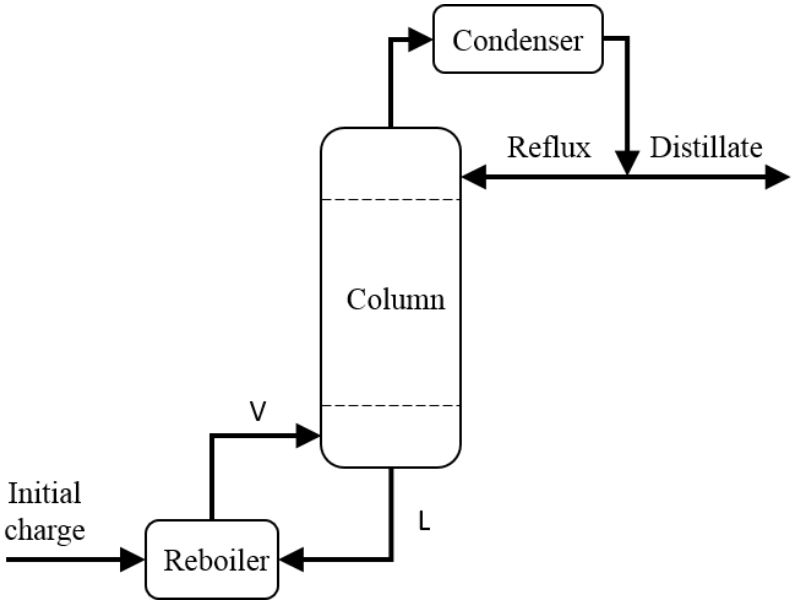

Figure 2.10 Schematic of a batch distillation system

Despite its advantages, batch distillation also results in operation problems such as the difficulties in deciding when to switch from one output stream to another, and finding the optimal reflux ratio, since the feed composition in the batch continuously changes as light

key is constantly removed from the still. Apart from that, it also takes time to charge and start up the column during each batch in order to establish the required parametric conditions for distillation, thus wasting time and energy (Fidkowski, 2013). In contrast, continuous distillation, which are designed to operate 24 hours a day, 7 days a week throughout the year, offers advantage over the efficiency and production quantity. The quantity is limited only by the amount of upstream feed. Therefore, it is more economical to adopt continuous distillation for large scale production (Kister, 1992).

The most affordable and easy way to carry out distillation is by conducting it at atmospheric pressure. The atmospheric boiling points of biodiesel generally range from 330°C to 357°C (Lieu et al., 2016). Due to the presence of esters with high boiling points, atmospheric distillation is not a feasible method for biodiesel distillation as the boiling temperatures of esters exceeded their respective thermal decomposition temperature (Mohammad Fauzi et al., 2014). Thermal decomposition (cracking) would alter the distillation characteristics of the biodiesel and results in inaccurate distillation information of the original fuel.

Instead, vacuum distillation can be used to separate the esters as the boiling point of the esters will decrease under reduced pressure. Thus, the esters can be boiled at lower temperatures, without the risk of cracking. Although vacuum distillation has not been vastly researched in the biodiesel industry to modify the ester compositions of biodiesel, it has been around for a long time for pure products separation from esters mixtures. For instance, Scott et al. (1952) developed a still to carry out vacuum fractionation of C18 unsaturated acid esters to as low as 0.1 mm Hg pressure in order to measure their respective boiling points.

Although vacuum fractional distillation is not commonly researched for the case of biodiesel, this operation method has been utilized by researchers to improve the quality of other biofuels such as algal bio-oil that was produced via pyrolysis (Choi et al., 2017; Nam et al., 2016). Pyrolysis is the thermal decomposition of organic matters in the absence of oxygen. The composition of bio-oil includes alkanes, alkenes, aromatics, carboxylic acids, and etc. (Atabani et al., 2012). Although the components to be separated

in bio-oil during the distillation process are different from biodiesel, the idea behind, which is to improve the fuel quality, is the same.

The amount of recent work related to vacuum distillation of biodiesel that are available in the open literature are scarce. A recent research work which may be consider closely related to the vacuum distillation of biodiesel was carried out by Iakovlieva et al. (2017). Their team conducted a vacuum fractional distillation on rapeseed oil esters in order to blend the distilled esters into jet fuel as bio-additives. The distillation of esters was performed under reduced pressure at 0.4–0.7 kPa at a temperature range of 165–215 °C to obtain several ester fractions. The rate of distillation was adjusted to 1–2 drops per second. It was reported that the application of vacuum distillation improved the quality of the rapeseed oil esters by reducing 17.7% of other undesired products present in it (eg. glycerides, glycerol, alcohol, and impurities) down to about 1%. The PP of the esters also reduced from -16 °C to -18.5 °C after the vacuum distillation.

On the other hand, Adewale et al. (2017) who conducted enzyme-catalyzed esterification on crude tall oil (53.36% FFA) also carried out fractional distillation on the biodiesel with the purpose of separating FAME from the rest of the crude tall oil biodiesel components (e.g. resin acid, unsaponifiable matters). The boiling points of the FAMEs were lower than that of the other undesired biodiesel components. Thus, the FAMEs could be collected in the form of distillates. Five fractions were obtained during the fractional distillation at temperature range of 210-238 °C and 20 mmHg. FAME components were mostly recovered in the first two fractions, whereby the concentration of palmitate in Fraction 1 collected at 210 °C was higher than Fraction 2 collected at 220 °C while the concentration of oleate was higher in Fraction 2 compare to Fraction 1.

2.11 Distillation column design

Fractional distillation, also referred to as fractionation, can be thought of as multiple separate distillations occurring within a single system. Fractional distillation is different from simple distillation as the objective of fractional distillation is to separate a highly

complex mixture of very broad boiling point range into usable fractions of relatively narrow boiling point range, rather than to end up with a pure chemical compound (Stauffer et al., 2008). It relies upon the same basic concept whereby compounds with lower boiling points vaporize more readily than higher boiling points compounds, resulting in a vapour, with a composition richer in the lower boiling point compounds, which is different from the source material. Fractional distillation is utilised for a more efficient separation process compare to simple distillation. The internal of a fractional distillation column consists of either trays or packing materials to facilitate fractional distillation. The column performance increases with an increasing number of plates (Buszewski, 2000). Separations that occur on the plates or trays of a fractional distillation column heavily depends on the vapour-liquid equilibrium (VLE) of the mixture. VLE determines the number of stages required in the column to achieve the degree of separation needed.

An ideal distillation stage, or theoretical plate, operates in steady state and contains two fluid streams, namely the liquid (L), and the vapour (V). All products which enter the stage are perfectly mixed and intimately contacted while the total vapour product and total liquid product that leave the stage are in equilibrium (Kister, 1992). For an ideal plate *n* as shown in Figure 2.11, the vapour and liquid leaving the *n*-th plate are in equilibrium, with their concentration termed as y_n and x_n respectively. As the vapour travels up the column, it is enriched in the more volatile component while the liquid is enriched with the heavy fractions (less volatile component) as it flows downward.

A column could be separated into two sections, the upper (rectifying) section and the lower (stripping) section. The assumption of constant molar overflow in McCabe-Thiele method simplifies the energy balance equations in the system. Thus, this gives the vapour-liquid equilibrium equation for plate *n* in rectifying section as (McCabe et al., 2005):

$$y_{n+1} = \frac{L_n}{L_n + D} x_n + \frac{D}{L_n + D} x_D \tag{2.9}$$

whereas the vapour-liquid equilibrium equation across plate *m* at the stripping section is described as:

$$y_{m+1} = \frac{L_m}{L_m - B} x_m - \frac{B}{L_m - B} x_B \tag{2.10}$$

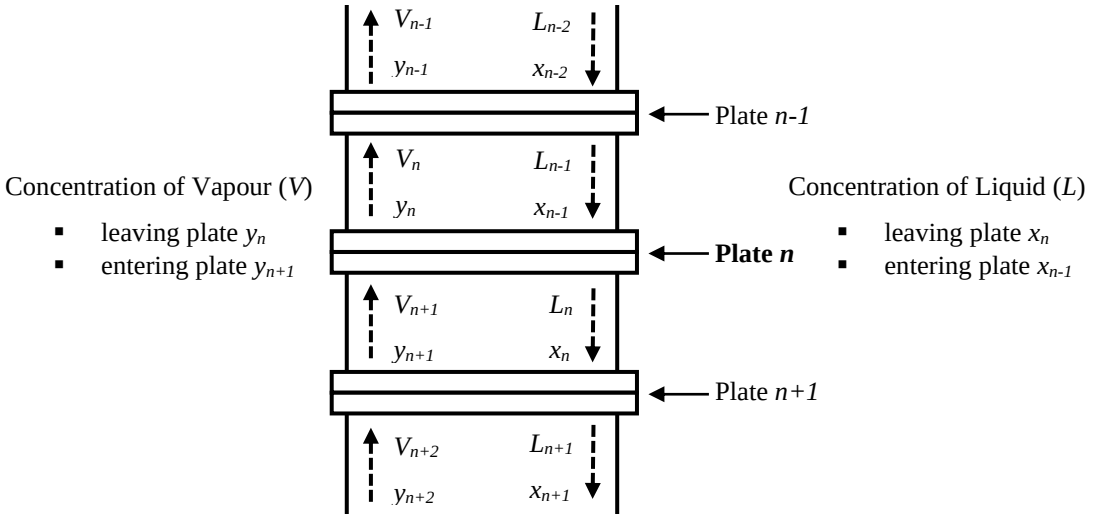

Figure 2.11 Material-balance diagram for plate *n* in a fractional distillation column

The process design of a column is carried out in a stepwise approach. The shortcut method is first used to eliminate the least-desirable options and provides a starting point for the rigorous step which fine-tunes the design and completes the column optimization process. The shortcut method (FUG method) has been utilised by several researchers to carry out column designs (Gadzama et al., 2016; Narvaes-Garcia et al., 2015).

Using the approximate calculation method, FUG method and Kirkbride's correlation, the design parameters of a fractional distillation column such as the number of stages, reflux ratios, and optimum feed stage location can be identified. The steps taken are as follows:

Step 1: Identify the K_i (or Henry's law constant) to determine the relative volatility of each individual esters.

$$K_i = \frac{P_{i,sat}}{P_i} \tag{2.11}$$

$$\alpha_i = \frac{K_i}{K_{HK}} \tag{2.12}$$

K_i measures the tendency of component *i* to vaporize.

Step 2: Estimate the minimum number of theoretical stages required under total reflux condition using Fenske equation (Jones & Pujadó, 2006)

$$N_{\min} = \frac{\log\left[\left(\frac{X_{D,LK}}{X_{D,HK}}\right)\left(\frac{X_{B,HK}}{X_{B,LK}}\right)\right]}{\log \alpha_{avg}} \tag{2.13}$$

where $X_{D,LK}$ is the mole fraction of light key component in the distillate, $X_{D,HK}$ is the mole fraction of heavy key component in the distillate, $X_{B,LK}$ is the mole fraction of light key component in the bottom, $X_{D,LK}$ is the mole fraction of heavy key component in the bottom, and α_{avg} is the average volatility of the light key to the heavy key component.

Step 3: Estimate distillate and bottom composition using Geddes-Hengstebeck equation

$$\log\left(\frac{X_{D,i}}{X_{B,i}}\right) = \log\left(\frac{X_{D,HK}}{X_{B,HK}}\alpha^{-N_{\min}}\right) + N_{\min}\log\alpha_i \tag{2.14}$$

From mass balance,

$$D_i = \frac{F_i}{1+\frac{B_i}{D_i}} \tag{2.15}$$

$$B_i = F_i - D_i \tag{2.16}$$

Step 4: Estimate minimum reflux ratio using Underwood equations and determine operating reflux ratio

$$\sum \frac{\alpha_i X_F}{\alpha_i - \theta} = 1 - q \tag{2.17}$$

$$\sum \frac{\alpha_i X_{D,i}}{\alpha_i - \theta} = R_m + 1 \tag{2.18}$$

Iterate θ until Equation (2.17) is equal to zero (q = 1 for feed in the form of saturated liquid). This gives the minimum reflux ratio. The operating reflux ratio is assumed to be 1.3 times of R_m.

Step 5: Estimate number of equilibrium stages required at operating reflux ratio using Regressed equation from Gilliland graphical method

$$\frac{N-N_{\min}}{N+1}=1-\exp\left[\left(\frac{1+54.4\psi}{11+117.2\psi}\right)\left(\frac{\psi-1}{\psi^{0.5}}\right)\right] \tag{2.19}$$

$$\psi=\frac{R-R_m}{R+1} \tag{2.20}$$

Step 6: Estimate feed tray location using Kirkbride correlation

$$\log\left(\frac{N_r}{N_s}\right)=0.206\log\left[\left(\frac{B}{D}\right)\left(\frac{X_{F,HK}}{X_{F,LK}}\right)\left(\frac{X_{B,LK}}{X_{D,HK}}\right)^2\right] \tag{2.21}$$

After FUG calculation, the diameter of the column can be determined by taking flooding condition into considerations for both rectifying and stripping sections. The flooding velocity with liquid surface tension correction at each section is expressed as:

$$u_f=C_{sb}\left(\frac{\sigma_s}{0.02}\right)^{0.2}\sqrt{\frac{\rho_L-\rho_v}{\rho_v}} \tag{2.22}$$

using Fair's correlation where C_{sb} is the Souders and Brown factor (Peters et al., 2004), which is a function of tray spacing with the liquid-vapour flow factor, F_{LV} acting as the parameter. The F_{LV} factor is given by

$$F_{LV}=\frac{L}{V}\sqrt{\frac{\rho_v}{\rho_L}} \tag{2.23}$$

By assuming 80% of flooding, the actual vapour velocity u_n is determined from:

$$\text{Percentage flooding}=\frac{u_n}{u_f} \tag{2.24}$$

The net column area required at the actual vapour velocity is expressed as:

$$A_n = \frac{Q}{u_n} = \frac{V}{\rho_v u_n} \tag{2.25}$$

where V is the maximum vapour rate (kg/s). The column diameter could then be calculated by estimating the cross sectional area of the column. Assuming a downcomer area of x = 15% (i.e. $A_d = xA_c$),

$$A_c = A_d + A_n = \frac{A_n}{1-x} = \frac{\pi}{4} D_c^2 \tag{2.26}$$

To convert the equilibrium stages to actual stages, the overall tray efficiency is required. A simple analytical expression was developed by Lockett (1986):

$$E_o = 0.492\left[\mu_L \left(\alpha_{LK/HK}\right)_{av}\right]^{-0.245} \tag{2.27}$$

The height of the column is estimated using Equation (2.28) with 10% additional height allowance for column operation such as phase disengagement and required internal hardware (Peters et al., 2004).

$$H_c = \left(N_{act} - 1\right) l_t + \Delta H = \left(\frac{N}{E_o} - 1\right) l_t + 0.1\left(\frac{N}{E_o}\right) l_t \tag{2.28}$$

Subsequently, the tray design is carried out by using the trial-and-error approach stated in the design guidelines compiled by Towler and Sinnott (2013) and Kister (1992). The preliminary data required for the plate-design include the vapour and liquid flow rates, the physical properties of the streams, the trial plate spacing, and the column diameter based on flooding considerations. To decide the liquid flow arrangement on the plate design, the maximum volumetric liquid rate (m^3/s) has to be determined by using the following expression:

$$L_{\max} = \frac{L_m' M_L}{3600 \rho_L} \tag{2.29}$$

where L_m' is the liquid molar flow rate below the feed stage (kmol/hr) and M_L is the molecular weight of the liquid (bottom stream). This is followed by the provisional plate design where the net area A_n and active area A_a are determined. For single pass plate,

$A_n = A_c - A_d$ and $A_a = A_c - 2A_d$. The hole area on the plate can be assumed to be 10% of A_a (Towler & Sinnott, 2013).

Another thing worth taking note of, is that the hole area of the plates should not be too large such that at the lowest operating rate, the vapour velocity would still be well above the weep point. Weep point refers to the lower limit of operating range when excessive amount of liquid leak through the plate holes. Eduljee (1959) proposed a correlation to predict the vapour velocity, which is also known as the minimum design vapour velocity:

$$u_h = \frac{\left[K_2 - 0.90\left(25.4 - d_h\right)\right]}{\left(\rho_v\right)^{0.5}} \tag{2.30}$$

where K_2 is a constant obtained from Figure 2.12, which depends on the depth of the clear liquid on the plate, $h_w + h_{ow}$. The actual minimum vapour velocity (70% Q/A_h) has to be higher than the vapour velocity at the weep point to ensure stable operation of the distillation column.

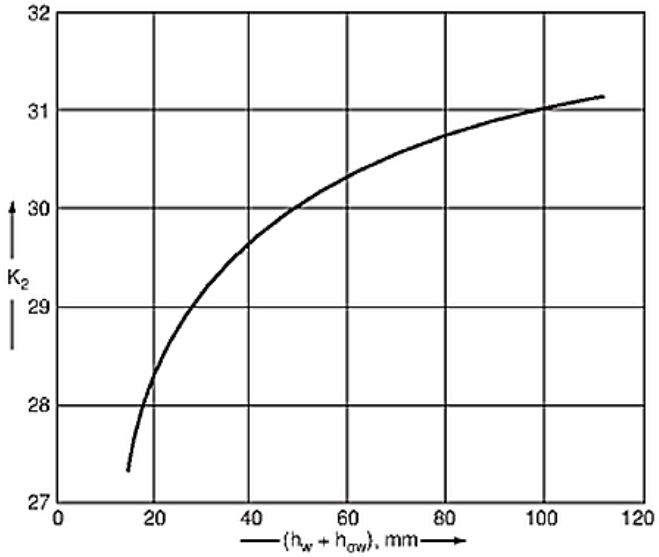

Figure 2.12 Weep-point correlation (Eduljee, 1959)

The height of the liquid crest over the weir, h_{ow} is expressed as:

$$h_{ow} = 750\left[\frac{L_w}{\rho_L l_w}\right]^{2/3} \tag{2.31}$$

Meanwhile, for vacuum operation, the weir height h_w of the plate is adjustable between 6-12 mm to reduce the pressure drop. This parameter determines the volume of liquid on the plate. A high weir will increase plate efficiency at the expense of a higher pressure drop over the plate (Towler & Sinnott, 2013).

The total pressure drop h_t over the plates can be estimated by summing up the dry plate drop, head of clear liquid ($h_w + h_{ow}$) and residual loss. The dry plate drop is expressed as:

$$h_d = 51\left[\frac{u_h}{C_0}\right]^2 \frac{\rho_v}{\rho_L} \tag{2.32}$$

where the orifice coefficient C_0 is obtained from Figure 2.13. It is a function of the plate thickness, hole diameter and the hole to perforated area ratio.

As for the residual head or residual loss h_r, the expression is as follows (Hunt et al., 1955):

$$h_r = \frac{12.5\times10^3}{\rho_L} \tag{2.33}$$

Apart from the resistance of liquid to flow in the downcomer, the total pressure drop over the plate also leads to downcomer liquid backup. If the level of liquid and froth in the downcomer rises above the outlet weir of the plate above, the column will flood. The downcomer backup h_b is expressed as:

$$h_b = \left(h_w + h_{ow}\right) + h_t + h_{dc} \tag{2.34}$$

The last term h_{dc} refers to the head loss in the downcomer due to flow resistance which is caused by the constriction at the downcomer outlet. It is given by:

$$h_{dc} = 166\left[\frac{L_{wd}}{\rho_L A_m}\right]^2 \tag{2.35}$$

where L_{wd} is the liquid flow rate in downcomer (kg/s) and A_m is selected from either the downcomer area or the clearance area under the downcomer A_{ap} , whichever is smaller.

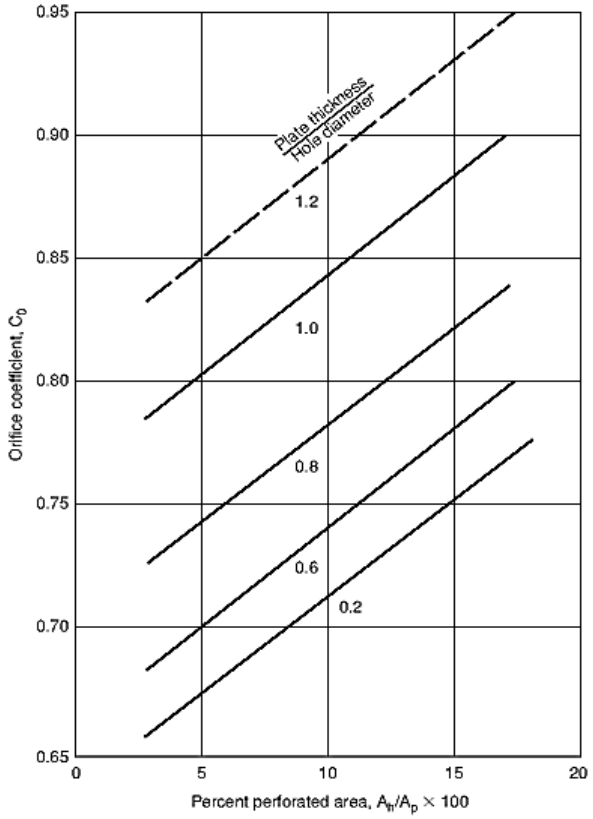

Figure 2.13 Orifice coefficient of sieve plates (Towler & Sinnott, 2013)

The A_{ap} is expressed as:

$$A_{ap} = h_{ap} l_w \tag{2.36}$$

where $h_{ap} = h_w - 5\,(\text{mm})$.

To avoid flooding at the downcomer, the following requirements have to be met:

$$h_b \le \frac{1}{2}\left(l_t + h_w\right) \tag{2.37}$$

$$t_r = \frac{A_d h_b \rho_L}{L_{wd}} \tag{2.38}$$

Equations (2.23) and (2.24) are used to check the entrainment by referring to Figure 2.14. As a rough guide, the entrainment should be less than 0.1 such that it has minimal effect on the plate efficiency.

The details of the plate layout are determined in the following step. The available perforated area on the plate will be reduced by the use of calming zones at the inlet and outlet sides of the plate, as well as the obstruction caused by structural members such as support rings and beams. The recommended width of each calming zone, w_{cz} is 75 mm for D_c below 1.5 m, and 100 mm for larger D_c. Meanwhile, the width of the support ring around the plate, w_{us} is fixed at 50 mm.

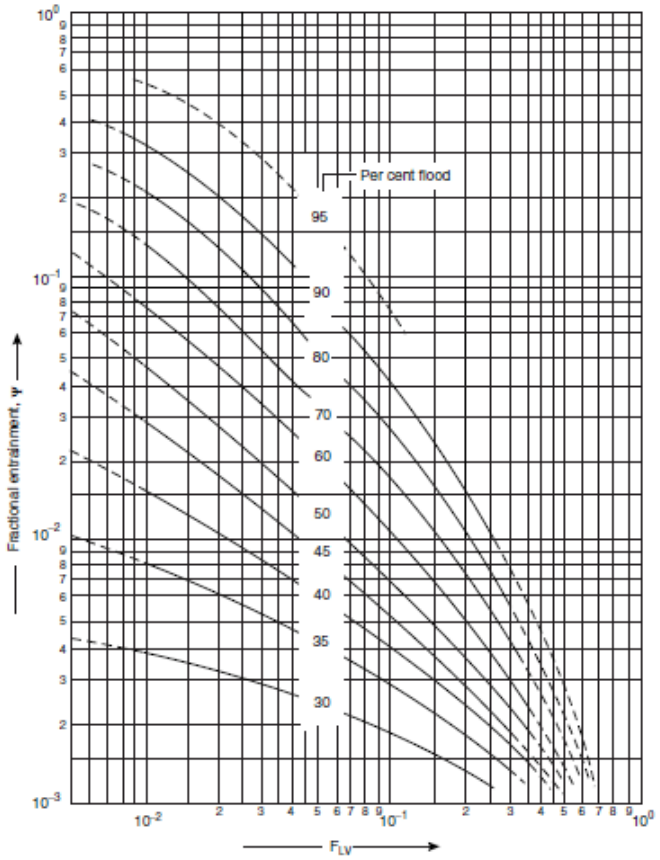

Figure 2.14 Entrainment correlation for sieve plates (Fair, 1963)

The total perforation area of a plate is given as

$$A_p = A_a - A_{us} - A_{cz} \tag{2.39}$$

where A_{us} is the area of unperforated edge strips and A_{cz} is the area of calming zones.

In order to determine A_{us}, the mean length of the unperforated edge strips has to be solved first:

$$l_{us} = \left(D_c - w_{us}\right)\pi \times \frac{180 - \theta_c}{180} \tag{2.40}$$

$$A_{us} = w_{us} \times l_{us} \tag{2.41}$$

whereas for calming zones, the mean length and area for calming zones are given as:

$$l_{cz} = l_w + w_{us} \tag{2.42}$$

$$A_{cz} = 2\left(l_{cz} \times w_{cz}\right) \tag{2.43}$$

For hole pitch arranged in an equilateral triangular pattern, the ratio of the total hole area over the perforated area is expressed as:

$$\frac{A_h}{A_p} = 0.9\left[\frac{d_h}{l_p}\right]^2 \tag{2.44}$$

The distance between the hole centres, or the hole pitch l_p should be

$$2.5 \le \frac{l_p}{d_h} \le 4.0 \tag{2.45}$$

The total amount of holes on the plate is calculated using Equation (2.46):

$$N_h = \frac{A_h}{A_h^{'}} \tag{2.46}$$

where $A_h^{'}$ is the area of a single hole.

2.12 Research gaps

The current status of studies on the microwave-assisted biodiesel production are still at laboratory scale (Tabatabaei et al., 2019). This implies that microwave technology in biodiesel production is still in developing stage which requires more investigation and research. Thus, in this work, the author would like to focus on exploring the effects of microwave technology on the production of low-cost biodiesel from alternative feedstock, PFAD. There is a lack of literature that characterize the effect of microwave power levels and irradiation time towards the reaction rate of microwave-assisted esterification of PFAD, as well as the investigation of its chemical reaction kinetics under microwave irradiation. Numerous researchers have proved that microwave technology is capable to greatly reduce the reaction time needed for the biodiesel production. Yet, little research has been done on the effect of microwave power variation on the reaction. Despite giving promising experimental results, to date, there is a lack of robust models which can describe the microwave-assisted esterification. To the best of author's knowledge, no numerical simulation which model the microwave-assisted esterification reaction of PFAD biodiesel has been reported. The temperature distribution under pulsed microwave irradiation during the entire reaction period has not been computed before as well. Therefore, there is a need for the development of multiphysics model in order to understand and optimize the microwave reactors for biodiesel production. From the literature review conducted, there is evidently no comprehensive model that could simulate the entire microwave-assisted biodiesel production process. Thus, the present study aims to develop and correlate a three-dimensional numerical model that accounts for the electromagnetics, heat transfer, fluid transport, and chemical kinetics for a complete microwave-assisted biodiesel production process. The numerical model would model the electromagnetic field and make realistic temperature prediction on the PFAD esterification while taking the chemical reaction into consideration. The simulated values would then be compared with the experimental results.

On the other hand, the current technology used to improve cold flow properties of biodiesel is known as the winterization technique, where the liquid fuel is gradually cooled below the melting points of the undesired esters such that the solidified ester

crystals could be separated from the biodiesel. Although this improves the biodiesel quality, the method itself is time consuming as it has to be repeated five to six times. Nevertheless, the low product yield (about 25 %) and 20% loss of starting materials have hinder its application in the industry. Therefore, an approach that is entirely the other way round is proposed in this project to remove the esters, which is through vacuum distillation. To the best knowledge of the author, this method has yet to be researched within the context of improving the cold flow behaviour of biodiesel. This project will provide a different point of view to produce export grade biodiesel with good cold flow properties via this alternative approach (vacuum distillation).

CHAPTER 3 RESEARCH METHODOLOGY OF MICROWAVE-ASSISTED PFAD ESTERIFICATION EXPERIMENT

This chapter covers the research methodology implemented to carry out the experiment of microwave-assisted PFAD esterification. The materials and experiment procedures are also explained here. This chapter is published in Applied Energy journal, https://doi.org/10.1016/j.apenergy.2019.01.052

3.1 Materials and apparatus

The PFAD samples was provided by Sarawak Oil Palm (SOP) Edible Oils Refinery Plant in Bintulu, Sarawak. Its FFA content is specified to be above 80%. The sample has a density of 0.898 kg/m^3 at 40 °C and the moisture and impurities content was below 0.4%. Methanol (ACS grade), sulphuric acid 95–97% (ACS grade), n-hexane (analytical grade), KOH pellets (ACS grade) and the certified reference material (FAME-mix RM6 and methyl heptadecanoate) for gas chromatography analysis were purchased from Merck Malaysia.

Using the right temperature measuring apparatus during microwave processing experiment is important. Mazubert et al. (2014) reported that poor temperature measurements in microwave reactors would give misleading reaction performances. Under microwave irradiation, charged molecules generated heat as they tried to align with the applied electric field at a very fast rate. As the heat could not be distributed over the entire volume evenly over a short time, this resulted in uneven heating or instantaneous

localized superheating, where the localized temperature would be much greater than the overall recorded temperature of the bulk reaction mixture. Hence, the bulk temperature might not be an accurate measure of the temperature at which the actual reaction took place (Gude et al., 2013). As a result, infrared red sensor which detected surface temperature was not suitable for temperature measurement under microwave irradiation. Monitoring temperature with an optical fibre sensor helped reduce incorrect temperature recording. Thus, fibre optic probe from the Luxtron Fibre Optic Thermometry (FOT) Lab Kit was used in this experiment.

3.2 Biodiesel production experiment procedures

A total of 80 g PFAD was prepared in a three-neck flask and placed in a 60 °C water bath such that the PFAD remained in liquid form. Methanol catalyzed with 1 wt.% sulphuric acid was added to the flask at a 1: 9 PFAD-to-methanol molar ratio during the experiment. The experimental setup is shown in Figure 3.1. The actual experiment setup is shown in Plate 1 and Plate 2 under Appendix A.

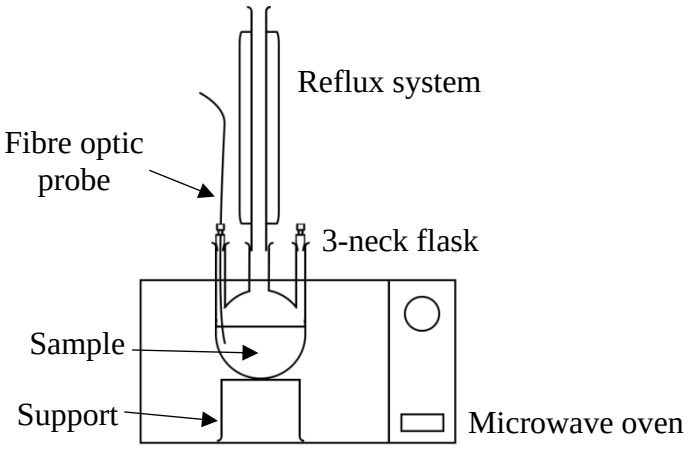

Figure 3.1 Schematic for microwave-assisted esterification

The entire setup was enclosed in a custom-built metal netting cage to reduce microwave leakage. The microwave oven used was a modified 20 liter domestic oven model,

Samsung ME711K (Malaysia). Its rated power consumption was 1150 W, and the output power could be varied from 100 to 800 W (max). After placing the three-neck flask in the microwave oven, the fibre optic probe was dipped into the liquid for temperature measurement during the experiment before the microwave oven was switched on. The experiments were conducted at eight different microwave irradiation periods (i.e. 1, 2, 3, 4, 5, 10, 15, and 20 min). The microwave power level was tested at three levels: 100W, 240W, and 300 W. Since there was no temperature-controlled system installed in the current microwave oven, it was not possible to maintain the experimental temperature at a fixed value. Each run was carried out three times to minimise the experimental errors. The biodiesel sample was taken out from the setup after the experiment was complete. No sample was extracted from the mixture while the experiment is ongoing.

After the experiment, the three-neck flask was immediately removed from the setup and immersed in a cool water bath for 5 min. The reacted mixture was subject to gravitational separation in a separating funnel. The collected biodiesel was washed several times with warm distilled water. Dissolved impurities and moisture were further removed through a centrifuge at 4000 rpm for 10 min. The weight of the centrifuged sample was recorded for calculating the biodiesel yield.

3.3 Experimental data analysis methods

After the experiment complete, four data analysis methods were used to interpret the experiment results, including biodiesel yield calculation, reaction kinetics analysis, GC-FID analysis, and dielectric properties measurement.

3.3.1 Biodiesel yield calculation

The actual biodiesel yield of PFAD was calculated as follows (Mohammad Fauzi et al., 2014):

$$\text{Actual Biodiesel Yield (\%)} = \frac{m_{\text{sample}}}{m_{\text{PFAD}}} \times \frac{AV_{\text{PFAD}} - AV_{\text{BD}}}{AV_{\text{PFAD}}} \times 100\% \qquad (3.1)$$

where AV_{PFAD} is the acid value of the PFAD feedstock and AV_{BD} is the acid value of the product (biodiesel) measured after the experiment. The calculation of the acid value was based on the mass of KOH required to neutralize 1 g of the feedstock or product diluted in an ethanol solution via titration, which was as follows:

$$AV = \frac{m_{\mathrm{KOH}}}{m_{sample}} \tag{3.2}$$

The mass of KOH could be obtained from the titration results by multiplying the titrant volume (L) with the molarity (mol/L) and molar mass (g/mol) of KOH.

3.3.2 Reaction kinetics analysis of microwave-assisted PFAD esterification

The rate equation for the esterification reaction of FFA and methanol is expressed as follows:

$$\dot{R} = \frac{d[\mathrm{FFA}]}{dt} = k_r \left[\mathrm{FFA}\right]^n \left[\mathrm{MeOH}\right]^m \tag{3.3}$$

where k_r represents the rate constant. When the molar concentration of methanol is much higher than the stoichiometric requirement for the esterification, the concentration of methanol could be considered as constant. Thus, Equation (3.3) could be rewritten as follows:

$$\dot{R} = \frac{d[\mathrm{FFA}]}{dt} = k_r \left[\mathrm{FFA}\right]^n = A\exp\left(\frac{-E_a}{R_U T}\right)\left[\mathrm{FFA}\right]^n \tag{3.4}$$

where k_r represents the rate constant of the total reaction.

By integrating Equation (3.4) and rearranging the terms, the rate equation for a first-order reaction (n = 1) is expressed as follows:

$$\left[\mathrm{FFA}\right] = \left[\mathrm{FFA}\right]_0 e^{-k_r t} \tag{3.5}$$

Similarly, the integrated rate equation for a second-order reaction (n = 2) is as follows:

$$\frac{1}{[\mathrm{FFA}]} = \frac{1}{[\mathrm{FFA}]_0} + k_r t \tag{3.6}$$

3.3.3 GC-FID analysis

Gas chromatography equipped with a flame ionisation detector (GC-FID) is the recommended method in EN 14214 standard (British Standards Institution, 2014) while gas chromatography equipped with mass spectrometry (GC-MS) is also used by some researchers (Hiwot, 2017; Iakovlieva et al., 2017; Nisar et al., 2018) for the same purpose. Both methods could identify the composition of fatty acid methyl esters (FAME) present in the final biodiesel sample. This was practised by various researchers (Hiwot, 2017; Ho et al., 2015; Y. Li et al., 2013). In this study, GC-FID analysis was carried out on the PFAD biodiesel samples.

The analysis was carried out using the Agilent 6890N Network GC system with an FID detector with operating conditions as reported by Yeong et al. (2019). The GC system was installed with an Agilent HP-5 column (30 m × 320 µm × 0.25 µm) (Y. Li et al., 2013). The injector and detector temperatures were set at 250 °C and the carrier gas used was helium with a 1 mL/min flow rate. Initially, the oven temperature was set at 140 °C. It was then ramped up at 15 °C/min rate to 200 °C and held for 2 min. Subsequently, the temperature was increased by 10 °C at 5 °C/min intervals and held for another 2 min. This increment step was repeated until the final temperature reached 240 °C. The volume of injected sample was 1 µL at 100 mL/min split flow. For quantitative FAME conversion, a sample was prepared in a 2 mL vial by diluting 50 mg of biodiesel sample and 10 mg of methyl heptadecanoate in 1 mL n-hexane. Methyl heptadecanoate with known concentration was used as an internal standard to determine the precise concentration percentage for the peaks shown by the biodiesel compound in the chromatogram. The relative concentration of the other esters was calculated by comparing the area of the respective peaks with the peak of the methyl heptadecanoate in the chromatogram.

On top of that, the identification of the composition of the major fatty acids in the biodiesel sample was carried out by comparing the components with FAME-mix RM6, which was

used as the reference standard (Ho et al., 2015). During GC-FID analysis, as the instrument detects the presence of certain esters in the sample, the detector signals will increase and plot in the form of 'peaks' on a chromatogram. These peaks that are recorded in the chromatogram over time were compared with the Supelco FAME mix RM-6 reference standard in order to identify the individual ester components. The FAME components with their specific concentrations in the FAME reference which serve as a guidance to calculate the concentration of the respective components present in the PFAD biodiesel sample are listed in Table 3.1.

Table 3.1 Components in Supelco FAME mix RM-6 with weight percentage

Component	**Weight Percentage (wt.%)**
Methyl myristate, C14:0	2
Methyl palmitate, C16:0	30
Methyl palmitoleate, C16:1	3
Methyl stearate, C18:0	14
Methyl oleate, C18:1	41
Methyl linoleate, C18:2	7
Methyl linolenate, C18:3	3

The FAME conversion was calculated using Equation (3.7) as expressed in the EN 14103 standard (British Standards Institution, 2011):

$$\text{Ester Content (\%)} = \frac{\sum A - A_{IS}}{A_{IS}} \times \frac{m_{IS}}{m} \times 100\% \tag{3.7}$$

where $\sum A$ is the sum of all FAME peak areas, A_{IS} is the internal standard (methyl heptadecanoate) peak area, m_{IS} is the mass of the internal standard, and m is the mass of the sample.

3.3.4 Measurement of dielectric properties

To carry out theoretical prediction, knowing the dielectric properties of materials is essential (Ratanadecho et al., 2002). In order to study the heat transfer behaviour of the PFAD feedstock (before esterification) and PFAD biodiesel (after esterification), samples of the purified biodiesel were sent to Universiti Teknologi Malaysia in Johor for dielectric measurement analysis. The data would then be used in the esterification modelling model.

The relative complex permittivity, ε_r of PFAD and PFAD biodiesel were measured via an open-ended co-axial probe method, using the Keysight 85070E dielectric probe. The aperture probe was calibrated before the permittivity measurements were carried out. The probe calibration consisted of air, short-circuits and deionised water. After the calibration, the aperture probe was immersed in the sample to measure its relative complex permittivity. Three readings were taken for each sample. The setup is shown in Figure 3.2.

The dielectric probe was attached to the Keysight E8362B network analyser and controlled with a computer. The sample was heated up using a Fisher Scientific Isotemp Stirring Hotplate; the temperature of the sample was monitored by using an 80BK-A Type K thermocouple temperature probe that was attached to a Fluke 289 multimeter. Three samples of each substance were measured at 2.45 GHz frequency at various temperatures (25 to 120 °C).

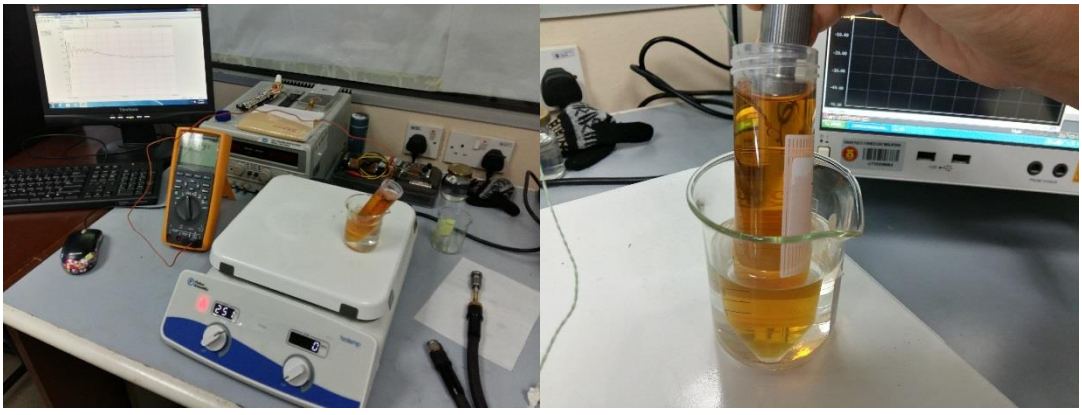

Figure 3.2 Dielectric properties measurement of PFAD and biodiesel samples

3.4 Summary

The preparation required and experiment procedures for microwave-assisted esterification of PFAD feedstock into biodiesel were explained in detail. The parameters studied during the experiment would be the microwave power levels and microwave irradiation periods. After completing the experiments, the yield of biodiesel would be recorded and further data analysis including the study of reaction kinetics of the PFAD esterification, characterization of the biodiesel through GC-FID, as well as the dielectric properties measurement of the PFAD biodiesel would then be carried out.

CHAPTER 4 EXPERIMENTAL RESULTS & ANALYSIS OF MICROWAVE-ASSISTED PFAD ESTERIFICATION

The experimental results for microwave-assisted PFAD esterification were obtained and analysed in this chapter. This includes the results of the final yield of PFAD biodiesel obtained using microwave-assisted esterification method, plus the effects of microwave power dissipation intensity and irradiation time on the yield. Furthermore, the reaction kinetics of the batch production of biodiesel, as well as the dielectric properties of the materials are also discussed. This chapter is published in Applied Energy journal, https://doi.org/10.1016/j.apenergy.2019.01.052

4.1 Biodiesel yield

The biodiesel yields obtained from the experiment at various power levels and reaction time are shown in Table B-1. Figure 4.1 depicts the change in biodiesel yield over time at different microwave power dissipation levels. The chosen range of microwave irradiation time was selected based on the study conducted by Lokman et al. (2014) who studied the optimal parameters for batch type microwave-assisted PFAD esterification. Their investigation revealed that the change in yield would be minimal (< 1%) between 15-45 min (900–2700 s) range. Thus, studying biodiesel yield for a longer microwave irradiation time is of less importance.

The highest biodiesel yield obtained was 92.39% under 1200 s (20 min) long of 300 W microwave irradiation, where the amount of microwave energy supplied to the reaction

mixture is the highest among all parametric conditions. This power level was similar to the 40% power dissipation level (320W) which gave the highest level of increase in yield as reported by Patil et al. (2010). However, the lowest yield result (82.75%) was observed at 300 s of 240W microwave irradiation instead of at 300 s of 100 W (83.35%). This minute difference might be a result of human errors which occurred during the experiments as the percentage error recorded for 100 W experiment condition was obviously larger than 240 W. Thus, in general, it could be concluded that the final yield of PFAD biodiesel increased with longer microwave irradiation time and higher microwave power level. With higher amount of heat energy supplied from the microwave, this encouraged the reaction between PFAD feedstock and methanol for better yield performance.

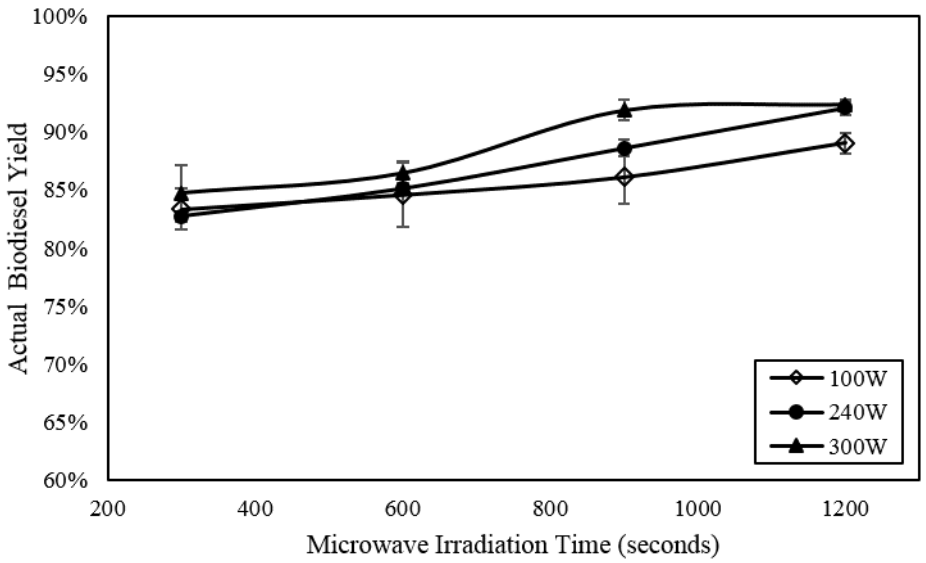

Figure 4.1 Actual biodiesel yield of microwave-assisted PFAD esterification

Nonetheless, when taking energy saving into consideration, the optimal parametric conditions for microwave-assisted PFAD esterification would be at 900 s of 300 W microwave irradiation. Another 300 s of microwave irradiation only increased the yield by a mere 0.5% which hinted that the effect of microwave irradiation time towards the biodiesel yield has greatly reduced. This optimal reaction time agreed with the optimal

time obtained by Lokman et al. (2014) who used 1 wt.% sulphuric acid catalyst and 1:9 methanol-to-oil molar ratio as well. They managed to produce 99.5% yield under 15 minutes of 800 W microwave power and constant mechanical stirring. Meanwhile, the biodiesel yield obtained in this study after 15 min of microwave irradiation was lower, which was at 91.88%. This difference in the observed yield was considered to be acceptable as the microwave power used in this study was 62.5% lower, i.e. 300 W and no mechanical stirring was involved in this study to improve the reaction rate. In other words, the sole application of 300 W microwave power could substantially improve the reaction rate of PFAD esterification to over 90% within 15 min even without any stirring mechanism. This showed the great potential of microwave technology in biodiesel production.

Therefore, in this study, the optimal condition for the batch production of PFAD biodiesel from microwave-assisted PFAD esterification to achieve 91.88% yield was 300 W microwave heating, 1:9 PFAD-to-methanol molar ratio, and 1 wt.% sulphuric acid catalyst at 15 min reaction time. As the initial volume of PFAD was 70.92 ml (80g), the specific energy required at the optimal condition (300 J/s × 900 s) was 3.81 kJ/ml.

As described Section 2.4, there are several parameters which affect the esterification reaction. However, only two parameters related to the effect of microwave (microwave irradiation periods and microwave power levels) were studied in this work. The investigation of other parameters (e.g. catalyst loading, oil-to-methanol molar ratio) had been studied extensively by other researchers such as Chongkhong et. al. (2007) and Lokman et. al. (2014). Thus, these parameters were not studied in this work. In addition, the stirring mechanism was not included in the set up to avoid the difficulty in differentiating and identifying the significance of the sole effects of microwave irradiation towards esterification in this work.

4.2 Effect of microwave irradiation time

The amount of heat energy supplied by the microwave to the esterification reaction could be controlled via the total irradiation time or the intensity of the microwave power. As shown in Figure 4.1, in general, the biodiesel yield increased as the irradiation time increased but the yield was not linearly proportional to the irradiation time. The conversion rate of PFAD into biodiesel was the highest during the first 300 s of microwave heating, reaching over 80% biodiesel yield, regardless of the microwave power level. This implied that a huge portion of the esterification reaction of FFAs into FAMEs took place during the first 300 s. As the reaction time continued to increase to 1200 s, the biodiesel yields still improved, but only by another 5 to 9%, which were relatively slower compare to the first 300 s. The slow conversion rate could be attributed to the huge drop in FFA concentration over time which reduced the effective area of reaction between the reactants as the process continues. To get a clearer picture of the reaction changes within the first 300 s, additional experiment runs were carried out at 300 W microwave power from 60 to 240 s. Their respective biodiesel yields were calculated and shown in Table B-2 (in Appendix B). Using the data in Table B-2, the actual biodiesel yield obtained under 300 W microwave power level was plotted in Figure 4.2.

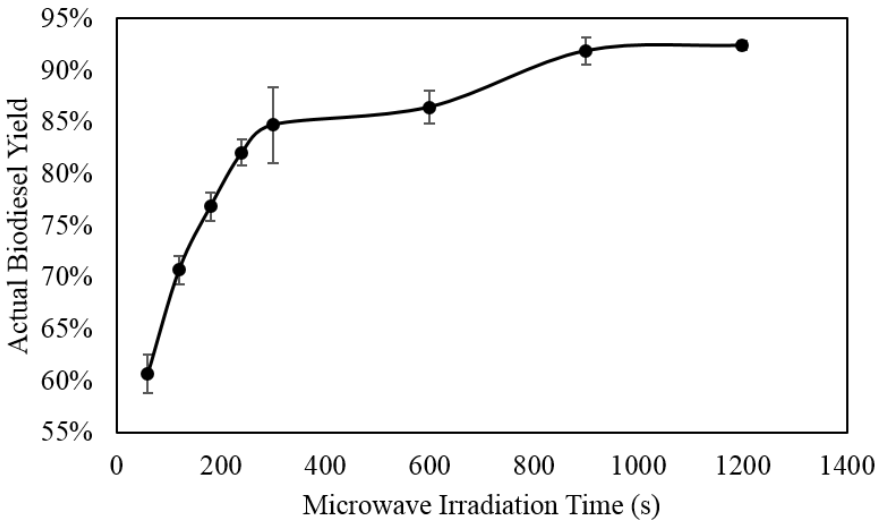

Figure 4.2 Actual biodiesel yield of PFAD in microwave-assisted esterification (300 W)

Each experiment was conducted in three replicates and the mean values of the yield were recorded. The deviation of yield values was less than 1.00% in general with the highest error recorded at 300 s (± 2.44%). This could be due to human error during the experiment.

It is clear that more than 60% of the PFAD was converted into biodiesel within the first minute. After 300 s of microwave irradiation, the biodiesel yield obtained increased to 84.72%. Figure 4.2 clearly shows that the yield did not increase linearly with time. The highest reaction rate was observed during the first 300 s, followed by a slower reaction rate between 300 and 600 s, which slightly increased again from 600 to 900 s, and gradually slowed down between 900 to 1200 s. This yield pattern was similar to the results reported by Lieu et al. (2016). The reaction occurred vigorously during the first 300 s as methanol exist in abundance and the equilibrium of the esterification reaction was shifted to the right. In addition, the microwave irradiation also provided energy to enhance the reaction rate. As the concentration of PFAD feedstock greatly reduced, the reaction slowed down. The reason for the slight increase in reaction rate between 600 to 900 s was unknown but could be due to the presence of optimal microwave power level.

The initial acid value of PFAD feedstock was determined to be 209.27 mg KOH/g. This value suggested the presence of a high amount of unreacted FFAs within the PFAD feedstock. As PFAD converts into biodiesel during the chemical reaction, the acid value reduced, indicating that the FFAs have been esterified into FAMEs. After 900 s of reaction time, the acid value of the PFAD biodiesel sample had significantly reduced to 11.41 mg KOH/g, as tabulated in Table B-2. This implied that the esterification of PFAD feedstock under microwave irradiation was a highly feasible production method of PFAD biodiesel. Nonetheless, this had yet to satisfy the requirement of EN 14214 or ASTM D6751 standards, which is < 0.5 mg KOH/g. To remove these unreacted FFAs, one might add some KOH solution to the biodiesel sample during the post-washing process in order to trigger saponification reaction. This would allow the FFAs to be removed in the form of soap. However, if one's main concern was to retain these FFAs to further increase the final biodiesel yield, it would be wise to introduce additional methods such as ultrasound

cavitation or continuous flow system to improve the mass transfer, rather than prolonging the microwave irradiation time.

On the other hand, Tabatabaei et al. (2019) commented that both mass transfer and yield would decrease at higher temperature due to the loss of reactants via vaporization. This effect was not observed in the study. At all microwave power levels, as the time passed and the superheated reaction temperature became much higher than the boiling temperature, the biodiesel yield did not decrease. The biodiesel yield still increased at higher temperature but at a slower rate. This negative effect on the mass transfer and yield had been eliminated in this experiment not only by having high PFAD-to-methanol molar ratio, but also by using a reflux system which condensed large amount of methanol that vaporized during the experiment such that the methanol would dripped back into the reaction mixture. Furthermore, this dripping action might indirectly promote mass transfer in the reaction mixture as well and improved the esterification rate.

4.3 Effect of microwave power level

According to Tabatabaei et al. (2019), the optimum reaction temperature for non-enzymatic conventional biodiesel production was near the boiling point of alcohol. Under microwave irradiation, it was obvious that the esterification of PFAD was successfully carried out near the boiling point of methanol. Interestingly, the temperature profiles of PFAD esterification as shown in Figure 4.3 suggested that the importance of reaction temperature in governing the biodiesel yield under microwave irradiation might be low. For instance, at t = 300 s, the reaction temperature was 59 °C at 100 W and 74 °C at 300 W, respectively. However, the yield obtained at both microwave power levels was similar although the temperature difference was as large as 15 °C. The biodiesel yield at 59 °C was only 1.37 % lower than that at 74 °C. This should not be the case as similar yields should only be obtained at similar temperatures. This was supported by the results obtained by Lokman, Rashid, and Taufiq-Yap (2015). The biodiesel yield they obtained at 60 °C and 75 °C under the same microwave power setting were 58% and 80%

respectively, which vary by a 22% difference. Therefore, this implied that obtaining similar yield was most probably a result of the intensity of the microwave power.

Based on the experiment data listed in Table B-1, one could deduce that the higher the microwave power level, the better the biodiesel yield. However, using microwave power level which was too high could negatively affect the cost effectiveness of utilizing this heating technology in biodiesel production. Besides, using high microwave power level would also result in the occurrence of superheating. This superheating effect could often be observed in multimode domestic microwave ovens without any stirring mechanisms. It was expected that the effect would disappear if the experiments were carried out with well-stirred mixtures at low microwave power level (Perreux & Loupy, 2001). Similar phenomenon was observed in this study.

The temperature profiles for the three microwave power levels were plotted in Figure 4.3.

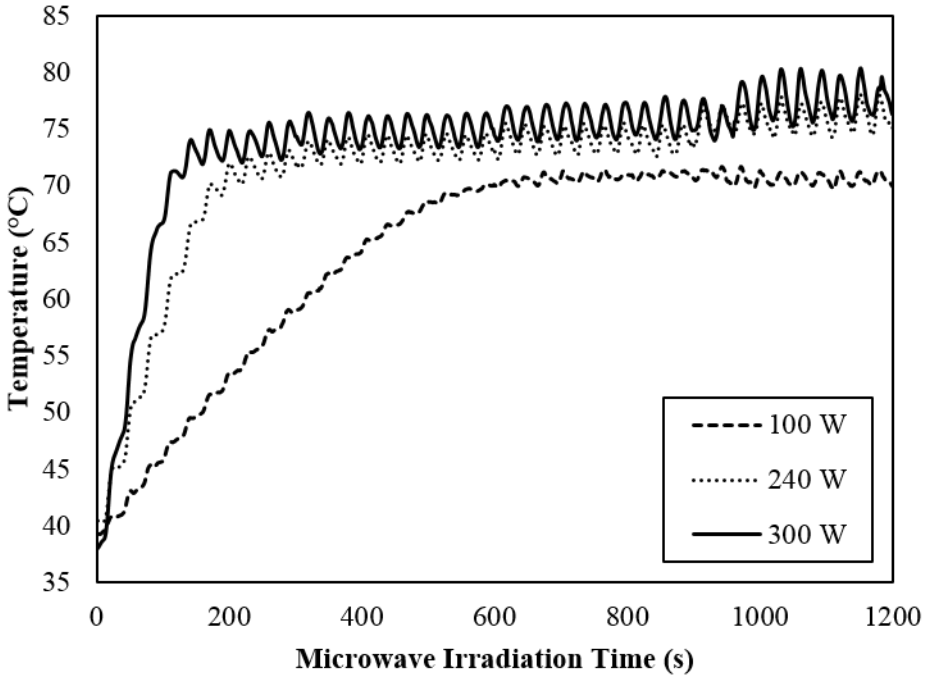

Figure 4.3 Experimental temperature profiles at different microwave power dissipation levels

In this study, the reaction temperature was uncontrollable as the temperature of the reaction mixture was affected by the microwave power level used during the experiment. In other words, the power level of the multimode microwave oven was fixed at a testing value but the temperature profile of the reaction mixture would constantly vary with the ON and OFF operation time of the magnetron and the total heat content within the liquid. The boiling point of methanol was 65 °C. When the temperature measurement of the reaction mixture exceeded 65 °C, this indicated the presence of localised superheating in the liquid. Superheating effects were observed at all microwave power levels but began at different microwave irradiation time in the absence of stirring. The superheating effect started roughly after 100 s under 300 W; 150 s under 240 W; and 500 s under 100 W microwave power. In addition, the superheated temperature profiles at the three microwave power levels also showed some difference. At 100 W, the superheated temperature range was about 70 °C while the average superheated temperature at 240 W after 150 s was 71 °C. The superheated reaction temperature profile at 300 W after 100 s fluctuated about 76 °C with ± 2 °C difference. These temperature values were acceptable as the superheated temperature of boiling methanol under microwave exposure recorded by Perreux and Loupy (2001) was as high as 84 °C.

With the reaction temperature exceeding the boiling point of methanol, the methanol would vaporise continuously. Nonetheless, the reaction between the liquid PFAD feedstock and liquid methanol would still occur simultaneously because the methanol had been supplied in excess (9 times more than PFAD feedstock in terms of molar ratio). In addition, a water-cooled reflux system had also been installed to the system to condense the evaporated methanol and return it to the reaction mixture, making sure that sufficient amount of methanol was available for esterification throughout the experiment.

The fluctuation at each temperature profile was due to the cyclic microwave heating pattern. At 300 W, the temperature variation during each cycle was relatively similar to 240 W (± 2 °C) and slightly larger compare to 100 W (± 1 °C). This showed that as the microwave power level increased, the superheating effect also increased, causing the average superheated temperature range of reaction mixture at higher microwave power

level to increase as well. During the experiment of the PFAD esterification, methanol and water which were polar molecules, selectively absorbed microwaves and subsequently released heat energy into the reaction mixture. As methanol existed in abundance in the reaction mixture, it was responsible for most of the energy conversion from microwave to heat energy. During the first 300 s of the experiment, most of the heat energy was utilised in the esterification reaction to convert the FFAs in PFAD feedstock into esters. Thus, the esterification rate at all microwave power levels were very high. As the reaction temperature rose above the boiling point of methanol, the reaction rate began to slow down. Apart from the reduction in the concentration of FFA available for esterification reaction, another reason which might result in the slow reaction rate could be the boiling methanol. A huge portion of the heat energy which was absorbed from the microwaves at the later stage was used for the vaporization of boiling methanol instead of improving the rate of esterification.

Figure 4.4 shows the energy consumption at various microwave power levels to achieve the respective biodiesel yields.

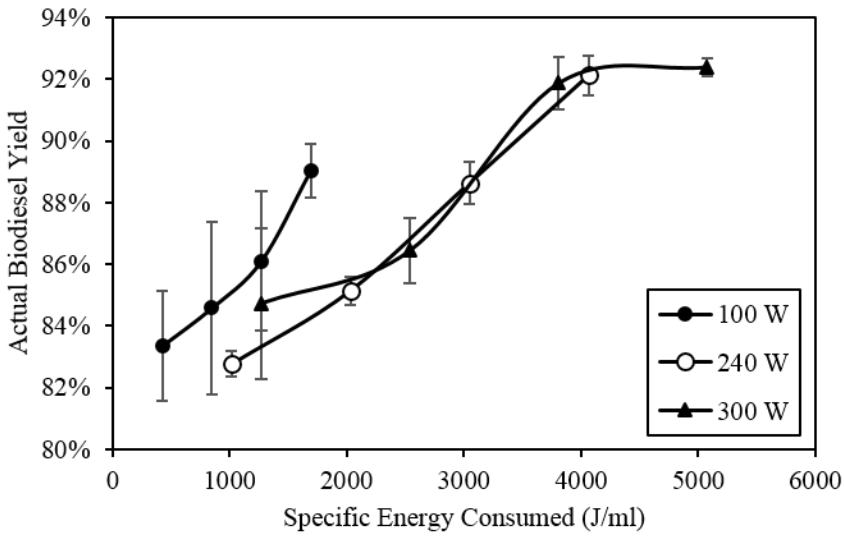

Figure 4.4 Energy consumption for biodiesel production at various microwave power levels

The energy consumption (J/ml) was obtained from the basic calculation of microwave power (W) and time (s) divided by the initial volume of PFAD (ml). The data is shown in Table B-3 in Appendix B. As observed, it was reasonable to deduce that the actual biodiesel yield obtained increased with the higher consumption of microwave energy, but up to an optimal value. The rate of yield attained reduced considerably and reached a plateau when the amount of microwave energy consumed by the reactant (PFAD) exceeded 4 kJ/ml.

Should the total energy consumption be the main criterion for selecting optimal operating condition (without considering the microwave irradiation time), 100 W might be thought to be the preferable microwave power level at first glance. As shown in Figure 4.4, higher biodiesel yield could be obtained at the same energy consumption level by using low power setting. For instance, when the energy consumption was 1269.04 J/ml, the actual biodiesel yield obtained at 100 W (900 s) was 86.09% as compared to 84.72% at 300 W (300 s). At 1692.05 J/ml specific energy consumption, the yield obtained at 100 W was 89.02%, which was comparatively higher than 240 W and 300 W which would give yield around 85%. However, this observation was insufficient to indicate that 100 W microwave power level was more superior because this higher yield was only possible at the expense of prolonged irradiation time. As such, the higher yield observed at 100 W under the same amount of energy consumption might arguably be the result of having longer reaction time for the occurrence of esterification reaction instead of implementing low microwave power level setting. At 240 W and 300 W microwave power levels, the graphs of yield versus the energy consumed were found to be plotting closely together along a linear line when the energy consumption ranged between 1200 to 4000 J/ml. This was probably because the difference between the power level was relatively small (60 W). Thus, the effect of another factor, longer reaction time for esterification, on the biodiesel yield would be less significant on the graph of energy consumption versus yield. The effect became significant as observed in the case of 100 W and shown by the shift of the line to the left. In summary, the effect of microwave power levels on the biodiesel yield

should be attribute to both the total energy consumed by the reacting mixture as well as the irradiation time.

4.4 Reaction kinetics of microwave-assisted PFAD esterification

The reaction order for the microwave-assisted PFAD esterification was determined by curve fitting the reaction rate equations with the biodiesel yield. The experimentally measured temperatures were used for the temperature terms in Equations (3.5) and (3.6) to obtain the instantaneous temperature at the measured data points. As the temperature varied greatly during each cycle, empirical functions were developed to predict the instantaneous temperatures. These equations are only applicable for the current reactor.

The estimated temperature profile functions (as depicted in Plate 4 in Appendix B) for the three microwave power levels during the experiment are expressed as:

$$T_{100\mathrm{W}} = 3e^{-8}t^3 - 0.001t^2 + 0.1029t + 37.164 \qquad (4.1)$$

$$R^2 = 0.9954$$

$$T_{240\mathrm{W}} = 6.9714 \ln t + 28.797 \qquad (4.2)$$

$$R^2 = 0.8506$$

$$T_{300\mathrm{W}} = 6.1861 \ln t + 35.845 \qquad (4.3)$$

$$R^2 = 0.7722$$

These functions were used in predicting the reaction rate constant k_r. Although R^2 for the empirical temperature function of 300W is quite low, the percentage error for the predicted temperature profile obtained using the empirical function is less than 3% (unit in Kelvin), when compared to the experimental temperature profile. Thus, this should give relatively close rate constant and subsequently, accurate final [FFA]. The fatty acid conversion was curve-fitted to both equations with the aid of Microsoft Excel solver using

the least squares method. The comparison between the experimental and predicted fatty acid conversion of the two reaction orders were shown in Figure 4.5.

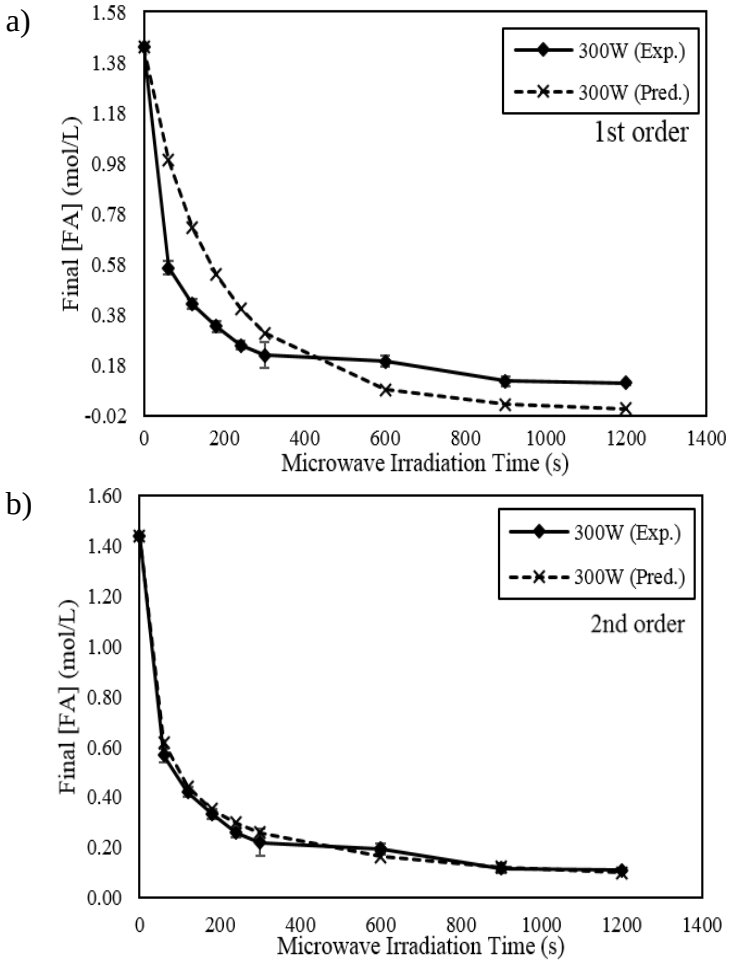

Figure 4.5 Comparison between reaction rate of PFAD esterification under 300 W microwave power with a) first-order; b) second-order reaction kinetics (curve-fitting)

The sum of squared error (SSE) was 0.0406 for the first-order curve-fitting and 0.0027 for the second-order curve-fitting. The predicted final concentration of the PFAD in the biodiesel sample was observed to be in good agreement with the experimental data using second-order reaction kinetics. Thus, the microwave-assisted PFAD esterification was deduced to follow the second-order reaction kinetics. Table 4.1 shows the comparison

between the actual and predicted reaction rate of PFAD esterification under 100 W, 240 W and 300 W with second-order reaction kinetics.

Table 4.1 Comparison between actual and predicted final fatty acid concentration of PFAD esterification

Microwave Irradiation Time (s)	**Final Fatty Acid Concentration (mol/L)**	**Predicted Fatty Acid Concentration (mol/L)**		**Squared Error**	**Rate constant, k (M^{-1} s^{-1})**
100W					
0	1.4938	1.4938		-	0.02114
300	0.2487	0.2981		0.0024	0.00895
600	0.2303	0.2269		0.0000	0.00623
900	0.2078	0.1660		0.0017	0.00595
1200	0.1640	0.1191		0.0020	0.00644
			SSE	0.0062	
240W					
0	1.4938	1.4938		-	0.02846
300	0.2577	0.2933		0.0013	0.00913
600	0.2221	0.1901		0.0010	0.00765
900	0.1698	0.1450		0.0006	0.00692
1200	0.1177	0.1190		0.0000	0.00644
			SSE	0.0029	
300W					
0	1.4938	1.4938		-	0.04024
300	0.2282	0.2599		0.0010	0.01059
600	0.2026	0.1636		0.0015	0.00907
900	0.1213	0.1228		0.0000	0.00830
1200	0.1137	0.0997		0.0002	0.00780
			SSE	0.0027	

It was found that the individual squared errors between the experiment data points and the model were minimal at all three power levels (< 0.0025). The curve at 300 W had the lowest SSE at 0.0027. Even the highest SSE was only 0.0062 at 100 W. As shown in Figure 4.6, the fitted line plots were very close to the experimental values, showing that

they were in good agreement. Nonetheless, the plots at 240 W and 300 W were closer to the experimental values as compared to the line plot of 100 W.

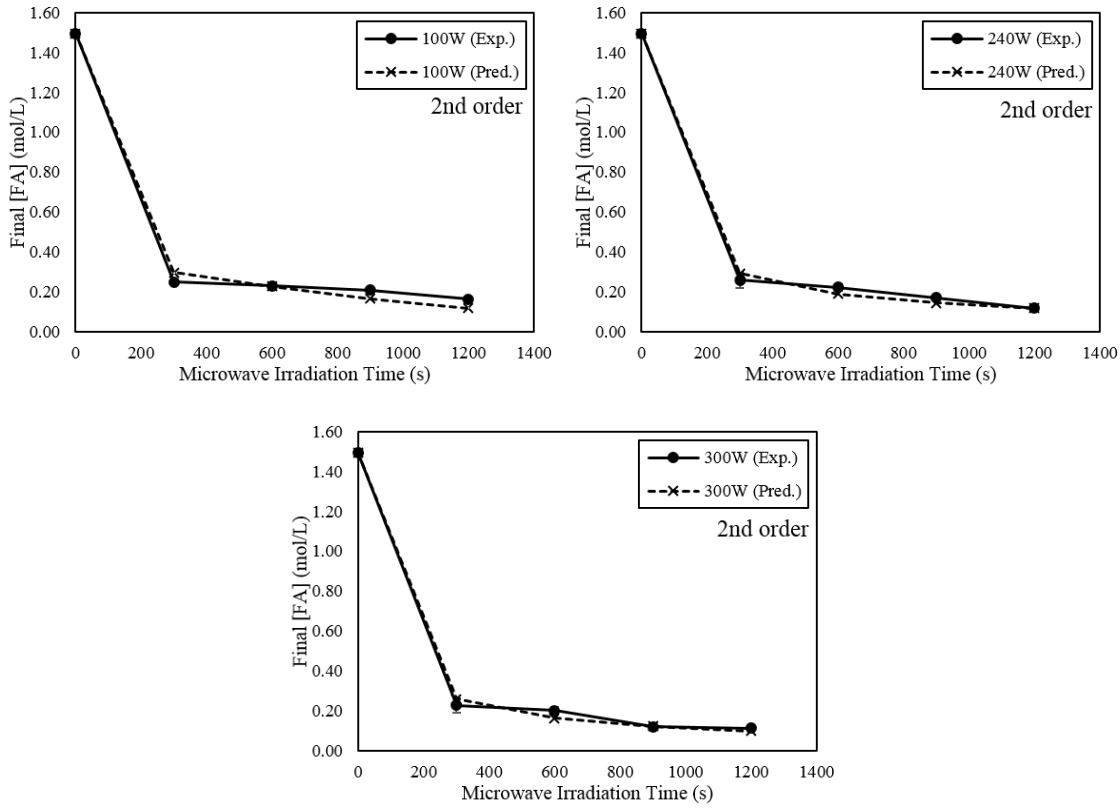

Figure 4.6 Comparison of estimated PFAD esterification reaction rate with experimental data

Microwave irradiation could affect the pre-exponential factor or activation energy in the Arrhenius equation due to the orientation effects of dipolar molecules in the presence of an electric field (Nomanbhay & Ong, 2017; Rodríguez et al., 2015). Table 4.2 shows the activation energies and frequency factors determined for the PFAD esterification reaction at the three tested microwave power levels. It was observed that the frequency factor slightly increased with higher level of microwave power. This implied that with stronger microwave power, higher amount of heat energy was supplied and the frequency of collisions with correct orientation between the particles increased. These values would be used as the input for modelling the reaction rate in the numerical model.

Table 4.2 Activation energies and frequency factors for microwave-assisted PFAD esterification under various power level

Microwave Power (W)	**Frequency factor, A (M^{-1} s^{-1})**	**Activation energy, E_a (J/mol)**
100	2.02×10^{-8}	-36000
240	2.87×10^{-8}	-36000
300	3.65×10^{-8}	-36000

The value of the activation energy required for microwave-assisted PFAD esterification was determined to be -36 kJ/mol. This was similar to the finding by Hong et al. (2012), and 10 kJ/mol higher than the activation energy reported by Jermolovicius et al. (2017). The difference in the values was possibly because the oil feedstock and alcohol used were different from those in this study. The negative activation energy as found in this study suggested that the reaction rate would decrease with an increase in temperature (Jermolovicius et al., 2017). Esterification is a form of bimolecular reaction as molecules of fatty acid and alcohol collide and exchange groups of atoms (Zhang et al., 2012); it was previously reported that negative activation energy could appear in bimolecular reactions that occur too fast (Benson & Dobis, 1998). It is therefore reasonable to deduce that the application of microwave energy, which excites the molecules rapidly, results in negative activation energy of microwave-assisted PFAD esterification. In fact, more than 60% of the reaction occurred within the first minute, where the average temperature was still relatively low, i.e. in the 38–60 °C range, compared to the remaining time duration. As the temperature increased, the reaction rate slowed down. This was also due to the fact that the concentration of FFA available for esterification had reduced substantially after the first minute.

4.5 GC-FID analysis

GC-FID analysis was carried out to characterize the biodiesel produced from PFAD. The FAME conversion in the biodiesel sample was verified to be greater than 96.5% (mol/mol), which was in accordance with the specifications stated in EN 14214 standard (British Standards Institution, 2014). The normalised mass fractions of the FAMEs were listed in Table 4.3.

Table 4.3 Ester components in PFAD biodiesel with their respective mass fractions

Ester	Retention Time (min)	Lipid number	Molar mass (g/mol)	Normalized Mass %
Methyl palmitate	9.187	C16:0	270.5	47.51
Methyl stearate	12.782	C18:0	294.5	4.76
Methyl oleate	12.374	C18:1	296.5	38.69
Methyl linoleate	12.211	C18:2	298.5	9.04

Since the FAMEs were directly converted from PFAD, it was reasonable to deduce that the fatty acids in PFAD would have identical mass fractions as those in the FAMEs. The value of the mass fractions obtained were similar to the result obtained by Lokman, Rashid, and Taufiq-Yap (2015), where the four major fatty acids in PFAD were reported to be palmitic acid (45.68 wt.%), oleic acid (40.19 wt.%), linoleic acid (7.9 wt.%), and stearic acid (4.25 wt.%), with a molecular weight of 232.3 g/mol. In addition, the molecular weight of the PFAD feedstock used in this study was estimated to be 260.17 g/mol based on the normalised mass fraction identified in Table 4.3.

4.6 Dielectric properties measurement

The response to an applied electric field (microwave) is dependent on the dielectric properties of the material. The dielectric properties of PFAD and biodiesel samples at 2.45 GHz were measured and plotted in Figure 4.7.

The dielectric constants of PFAD were observed to range between 2.47–2.9 over a temperature range of 25–120 °C. Rudan-Tasic and Klofutar (1999) reported that the dielectric constant of oils lied in the range of 3.0–3.2; since PFAD is a type of low quality oil, therefore, the obtained values were considered acceptable. It was observed that the dielectric constant and loss factor of PFAD were generally lower than those of biodiesel. Once PFAD was converted into biodiesel, the dielectric constant increased to the range of 2.92–3.52. Similarly, the loss factor of the PFAD, which was between 0.11–0.24, also increased after the esterification.

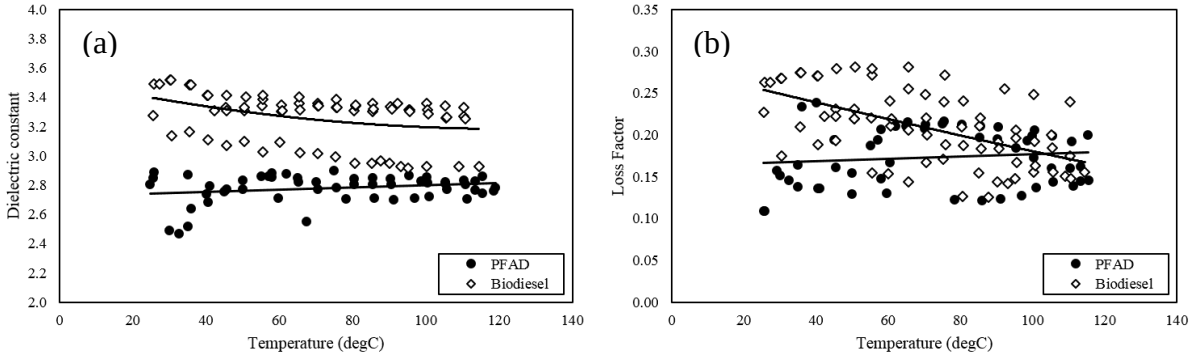

Figure 4.7 (a) Dielectric constant, and (b) loss factor measurement for PFAD and biodiesel at f = 2.45 GHz

The empirical equations for the respective dielectric properties of PFAD and biodiesel with respect to temperature (°C) are expressed as follows:

PFAD:

$$\varepsilon_r{}'_{\mathrm{PFAD}} = 0.008T + 2.7216 \tag{4.4}$$

$$\varepsilon_r{}''_{\mathrm{PFAD}} = 0.0001T + 0.1625 \tag{4.5}$$

Biodiesel:

$$\varepsilon_r{}'_{\mathrm{BD}} = 2e^{-5}T^2 - 0.0055T + 3.5216 \tag{4.6}$$

$$\varepsilon_r{}''_{\mathrm{BD}} = -0.001T + 0.2777 \tag{4.7}$$

Although both dielectric constant and loss factor of PFAD did not vary much across the temperature range, the effect of temperature on biodiesel was more obvious. While both values were observed to decrease with increasing temperature, the change in the values was considered insignificant (<0.6 for dielectric constant, <0.13 for loss factor). Hence for simplicity of modelling, the dielectric properties of PFAD and its biodiesel could be considered to be constant within the 25–120 °C temperature range. At 2.45 GHz, the average relative complex permittivity of PFAD was 2.78–0.17*j* while for biodiesel it was 3.26–0.21*j*.

4.7 Summary

The biodiesel yield obtained from the microwave-assisted esterification of PFAD feedstock was presented and discussed. The optimal parametric conditions for PFAD esterification at 1:9 methanol-to-oil molar ratio and 1 wt.% sulphuric acid catalyst loading were 900 s of 300 W microwave irradiation in order to produce 91.88% yield. In general, the biodiesel yield was positively correlated with both microwave irradiation time and microwave power levels. It was found that the reaction kinetics of the PFAD esterification became second order under microwave irradiation. The values of activation energy and pre-exponential factor at each microwave power level were determined as well. GC-FID analysis was conducted to identify the ester composition of PFAD. In addition, the dielectric constant and loss factor of PFAD biodiesel at 2.45 GHz microwave were also measured and reported.

CHAPTER 5 RESEARCH METHODOLOGY OF MICROWAVE-ASSISTED PFAD ESTERIFICATION SIMULATION

This chapter explains the model development of microwave-assisted PFAD esterification. The assumptions and limitations of the model are shown. The model description, the governing equations used as well as the input, boundary and initial conditions of the model are also specified. This chapter is published in Applied Energy journal, https://doi.org/10.1016/j.apenergy.2019.01.052

5.1 Assumptions and limitations of the model

The following assumptions were made in the current mathematical model:

1. Air would not be heated by microwave as it is microwave-transparent (i.e. $\varepsilon_r' = 1$) (Ratanadecho et al., 2002). The temperature of the air surrounding the reaction medium remains constant during the esterification process.
2. The PFAD and biodiesel remain in the liquid phase during the production process because of their relatively higher boiling points (i.e. >300 °C) at atmospheric pressure.
3. The liquid phase is assumed to be in the laminar regime due to the absence of mechanical stirring of the liquid.
4. Methanol and water vaporise due to their lower boiling points which are 64.7 °C and 100 °C respectively, under the standard atmospheric pressure.

5. The effect of boiling nucleation at high temperatures due to the insertion of the fibre optic probe into the liquid medium is neglected.
6. The liquid mixture is assumed to be a homogenous single phase solution (Selemani, 2018).

5.2 Model description

The computational domain consisted of a microwave oven cavity with the flask located in the middle, as shown in Figure 5.1. Only the bottom section of the flask, which contained the liquid sample, was included in the numerical model as the upper section contained only air, which was the same as the microwave oven domain. The esterification reaction was simulated in a liquid medium which was a mixture of PFAD, methanol, biodiesel, and water. The sulphuric acid catalyst was omitted from the model as it was neither consumed nor produced during the reaction. The microwave oven domain had been represented by an enclosed rectangular box with a rectangular waveguide attached on the right wall.

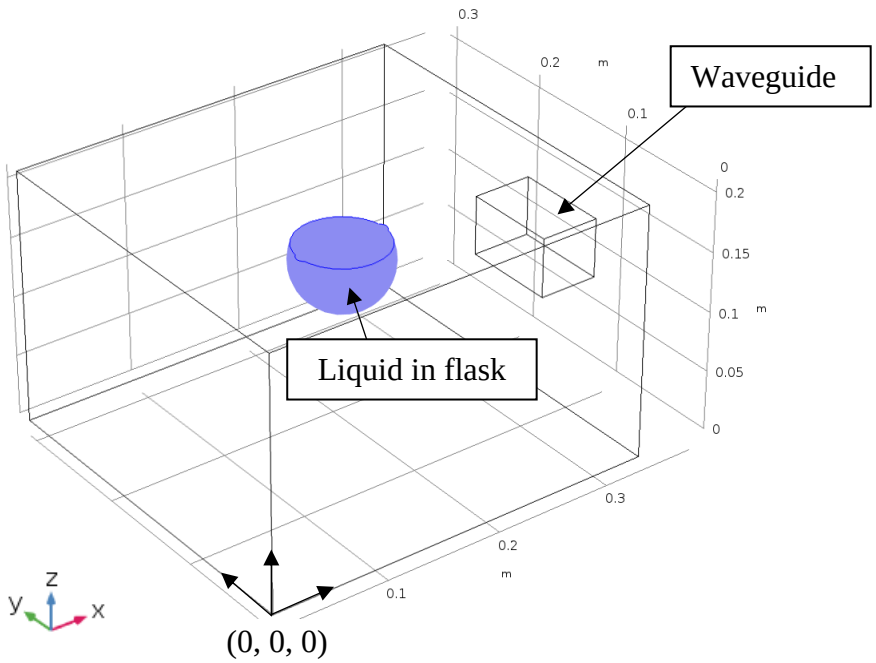

Figure 5.1 Esterification model

In the experiment, the temperature profile of the liquid was obtained using the fibre optic probe at a specific point as shown in Figure 3.1. Thus, the same location was chosen for temperature prediction in the model to facilitate result comparison. The Cartesian coordinate for this point was 0.142 m (x) × 0.152 m (y) × 0.155 m (z), as shown in Figure 5.2.

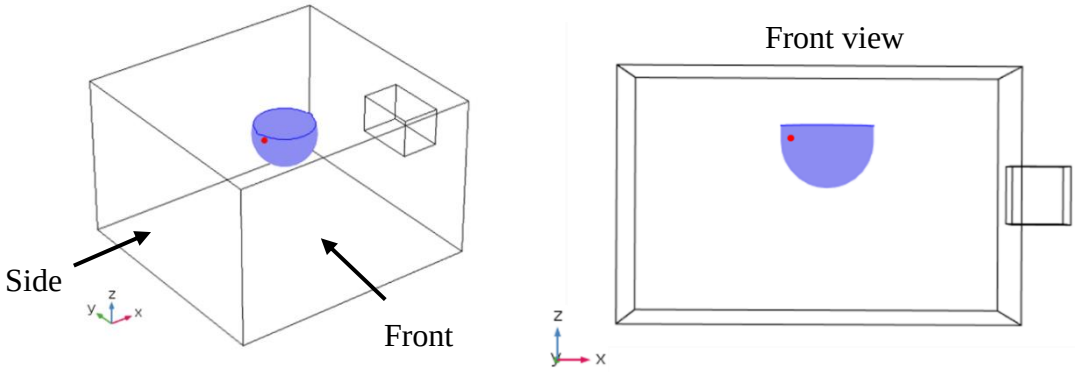

Figure 5.2 Temperature measuring point

The microwave generated by the magnetron was modelled as a plane wave emitted from the waveguide. It was transmitted from the waveguide into the oven cavity to heat up the reaction mixture in the flask. The liquid underwent cyclical volumetric heating which resulted in temperature fluctuations during the reaction process. As the microwave heating continued, the liquid temperature continued to increase and exceeded the boiling point of methanol (64.7 °C). A part of the liquid methanol boiled and vaporised; this was subsequently cooled and condensed by a reflux system (not modelled in the numerical model) and returned to the flask. This effect of vaporisation and condensation of methanol would prevent further increase in the liquid temperature and cause the temperature to oscillate within a constant range, unless extra heat energy was supplied to or lost from the system.

Without any stirring mechanism involved in the system, microwave heating would lead to uneven temperature distribution in the liquid due to the formation of hot and cold spots caused by the alternating electric field. Hence, the local temperature at certain parts of the liquid might exceed the boiling point of water, causing the water to vaporise. Therefore, the vaporisation effect of water was included.

5.3 Governing equations

The current model solves for the electric field distribution, mass, momentum, energy, and energy balance of the liquid mixture.

5.3.1 Electromagnetic field

The electromagnetic wave distribution inside the modified microwave oven was governed by Maxwell's equations. The wave equation can be expressed as (Law et al., 2016):

$$\nabla \times \left(\nabla \times \mathbf{E} \right) - \omega^2 \kappa \varepsilon \mathbf{E} = 0 \tag{5.1}$$

where ω, κ and ε are the angular frequency, magnetic permeability and complex permittivity of a material, respectively. This equation was solved for the entire computational domain which included the microwave cavity and biodiesel liquid mixture.

5.3.2 Mass-momentum conservation

Navier-Stokes equations solved for the mass and momentum conservation of the liquid phase of the biodiesel liquid mixture. In the absence of an external mixing mechanism, the system was assumed to operate under laminar flow condition. Thus, the equations were as follows (COMSOL Inc.):

$$\partial \rho / \partial t + \nabla \cdot \left(\rho \mathbf{u} \right) = 0 \tag{5.2}$$

$$\rho \, \partial \mathbf{u} / \partial t + \rho \mathbf{u} \cdot \nabla \mathbf{u} = -\nabla p + \left[\mu \left(\nabla \mathbf{u} + \left(\nabla \mathbf{u} \right)^T \right) - 2/3 \left(\mu \left(\nabla \cdot \mathbf{u} \right) \right) \right] - \rho \mathbf{g} \tag{5.3}$$

where μ is the molecular viscosity coefficient, and **g** is the gravitational acceleration.

5.3.3 Chemical species conservation

In this study, the following species were calculated: PFAD, methanol, biodiesel, and water. The conservations of the concentration of each species are expressed as follows:

$$\frac{\partial c_{\mathrm{PFAD}}}{\partial t}+\nabla\cdot\left(-D^{m}_{\mathrm{PFAD}}\nabla c_{\mathrm{PFAD}}\right)+\mathbf{u}\cdot\nabla c_{\mathrm{PFAD}}=\dot{R}_{\mathrm{PFAD}} \tag{5.4}$$

$$\frac{\partial c_{\mathrm{MeOH}}}{\partial t}+\nabla\cdot\left(-D^{m}_{\mathrm{MeOH}}\nabla c_{\mathrm{MeOH}}\right)+\mathbf{u}\cdot\nabla c_{\mathrm{MeOH}}=\dot{R}_{\mathrm{MeOH},\,vap} \tag{5.5}$$

$$\frac{\partial c_{\mathrm{BD}}}{\partial t}+\nabla\cdot\left(-D^{m}_{\mathrm{BD}}\nabla c_{\mathrm{BD}}\right)+\mathbf{u}\cdot\nabla c_{\mathrm{BD}}=\dot{R}_{\mathrm{BD}} \tag{5.6}$$

$$\frac{\partial c_{\mathrm{H_2O}}}{\partial t}+\nabla\cdot\left(-D^{m}_{\mathrm{H_2O}}\nabla c_{\mathrm{H_2O}}\right)+\mathbf{u}\cdot\nabla c_{\mathrm{H_2O}}=\dot{R}_{\mathrm{H_2O},\,vap} \tag{5.7}$$

The first term on the left-hand side of Equations (5.4) – (5.7) referred to the changes in the concentration of the species with time. The second term accounted for the diffusive interaction between the dilute species and the solvent, while the third term described the convective transport of the species due to the velocity field **u**. The reaction kinetic terms were on the right-hand side of the equations. These reaction kinetics were discussed in the following section.

The FAME, $\mathrm{R\text{-}COOCH_3}$ was produced via the following chemical reaction (Leung et al., 2010):

$$\mathrm{R\text{-}COOH+CH_3OH \rightarrow R\text{-}COOCH_3+H_2O} \tag{5.8}$$

The reaction between the PFAD (R-COOH) and methanol (CH_3OH) produced FAME and water (H_2O). For PFAD, the effective reaction rate for esterification with second-order reaction kinetics, could be expressed as follows:

$$\dot{R}_{\mathrm{PFAD}}=-k_r[\mathrm{PFAD}]^2=-A\exp\left(\frac{-E_a}{R_U T}\right)[\mathrm{PFAD}]^2 \tag{5.9}$$

The negative sign indicated that the amount of PFAD decreased as the reaction proceeded.

Furthermore, biodiesel was produced at the same rate as the PFAD according to Equation (5.8):

$$\dot{R}_{\mathrm{BD}} = -\dot{R}_{\mathrm{PFAD}} = A\exp\left(\frac{-E_a}{RT}\right)\left[\mathrm{PFAD}\right]^2 \tag{5.10}$$

In the current model, only methanol and water experienced a phase change as they vaporised during the biodiesel production, while FAME and PFAD were assumed to remain in the liquid phase because their boiling points are greater than 300 °C, which were beyond the operating temperature range (i.e. between 38 °C and < 100 °C) of this reaction. Thus, $\dot{R}_{i,vap} = 0$ for FAME and PFAD.

The vaporisation rate, $\dot{R}_{\mathrm{MeOH},vap}$ for methanol was calculated as follows:

$$\dot{R}_{\mathrm{MeOH},vap} = -A_{\mathrm{MeOH}} e^{\frac{-E_{\mathrm{MeOH}}}{R_U T}} \left(c_{\mathrm{MeOH}} - c_{\mathrm{MeOH},sat}\right) \tag{5.11}$$

where $c_{\mathrm{MeOH},sat}$ is the saturation concentration (mol m^{-3}) of methanol, and c_{MeOH} (mol m^{-3}) is the concentration of methanol at any time during the reaction. The vaporisation of methanol occurred when T > 64.7 °C.

The vaporisation rate, $\dot{R}_{\mathrm{H_2O},vap}$ for water was calculated as follows:

$$\dot{R}_{\mathrm{H_2O},vap} = -k_{c,\mathrm{H_2O}} \left(c_{\mathrm{H_2O}} - c_{\mathrm{H_2O},sat}\right) \tag{5.12}$$

where $k_{c,\mathrm{H_2O}}$ is the mass transfer coefficient (s^{-1}) of water. This vaporisation effect occurred when T > 100 °C.

The saturation concentration of vapour was calculated as:

$$c_{i,sat} = \frac{P_{i,sat}}{RT} \tag{5.13}$$

The saturation pressure, $P_{i,sat}$ (mm Hg), was calculated using the Antoine equation as follows (Dortmund Data Bank, 2018):

$$P_{i,sat} = 10^{A-\frac{B}{T+C}} \tag{5.14}$$

The numerical values of the constants A, B, and C for water and methanol were listed in Table 5.1, along with the valid temperature range.

Table 5.1 Antoine equation parameters for water and methanol (Dortmund Data Bank, 2018)

Material	**A**	**B**	**C**	**Temperature Range (°C)**
Water	8.07131	1730.63	233.426	1 – 100
Water	8.14019	1810.94	244.485	> 100
Methanol	8.08097	1582.27	239.700	15 – 100
Methanol	7.97010	1521.23	234.000	> 100

Mass transfer due to concentration gradient between the liquid-air interface had not been considered in this study; and the phase changes of methanol and water were assumed to take place throughout the volume of the liquid, as a result of the volumetric heating of the microwave.

5.3.4 Energy conservation

The heat transfer in the liquid phase was described by Fourier energy equation as follows (COMSOL Inc.):

$$\rho c_p \frac{\partial T}{\partial t} + \rho c_p \mathbf{u} \cdot \nabla T - \nabla \cdot (k \nabla T) = \dot{Q}_{MW} + \dot{Q}_{\Delta H} - \sum \Delta H_{i,vap} \dot{R}_{i,vap} \tag{5.15}$$

The microwave heating effect, $\dot{Q}_{MW}$ is a function of the absorbed electric field as well as the dielectric loss factor. For instance, during the experiment, the microwave power at 300 W was switched on for 13 s and subsequently switched off for 17 s in a single cycle. The heat source could imitate the cyclic pattern by multiplying the electromagnetic heat source term with a periodic piecewise function, as follows:

At 300W,

$$\dot{Q}_{MW} = \begin{cases} 2\pi f \varepsilon_0 \varepsilon_r'' |\mathbf{E}|^2 & \text{if} \quad 0 \le t < 13 \\ 0 & \text{if} \quad 13 \le t \le 30 \end{cases} \tag{5.16}$$

At 240W,

$$\dot{Q}_{MW} = \begin{cases} 2\pi f \varepsilon_0 \varepsilon_r'' |\mathbf{E}|^2 & \text{if} \quad 0 \le t < 12 \\ 0 & \text{if} \quad 12 \le t \le 30 \end{cases} \tag{5.17}$$

At 100W,

$$\dot{Q}_{MW} = \begin{cases} 2\pi f \varepsilon_0 \varepsilon_r'' |\mathbf{E}|^2 & \text{if} \quad 0 \le t < 10 \\ 0 & \text{if} \quad 10 \le t \le 30 \end{cases} \tag{5.18}$$

Enthalpy change occurred in the system when the reactants were transformed into products via esterification (exothermic). This introduced a heat source, $\dot{Q}_{\Delta H}$ into the system, which is expressed as follows:

$$\dot{Q}_{\Delta H} = \Delta H_r \dot{R} \tag{5.19}$$

The heat source from the exothermic esterification reduced as the reaction proceeded. The enthalpy of reaction was equivalent to the total sum of the enthalpy of formation of liquid for each methyl ester in the biodiesel, according to Hess Law and their respective mole fractions. The net enthalpy of reaction was calculated to be -8.60 kJ/mol at std condition.

During the reaction, a reflux system resulted in the condensation of the vapour back into the reaction mixture. This cooling effect had been accommodated by the vaporisation function of methanol and water, which was represented by the third term on the right-hand side of Equation (5.15).

On the other hand, the complex permittivity, ε of a liquid mixture depended on the molar fraction of each individual component. Thus, ε was calculated as the sum of the product of the molar fraction and the relative complex permittivity of a species *i*, which is expressed as follows:

$$\varepsilon = \varepsilon_0 \sum_{i=1}^{4} \left(x_i \varepsilon_{r,i} \right) \tag{5.20}$$

$$\varepsilon_r = \varepsilon_r' - j\varepsilon_r'' \tag{5.21}$$

where ε_0 is the permittivity of free space (8.854×10^{-12} F/m) and x_i is the molar fraction. The relative complex permittivity, ε_r, consists of a real part, ε_r', and a complex part, ε_r'', which are known as the dielectric constant and loss factor, respectively (Law et al., 2016). The dielectric constant indicates the electrical energy storage capacity of the material whilst the dielectric loss factor expresses the degree of conversion of the stored electrical energy that is released in the form of heat.

The molar fraction x_i, is determined by the ratio of the individual species concentration to the total concentration, as shown in Equation (5.22).

$$x_i = \frac{c_i}{c_{tot}} \tag{5.22}$$

The dynamic viscosity, thermal conductivity, specific heat capacity and density of the liquid mixture were also calculated based on the molar-averaged principle, which are expressed as follows:

$$\mu = \sum_i x_i \mu_i \tag{5.23}$$

$$k = \sum_i x_i k_i \tag{5.24}$$

$$c_p = \sum_i x_i c_{p,i} \tag{5.25}$$

$$\rho = \sum_i x_i \rho_i \tag{5.26}$$

5.4 Input, boundary and initial conditions

The input parameters for the model were listed in Table 5.2.

Table 5.2 Input details of the esterification model

Parameters	**Unit**	**Value**	
Oven dimension	mm	330 (w) × 309 (d) × 211 (h)	
Waveguide	mm	45 (w) × 85 (d) × 56 (h)	
Flask diameter	mm	80	
Material properties	**Symbol**	**Unit**	**Value**
Specific heat capacity of methanol (Central, 2010)	$c_{p,\mathrm{MeOH}}$	J kg^{-1} K^{-1}	2520
Density of methanol (National Center for Biotechnology Information, 2004)	ρ_{MeOH}	kg/m^3	792
Thermal conductivity of methanol (Engineering ToolBox, 2008)	k_{MeOH}	W m^{-1} K^{-1}	0.20
Dynamic viscosity of MeOH @70^{o}C (Alam et al., 2018)	μ_{MeOH}	mPa.s	0.34
Complex relative permittivity of MeOH (Singh, 2010)	$\varepsilon_{\mathrm{MeOH}}$	-	26.39-10j
Enthalpy of vaporisation of methanol (Wu et al., 2013)	$\Delta H_{\mathrm{MeOH},vap}$	J/mol	35210
Specific heat capacity of PFAD*	$c_{p,\mathrm{PFAD}}$	J kg^{-1} K^{-1}	2183
Density of PFAD*	ρ_{PFAD}	kg/m^3	885.6
Thermal conductivity of PFAD (Chempro)	k_{PFAD}	W m^{-1} K^{-1}	0.17
Dynamic viscosity of PFAD (Chempro)	μ_{PFAD}	mPa.s	12.75
Complex relative permittivity of PFAD*	$\varepsilon_{\mathrm{PFAD}}$	-	2.78-0.17j
Specific heat capacity of biodiesel (Jaimes et al., 2010)	$c_{p,\mathrm{BD}}$	J kg^{-1} K^{-1}	1880
Density of biodiesel*	ρ_{BD}	kg/m^3	879
Thermal conductivity of biodiesel (Saeed et al., 2017)	k_{BD}	W m^{-1} K^{-1}	0.18
Dynamic viscosity of biodiesel (Pratas et al., 2010)	μ_{BD}	mPa.s	2.10
Complex relative permittivity of biodiesel*	$\varepsilon_{\mathrm{BD}}$	-	3.26-0.21j
Specific heat capacity of water (Engineering ToolBox, 2003)	$c_{p,\mathrm{H_2O}}$	J kg^{-1} K^{-1}	4184
Density of water (Engineering ToolBox, 2003)	$\rho_{\mathrm{H_2O}}$	kg/m^3	1000

Material properties	Symbol	Unit	Value
Thermal conductivity of water @70°C (Engineering ToolBox, 2018)	k_{H_2O}	W m^{-1} K^{-1}	0.66
Dynamic viscosity of water @70°C (Alam et al., 2018)	μ_{H_2O}	mPa.s	0.42
Complex relative permittivity of water (Komarov et al., 2005)	ε_{H_2O}	-	78-12.5j
Enthalpy of vaporisation of water (Nakamura et al., 2005)	$\Delta H_{H_2O,vap}$	J/mol	40650
Enthalpy of reaction*	ΔH_r	J/mol	8603
Initial concentration of methanol*	$c_{0,MeOH}$	mol/m^3	13657.48
Initial concentration of PFAD*	$c_{0,PFAD}$	mol/m^3	1517.5
Diffusion coefficient of methanol (Derlacki et al., 1985)	D^m_{MeOH}	m^2/s	2.1×10^{-9}
Diffusion coefficient of PFAD*	D^m_{PFAD}	m^2/s	1×10^{-9}
Diffusion coefficient of biodiesel*	D^m_{BD}	m^2/s	1×10^{-9}
Diffusion coefficient of water (Derlacki et al., 1985)	$D^m_{H_2O}$	m^2/s	2.1×10^{-9}

**in this work*

5.4.1 Maxwell's equations

As the skin depth of the oven walls (metal) is much smaller than the dimensions of the microwave oven, therefore, the electromagnetic fields penetrate a negligible distance into the walls. Hence, it is not necessary to solve Maxwell's equations for the inside of the walls. In other words, the wave did not penetrate through the object. The interaction between the oven walls and microwave irradiance was described by an impedance boundary condition. For microwave irradiance travelling through any arbitrary medium 1 to medium 2, the equation is expressed as follows (Law et al., 2018):

$$\frac{1}{\mu_{r1}}\mathbf{n}\times\left(\nabla\times\mathbf{E}\right)-\frac{jk_0}{\eta}\mathbf{n}\times\left(\mathbf{n}\times\mathbf{E}\right)=0 \tag{5.27}$$

where $k_0=\omega\sqrt{\varepsilon_0\mu_0}$ and $\eta=\sqrt{\mu_{r2}/\varepsilon_{r2}}$.

For the interaction between microwave irradiance and the glass flask, the following equations were implemented to ensure continuity between the electric field strength and displacement current density, $\mathbf{D}$ ($= \varepsilon \mathbf{E}$) (Thidé, 2004), which is expressed as follows:

$$\mathbf{n} \times \left(\mathbf{E}_1 - \mathbf{E}_2 \right) = 0 \tag{5.28}$$

$$\mathbf{n} \cdot \left(\mathbf{D}_1 - \mathbf{D}_2 \right) = 0 \tag{5.29}$$

At 2.45 GHz microwave frequency, the propagating mode through the waveguide is specified to be TE_{10} mode.

5.4.2 Mass – momentum conservation equations

A no slip condition was applied between the liquid and the wall of the flask, and atmospheric pressure was applied at the interface between the liquid and gas.

5.4.3 Species conservation equation

The mixture of the four components was considered as a single phase solution (Selemani, 2018). The initial concentrations of PFAD and methanol were presented in Table 5.2, while the initial concentrations of FAME and water were set to zero. As esterification occurred, the concentrations of FAME and water (products) increased while those of PFAD and methanol (reactants) decreased.

5.4.4 Energy conservation equation

The temperature of the liquid mixture is also affected by the heat loss to the environment. Two main heat loss mechanisms — convection and radiation were considered in this study (COMSOL Inc., 2012):

$$-\mathbf{n} \cdot \left(k \nabla T \right) = h_c \left(T_\infty - T_{ref} \right) + \gamma \sigma \left(T_\infty^4 - T_{ref}^4 \right) \tag{5.30}$$

The convective coefficient, h_c was assumed to be 28 W/(m^2.K) (Conti et al., 2014). The reference temperature, T_{ref} , in the microwave oven cavity was taken as 298 K. The emissivity, γ, of glass was taken as 0.84 (Carwile & Hoge, 1966), while the value of σ is 5.67×10^{-8} W.m^{-2}.K^{-4}.

5.5 Summary

The development details of the numerical model for microwave-assisted PFAD esterification was covered in this chapter. The model consisted of a flask which was filled with the reaction mixture of PFAD feedstock and methanol that located inside a microwave oven cavity. The multiphysics model was governed by electromagnetic propagation (Maxwell's equations), mass-momentum (Navier-Stokes equations), chemical species, and energy conservations (heat transfer). The important input parameters, boundary, initial conditions, as well as the limitations of the model were also specified in the chapter.

CHAPTER 6 SIMULATION RESULTS & ANALYSIS OF MICROWAVE-ASSISTED PFAD ESTERIFICATION

In this chapter, the simulation results obtained from the numerical model of microwave-assisted PFAD esterification are discussed. This chapter is published in Applied Energy journal, https://doi.org/10.1016/j.apenergy.2019.01.052

6.1 Grip independence study

The model was calculated using a workstation with 14 cores and 2.3 GHz clock speed processor (Intel Xeon CPU E5-2695 @ 2.3 GHz). A frequency-transient solver was used to simulate the reaction for 1200 s at intervals of 5 s. The simulation solved Maxwell's equations in the frequency domain, while the other equations were solved transiently.

The element type used in this model was free tetrahedral. The mesh setting was user-controlled and the element size was calibrated to the default setting for fluid dynamics. To examine the effect of mesh size refinement on the model solution, the temperature profile of the process using different mesh sizes was studied, as shown in Figure 6.1.

The mesh with the lowest number of elements (28971, coarse) was studied first, followed by normal mesh (92229 elements), and fine mesh (193330 elements). Overall, the temperature profiles for all the three configurations were similar during the entire 1200 s of simulated time. This indicates that the mesh size did not have an adverse effect on the simulated temperature profile. However, there was a distinct difference in the actual computational time required by each mesh. The computational time for the coarse mesh

was the highest, which was 36.7 h; while for a normal mesh it took only 11 h to complete the simulation. The time taken by a fine mesh was 14.5 h. The reason for the unusually high computational time for the coarse mesh was due to the higher residual error, which badly affected the convergence, thereby prolonging the solving process. As the mesh size was refined to normal setting, the simulation time was reduced by 70%. However, with further refinement, the simulation time increased by another 3.5 h because the number of elements doubled and therefore, higher computational time was required. Hence, the simulation model with 92229 elements was sufficient to obtain satisfactory results while taking the computational cost into consideration.

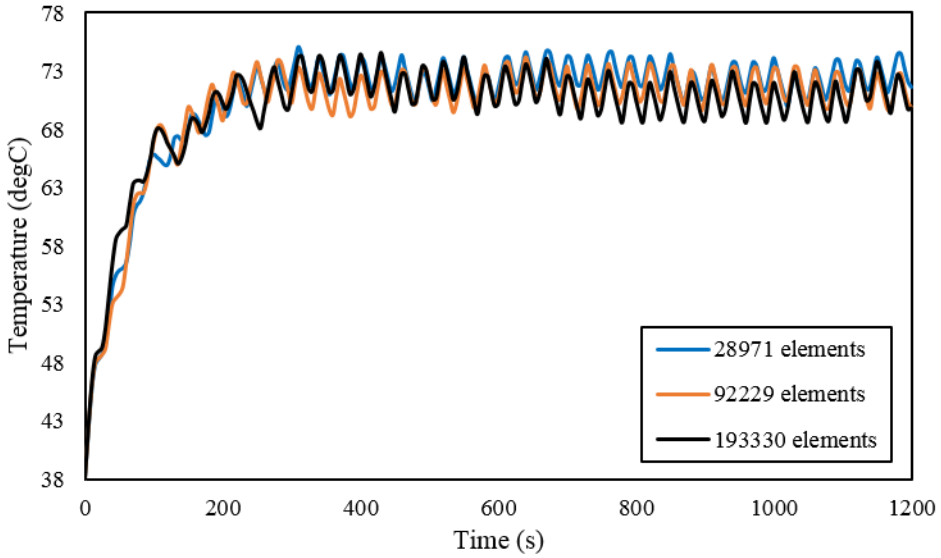

Figure 6.1 Effect of mesh size refinement on temperature change

6.2 Model Results

The simulation results were divided into two sections. The first section discussed the phenomena that were obtained from the numerical model at 300 W microwave power level. In the second section, the models simulated under 100 W and 240 W were compared with the 300 W model, such that the similarities and differences under three microwave power levels were obtained and discussed.

6.2.1 Esterification model under 300 W microwave power

Figure 6.2 shows the experimental and simulation temperatures during the esterification at the temperature measuring point (see Figure 5.2). Apparently, both temperature profiles have similar patterns. The average error of the temperature prediction was found to be less than 3% (unit in Kelvin). Since this model is developed for the first time, there is no solid reference for a general rule of thumb for an acceptable margin of error for the simulation. With the percentage error lower than 3%, it was presumed that the model provides good agreement with the experimental results.

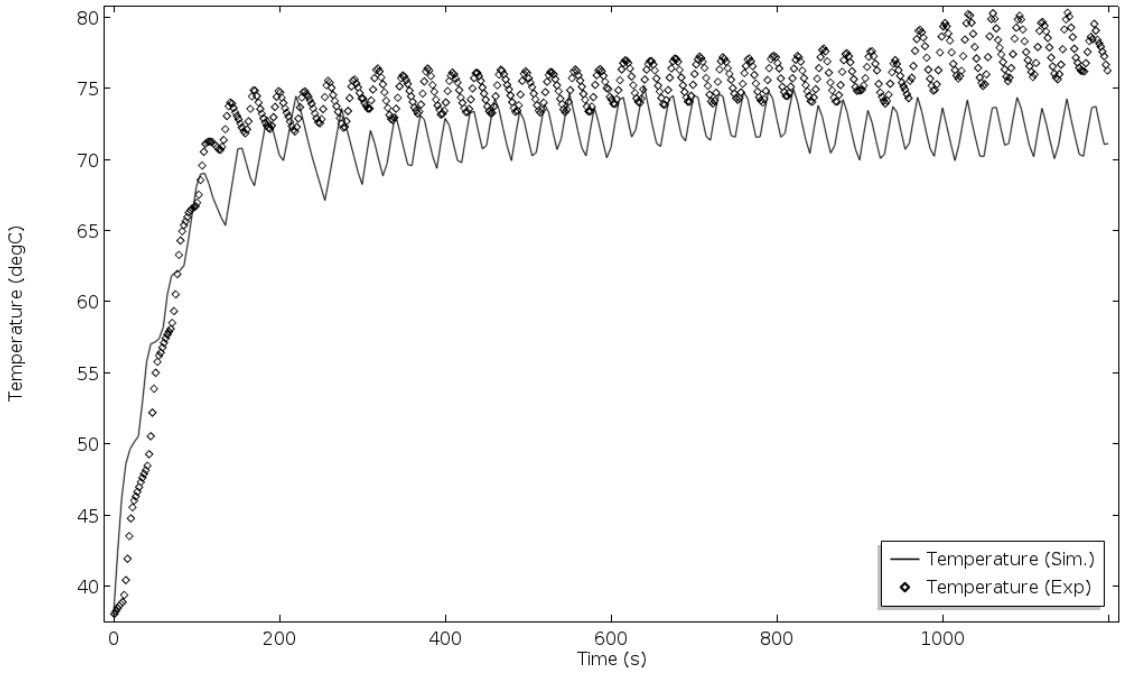

Figure 6.2 Temperature profile during PFAD esterification at 300 W microwave power

In the experiment, the temperature of the reaction mixture surged quickly from 38 °C to above 70 °C in less than 150 s. This rapid heating rate was due to the presence of a large amount of methanol — a polar solvent with a high dielectric constant and loss factor. Methanol absorbed the electrical energy from the microwave, and released them into the reaction mixture, which subsequently increased the temperature. After the stage of rapid temperature increment, some of the methanol was observed to vaporise during the

experiment. The reflux system had condensed a considerable amount of methanol vapour and continuously returned them to the flask throughout the experiment. Under this reflux condition, the system had reached its steady state where the reaction temperature became relatively stable and oscillated within the range of 71–80 °C, which was around 6 to 15 °C higher than the usual boiling point of methanol. The temperature did not rise higher in spite of the subsequent pulsed microwave heating.

Under normal circumstances, all the liquid methanol in the mixture should have turned into vapour before the reaction temperature could rise higher, as methanol has a normal boiling point of 64.7 °C. However, it is well known that microwave dielectric heating would lead to the superheating of a liquid where the temperature of the liquid rises above its boiling point without boiling. This phenomenon coincided with the results found by Chemat and Esveld (2001). They reported that the liquid methanol experienced superheating, even when the fibre optic probe had provided a nucleation site for the formation of bubbles that promote flow disturbance. This phenomenon of bubbles germination was reported to reduce the magnitude of the superheating temperature range of pure methanol from 14 °C to 5–6 °C. The experimental temperature profile in Figure 6.2 showed that the superheated temperature range could still increase to 15 °C above the boiling point of methanol when the microwave was switched on. Thus, the flow disturbance caused by the bubbles is assumed to be rather insignificant and therefore, can be ignored in a simplified esterification model.

Figure 6.2 shows that the reaction temperature could decrease by as much as 4 °C in a single cycle when the microwave energy is intermittently turned off. This is due to the presence of other heat transfer mechanisms, such as the vaporisation-condensation phenomenon of methanol and water, as well as the radiation loss or convective loss across the flask surface. The vaporisation rate of methanol was included in this model as the reaction temperature mostly occurred above the normal boiling point of methanol. Therefore, a large amount of heat energy would be absorbed by the methanol molecules as they converted into gaseous phase. As a result of this phase change, the methanol vapour would consume a significant amount of heat energy from the mixture, contributing

to the drop in the reaction temperature. Since there is no literature data available for the vaporisation rate of methanol and water under microwave irradiation, the A_{MeOH} and E_{MeOH} values in Equation (5.11) and $k_{\mathrm{H_2O}}$ value in Equation (5.12) were fine-tuned against the temperature measurement data. The values for A_{MeOH}, E_{MeOH} and $k_{\mathrm{H_2O}}$ were found to be 2×10^5 s^{-1}, 54500 J/mol and 0.001 s^{-1}, respectively.

It is evident from Figure 6.2 that the major heat source which increased the reaction temperature was the microwave energy generated from the magnetron of the microwave oven. Figure 6.3 depicts the volume-averaged power density generated from the cyclic microwave power.

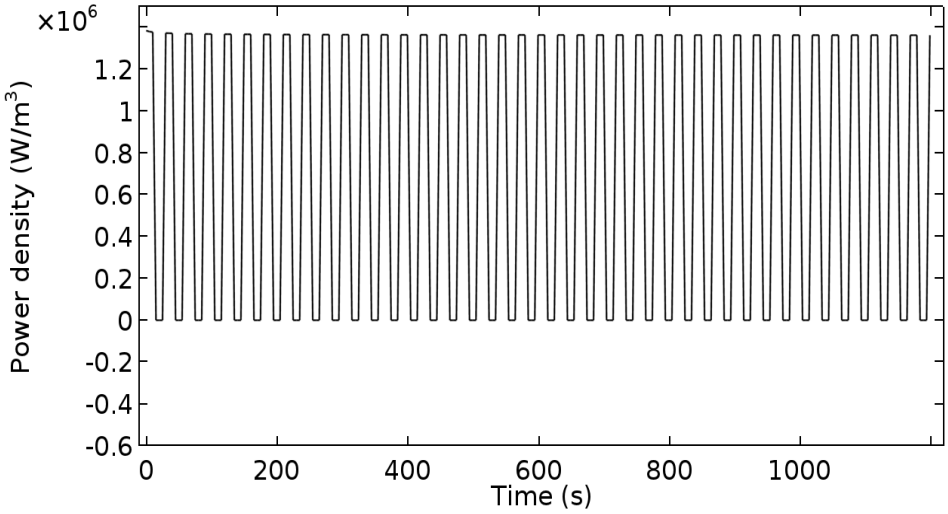

Figure 6.3 Power density of microwave heating during PFAD esterification

As denoted in Equation (5.16), only 13 s of microwave energy was supplied to the reaction mixture in a single 30 s cycle; and over the 1200 s period, there were 40 such cycles; thus, the effective microwave irradiation time was only 520 s. Nonetheless, the microwave power had provided a high dosage of heat energy to the reaction mixture, with the power density instantaneously reaching a value as high as 1.38×10^6 W/m^3. However, not all parts of the liquid experienced uniform microwave heating. As shown in Figure

6.4, a higher density of microwave power focused on the central region as well as the upper left region (close to the surface) of the liquid.

It is well known that microwave would create hot and cold spot regions inside the microwave oven cavity due to the constructive and destructive interference of the electromagnetic waves. Figure 6.5 illustrates the electric field distributions inside an empty microwave oven, as well as inside the microwave oven after placing a flask in it (see Figure 5.1), in three cross-sectional views, i.e. the *xy*-, *yz*-, and *xz*-planes.

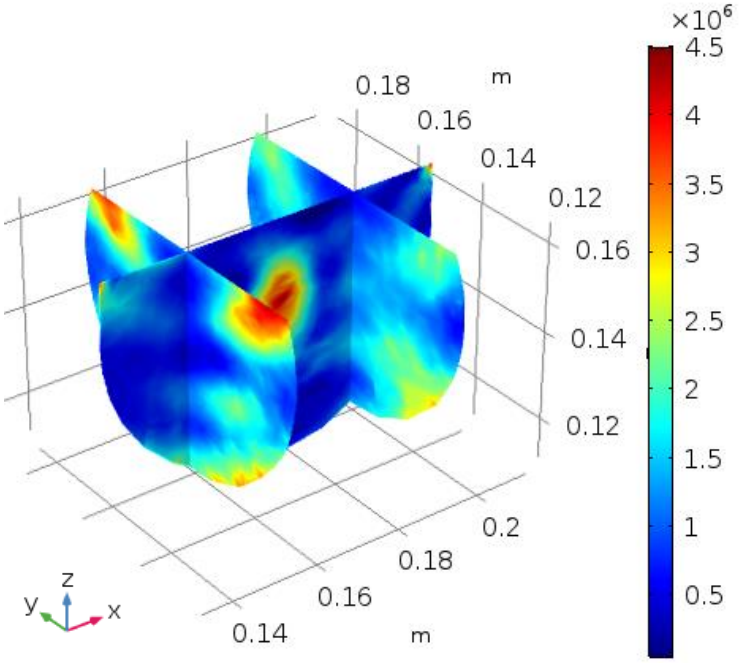

Figure 6.4 Power density distribution (W/m^3) in liquid (300 W)

According to Kesbi et al. (2018), it is possible to obtain the inner electric field intensity by measuring the surface temperature changes of the sample with a non-contact infrared thermometer and then perform theoretical analysis on the data, only if the microwave is acting as a plane wave normal to the sample surface. However, the microwave in this experiment is not always normal to the sample surface. This makes it difficult to validate the electric field intensity results via experimental approach. Thus, the electric field

distribution as well as the electric field vector (as shown in Figure 6.6) in the liquid were investigated using simulation approach only.

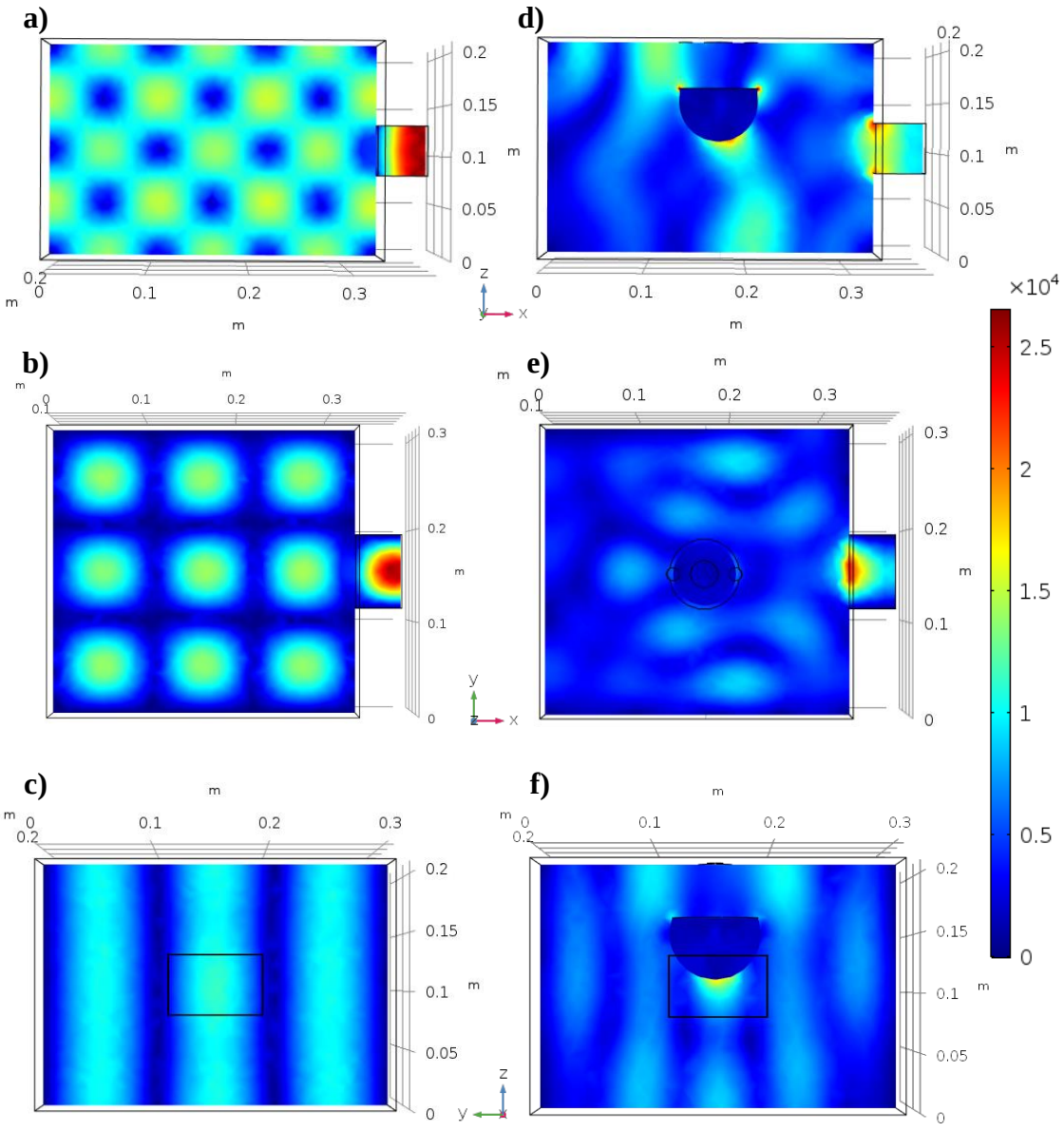

Figure 6.5 Electric field distribution (V/m) of 300 W in the empty microwave oven: a) front view, b) top view, c) side view; and in the microwave oven with flask: d) front view, e) top view, f) side view

In an empty microwave oven, the electric field distributions were observed to be very organised in all the planes, and the hot and cold spot regions could also be clearly distinguished. However, when the flask was placed inside the oven, the electric field distribution was heavily disturbed, as shown in Figure 6.5(d), (e), and (f). The pattern of the hot and cold spots had entirely changed and the overall strength of the electric field had decreased. This was due to the absorption of microwave energy by the reaction mixture. As shown in Figure 6.5(d), the intensity of the electric field was higher at the waveguide, the upper left region, and the bottom right region of the flask. Meanwhile, Figure 6.5(e) shows a stronger electric field at the waveguide, as well as around the flask; however, the strength of the electric field near the left wall of the microwave oven is observed to be weak. Figure 6.5(f) shows a stronger electric field focused near the bottom of the flask and a small area near the surface of the liquid. Further down the back wall or on the door side of the microwave oven, the electric field is observed to be weaker.

Figure 6.6 shows the electric field vectors within the reaction mixture in the *yz*-plane. Apparently, the electric field pattern remains the same at t = 20 s and t = 500 s; and only the electric field intensity gradually changes over time. At t = 20 s, strong electric field is observed on both sides close to the bottom of the flask, as well as in the region towards the right of the central region, as indicated by the red coloured vectors. With increasing time, the electric field near the bottom region is observed to become weaker, while the electric field at the central region becomes stronger. This shift in the local electric field strength would result in a higher heating rate at the central region of the liquid, which translates to increased temperature.

Apart from the heat energy supplied from the magnetron of the microwave oven, there were other heat sources and heat sinks that also affected the temperature of the liquid. In total, there were two heat sources (microwave, reaction enthalpy), two heat sinks (methanol vaporisation, water vaporisation) and two heat fluxes across the flask surface (convective loss, radiation loss). Figure 6.7 shows the reaction enthalpy (heat source) and the net vaporisation of methanol and water (heat sinks) while the heat fluxes are shown in Figure 6.8.

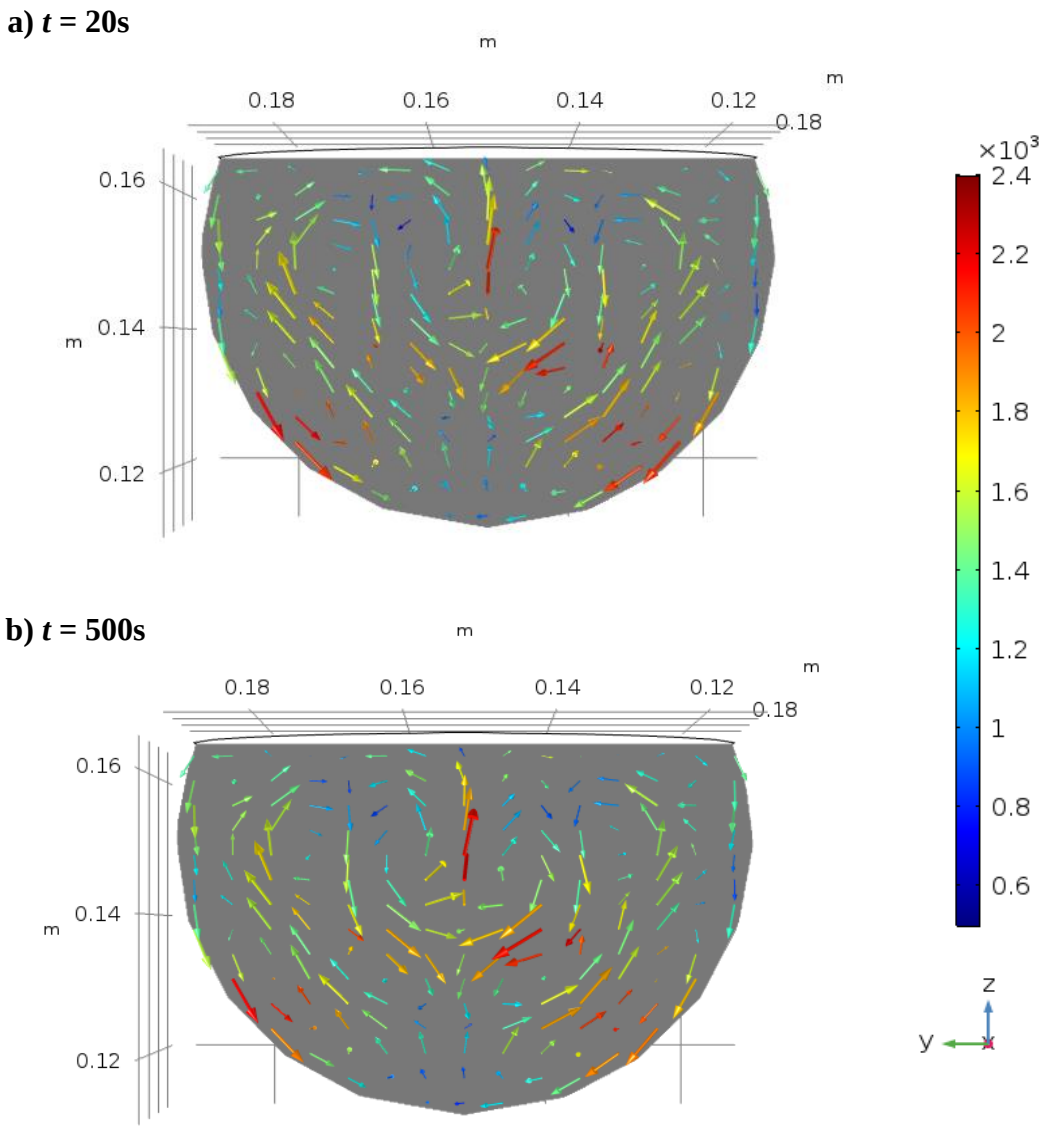

Figure 6.6 Electric field vector (V/m) in the liquid (in the *yz*-plane) at 300 W when a) *t* = 20 s; and b) *t* = 500 s

The heat energy provided by the reaction enthalpy was the highest at the beginning of the process as esterification occurred rapidly during that time. After most of the PFAD had reacted to form biodiesel, the heat released from the reaction enthalpy quickly diminished and approached zero as the process continued. Thus, the amount of heat generated decreased rapidly as the reaction slowed down. In the meantime, the system temperature

had reached the boiling point of methanol. This triggered the vaporisation effect of methanol, causing a high amount of net heat loss in the system. Subsequently, the liquid temperature decreased while microwave power was temporarily switched off in the 30 s cycle. The heat loss due to the vaporisation of water was observed to be minimal and could be neglected. This indicates that the local temperature in any part of the liquid could hardly reach 100 °C.

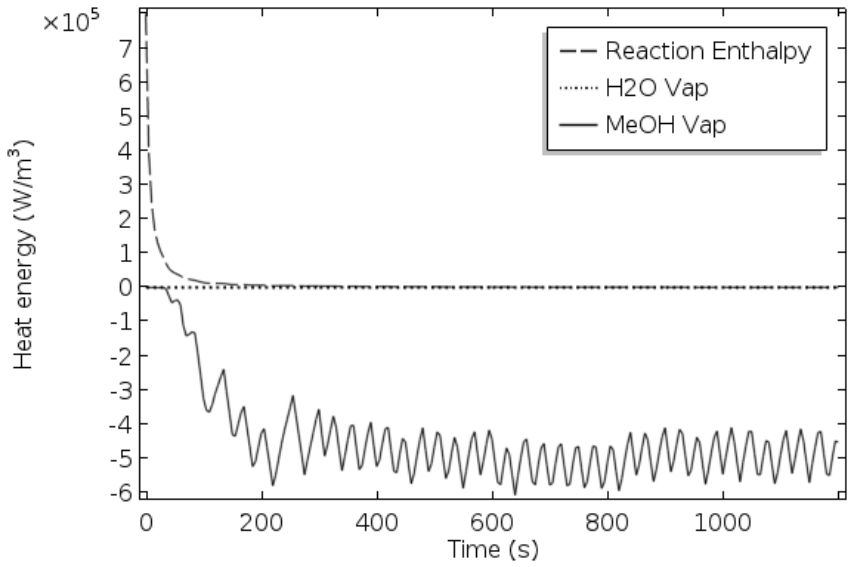

Figure 6.7 Other heat source and heat sinks in PFAD esterification

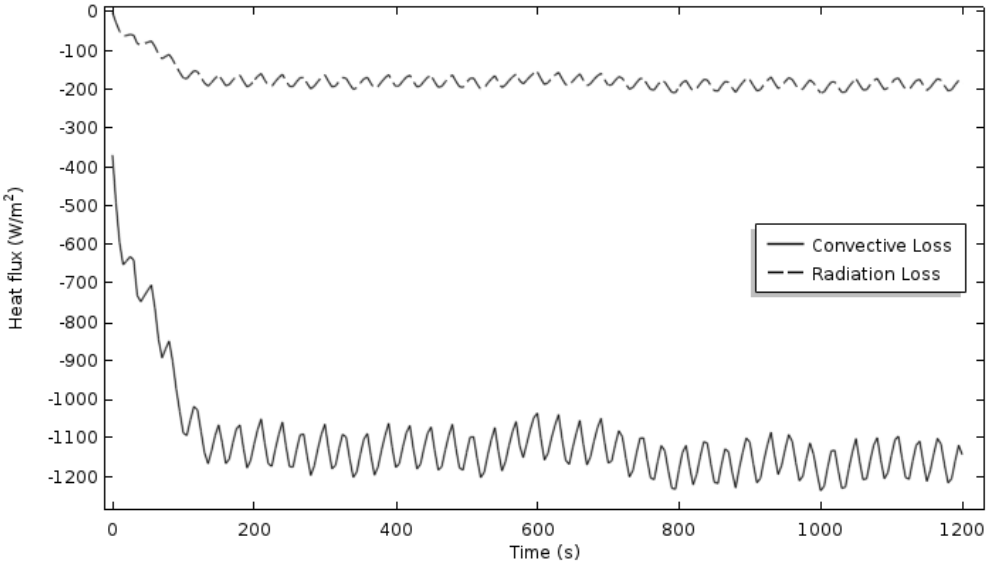

Figure 6.8 Heat fluxes in PFAD esterification (300 W)

On the other hand, the heat energy that was stored in the liquid was also lost through convection and radiation via the glass flask. The heat flux profile in Figure 6.8 shows that convective loss had a higher contribution to the temperature change in the liquid than thermal radiation loss. Due to the convective loss the liquid near the wall of the flask was cooler compared to the central region of the liquid. This effect is clearly visible in Figure 6.9, which shows the temperature distribution in the reaction mixture for four different timeframes.

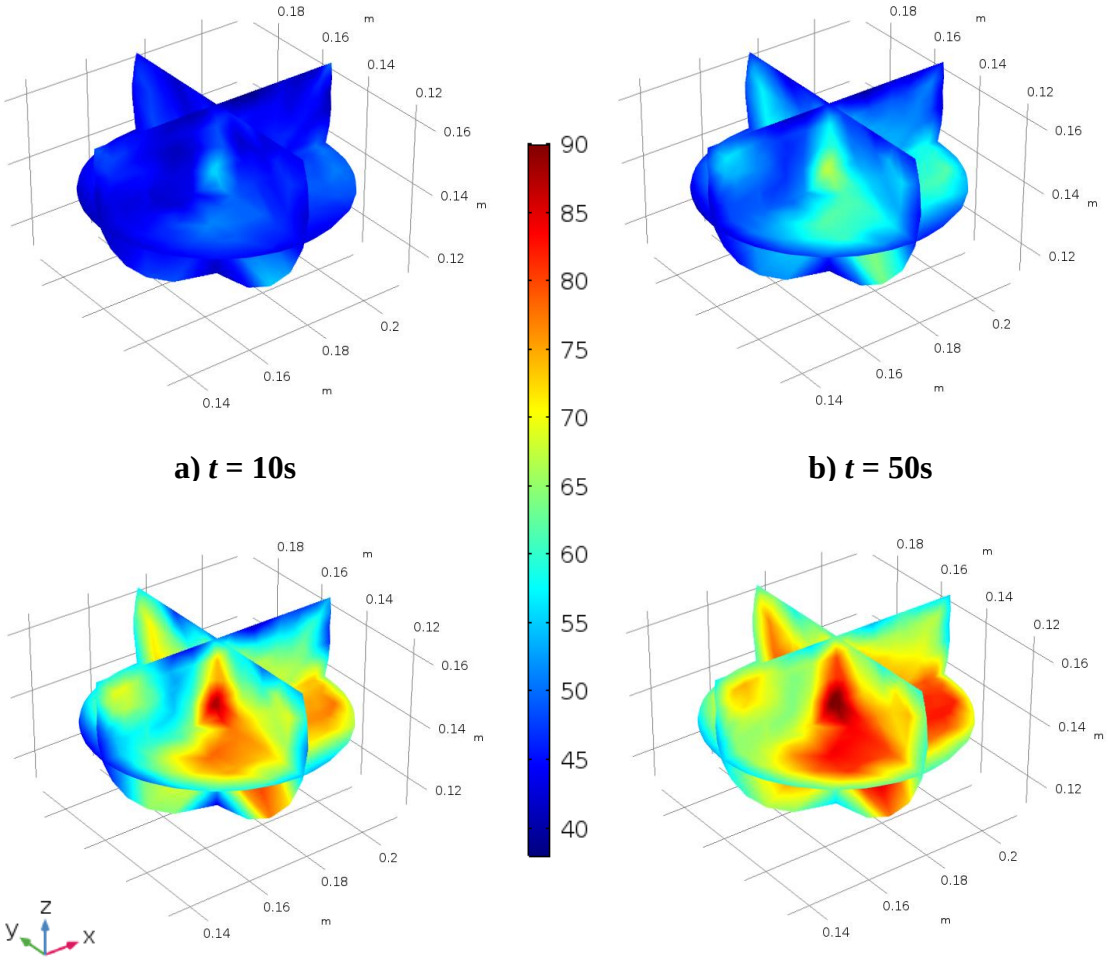

Figure 6.9 Temperature distribution (°C) of reaction mixture during 300 W microwave-assisted esterification (1:9 molar ratio) at a) t = 10 s; b) t = 50 s; c) t = 100 s; and d) t = 500 s

The electric field distribution (see Figure 6.5) due to the presence of the reaction mixture in the microwave oven was found to correlate with the temperature distribution within the liquid. Initially, the temperature of the liquid was 38 ^{o}C. After 10 s of microwave irradiation, the liquid temperature at the centre began to rise due to volumetric heating effect of the microwave. When t = 50 s, part of the liquid that is closer to the waveguide (cyan region) is observed to heat up faster compared to the left side of the flask. The location where the temperature was the highest, is found to correspond to the strongest electric field, as shown in Figure 6.5(d) and (f). A higher temperature is also observed at the upper left section of the liquid where the electric field is stronger. The temperature distribution of the fluid remained uneven throughout the simulation time, indicating that the fluid velocity, which can promote temperature homogenisation, was very weak.

According to Asada et al. (2015), the velocity resulted from convection could be monitored using Particle Imaging Velocimetry technique during the experiment. However, this technique was not adopted due to equipment constraints whereby the optical fibre could not be placed close to the liquid medium within the microwave cavity of the domestic microwave oven. Therefore, the velocity field in the liquid is studied with this numerical model only, as illustrated in Figure 6.10.

The highest velocity magnitude recorded was only 1.38×10^{-4} m/s which occurred at t = 5 s, indicating that the convection in the reaction mixture was very weak. At t = 0 s, the esterification reaction had not yet occurred; and hence, the velocity vectors were seen pointing downwards. This was mainly due to the gravitational acceleration term as indicated in Equation (5.3). At t = 5 s, the rapid chemical reaction caused liquid motion due to the density change in the reaction mixture.

As listed in Table 5.2, the densities of the four species were assumed to be temperature independent (constant values). Thus, the density differences would only occur when the esterification took place. During the initial stage of the reaction, there was a rapid change in the species concentration. The reactants (PFAD and methanol) were quickly converted into the products (biodiesel and water). Consequently, the density, along with other thermophysical properties (see Figure 6.11) of the reaction mixture, were changing as

well. As the reaction rate decreased, so did the convection within the liquid. The liquid motion disappeared gradually as shown in Figure 6.10(c), (d), (e) and (f). This caused the velocity in the liquid to gradually diminish over the period of time.

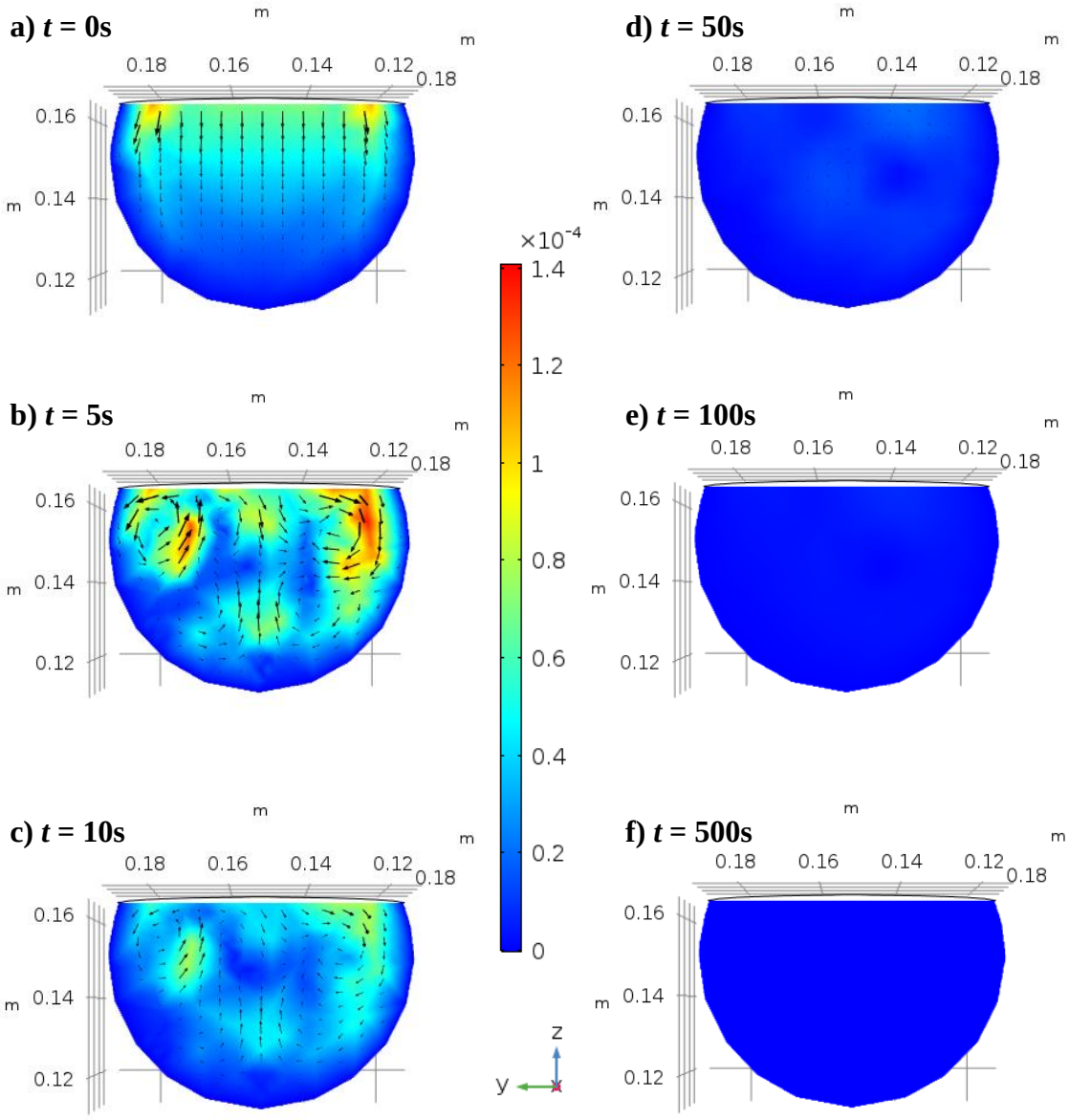

Figure 6.10 Velocity field in liquid (m/s) in *yz*-plane at 300 W microwave irradiation when a) t = 0 s; b) t = 5 s; c) t = 10 s; d) t = 50 s; e) t = 100 s; and f) t = 500 s

Figure 6.11 shows that the esterification would increase the values of c_p, ρ, and k of the reaction mixture. In contrast, the μ value of the liquid decreased as the PFAD, which has the highest μ among all the species, was being consumed. Apart from these parameters, the dielectric properties of the reaction mixture were changing as well. As shown in Figure 6.12, the dielectric constant increased by 20%, i.e. from 24 to 29, while the loss factor only reduced 2.2%, i.e. from -9.02 to -9.26. It is noteworthy that these changes were solely caused by the esterification reaction as the dielectric properties of the four species were assumed to be temperature independent. The significant increase in the dielectric constant, indicates that the reaction mixture would become a better dielectric and harness a greater amount of electrical energy from the microwave at the end of the reaction.

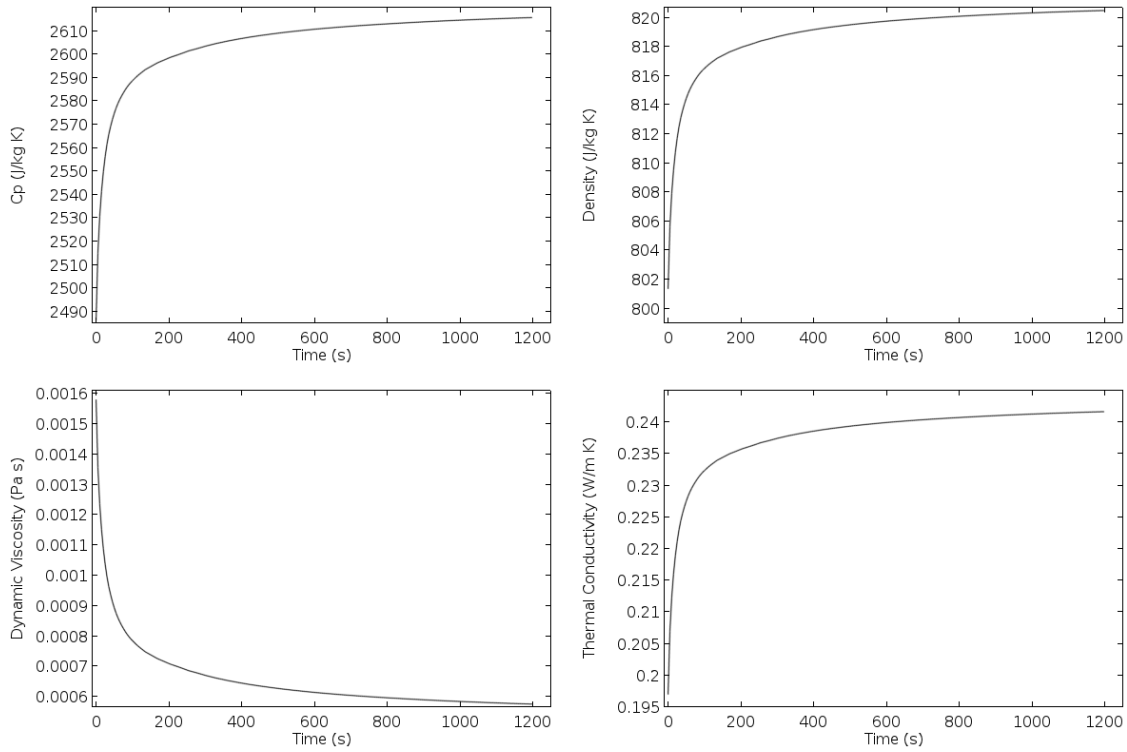

Figure 6.11 Change in thermophysical properties (c_p, σ, μ and k) of the reaction mixture during esterification

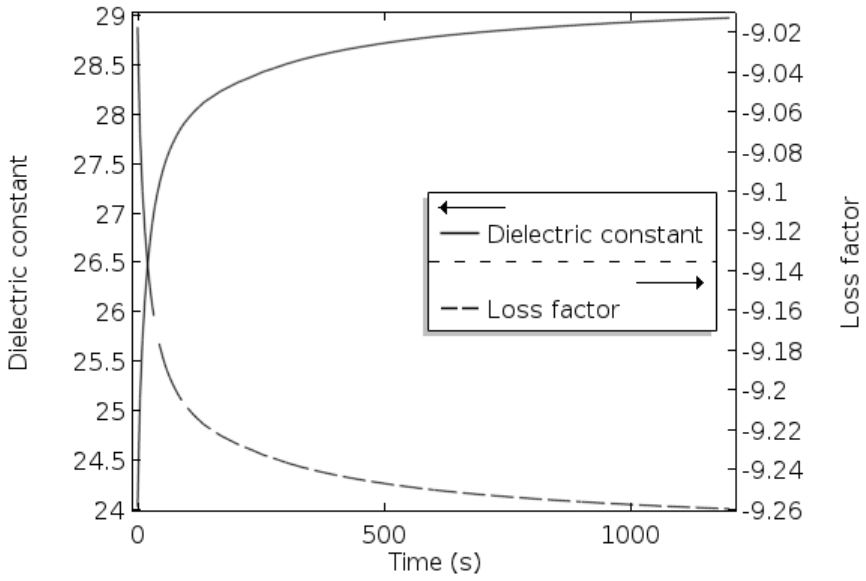

Figure 6.12 Dielectric properties of the reaction mixture during esterification

6.2.2 Effect of microwave power level on PFAD esterification

The effect of microwave power level on the PFAD esterification were further investigated via numerical method. Figure 6.13 shows the simulated and experimental temperature profiles of the PFAD esterification at 100 W and 240 W. By comparing Figure 6.13(a) with Figure 6.13(b), it is observed that as the reaction temperature became relatively steadier (when methanol begins to vaporize), the temperature variation within each cycle also reduced as the microwave power level reduced. The change in the temperature within a single ON/OFF cycle at 100 W was only ± 1 °C, but at 240 W, it varied by ± 3 °C, which was still lower than the 4 °C at 300 W.

The simulated temperature profiles during the initial heating stage at 100 W (up to 300 s) and 240 W (up to 150 s) were over-predicted when compared to the experimental results. In contrast to numerical simulation, there would be inevitable loss in the microwave power that were absorbed by the liquid during experiments which lead to lower heating rate. Hence, the simulated temperature values were higher. In addition, it could be difficult to precisely simulate the actual localised heating phenomenon that occurred at the location

of a single temperature measuring point in the experiment. Therefore, the temperature values at the temperature measuring point could be over predicted.

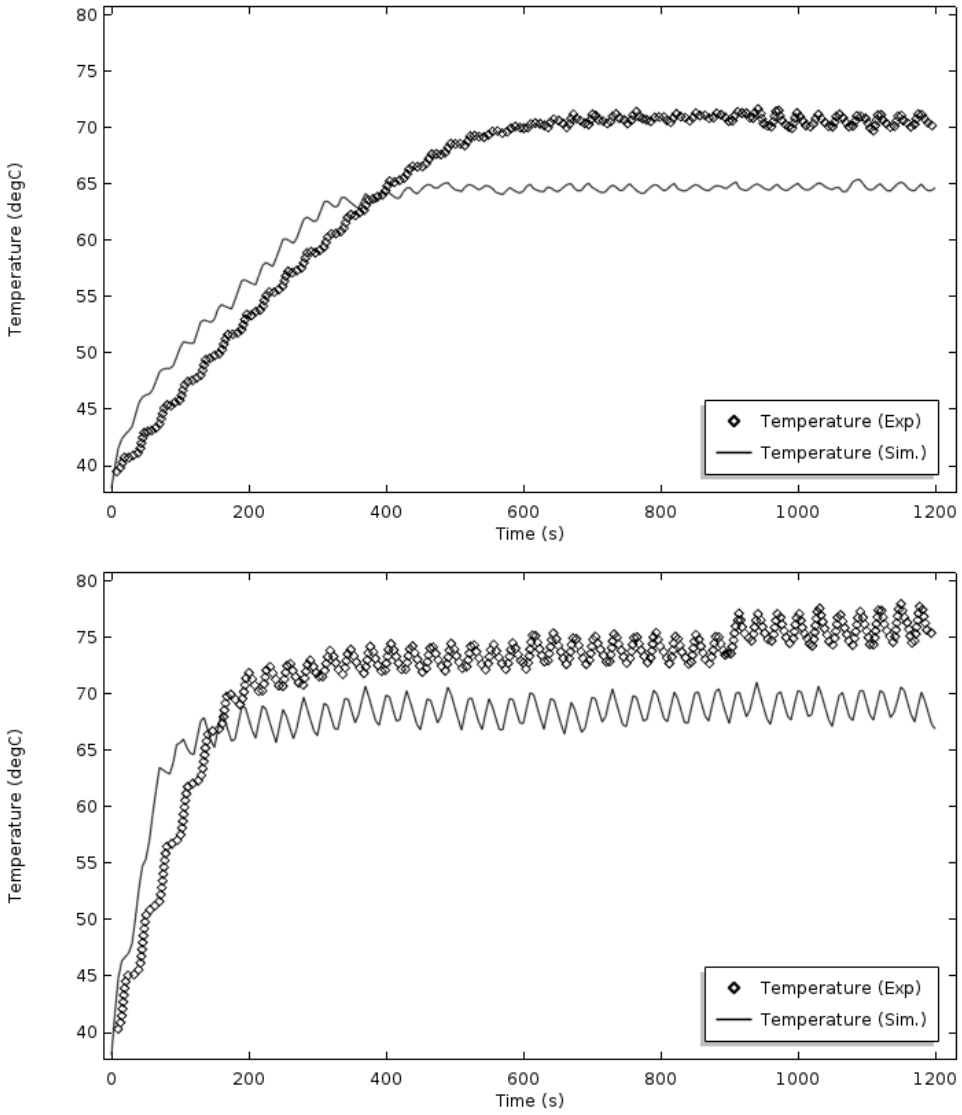

Figure 6.13 Simulated and experimental temperature profiles during PFAD esterification at a) 100 W (top); and b) 240 W (bottom) microwave power level

However, it was observed that the predicted temperature values became lower than the experimental profiles after the system reached its steady state. This was possible as the

vaporization effect of methanol began to involve in the model. As observed from the experimental profiles, the temperature profile became stable around 70 °C (100 W) or above (240 W & 300 W). This indicated that the methanol in the reaction mixture were superheated due to the microwave irradiation. In the simulation setting, the vaporization rate of methanol was set to occur right after the liquid temperature exceeded 64.7 °C, which was valid under normal circumstances without microwave irradiation. Based on the simulated temperature profiles in Figure 6.13(a), the vaporisation of methanol could be set to occur at 70 °C, about 5 °C higher than the its boiling point as a measure to cater the effect of microwave in superheating methanol. This could help in producing closer prediction over the temperature profile. Furthermore, the complex relative permittivity of methanol and water (refer Table 5.2) were assumed to be temperature independent constants, for model simplification. This could be another reason which contribute to the overestimation of temperature values at the beginning stage and under prediction at the later stage of microwave heating respectively. Nonetheless, the overall patterns between the experimental and simulated temperature profiles were in good agreement.

The changes in the temperature distribution within the reaction mixture under 100 W and 240 W at various times are shown in Figure 6.14. Similar to Figure 6.9, the result shows that the highest temperature were observed at the centre region of the reaction mixture with the temperature decreasing towards the side walls of the flask. Obviously, with higher amount of energy supplied from the microwave electric field, the temperature difference within the reaction mixture under 240 W microwave irradiation was more drastic as compared to under 100 W.

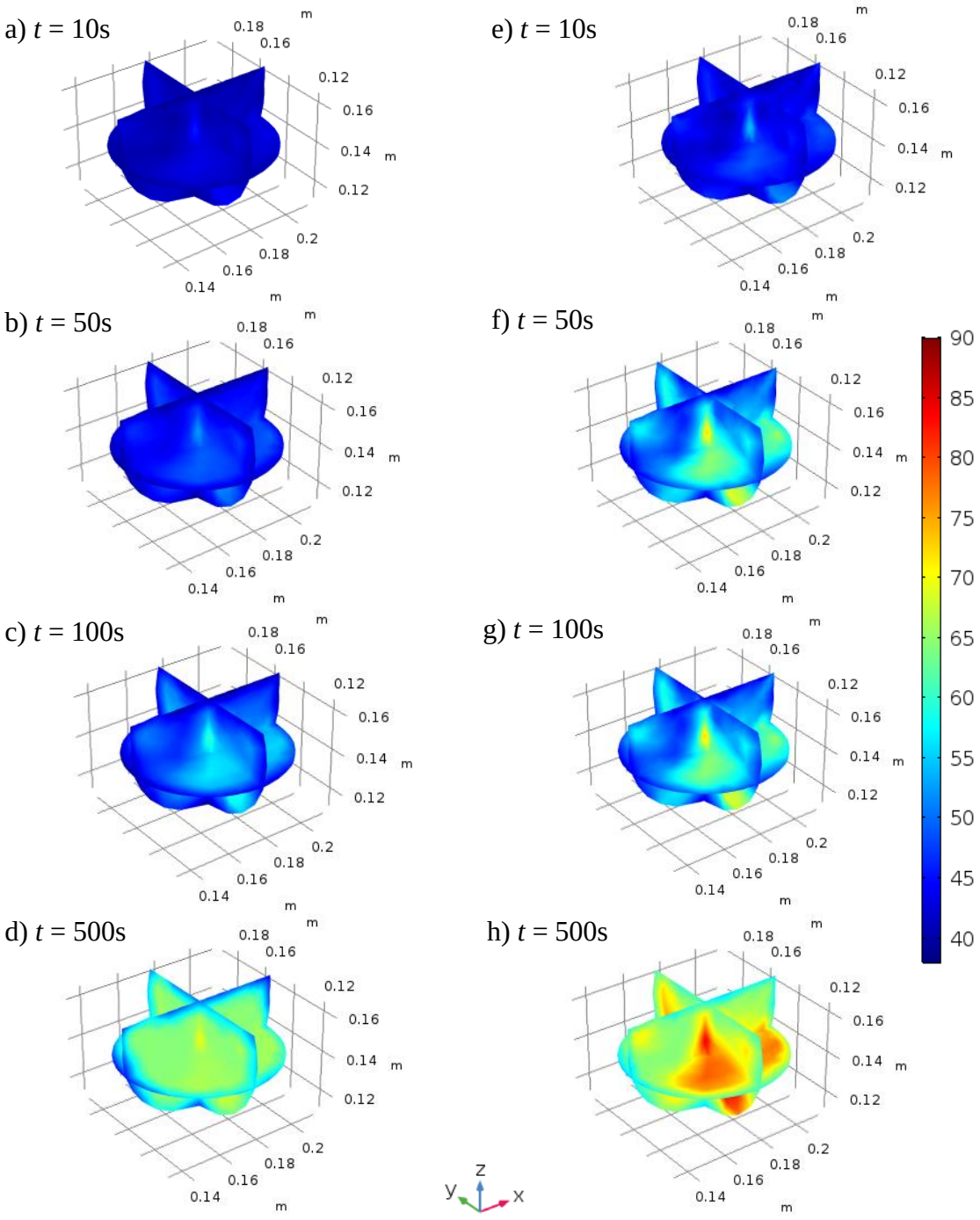

Figure 6.14 Temperature distribution (°C) of reaction mixture during 100 W at a) *t* = 10 s; b) *t* = 50 s; c) *t* = 100 s; d) *t* = 500 s; and 240 W at e) *t* = 10 s; f) *t* = 50 s; g) *t* = 100 s; h) *t* = 500 s

Over the 1200 s period, the effective microwave irradiation time was 400 s for 100 W and 480 s for 240 W. The volume-averaged instantaneous power density at 100W was 4.52×10^5 W/m^3, which was one third of the power density at 300 W and the instantaneous power density at 240W was 1.09×10^6 W/m^3. As shown in Figure 6.15, the patterns of the power density distribution at 100 W and 240 W were similar to 300 W (see Figure 6.4), with the only difference in their magnitudes. Same also applies to the electric field distribution and the electric field vectors. As illustrated in Figure 6.16, it is found that the patterns of the electric field distribution at 100 W and 240 W were the same as 300 W (see Figure 6.5). The vectors in the electric fields at Figure 6.17 shows that the electric field magnitude slowly increased as time progressed from 20 s to 500 s, especially at the central region of the liquid. As the dielectric constant of the reaction mixture increased from 24.5 to 28.7, the electric field energy which could be absorbed also increased.

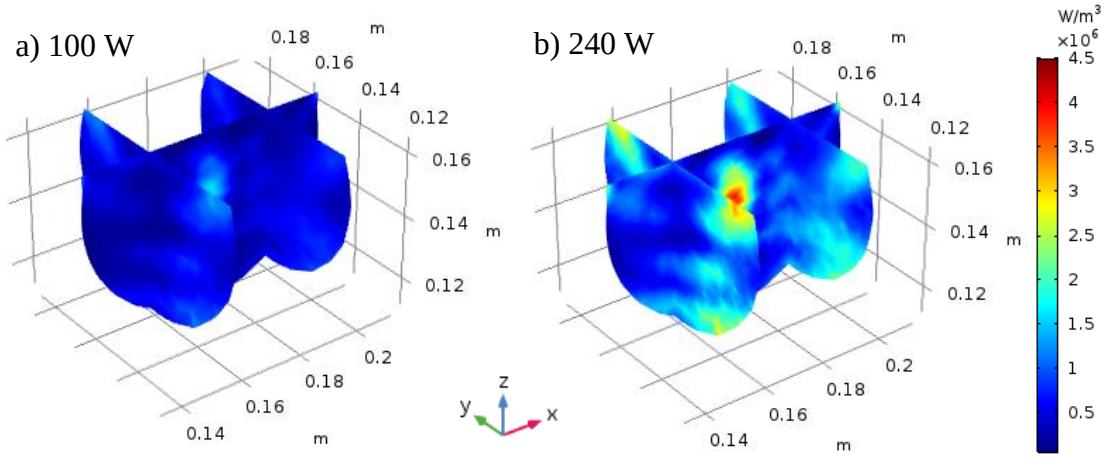

Figure 6.15 Power density distribution (W/m^3) in liquid at a) 100 W and b) 240 W microwave power

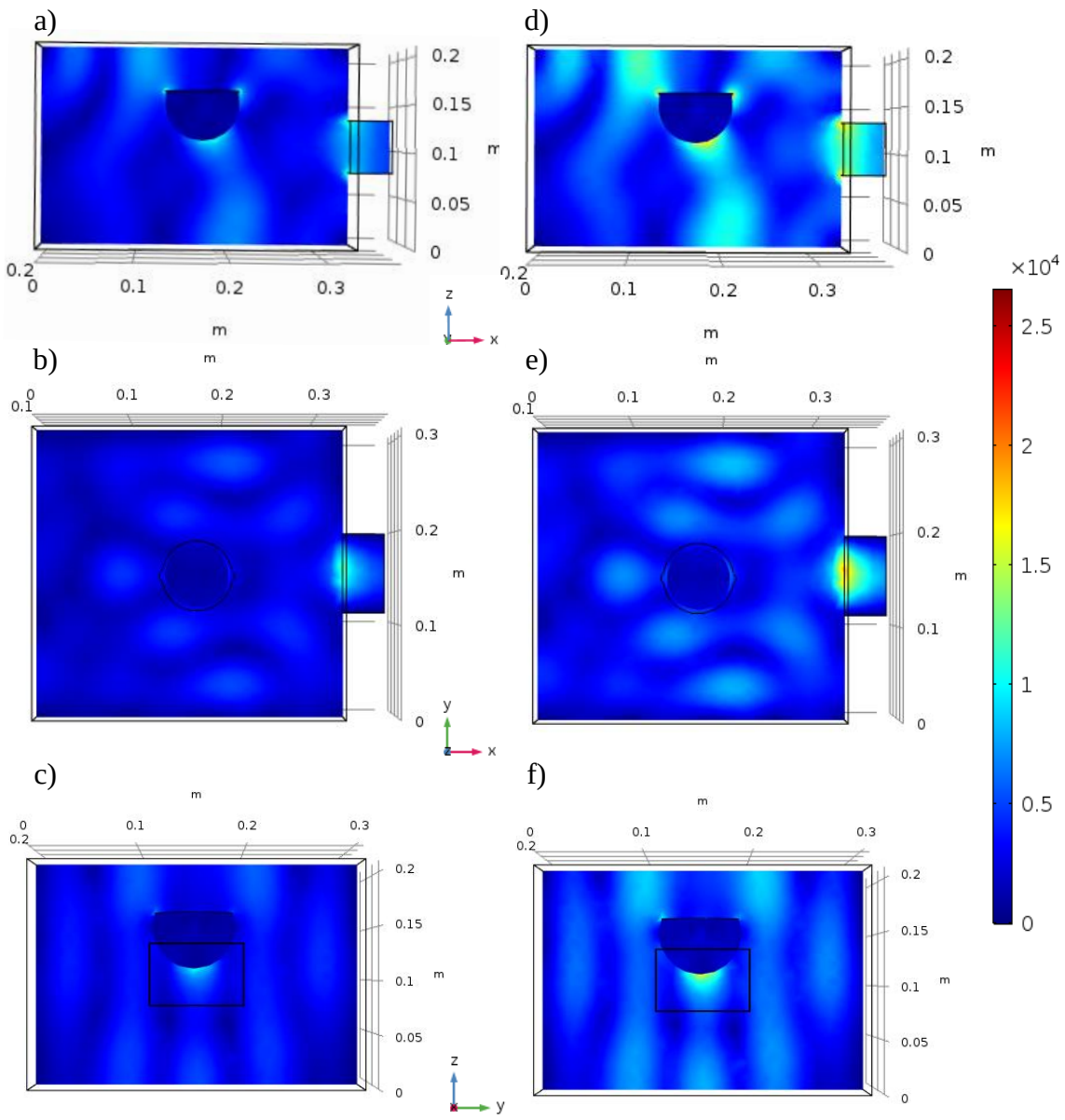

Figure 6.16 Electric field distribution (V/m) under microwave power of 100 W: a) front view, b) top view, c) side view; and of 240 W: d) front view, e) top view, f) side view

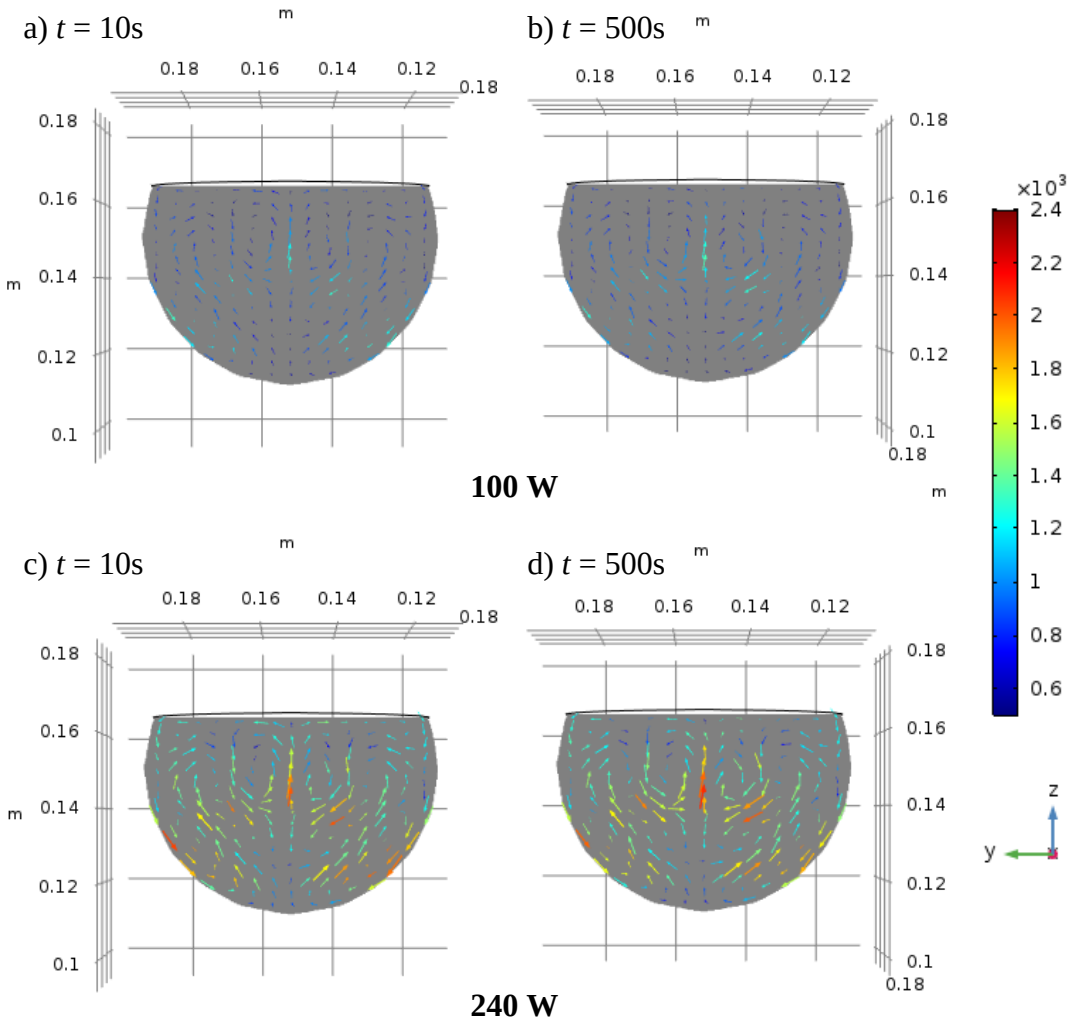

Figure 6.17 Electric field vector (V/m) in the liquid (in the *yz*-plane) at 100 W when a) *t* = 20 s; b) *t* = 500 s; and at 240 W when c) *t* = 20 s; and d) *t* = 500 s

Apart from the microwave power, the other heat source (reaction enthalpy) and heat sinks (vaporization of methanol and water) which affect the heating during the PFAD esterification under 100 W and 240 W microwave irradiation were depicted in Figure 6.18. The reaction enthalpy also contributed to the rise of temperature during the initial heating stage. The initial value of the reaction enthalpy was not affected by the microwave power levels as this energy source was decided by the concentration of the reactants. This heat source quickly decayed after most of the esterification reaction took place. Then, this was

followed by the vaporisation of methanol when the reaction temperature exceeded the boiling point of methanol. The heat energy released from the methanol vaporization at 100 W was within 2×10^5 W/m^3. As for the case of 240 W, the heat loss increased more than double to within 5×10^5 W/m^3. The vaporisation of water at both 100 W and 240 W were negligible. This implies that the heat sink due to vaporisation of water could be safely neglected from the model as the temperature of the reaction mixture did not exceed the boiling point of water.

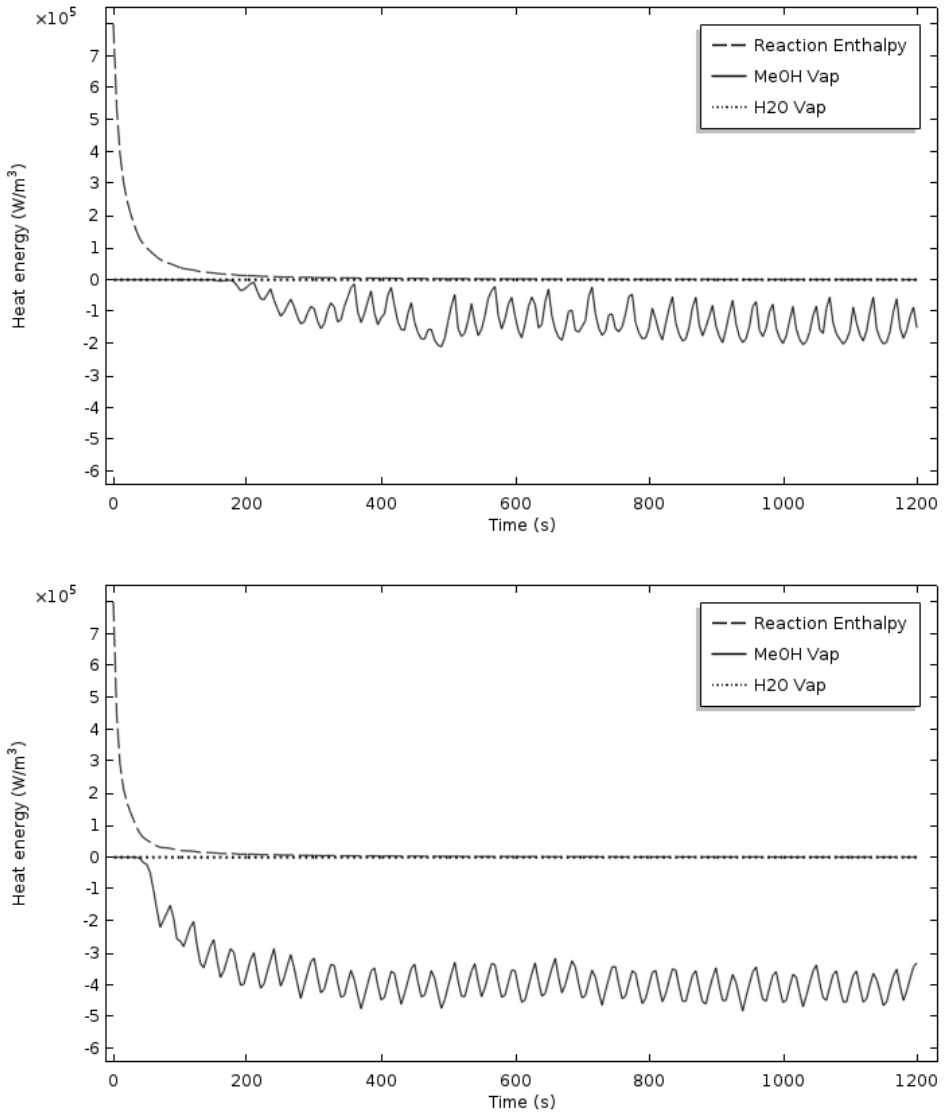

Figure 6.18 Heat source (reaction enthalpy) and heat sinks in PFAD esterification under a) 100 W (top); and b) 240 W (bottom)

It is observed that the convective loss and radiation loss across the flask surface at 100 W and 240 W which are depicted in Figure 6.19 had little influence over the overall heating rate of the PFAD esterification. Among the three heat sinks, heat energy released due to radiation loss was the lowest. The values were only about -100 W/m^3 at 100 W to -200 W/m^3 at 300 W (see Figure 6.8), which was less than 0.1% as compared to the heat loss resulting from methanol vaporization. Even the heat loss from convection was relatively small, with scale about 0.2–0.4% to the heat loss from methanol vaporization. This could be a result of minimal fluid flow.

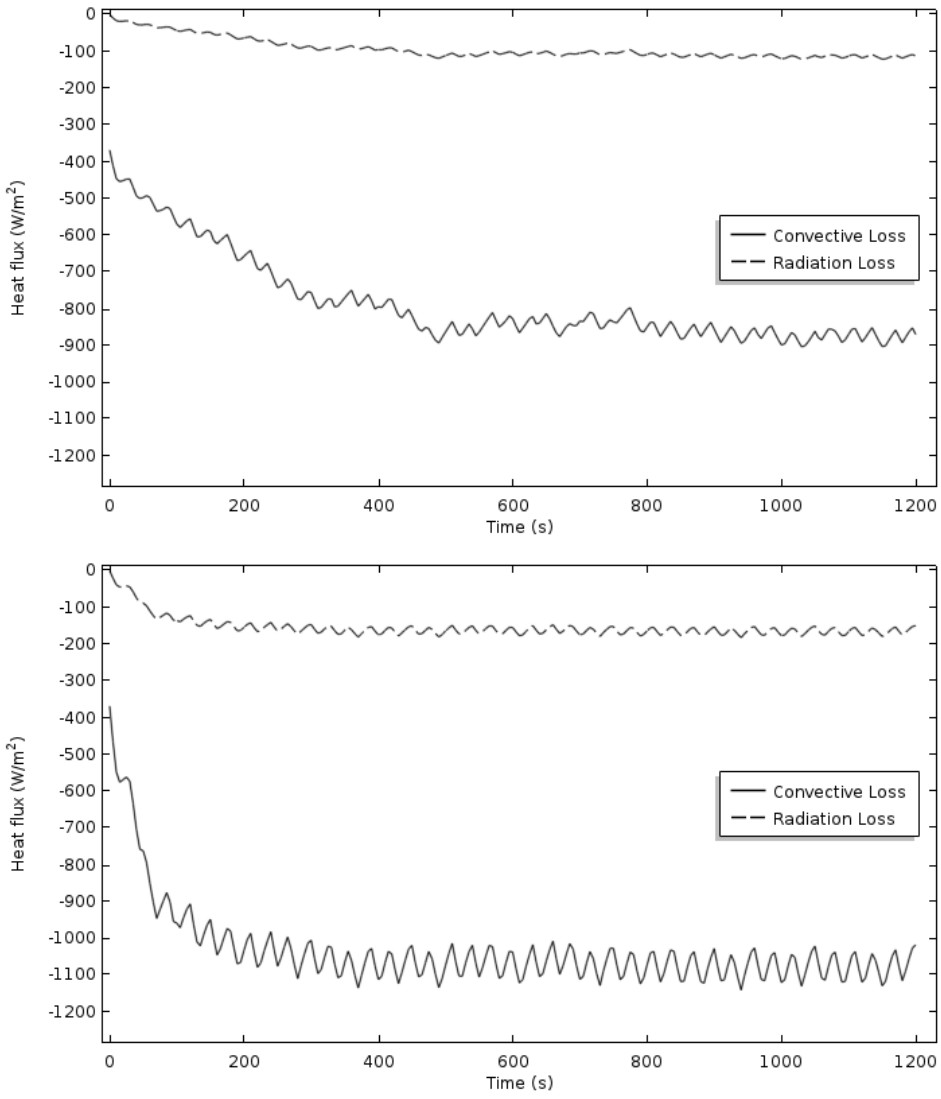

Figure 6.19 Heat fluxes in PFAD esterification under a) 100 W (top); and b) 240 W (bottom)

The velocity field within the reaction mixture at various times under 100 W microwave irradiation is shown in Figure 6.20. At t = 0 s, the gravity effect played a role in the fluid flow. As the heating proceeds, the local heating near the liquid surface above the central region promoted the convective flow of the liquid, causing the liquid to flow from the hotter region at the centre to the cooler region at the side walls of the flask. In this stage of heating, the effect of convective flow was stronger at the upper portion of the liquid. However, the convection played a smaller role near the bottom region where the temperature distribution was still primarily by conduction. After t = 50 s, the fluid velocity became much slower compare to the earlier stage of heating. This suggests that the velocity of the fluid flow under microwave irradiation was the highest during the initial period when esterification reaction was occurring rigorously and subsequently decreased as the concentration of the limited reactants (PFAD) reduced.

The velocity field in the liquid at 240 W microwave irradiation is shown in Figure 6.21. The pattern of the velocity field at 240 W over time was similar to 100 W. By comparing Figure 6.10, Figure 6.20, and Figure 6.21, it is seen that at t = 0 s, the fluid flow was affected by the microwave power levels for some unknown reasons. At t = 5 s, the fluid velocity increased as the microwave power level increased. However, at t = 10 s, the velocity field at the upper portion of the reaction mixture at 240 W was weaker than at 100 W. This inconsistency implies that the magnitude of the microwave power level may not have a direct correlation to the velocity field in the liquid. Another possible reason which affect the accuracy of the velocity field calculation might be the use of constant values (temperature independent) for the thermophysical properties and dielectric properties of the chemical species, especially methanol which plays an important role in microwave dielectric heating. A quick check on the thermophysical properties and dielectric properties over time at the three microwave power levels shows that the changes were similar without significant differences as they were only affected by the changes resulting from the occurrence of esterification reaction.

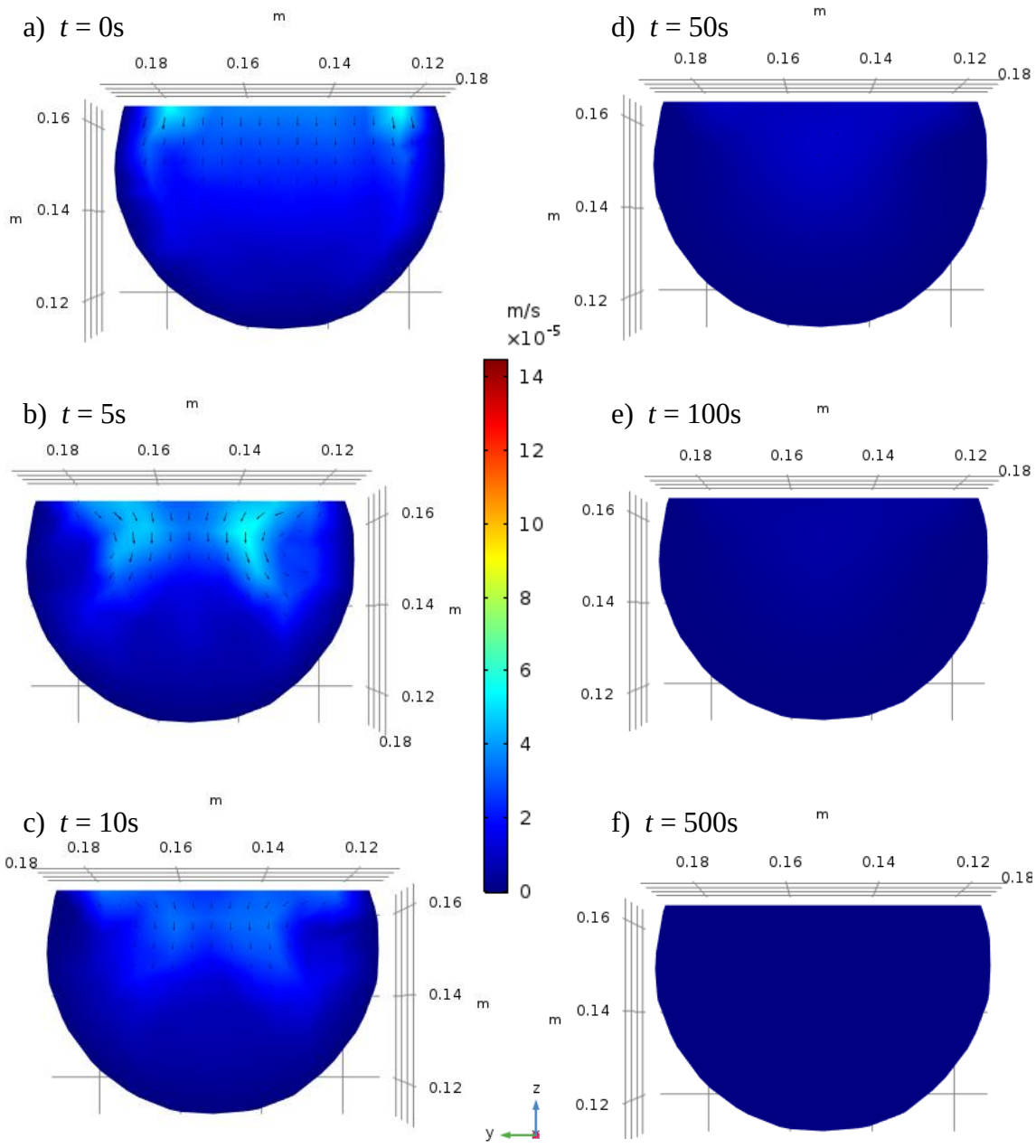

Figure 6.20 Velocity field in liquid (m/s) in *yz*-plane at 100 W microwave irradiation when a) t = 0 s; b) t = 5 s; c) t = 10 s; d) t = 50 s; e) t = 100 s; and f) t = 500 s

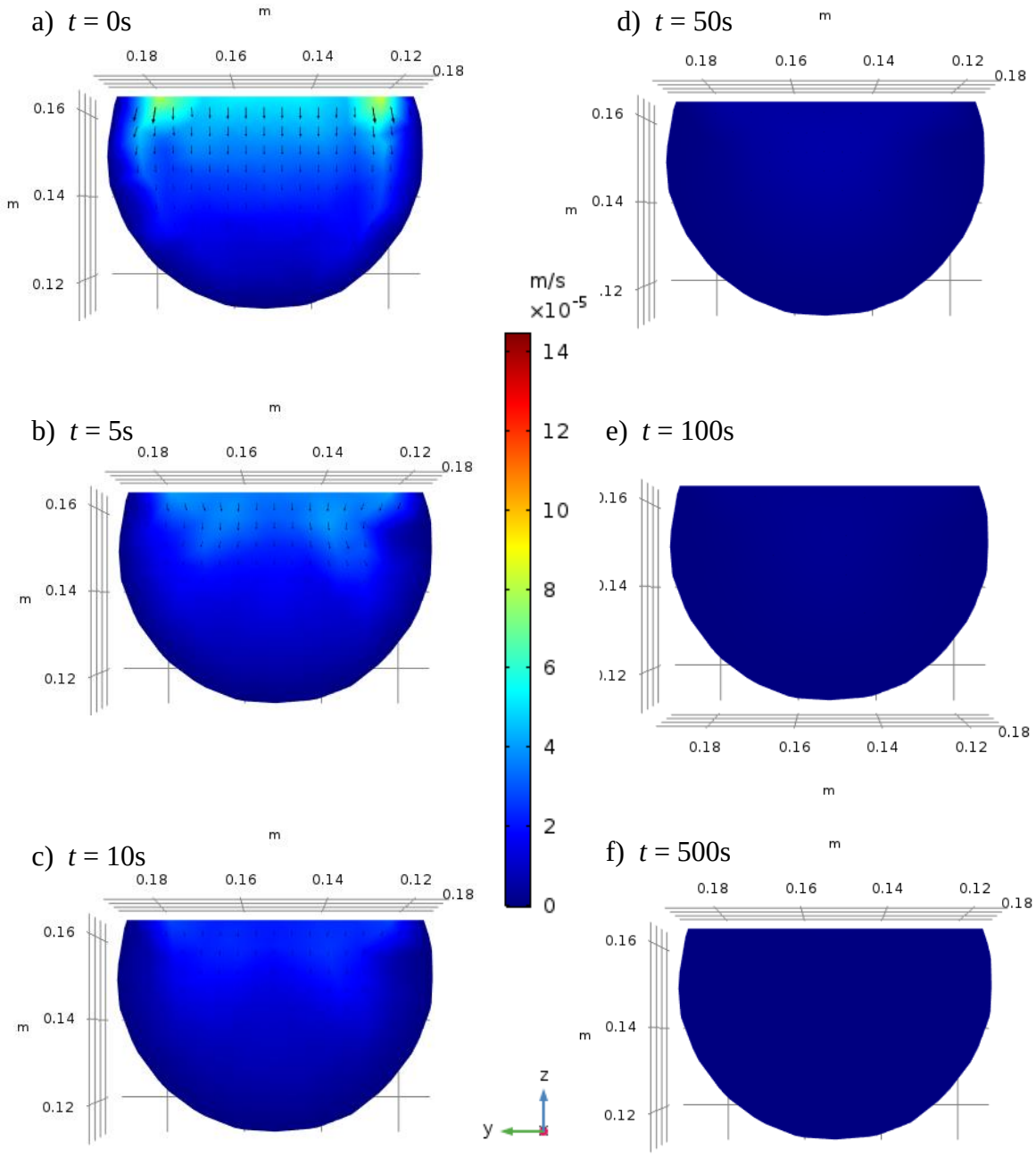

Figure 6.21 Velocity field in liquid (m/s) in *yz*-plane at 240 W microwave irradiation when a) t = 0 s; b) t = 5 s; c) t = 10 s; d) t = 50 s; e) t = 100 s; and f) t = 500 s

6.3 Significance of fluid dynamics in the esterification modelling

During the simulation, the velocity field in the liquid (under 300 W microwave irradiation) was negligibly small (< 1.4×10^{-4} m/s) throughout the process. This raises a question regarding the necessity of solving the fluid transport equations to accurately model the esterification reaction. To investigate this, the Navier-Stokes equations (Equation (5.2) and (5.3)) were not solved in this case study. Without solving the equations, the simulation run time was substantially reduced from 11 h to 73 min.

The species concentration with and without solving Navier-Stokes equations were compared. As shown in Figure 6.22, the changes in the species concentration of PFAD, biodiesel, and water were similar. The concentration of biodiesel and water were slightly over predicted while the concentration of the methanol was obviously over predicted.

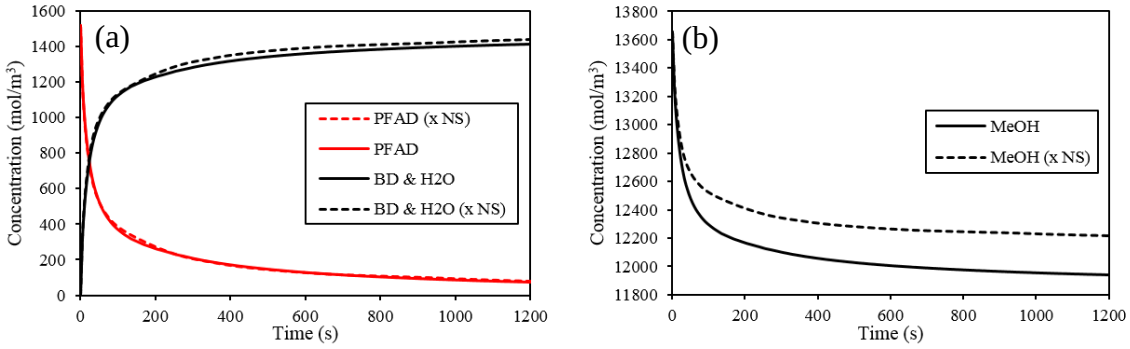

Figure 6.22 Change in species concentration in PFAD esterification without solving Navier-Stokes equations, for: a) PFAD, biodiesel, and water; b) Methanol

Furthermore, when the Navier-Stokes equations were not solved, the third term in Equation (5.4) to (5.7), $\mathbf{u} \cdot \nabla c_i$,which describes the convective transport due to velocity field **u** would be equivalent to zero. In other words, the concentration of a species with respect to time, $\partial c_i / \partial t$ would be purely based on the diffusion and reaction rates. It is well understood that diffusion is usually much slower than convection. Thus, the change in concentration over time would be slower as well. For PFAD, biodiesel, and water,

which exist in low concentrations, not solving the Navier-Stokes equation was observed to have little impact on their concentrations. However, for methanol, which exist in abundance, the effect would be amplified, causing the final predicted concentration to be much higher than the values obtained in the original esterification model.

Apart from the species concentration, it is also observed that the Navier-Stokes equations have a significant effect on the temperature profile simulation. The temperature profile result of the case study is depicted in Figure 6.23.

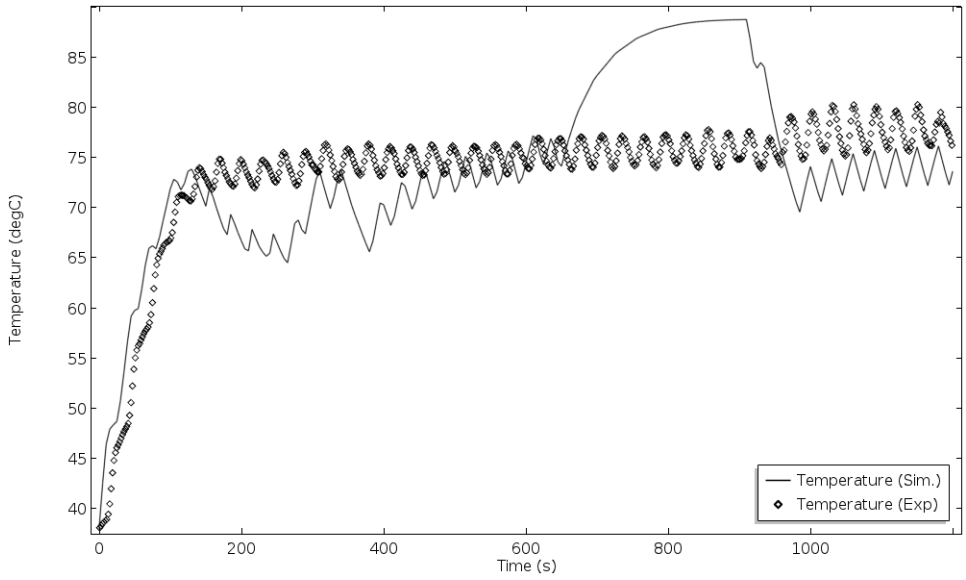

Figure 6.23 Temperature profile during PFAD esterification (300 W) without solving Navier-Stokes equations

In the beginning, the predicted temperature profile without solving Navier-Stokes equations is observed to be slightly higher than the experimental temperature, which is similar to the original simulated temperature profile shown in Figure 6.2. However, the temperature profile changed beyond the boiling point of methanol.

Beyond 70 °C at t = 100 s, the temperature began to oscillate within the range 65–75 °C. However, as time approached 650 s, the temperature sharply increased until it reached 89 °C without showing any signs of the cyclic heating effect from microwave heating. It

then decreased rapidly to 70 °C at 900–1000 s before another round of temperature oscillations could take place.

The main reason for this occurrence in the simulation was due to the inability of the model to reflect the distribution of the actual reactants in the reaction solution. Therefore, without accounting for the convective transport term in Equation (5.4), the concentration of methanol in certain regions of the liquid would be over predicted. As the diffusion rate is slow, the heat energy could not effectively flow from the high energy region to the low energy region; and methanol, which continued to absorb a huge amount of microwave energy, would then cause the local temperature to rise too quickly, creating 'overheated' hot spots between 600 and 800s. In fact, the highest temperature observed in the model was over 118 °C in the central region, as shown in Figure 6.24(b). Due to the localised high temperature, the vaporisation of water was initiated. Since this is an endothermic process, the reaction mixture was cooled, causing a sharp decrease in the local temperature, which was restored to the normal temperature range, i.e. around 70–75 °C during 900–1000 s.

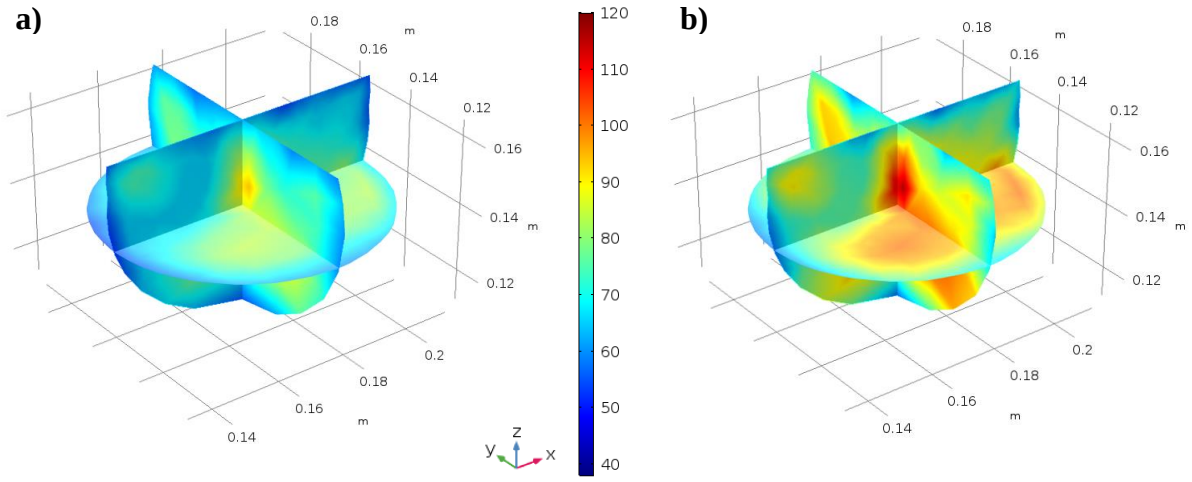

Figure 6.24 Temperature distribution (°C) at 800 s, a) with; and b) without solving Navier-Stokes equations

This analysis has established the importance of including fluid flow calculations. Moreover, the vaporisations of methanol and water are also important because these two mechanisms provide a cooling effect for the microwave-assisted biodiesel production. Therefore, these factors should be considered to obtain good model predictions.

6.4 Summary

The underlying physics for the esterification of PFAD under microwave irradiation were investigated and discussed in this chapter. Increasing microwave power levels were found to increase the intensity of the electric field, power density and reaction temperature. It also increased the heat energy released by the heat sinks and heat fluxes, especially the vaporization effect of methanol. Without the presence of stirring mechanism, the temperature distribution within the reaction mixture was observed to be non-uniform. High microwave power level increased the electric field intensity and subsequently increased the temperature difference across the centre and outer region of the reaction mixture. On the other hand, the fluid flow calculations should be included in the numerical model regardless how insignificant the fluid velocity was. Nonetheless, the intensity of the velocity field in the reaction mixture seemed to not correlate with the microwave power levels.

CHAPTER 7 RESEARCH METHODOLOGY OF PFAD BIODIESEL DISTILLATION EXPERIMENT & COLUMN DESIGN

This chapter covers the research methodology implemented to carry out the experiment of PFAD biodiesel distillation for improving cold flow properties, as well as the design procedures using FUG distillation calculation method and Kern's method to design a distillation column for the aforementioned purpose.

7.1 Materials

The PFAD biodiesel sample for distillation experiment was prepared in bulk using the optimal parametric condition concluded in Chapter 4. The n-hexane (analytical grade), FAME-mix RM6 reference standard and methyl heptadecanoate for GC-FID analysis were purchased from Merck Malaysia.

7.2 Lab scale vacuum distillation setup

A simple distillation under reduced pressure was used in this experiment setup as one of the main objectives of this study is to investigate the feasibility of using vacuum distillation to improve the cold flow behaviour of biodiesel. The test was conducted in lab scale and the esters to be separated were produced in small quantities. To facilitate vacuum distillation of PFAD biodiesel, understanding the FAMEs composition of the biodiesel and their respective melting points was necessary for the determination of the key components for distillation as FAMEs with high melting points would crystallize

faster at low temperature. In this work, methyl palmitate with high melting point was selected as the light key component (to be removed as distillate) while methyl oleate was selected as the heavy key component.

A schematic diagram of the distillation setup is depicted in Figure 7.1. The actual distillation setup is shown in Plate 3 under Appendix A.

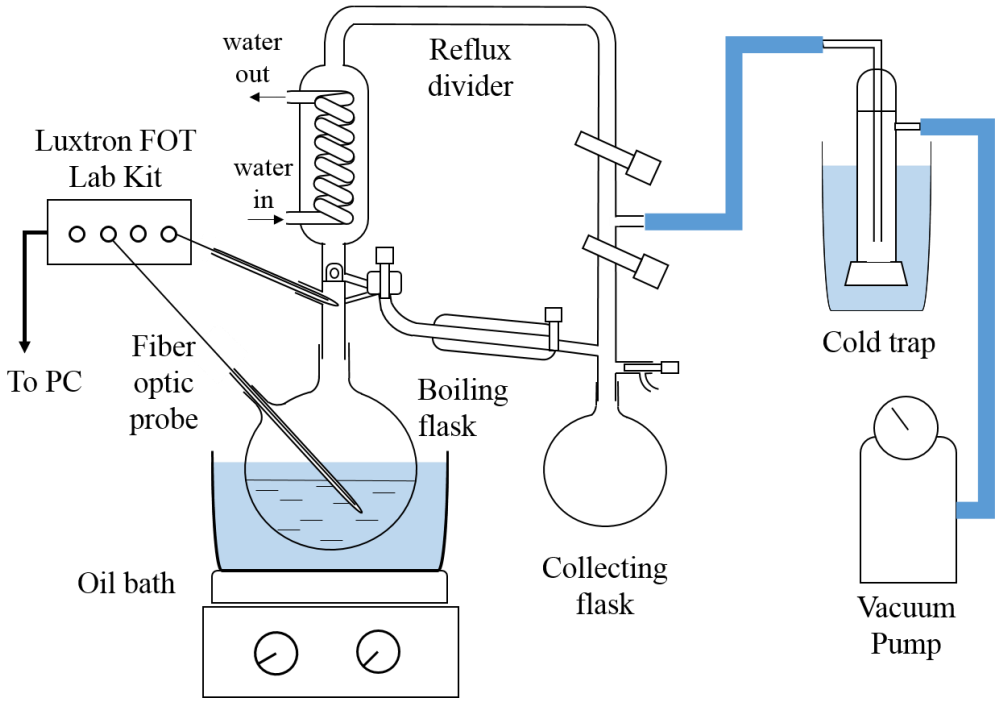

Figure 7.1 Schematic of vacuum distillation experiment setup

The glassware required in the experiment were a 1 L boiling flask, a reflux divider, a cold trap, and a 500 ml collecting flask. The reflux divider (LSG 09089 model) was purchased from Normag, Germany. It consists of a jacketed water-cooled coiled condenser, a ground joint fitting for insertion of temperature measuring device, a distillate drain section (with two glass needle valves), a side-arm vacuum frame for venting or connection to the vacuum supply (with two spindle valves), and a stopcock valve above the receiving end joint. Fibre optic probes were inserted at two temperature measuring locations: i) take-off section with ground joint fitting between the boiling flask and reflux divider; and (ii) in the boiling flask, to record the instantaneous vapour and reboiler temperature respectively.

The 1 L boiling flask was half filled with the biodiesel sample to allow additional room for bubbling during the boiling stage in experiment. This also helps in preventing splashing of the sample into the reflux divider. During the experiment runs, the flask was heated in an oil bath which is maintained at 210°C under a reduced pressure of 100 kPa (1 kPa absolute pressure). All the connecting joints of the glassware were lubricated with Dow-Corning high vacuum silicone grease. The flask was connected to a reflux divider which was a combination of a coil condenser and vacuum control valves that connect to a vacuum pump fitted with a cold trap. The collecting flask could be disconnected from the reflux divider from time to time by shutting off the needle valve and spindle valve which were closest to the collecting flask. The valves could be turned on to reintroduce vacuum into the collecting flask again. The distillates were collected in 10-minute interval and characterized using GC-FID analysis. The experiment ended when the distillate that could be collected during the 10-minutes interval significantly reduced (i.e. distillation rate < 3g/10 min).

7.3 Data analysis methods

After the distillation experiment was completed, both the distillate and bottom product (biodiesel) samples were subjected to GC-FID analysis for FAMEs identification, as detailed in Chapter 3.3.3, before the following tests were carried out to determine the cold flow properties of the distilled biodiesel samples.

7.3.1 Cloud point test

Biodiesel sample was poured into a test jar and pre-heated in a 40°C water bath before test. Then, the sample was setup in a test jar according to ASTM standard D2500 (ASTM, 2011). A thermometer was inserted into the test jar until the bulb reached the bottom surface. The temperature when a cloud of wax formed at the bottom was recorded as the cloud point. The test was carried out in triplicates.

7.3.2 Pour point test

The pour point test of the biodiesel sample was conducted according to ASTM standard D97 (ASTM, 2015). Biodiesel sample was poured into a test jar. Then, a thermometer was inserted into the jar such that the bulb was 1 inch from the bottom surface of the test jar. The test jar was placed in the cloud and pour point bath (0 °C). The condition of the biodiesel sample was inspected every 3 °C drop in the temperature. The temperature when the biodiesel sample did not flow at all after tilted horizontally for 5 seconds was recorded. The pour point of the tested sample was identified by adding 3 °C to the recorded temperature. The test was repeated in triplicates.

7.3.3 CFPP test

The CFPP of biodiesel gives a proper estimate of the lowest temperature at which the fuel could flow trouble-free in the fuel systems. The biodiesel sample was added into a CFPP apparatus as illustrated in ASTM standard D6371-05 (ASTM, 2010). The sample, which was cooled at 1 °C interval, was drawn into a pipet through a wire mesh filter under controlled vacuum. This process was repeated until the amount of wax crystals formed was sufficient to stop or slow down the flow such that the time taken to fill the pipet exceeded 60 seconds. The indicated temperature for the last successful filtration was recorded as the CFPP.

7.4 Process design of vacuum distillation column

The design scope of a distillation column could be categorized into process design, operational design and mechanical design respectively. In this work, only the process design was carried out. The scope included the design methodology of the column, assumptions made, design considerations, as well as the selection of heat exchangers (reboiler and condenser).

7.4.1 Design methodology

A tray distillation column was designed in this work. The design procedures for the distillation column are as follows (Kister, 1992; Towler & Sinnott, 2013):

1. Collect data on operating conditions and physical properties for the column
2. Determine the number of stage and reflux ratio by using FUG method
3. Calculate column diameter for both rectifying and stripping sections by taking flooding condition into considerations
4. Determine overall tray efficiency and number of actual stages
5. Selection of tray spacing
6. Determination of column height
7. Plate design
    i. Decide liquid flow arrangement
    ii. Make a trial plate layout design for downcomer area, active area, hole area, hole size, weir height, tray thickness by selecting the parameters within recommended ranges, weir length and downcomer width.
    iii. Check weeping rate, plate pressure drop, downcomer back-up, downcomer residence time. If the results are not satisfactory, return to step ii.
    iv. Design plate layout details (e.g. calming zone, unperforated area)
    v. Recalculate percentage flooding based on the chosen column diameter
    vi. Check entrainment
    vii. Calculate perforated area and determine hole pitch
    viii. Calculate number of holes
8. Design and determine the specifications of peripheral equipment (condenser, reboiler)

7.4.3 Assumptions and limitations of column design

Also known as the shortcut method, FUG method posed some simplifying assumptions: constant molal overflow, zero holdup, and constant relative volatility throughout the column (Nisar et al., 2018). In order to ease the calculations, the energy balance of the

distillation process was simplified. The column was assumed to operate in vacuum at a constant pressure of 1 kPa under steady state condition. The vapour formed in the column was treated as ideal gas for the estimation of vapour density.

Furthermore, the composition of PFAD biodiesel feed was also simplified by only considering the four major ester components (methyl palmitate, methyl stearate, methyl oleate and methyl linoleate). Other components which had less than 1 wt.% composition were not taken for the calculation. In addition, the operation temperature, heat transfer rate, component thermal properties and heat transfer coefficients were all treated as constants. The column was assumed to be well insulated with negligible heat loss to the surrounding. Lastly, the external column pressure was assumed constant at 1 atm.

On the other hand, the designs of peripheral equipment were done by using Kern's Method, which excluded the effect of leakage and bypass streams in the prediction of pressure drop. Nonetheless, this method is simple to apply and accurate enough for preliminary design calculations and provides a reasonably satisfactory estimation of the heat transfer coefficient for the heat exchangers (Towler & Sinnott, 2013). For the calculation of log mean temperature difference for the shell and tube heat exchanger, the following assumptions were made in the derivation of the temperature correction factor, F_t:

1. Heat transfer areas at each tube pass are equal
2. Overall heat-transfer coefficient of streams at each tube pass is constant
3. Shell-side fluid in any pass is isothermal across any cross-section
4. No fluid leakage between shell passes

7.4.1 Design considerations

Prior to the column design process, the selection of key components during the vacuum distillation was carried out. The two main ester components in PFAD biodiesel were methyl palmitate and methyl oleate. In this design work, methyl palmitate was chosen as the light key due to its lower boiling point. Its higher melting point was bad for the cold

flow properties of the PFAD biodiesel and therefore should be removed. Methyl oleate with higher boiling point was selected as the heavy key. Most of the methyl palmitate were to be separated from the biodiesel in the form of distillate, while methyl oleate and the rest of the heavier esters would be collected as the bottom product, or the desired biodiesel with improved cold flow behaviour.

The recommended height-to-diameter ratio for a column ranged from 3 to 20 (ICARUS Corporation, 1998). According to Towler and Sinnott (2013), while designing the tray column, the tray spacing must be greater than the downcomer backup in order to prevent the occurrence of column flooding which could significantly decrease the separation efficiency. In fact, the downcomer backup should be 50% less than the sum of tray spacing and weir height, for safe design. In addition, the actual velocity of the vapour should not be lower than the minimum design vapour velocity. Else, weeping would occur in the column whereby liquid leak through the perforations on the tray. The percentage of flooding that is calculated must be below 100% in order to minimize the effect on the column efficiency. Apart from that, the fractional entrainment should not be greater than 0.1.

7.4.2 Design data & basis of design

The design data required for the distillation column design was extracted from Aspen Hysys as well as obtained from the experiment work. The design data and compositions of feed and product streams are summarized in Table 7.1.

Table 7.1 Physical properties and composition of feed and product streams of distillation column with utility used

Properties	**Unit**	**Feed**	**Distillate**	**Bottom**
Vapour fraction	dimensionless	0	0	0
Pressure	kPa	1	1	1
Temperature	°C	186.0	178.8	196.8
Molecular Weight	kg/kmol	283.5	271.3	295.0

Properties	Unit	Feed	Distillate	Bottom
Density	kg/m^3	746.17	750.43	738.49
Surface Tension	mN/m	196.0	200.2	188.9
Viscosity	mPa.s	0.4136	0.4382	0.3800
Mass Flow Rate	kg/h	3750	1745	2005
Volumetric Flow Rate	m^3/h	5.026	2.325	2.716
Heat Flow	10^6 kJ/h	-8.610	-4.476	-4.111
Mole Fraction (Methyl Palmitate)	dimensionless	0.4963	0.9680	0.0500
Mole Fraction (Methyl Stearate)	dimensionless	0.0476	0.0018	0.0909
Mole Fraction (Methyl Oleate)	dimensionless	0.3677	0.0300	0.6872
Mole Fraction (Methyl Linoleate)	dimensionless	0.0884	0.0002	0.1719

The distillation was conducted under vacuum at 1 kPa (i.e. 7.5 mmHg) absolute pressure to avoid thermal degradation of esters which could negatively affect the quality of biodiesel. The temperature of feed was set at 186 °C, the bubble point of the feed, to ease the design calculation.

7.4.5 Sizing and specification of peripheral equipment

A shell and tube exchanger consisted of a bundle of tubes enclosed in a cylindrical shell. The peripheral equipment of the distillation equipment, the condenser and reboiler, were designed as shell and tube exchangers following the guidelines provided by Towler and Sinnott (2013). The condenser cooled and condensed the vapour leaving the top of the distillation column by using cooling water as the cooling medium. The vapour which mainly comprised of methyl palmitate was condensed and collected as distillate. The condenser was modelled as a horizontal shell and tube exchanger. On the other hand, the biodiesel at the bottom of the column was heated and vaporised by using a kettle reboiler, with high pressure steam acting as the heating medium. Kern's method, which was based on the experimental work on commercial exchangers with standard tolerances, was adopted to give a reasonably satisfactory prediction of the heat-transfer coefficient and

pressure drop in the heat exchangers. A trial and error approach was necessary in the design of an exchanger as the heat transfer area must be known first before the physical layout of the exchanger could be determined. Refer Towler and Sinnott (2013) for the detailed step-by-step design procedures of the heat exchangers.

The design procedure for shell and tube heat exchanger was briefly shown as follows:

1) Define duty: heat transfer rate, fluid flow rates and temperatures
2) Collect fluid physical properties required (density, viscosity, heat capacity, thermal conductivity)
3) Select a trial value for the overall heat transfer coefficient U_o
4) Decide number of shell and tube passes. Calculate ΔT_{lm}, F_t and ΔT_m
5) Determine heat transfer area required, A_o
6) Decide the heat exchanger layout (type, tube size, material)
7) Calculate number of tubes required and shell diameter
8) Estimate tube-side heat transfer coefficient
9) Decide baffle spacing and estimate shell-side heat transfer coefficient
10) Calculate overall heat transfer coefficient, $U_{o,calc}$ and compare with the trial value.

    If the difference between $U_{o,calc}$ and U_o exceeds 30%, replace the trial value with $U_{o,calc}$ and return to step 5
11) Estimate tube and shell-side pressure drops

7.5 Prediction of cold flow properties

Several studies had been done to develop empirical correlations for the prediction of the biodiesel cold flow properties. Dunn and Bagby (1995) had proposed relationships between CP and PP for diesel/ester blends. Their analysis showed that CFPP with at least 10 vol% of methyl esters were linearly related to CP. According to Lopes et al. (2008) who developed a model to determine the CP of the binary mixtures of FAMEs, PP and CFPP could be related to the CP and be predicted from its value. Their results suggested that the CPs were dominated by the saturated esters with higher melting points.

Al-Shanableh et al. (2016) utilized artificial neural network for predicting the CP, PP and CFPP of biodiesel fuel based on the fatty acid composition of feedstock. They reported that the model could be trained to predict the cold flow properties of biodiesel with high accuracy (>94%). However, the model was not accessible for implementation at the moment. Nonetheless, there were two empirical correlations methods that were available in literature for the prediction of cold flow properties. The first method, which consisted of two sets of correlations, was proposed by Sarin et al. (2009) to predict CP and PP of biodiesel. The prediction for CFPP of biodiesel was also added to the first method by using the same sets of correlations as the backbone in the following year (Sarin et al., 2010). The two sets of correlations which were developed in the first method for the prediction of CP, PP and CFPP were based on: (i) the palmitic acid methyl ester; and (ii) the total unsaturated FAMEs. The first correlations based on methyl palmitate (P_{FAME}, wt.%) include

$$CP = 0.526P_{FAME} - 4.992 \quad (0 < P_{FAME} \leq 45) \tag{7.1}$$

$$PP = 0.571P_{FAME} - 12.24 \quad (0 < P_{FAME} \leq 45) \tag{7.2}$$

$$CFPP = 0.511P_{FAME} - 7.823 \quad (0 < P_{FAME} \leq 45) \tag{7.3}$$

And correlations based on the total content of unsaturated FAMEs (U_{FAME}, wt.%) are expressed as

$$CP = -0.576U_{FAME} + 48.255 \quad (0 < U_{FAME} \leq 84) \tag{7.4}$$

$$PP = -0.626U_{FAME} + 45.594 \quad (0 < U_{FAME} \leq 84) \tag{7.5}$$

$$CFPP = -0.561U_{FAME} + 43.967 \quad (0 < U_{FAME} \leq 84) \tag{7.6}$$

The second method was proposed by Su et al. (2011) which could quantitatively predict the three cold flow properties based on the weighted average number of carbon atoms in FAME and the composition of total unsaturated FAMEs. The correlations are expressed as follows:

$$CP = 18.134(N_c) - 0.790(U_{FAME}) \tag{7.7}$$

$$PP = 18.880(N_c) - 1.000(U_{FAME}) \tag{7.8}$$

$$\mathrm{CFPP} = 18.019(N_c) - 0.804(\mathrm{U_{FAME}}) \quad (7.9)$$

These correlations could help in validating the cold flow tests of PFAD biodiesel before and after distillation. Dunn (2018) evaluated six empirical correlation models using regression analysis solely in calculating the CP of biodiesel fuels in order to determine the best correlation models with 1:1 correlation between the calculated and measured CP data. He reported that Su's model demonstrated the best validation results with slope = 0.98, intercept = 2.3, and standard error of the *y*-estimate (σ_y) = 0.9, followed by Sarin's first correlation method, P_{FAME} (slope = 1.10, intercept = 2.2, and σ_y = 1.4). Although Sarin's second method (U_{FAME}) had a lower intercept and σ_y than Sarin's first method (intercept = 1.1, and σ_y = 1.3), Dunn ranked it last among the three models as its slope was 1.28.

7.6 Summary

In this chapter, the research methodology of using vacuum distillation technology in improving the cold flow properties of PFAD biodiesel was briefly explained. It was categorized into two parts: (i) vacuum distillation experiment, and (ii) preliminary design of vacuum distillation column. The experiment was carried out to check the feasibility of improving the cold flow properties of PFAD biodiesel via vacuum distillation, while the process design of a vacuum fractional distillation column described in the latter part was a trial effort done to introduce vacuum distillation technology into the biodiesel industry to post-process PFAD biodiesel in order to enhance its cold flow behaviour. By extracting the data of bottom product from the model, the cold flow properties of the distilled PFAD biodiesel would then be estimated via empirical correlations in order to check the possibility of turning the biodiesel into export grade biodiesel.

CHAPTER 8 RESULTS & DISCUSSION FOR VACUUM DISTILLATION EXPERIMENT OF PFAD BIODIESEL & COLUMN DESIGN

The results for the experiment of PFAD biodiesel distillation are presented and discussed in this chapter. The calculation process and results of the column design are also covered.

8.1 Lab scale vacuum distillation of PFAD biodiesel

The key component which was separated from the PFAD biodiesel during the vacuum distillation was methyl palmitate. As shown in Table 8.1, the FAME with the highest melting point was methyl stearate (37.7 ^{o}C), followed by methyl palmitate (28.5 ^{o}C). In spite of having higher melting points, methyl stearate was not selected as its composition was relatively low compared to methyl palmitate, which was only 4.76%. In contrast, the composition of methyl palmitate was 47.51%, which was the highest among the four esters present in the PFAD biodiesel. Therefore, it was necessary to remove methyl palmitate from the rest of the esters in order to lower the CP, PP and CFPP of PFAD biodiesel.

The experiment was carried out under vacuum. Bonhorst et al. (1948) reported that the decomposition of saturated acid esters would occurred progressively at temperature above 205 °C under atmospheric pressure. As depicted in Table 8.1, the boiling point of methyl palmitate was 184 °C at 10 mmHg. Thus, in order to avoid the thermal degradation of esters during the distillation process, the experiment was carried out at the boiling temperature of methyl palmitate under 100 kPa vacuum pressure.

Table 8.1 Fatty acid methyl esters in PFAD biodiesel with their respective melting and boiling points

Trivial Name	**Melting Point (°C)[a]**	**Boiling Point (°C/10 mmHg)[a]**	**Composition[b] (wt.%)**	**Composition[c] (wt.%)**
Methyl Myristate	18.1	161	negligible	1.93
Methyl Palmitate	28.5	184	47.51	45.68
Methyl Stearate	37.7	205	4.76	4.25
Methyl Oleate	-20.2	201	38.69	40.19
Methyl Linoleate	-43.1	200	9.04	7.90

[a] Cermak et al. (2012); [b] In this work; [c] Lokman et al. (2014)

The vacuum distillation experiment separated a good amount of esters from the heated PFAD biodiesel sample successfully. About 430 g of PFAD methyl esters were placed in the boiling flask during the distillation run. The total yield of distillate obtained was 39.76% while the bottom product was 59.62%.

The temperature profiles of the liquid (in boiling flask) and vapour (before condensed into distillate) were recorded starting from 70 minutes before the experiment to the subsequent 100 minutes until the distillation experiment completed. The changes in the temperature before and during the distillation experiment are shown in Figure 8.1. During the experiment, the vapour temperatures were observed to stay consistently about 10°C lower than the reboiler temperature throughout the distillation experiment. As observed in Figure 8.1, the biodiesel in liquid phase reached its boiling point about 35–40 minutes before the distillation began. The highest biodiesel temperature recorded was 194.8 °C at the 35th minute before the first distillate sample collection took place. At this stage, the molecules in the biodiesel sample possessed enough kinetic energy to escape from the liquid phase to vapour phase. This was shown by the immediate increase in vapour temperature. The vapour temperature directly rose from room temperature to over 180 °C as more vapour was continuously generated in order to achieve stable total reflux condition in the distillation system. This temperature profile indirectly signified that it

was nearly impossible to distil esters with lower boiling point than methyl palmitate (e.g. boiling point of methyl myristate: 161°C) that present in small portion in the PFAD biodiesel. In other words, only one distillate fraction was obtained as the vapour temperatures remained steady at 183–184 °C range during the experiment. This was acceptable as taking subsequent fractions at higher temperature would inevitably remove a higher amount of methyl oleate and methyl linoleate from the biodiesel which would beat the purpose of conducting distillation on PFAD biodiesel.

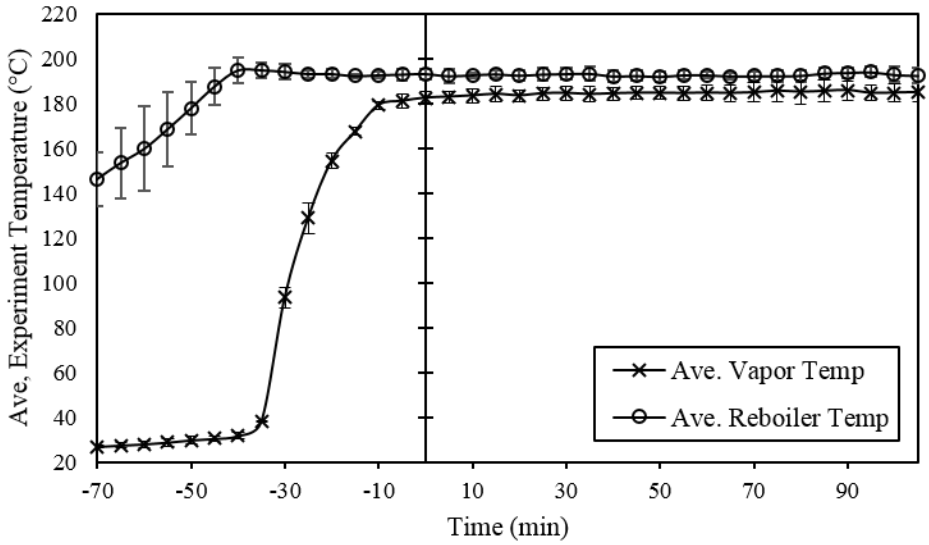

Figure 8.1 Vapour and reboiler temperature profiles before and during vacuum distillation

The light key component, methyl palmitate, was removed from the system and collected in the form of distillate every ten minutes at a reflux ratio of 1:1. The amount of distillate collected at each interval during the distillation experiment is plotted in Figure 8.2. It is noticed that the distillate removal rate increased for the first 60 minutes but decreased at a faster rate after that. By 60^{th} minute, the amount of distillate obtained was 29.99 wt.% of the initial feed. After 100 minutes, the mass fraction of distillate that was enriched with methyl palmitate increased to 39.76 wt.% whereas the bottom product left in the boiling flask was enriched in the higher boiling component (methyl oleate).

By the end of the experiment, the bottom product (distilled biodiesel) remaining in the boiling flask was collected. In order to study the efficiency of the vacuum batch distillation, the composition of the biodiesel samples before and after distillation were subjected to GC-FID analysis for fatty acid composition studies. The ester compositions in the PFAD biodiesel before and after the distillation are identified from chromatograms as shown in Figure 8.3. The results are listed in Table 8.2.

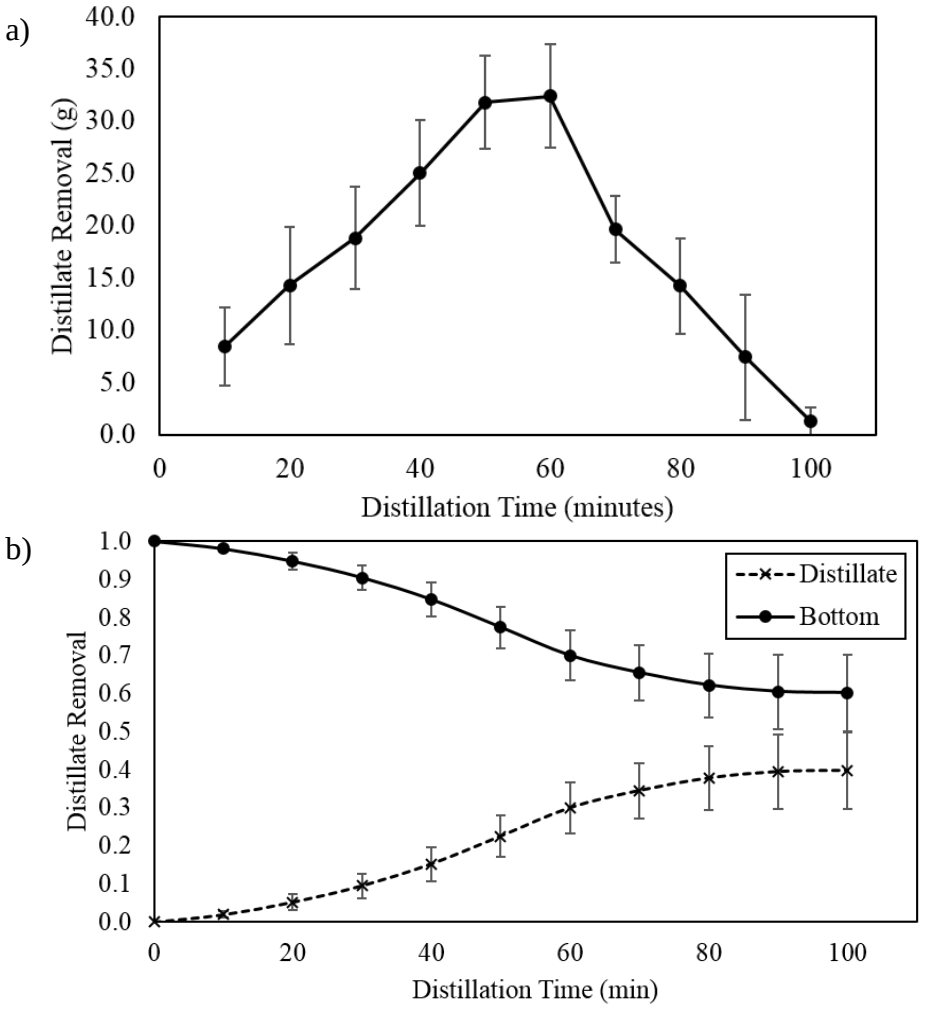

Figure 8.2 Distillate removal of PFAD biodiesel during vacuum distillation, a) at each interval; b) in a cumulative manner (mass fraction)

The PFAD biodiesel before distillation consisted of 47.36% methyl palmitate, 38.46% methyl oleate and 14.19% other esters. Upon GC-FID analysis, it is found that the methyl palmitate content in the distilled PFAD biodiesel decreased by 15.44% after the distillation, from 47.36% to 31.91%. Meanwhile, the mass fraction of other esters increased: methyl oleate has increased by 11.66%, followed by methyl linoleate (2.28%), and methyl stearate (1.85%). Hence, the dominant ester in PFAD biodiesel after distillation had changed from the saturated ester methyl palmitate to the unsaturated ester methyl oleate. The amount of total unsaturated FAMEs in the PFAD biodiesel increased 13.60% after the distillation. Hence, it can be deduced that the cold flow properties of the PFAD biodiesel would improve as unsaturated FAMEs have lower melting points than saturated FAMEs.

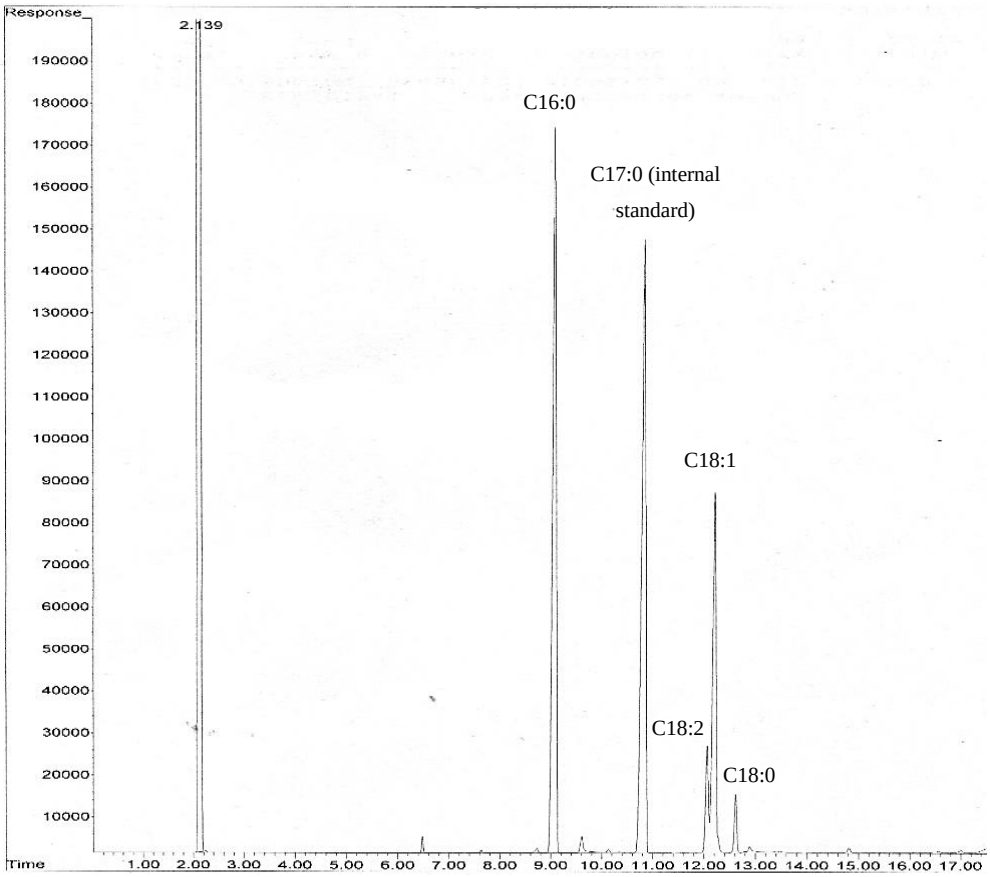

Figure 8.3 A typical chromatogram of the FAMEs in PFAD biodiesel

Table 8.2 Ester components in PFAD biodiesel with their respective mass fractions

Ester	Retention Time (min)	Molar mass (g/mol)	Normalized Mass Fraction (%)		
			Pre-distillation	Post-distillation	Change
Methyl palmitate (C16:0)	9.19	270.5	47.36	31.91	-15.44
Methyl stearate (C18:0)	12.78	294.5	5.01	6.86	1.85
Methyl oleate (C18:1)	12.37	296.5	38.46	49.78	11.32
Methyl linoleate (C18:2)	12.21	298.5	9.17	11.45	2.28
Total saturated FAMEs	-	-	52.37	38.77	-13.60
Total unsaturated FAMEs	-	-	47.63	61.23	13.60

On the other hand, the GC-FID analyses also showed that the ester conversion of the biodiesel sample had slightly decreased by 4.92 ± 3.93% after the vacuum distillation. This could be due to the removal of 40 wt.% of distillate during the distillation experiment, which indirectly increased the composition percentage of the other impurities remaining in the bottom samples. The ester compositions of the ten distillate samples collected during experiment at each 10-minute interval were also identified using GC-FID analysis. The results are shown in Table B-4 in Appendix B. The data in Table B-4 was also used to plot Figure 8.4 for better visualization of the changes occurred in the FAME compositions of distillate over time.

It was observed that among all the ten distillate samples, they were consisted of 60–69% methyl palmitate, 19–29% of methyl oleate, 5–7% of methyl linoleate, and 2–3% of methyl stearate. The first distillate sample contained the highest fraction of methyl palmitate (68.60%) and the lowest fraction of methyl oleate (19.17%). Its content of methyl stearate and linoleate were the lowest as well. In the subsequent samples, the fraction of methyl palmitate in distillate gradually dropped while the composition of the other three esters in the distillate samples slowly increased. The first four distillate

samples had relatively higher amount of methyl palmitate, ranging between 66.21% and 68.60%. This dropped to 60.80% at the sixth sample when the amount of distillate collected were the highest at 32.38 ± 4.95 g (refer Figure 8.2a). The composition of methyl palmitate in the remaining distillate samples stayed consistent in the range of 59.62% to 61.73%.

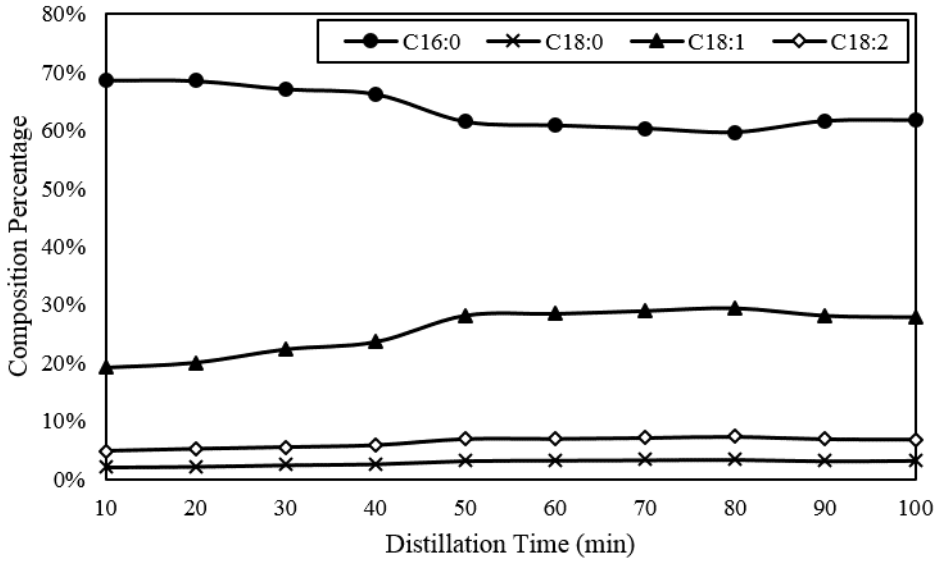

Figure 8.4 Methyl esters composition fraction in distillate samples over time

The entire mass balance of the vacuum distillation experiment is tabulated in Table 8.3. As shown in Figure 8.2b and Table 8.3, the yield of the bottom product (distilled biodiesel) obtained from the distillation was 59.62%, which was comparatively higher than using winterization technique. This claim was supported with the results reported by Dunn et al. (1996). They carried out winterization studies on a FAME mixture in order to lower its CP and PP by reducing the long-chain saturated esters (C16 or above) content through crystallization in refrigerated bath. The process of removing 12.5 wt.% total saturated FAMEs (methyl palmitate and stearate) took about one week's time and the product yield was only about 25%. Not to mention 20% of starting materials was lost during the process as well. In contrast, 13.60 wt.% of total saturated FAMEs were removed in this study, and the product yield was found to be 59.62% with only 0.62% loss of starting materials.

Therefore, vacuum distillation is relatively better than winterization technique for improving the cold flow characteristics of biodiesel, from the perspective of short processing time, high product yield and small loss.

Table 8.3 Mass balance of the vacuum distillation of PFAD biodiesel

Sample	**Mass (g)**	**Mass (%)**
Initial charge	435.87 ± 1.40	100.00 ± 0.32
Distillate	173.29 ± 10.64	39.76 ± 2.44
Bottom	259.87 ± 8.80	59.62 ± 2.02
Loss	2.71 ± 0.19	0.62 ± 0.04

Although the separation efficiency of the methyl palmitate from PFAD biodiesel via simple batch distillation under vacuum was better than winterization technique but it is still considerably low due to the small difference in boiling points. For instance, at an absolute pressure of 1.33 kPa (10 mmHg), which is close to the experimental operating pressure in this study, the difference between the boiling points of methyl palmitate (light key) and oleate (heavy key) was 17 °C (refer Table 8.1). Nevertheless, the purity of the distilled biodiesel could be further improved by performing separate simple distillations on the sample for another few more times. However, this would result in higher material loss. Simple distillation could be referred as one theoretical plate as only a single equilibrium stage between the liquid and vapour was involved. To attain higher yields with smaller loss and higher purity as well as better separation efficiency, fractional distillation could be carried out to establish higher number of vaporization-condensation cycles in the system. This could be done by inserting a fractionating column equipped with multiple plates into the simple distillation system setup. The ascending vapour would then be redistilled and condensed repetitively over the plates in the column, and better separation of the more volatile component would be obtained in the final product yield.

8.2 Cold flow properties

As shown in Table 8.2, the changes in the mass fraction of methyl stearate and linoleate in the biodiesel sample were minimal, which increase by 1.85% and 2.27% respectively. Meanwhile, there was a net 15.44% reduction of methyl palmitate (saturated ester) and a net increase of 11.32% of methyl oleate (unsaturated ester) in the distilled PFAD biodiesel sample. Thus, the degree of unsaturation in the distilled PFAD biodiesel increased, resulted in the drop in cloud point, which agrees with the findings by Elias et al. (2016). Simultaneously, the pour point and CFPP would inevitably reduce as well as they are related to the cloud point (Lopes et al., 2008). The cold flow properties of the PFAD biodiesel before and after the distillation experiment were measured and recorded in Table 8.4.

Table 8.4 Cold flow properties of PFAD biodiesel before and after simple vacuum distillation

PFAD Biodiesel	Pre-distillation	Post-distillation	Improvement
Cloud Point (℃)	20 ± 1	13 ± 1	7 ± 1
CFPP (°C)	19 ± 1	11 ± 1	8 ± 1
Pour Point (°C)	15 ± 1	9 ± 1	6 ± 1

Before the distillation is carried out, the CP, CFPP and PP of the PFAD biodiesel was 20 °C, 19 °C and 15 °C. After the distillation, the CP, CFPP and PP of the PFAD biodiesel reduced to 13 °C, 11 °C and 9 °C, respectively. The CFPP improved the most among the three properties. This could be due to the high correlation of CFPP values with the contents of methyl palmitate as well as the contents of total unsaturated FAMEs (Park et al., 2008; Sarin et al., 2010). As methyl palmitate reduced and total unsaturated FAMEs increased, this posed a greater effect on the CFPP than the CP and PP.

The improvement in cold flow properties showed that vacuum distillation is a feasible technique to enhance the cold flow properties of PFAD biodiesel even though the difference in the boiling points of the light key and heavy key was less than 20 °C. In spite of only 13.60% removal of the total saturated FAMEs in the distilled PFAD biodiesel, the

results showed that the cold flow properties of the PFAD biodiesel clearly improved by 35–42% (6–8 °C) after 100 minutes of simple vacuum distillation, which was significant. This implied that vacuum distillation is a feasible way to improve the cold flow characteristics of PFAD biodiesel.

Using the fatty acid compositions of PFAD biodiesel in Table 8.2 and cold flow properties data in Table 8.4, the three empirical correlation methods proposed by Sarin et al. and Su et al. in predicting the cold flow properties of PFAD biodiesel were evaluated. The values of CP, PP and CFPP for the PFAD biodiesel samples, as listed in Table 8.5, were predicted using Equations (7.1) to (7.9).

Table 8.5 Cold flow properties prediction of PFAD biodiesel samples before and after distillation via empirical correlations

Cold Flow Properties	**In this work**	**Sarin (P_{FAME})**	**% error**	**Sarin (U_{FAME})**	**% error**	**Su**	**% error**
Pre-distillation PFAD biodiesel							
CP (°C)	20	19.92	0.40%	20.82	4.10%	15.76	21.20%
PP (°C)	15	14.80	1.33%	15.77	5.13%	19.19	27.93%
CFPP (°C)	19	16.38	13.79%	17.24	9.26%	13.02	31.47%
Post-distillation PFAD biodiesel							
CP (°C)	13	11.79	9.31%	12.99	0.08%	10.72	17.54%
PP (°C)	9	5.98	33.56%	7.26	19.33%	11.53	28.11%
CFPP (°C)	11	8.48	22.91%	9.62	12.55%	7.76	29.45%

Looking at the pre-distillation PFAD biodiesel sample, it was found that Sarin (P_{FAME}) method could estimate the CP and PP of the biodiesel sample with minimal error (0.40–1.33%) but the CFPP value had a deviation of 13.79%. However, the mass fraction of methyl palmitate of the sample was 47.36% (as shown in Table 8.2), which was slightly higher than the upper boundary value $(0 < P_{FAME} \leq 45)$ given in Equation (7.1) to (7.3). for Sarin (P_{FAME}) method. Thus, the decision of implementing Sarin (P_{FAME}) method

solely based on the calculation on this sample could be doubtful. Meanwhile, the Sarin (U_{FAME}) method could predict all three cold flow properties for the PFAD sample with less than 10% error. The predicted values using Su's method was found to have the highest percentage error (21.20–31.47%) among the three methods.

As for the post-distillation PFAD biodiesel sample, it satisfied the requirement for using both Sarin's (P_{FAME}) (e.g. $0 < P_{FAME} \leq 45$ wt%) and (U_{FAME}) ($0 < U_{FAME} \leq 84$ wt%) correlations. It was found that Sarin (U_{FAME}) method gave the lowest percentage errors among the three methods. The CP value was estimated accurately but the errors for PP and CFPP prediction varied by 12.55–19.33%. Nonetheless, the percentage errors were lower when compared with Sarin (P_{FAME}) method. Thus, the accuracy of Sarin (P_{FAME}) correlations in predicting the cold flow properties of PFAD sample in this work was lower than Sarin (U_{FAME}) method. On the other hand, the errors generated for CP and CFPP values by using Sarin (P_{FAME}) method were lower than using Su's method. However, Sarin (P_{FAME}) method gave 33.56% error for the PP values, which was higher than Su's method (28.11%).

Among the three methods, it was found that the second correlation method, Sarin (U_{FAME}), could best predict the three cold flow properties of PFAD biodiesel samples in this work. In fact, this method predicted the cold flow properties of PFAD biodiesel sample with less than 2 °C deviation. The ranking was followed by Sarin (P_{FAME}) method, and lastly Su's method. Although this finding was different from that reported by Dunn (2018), the comparison between the three methods showed that Sarin (U_{FAME}) method was the most suitable approach for predicting the cold flow properties of PFAD biodiesel in this work.

As suggested in Chapter 8.1, in order to obtain PFAD biodiesel with better cold flow properties than what was shown in the experiment results, the separation efficiency of the distillation system should be enhanced by implementing vacuum fractional distillation. Table 8.6 shows the comparison between the quality of PFAD biodiesel sample processed through simple vacuum distillation as well as vacuum fractionation. The distillation column designed for the vacuum fractionation would be discussed in Chapter 8.3. As shown in Table 8.6, the quality of PFAD biodiesel distilled through vacuum fractional

distillation was much more favourable. The composition of methyl oleate increased 19.31% and the undesired methyl palmitate was further reduced by 27.32%. Thus, the cold flow properties of PFAD biodiesel which underwent vacuum fractionation could be expected to have better cold flow properties. The ester composition and cold flow properties of the feed, distillate and bottom streams during the vacuum fractional distillation of PFAD biodiesel were calculated and shown in Table 8.7.

Table 8.6 Ester composition comparison of PFAD biodiesel sample under different distillation methods

	Mass fraction (wt.%)		
Ester Composition	**Simple Vacuum Distillation[a]**	**Vacuum Fractionation[b]**	**Difference (%)**
Methyl Palmitate, C16:0	31.91	4.59	- 27.32
Methyl Stearate, C18:0	6.86	9.20	+ 2.34
Methyl Oleate, C18:1	49.78	69.09	+ 19.31
Methyl Linoleate, C18:2	11.45	17.16	+ 5.71

[a] Experiment data; [b] Simulated results

As discussed earlier, the Sarin (U_{FAME}) method could best estimate the cold flow properties of PFAD biodiesel and could be used for the cold flow properties prediction of the final biodiesel product obtained via vacuum fractional distillation. However, the CP, PP and CFPP of the bottom stream (distilled biodiesel) in Table 8.7 were calculated using Sarin's P_{FAME} method instead of Sarin's U_{FAME} method because its ester composition did not meet the requirement of the U_{FAME} correlation function whereby the mass fraction of the total unsaturated FAMEs should be $\leq$ 84%. The total unsaturated FAMEs in the bottom stream was 86.25 wt.%. The estimated CFPP was -5.48 °C, which hinted that the distilled PFAD biodiesel has the potential to be graded as summer biodiesel for temperate climates at grade C (max CFPP -5 °C) according to Europe EN 14214 standard (British Standards Institution, 2014).

Table 8.7 Ester composition in feed, distillate and bottom streams (mol% & wt.%) with their estimated cold flow properties under vacuum fractional distillation

Stream	**Feed**	**Distillate**	**Bottom**
Mole fraction			
Methyl Palmitate, C16:0	0.4963	0.9680	0.0500
Methyl Stearate, C18:0	0.0476	0.0018	0.0909
Methyl Oleate, C18:1	0.3677	0.0300	0.6872
Methyl Linoleate, C18:2	0.0884	0.0002	0.1719
Mass fraction			
Methyl Palmitate, C16:0	0.4745	0.9653	0.0459
Methyl Stearate, C18:0	0.0502	0.0020	0.0920
Methyl Oleate, C18:1	0.3854	0.0328	0.6909
Methyl Linoleate, C18:2	0.0920	0.0002	0.1716
Cold Flow Properties			
CP (°C)	20.76[a]	-	-2.58[b]
PP (°C)	15.71[a]	-	-9.62[b]
CFPP (°C)	17.19[a]	-	-5.48[b]

[a] Calculated using Sarin (U_{FAME}) method; [b] Calculated using Sarin (P_{FAME}) method

8.3 Distillation system design

As discussed in Chapter 8.1 and 8.2, in order to obtain PFAD biodiesel with better cold flow properties, implementing vacuum fractional distillation is the way to go. Additionally, judging from the long start-up time required during batch vacuum distillation (about 2 hours), it would be more time-effective and productive to design a vacuum fractional distillation column in continuous flow mode. The design of distillation system is divided into two parts: (i) column and tray design, and (ii) condenser and reboiler design.

8.3.1 Column and tray design

Since a simple distillation is relatively inefficient in separating the esters in PFAD biodiesel, a vacuum fractional distillation column was designed using FUG calculation to improve the separation efficiency of methyl palmitate from the PFAD biodiesel sample.

At the beginning of the design stage, the relative volatility of each individual esters in the PFAD biodiesel was first calculated. It was found that the relative volatility of methyl palmitate to methyl oleate was 2.32. Thus, the separation should be easy as the relative volatility between the two key components was higher than 1.1 (Martín, 2016).

The final mole fraction of light key (methyl palmitate) in the bottom product was set as 0.05. This assumption was reasonable as similar mass composition of methyl palmitate was found in the final product obtained by Dunn et al. (1996) while improving the low temperature properties of biodiesel through winterization. On the other hand, the final mole fraction of heavy key (methyl oleate) present in the distillate was assumed to be 0.03 so as to keep the loss of methyl oleate from the distilled PFAD biodiesel at a low level.

By using Fenske equation, the minimum number of stages required in the distillation column under total reflux condition was found to be 8 stages. The minimum reflux ratio calculated using Underwood Equation was 1.28, which gave an operating reflux ratio of 1.66, at 1.3 times of the minimum reflux ratio. Calculated using Gilliland correlation, the actual number of theoretical stages required in the distillation column was 17 stages (including 1 reboiler). The location of the feed tray was estimated to locate at the ninth stage counting from the top of the column. The results obtained from the manual calculation was validated with a shortcut column modelled using Aspen Hysys, as shown in Figure 8.5. The fluid property package used for predicting the equilibrium and liquid properties in the column was NRTL model (Abdurakhman et al., 2017; Basso et al., 2017). The results obtained, as shown in Table 8.8, were found to be identical.

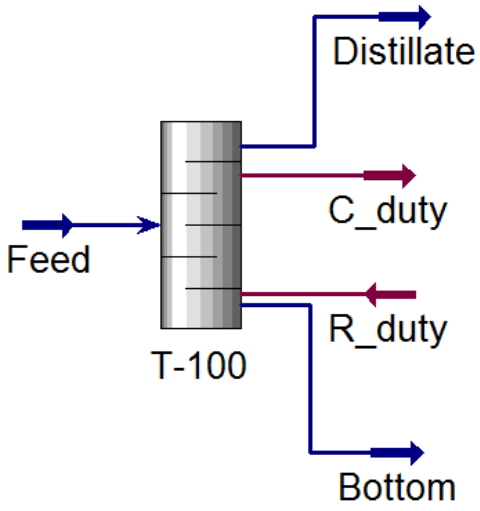

Figure 8.5 Shortcut distillation column model

Table 8.8 Comparison between manual FUG calculation and Hysys model

Performance	**Manual calculation**	**Hysys model**
Minimum number of Trays	7.635	7.287
Actual Number of Trays	16.64	15.975
Optimal Feed Stage	8.65	8.626
Minimum reflux ratio	1.28	1.254
Operating reflux ratio	1.664	1.630

From the distillation column model, additional details on the column and streams were obtained and shown in Table 8.9. The condenser and reboiler pressures were fixed at an absolute pressure of 1 kPa (under vacuum). The operating temperature of the feed stream was set at 186 °C such that the feed stayed as a saturated liquid (i.e. bubble point feed). The thermal condition of the feed is important as it determines the internal flows in the distillation column. No additional heat calculation was required for saturated feed and the feed could be added directly to the liquid flow (Price, 2003). The feed rate of PFAD biodiesel was set at 3750 kg/h or 13.23 kmol/h.

Table 8.9 Operating condition of the distillation column

Operating Parameters	**Value**
Condenser Temperature (°C)	178.8
Reboiler Temperature (°C)	196.8
Rectify Vapour (kmol/h)	16.913
Rectify Liquid (kmol/h)	10.482
Stripping Vapour (kmol/h)	16.913
Stripping Liquid (kmol/h)	23.710
Condenser Duty (10^4 kJ/h)	-106.96
Reboiler Duty (10^4 kJ/h)	109.23
Molar flow rate of distillate (kmol/h)	6.431
Molar flow rate of bottom (kmol/h)	6.797

Judging from the molar flow rate of the bottom product, the total yield of biodiesel with high purity of methyl oleate (69.09 wt.%) and low amount of methyl palmitate (4.59 wt.%) obtained via the fractional distillation column was 51.38%. This is better than using winterization technique but relatively lower than the 59.62% yield obtained using simple vacuum distillation. Nonetheless, the methyl palmitate content in the fractionated biodiesel had significantly reduced from 47.45 wt.% to 4.59 wt.%, as shown in Table 8.7. With the removal of methyl palmitate, the total saturated FAMEs in the biodiesel reduced from 52.47 wt.% at the feed stream to 13.79 wt.% at the bottom stream. This is great for the cold flow improvement of PFAD biodiesel. The distillation column was not designed to completely remove the saturated esters from the PFAD biodiesel as doing so would significantly reduce the ignition quality of the biodisel (Dunn et al., 1996; Edith et al., 2012).

With the obtained properties of distillate and bottom, the liquid and vapour rates were estimated and subsequently, the calculations for column sizing were conducted. With a plate spacing of 0.46 m (18 inch), the column diameter of the rectifying section and stripping section were calculated to be 1.86 m and 1.95 m respectively. There was a 4.6%

difference between the column diameter for both sections due to the variation in velocities of the vapour and liquid streams. Since the difference between the calculated column diameters was small, it is recommended to use a uniform column diameter for the entire column to simplify the fabrication work. Thus, the larger column diameter, 1.95 m, was chosen.

The overall tray efficiency was identified to be 49.71%. Therefore, the number of actual stages required was 34 stages. The column height was estimated to be 16.74m, giving a height-to-diameter ratio of 8.61. According to Price (2003), the height-to-diameter ratio of a distillation column should be less than 20 or 30 while ICARUS Corporation (1998) recommended the ratio should range between 3 and 20. Hence, the calculated ratio was acceptable.

Moving on to the plate design, the selection of plate type depends on the liquid flow arrangement, which was affected by the liquid flow rate and column diameter. The simplest type of most commonly used cross-flow plates, sieve plates, were used in this column design. As compared to valve plates and bubble cap plates, sieve plates are the most cost-effective and least prone to fouling. In addition, the cross-flow trays are also classified based on the liquid flow patterns on the plate. Judging from the calculated volumetric liquid rate (0.0032 m^3/s), using single pass plate was sufficient to accommodate the liquid flow pattern on the plates when the liquid weird load was 0.0021 m^3/s at a weir length of 1.58 m.

No weeping should occur in the column as the actual minimum vapour velocity (66.98 m/s) was higher than the minimum design vapor velocity (34.35 m/s). This would exert enough pressure to hold up the liquid on the tray. Another factor that could cause weeping is the total plate pressure drop, which consist of dry plate drop and wet plate drop. It is a good practice to keep the total pressure drop per tray within the level of 75.4 mm to 127 mm (Kister, 1992). In the calculation, it was discovered that the dry plate drop dominates and exceeded the recommended range. Therefore, the hole area was adjusted to 14% to reduce the dry plate drop, and subsequently reduced the total plate pressure drop. The calculated total plate pressure drop was 115.04 mm liquid, which was satisfactory.

Apart from that, weir height also affects the total plate pressure drop and downcomer liquid backup. The weir height of the vacuum column was set at 8 mm which was within the range 6 to 12 mm recommended by Towler and Sinnott (2013). It was found that at lower weir height setting, the head loss in downcomer would increase significantly, causing the downcomer backup to exceed the column design limitation (half of the sum of tray spacing and weir height, 0.234 m). This was due to the decrement of the A_{ap} with lower weir height. A smaller A_{ap} would amplify the head loss in downcomer, thus contributing to higher downcomer backup that led to column flooding. The downcomer backup of the column was found to be acceptable at 0.21 m and the downcomer residence time was well above 3 s (28.97 s).

Entrainment could occur in a column and negatively affect the plate efficiency when the liquid on the tray was undesirably carried by ascending vapour up to the tray above due to high vapour flow rate. Execessive entrainment should be avoided as this could lead to flooding. To keep the entrainment effect small, it is recommended to take the upper limit of ψ as 0.1. Nonetheless, the figure only served as a rough guide, instead of being a must-have requirement (Towler & Sinnott, 2013). At the column diameter specified, the percentage of flooding was found to be 76.93%. When the F_{LV} was 0.0015, the entrainment was approximately 0.12, which was slightly above the guideline ($\psi \leq 0.1$). This indicated that the entrainment would have a slight effect on the plate efficiency. The finalized plate layout which showcase the downcomer area, hole area, weir length, hole diameter, and etc. is shown in Figure 8.6. Overall, the column and tray design had fitted all of the design requirements, except the entrainment estimation which was least important, and therefore it could be concluded that the design was feasible and practical.

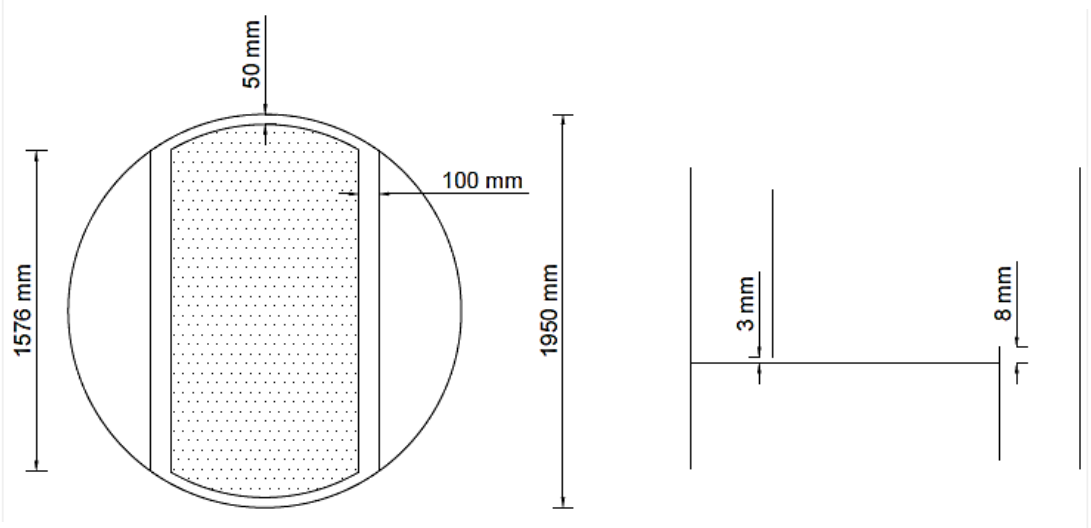

Cross sectional view **Side View**

Plate inner diameter	1.95 m	Plate material	Stainless steel
Hole size	5 mm	Plate spacing	0.46 m
Hole pitch	10.77 mm □	Plate thickness	3 mm
Active holes	14842	Plate pressure drop	115 mm liquid

Figure 8.6 Plate layout

8.3.2 Condenser and reboiler design

A condenser was designed to cool and condense the overhead vapour leaving the top of the column by using cooling water. In this work, the condenser was modeled as a horizontal shell and tube heat exchanger. The shell side consisted of the biodiesel vapour (distillate) and the tube side was allocated with cooling water. The chosen condenser design was a split-ring floating head type, with one shell and four tube passes that were arranged in square pattern. Tube with two passes design was not suitable as the tube side fluid velocity would be less than the recommended range of 1 to 2 m/s (Towler & Sinnott, 2013). The stream properties of the condenser were determined and shown in Table 8.10.

The logarithmic mean temperature difference ΔT_{lm} for the shell and tube streams was 141.76 °C. This temperature difference was not directly used for design as it was only applicable to the heat transfer in true countercurrent flow. By applying a correction factor,

the true temperature difference ΔT_m was found to be 141.42 °C, which was very close. The total heat load from the shell (distillate strean) was 1243.36 kW. To remove this amount of heat energy, the required mass flow rate of cooling water was 7.35 kg/s.

Table 8.10 Stream properties of condenser (1 Shell 4 Tube Passes)

Properties	**Unit**	**Shell (Distillate)**	**Tube (Cooling Water)**
T_{in}	°C	186.00	20
T_{out}	°C	178.77	60
T_{mean}	°C	182..39	40
k_f	W/m.°C	0.0845	0.6315
C_p	kJ/kg°C	2.4125	4.2270
μ	mNs/m^2	0.4382	0.65
ρ	kg/m^3	750	996
$\dot{m}$	kg/s	0.485	7.35
MW	kg/kmol	271.29	18.02

The overall heat transfer coefficient across the shell and tubes of the heat exchanger was assumed as 300 W/m^2.°C as the typical U_o for vacuum condenser with cooling water was between 200–500 W/m^2°C (Towler & Sinnott, 2013). The provisional area required for the heat transfer was found to be 43.96 m^2. With this piece of information, the physical layout of the tube was designed. The material was set as stainless steel 304 to prevent corrosion. For the outer diameter of the tube, it was set as 1 inch. This was one of the most commonly used sizes in the industry while the wall thickness of the tube was decided according to the Birmingham wire gage (BWG) (Edwards, 2008). By using 4.88 m long stainless steel 304 tubes (BWG8) with 25.4 mm outer diameter and 17.0 mm inner diameter, the number of tubes required was found to be 76 tubes. Hence, for 4 passes design, the tubes required per pass would be 19. The tube side fluid velocity was 1.71 m/s, which was satisfactory as the acceptable range was 1–2 m/s. Using 1.25 times square pitch, the tube bundle diameter was found to be 389 mm, and a 53 mm bundle diameter clearance

was required. Therefore, the shell inner diameter, which was the sum of tube bundle diameter and bundle diameter clearance, was 442 mm.

Subsequently, Kern's method was used to determine the heat transfer rate and pressure drop of the heat exchanger in order to check the validity of the initial assumption of the overall heat transfer coefficient. The shell side and tube side heat transfer coefficient were determined to be 499.45 W/m^2.°C and 5899.71 W/m^2.°C, respectively. The overall heat transfer coefficient was 305.75 W/m^2.°C with a percentage difference of only 1.92% when compared with the trial value (300 W/m^2.°C). The tube-side and shell-side pressure drop of the condenser heat exchanger were found to be 43.88 kPa and 1.10 kPa, respectively.

On the other hand, the reboiler for the distillation column was used to vaporize the bottom products by using high pressure steam (23.18 bar). The steam was set as the tube stream, and the biodiesel was the shell stream. Kettle reboiler design was chosen in this study as it was suitable for vacuum operation. The total heat load required for vaporizing the biodiesel was 155.64 kW. Detailed properties of the bottom products and high pressure steam streams are listed in Table 8.11.

Table 8.11 Stream properties for kettle reboiler

Properties	**Unit**	**Shell (Bottom)**	**Tube (Steam @23.18bar)**
T_{in}	°C	186.00	220
T_{out}	°C	196.77	220
T_{mean}	°C	191.38	220
k	W/m.°C	0.0763	0.0351
C_p	kJ/kg°C	2.485	3.598
ΔH_{vap}	kJ/kg	252.62	1862.95
μ	mNs/m^2	0.038	0.016
ρ	kg/m^3	738.49	10.18
$\dot{m}$	kg/s	0.56	2.03
MW	kg/kmol	295.03	18.02

Assuming the overall heat transfer coefficient of the reboiler was 600 W/m^2.°C, the area required for the heat transfer was equivalent to 9.17 m^2. By selecting U tubes with 4.8 m nominal length (d_o = 30 mm, d_i = 25 mm), the number of U tubes required for the process was 21. The tube bundle diameter of the kettle reboiler was found to be 235.41 mm. Using Mostinski's equation, the calculated heat flux based on the estimated area was 17.81 kW/m^2, which was satisfactory as the maximum allowable heat flux value was 30.10 kW/m^2. The nucleate boiling heat transfer coefficient was found to be 746.31 W/m^2.°C. For the reboiler, the overall heat transfer cofficient was 507.40 W/m^2.°C. This value was acceptable as it was close to the estimation of 600 W/m^2.°C for the design to stand. The pressure drop on the tube side was 12.62 kPa, which was well below the maximum allowable pressure drop of 221.67 kPa. The maximum vapor velocity at the kettle reboiler should be less than 19.78 m/s to avoid excessive entrainment. It is found that the maximum velocity of vapor at the liquid surface was 5.22 m/s. Thus, the overall design of the kettle reboiler was satisfactory.

8.4 Summary

The experimental results of the vacuum distillation of PFAD biodiesel were presented and discussed. The yield of distilled biodiesel was 59.62% with only 0.62% loss of starting materials. The fatty acid compositions of PFAD biodiesel before and after vacuum distillation were determined via GC-FID. It was found that a total of 15.44 wt.% methyl palmitate was removed from the distilled biodiesel. The cold flow properties of the distilled sample were significantly improved by 35–42% (6–8 °C). Besides, Sarin (U_{FAME}) correlations could be used to predict the cold flow properties of PFAD biodiesel with less than 2 °C deviation. The CFPP of PFAD biodiesel could be further reduced via vacuum fractional distillation in order to turn the biodiesel into export grade summer biodiesel. Furthermore, the design work and specifications of a vacuum fractional distillation column with the aim of enhancing the cold flow properties of PFAD biodiesel was presented in this chapter. The specifications of the condenser and reboiler for the distillation column which were designed based on Kern's method were shown as well.

The overall design specification of the vacuum tray distillation column is shown in Table 8.12.

Table 8.12 Specification sheet for vacuum fractional distillation column

Specifications	**Symbol**	**Unit**	**Detail**
Feed rate	F	kmol/h	13.2
Minimum number of theoretical stages	$N_{\min}$	-	8
Minimum reflux ratio	R_m	-	1.28
Operating reflux ratio	R	-	1.66
Actual number of theoretical stages	N	-	17
Optimal feed stage	-	-	9
Actual number of trays	N_{act}	-	34
Overall tray efficiency	E_o	%	49.71
Column diameter	D_c	m	1.95
Column length	l_c	m	16.74
Plate spacing	l_t	m	0.46
Weir length	l_w	m	1.58
Cross sectional area of column	A_c	m^2	2.97
Cross sectional area of downcomer	A_d	m^2	0.45
Hole area	A_h	m^2	0.27
Weir height	h_w	mm	8
Hole pitch	l_p	mm	11.18
Hole diameter	d_h	mm	5
Plate thickness	t_p	mm	3
Downcomer backup	h_b	mm	223.86
Type of cross-flow plate	-	-	Single pass sieve plate

CHAPTER 9 CONCLUSION & RECOMMENDATIONS

Part of this chapter (15%) is published in Applied Energy journal, https://doi.org/10.1016/j.apenergy.2019.01.052

Conclusion

The effects of microwave heating towards the biodiesel production as well as the feasibility of vacuum distillation technology towards the cold flow improvement of PFAD biodiesel have been investigated in this study. There were two major findings:

a) **A three-dimensional multiphysics model which describe the microwave-assisted esterification of PFAD was developed by solving the electromagnetism, chemical species, mass-momentum, and energy conservation equations.** The model was capable to provide good prediction of the temperature profile during the process at elevated temperature (above the boiling point of methanol) under microwave irradiation. The overall simulated temperature profile was in good agreement with the experimental results with less than 3% error. This was made possible by including the phase change effect due to methanol vaporization. In addition, to obtain excellent model prediction, the Navier-Stokes equations should always be included in the modelling of biodiesel production regardless how negligible the velocity change associated with the fluid flow is.

b) **Vacuum fractional distillation was found to be a feasible method to improve the cold flow characteristics of PFAD biodiesel to produce export grade biodiesel**. A great portion of methyl palmitate was successfully separated from the rest of the esters in the biodiesel. The yield of biodiesel obtained using fractional vacuum distillation was 51.38%, which was better than using winterization technique (~25%). The reduction of 42.77 wt% methyl palmitate from the biodiesel improved the CFPP of PFAD biodiesel from 19 °C to -5.48 °C, which satisfied the CFPP requirement for grade C summer biodiesel for temperate climates in EN 14214 standard.

The scientific contributions which could be obtained from this study were listed as follows:

- With the aid of microwave dielectric heating, the esterification reaction of PFAD was accelerated and found to follow a second order reaction kinetics, with an activation energy of -36 kJ/mol.
- The relative complex permittivity of PFAD and its biodiesel at 2.45 GHz for temperature range 25–120 °C could be considered as temperature-independent constants, which were 2.78-0.17*j* for PFAD and 3.26-0.21*j* for PFAD biodiesel.
- By using the esterification model, the inputs for vaporization effect of methanol under microwave irradiation, which was not available in literature, were fine-tuned against the temperature measurement data and reported in this study. The values for pre-exponential factor A_{MeOH} and activation energy E_{MeOH} of the vaporization reaction of methanol were found to be 2×10^5 s^{-1} and 54500 J/mol, respectively.
- In the esterification model, non-uniform heating could be observed from the esterification of PFAD and methanol under microwave irradiation. The changes in the localised temperature at the hot spots was sufficient to trigger vaporization reaction of methanol but insufficient to trigger the vaporization reaction of water. Thus, the vaporization reaction of water could be neglected.

- The separation of methyl palmitate (light key) from methyl oleate (heavy key) could be achieved using simple vacuum distillation but at low efficiency (i.e. removal of 15.44 wt% methyl palmitate). Higher separation efficiency could be achieved using vacuum fractional distillation (i.e. removal of 42.77 wt% methyl palmitate)
- The preliminary design of a vacuum fractional distillation column to improve the cold flow properties of PFAD biodiesel was created by using FUG method and presented in this study. The condenser and reboiler which were designed based on Kern's method were shown as well.
- In this study, Sarin (U_{FAME}) method was found to best predict the cold flow characteristics of PFAD biodiesel among the three empirical correlations (Sarin (P_{FAME}), Sarin (U_{FAME}) and Su's method) employed for the prediction of biodiesel cold flow properties, with less than 2 °C deviation.

The research gaps that have been identified included (i) limited studies on the microwave-assisted biodiesel production of low-cost biodiesel from PFAD, (ii) lack of robust model which can describe the microwave-assisted PFAD esterification, as well as (iii) the lack of study on vacuum distillation in modifying the ester compositions of PFAD biodiesel in order to improve its cold flow behaviour. In this work, the effects of microwave on the biodiesel yield was studied. The optimal parametric condition to achieve 91.88% biodiesel yield was reported to be 300 W microwave power, 15 min reaction time, 1:9 PFAD-to-methanol molar ratio, and 1 wt% sulphuric acid catalyst. The second research gap was narrowed down with the successful development of a three-dimensional multiphysics model of microwave-assisted esterification of PFAD feedstock. The power density, heat transfer, fluid velocity, electrical and temperature distribution within the reaction mixture across time were examined. Lastly, to taper the third research gap, a feasibility study on the cold flow improvement of PFAD biodiesel via vacuum distillation approach was carried out. It was proved that the vacuum distillation was a feasible method to improve the cold flow properties of PFAD biodiesel by modifying the ester compositions. The five research objectives of the study had been achieved.

Recommendations

The effect of microwave irradiation on microwave-assisted PFAD esterification can be further investigated by using a more sophisticated microwave reactor that could simultaneously control the temperature magnitude as well as the homogeneity in the reacting fluid. The difference between the reaction kinetics under domestic microwave oven (power-controlled) and scientific microwave oven (temperature-modulated) can be compared in the future work.

In order to further improve the robustness of the numerical model, there are several possible future investigations that can be done. For instance, the thermophysical parameters of the species can be changed to temperature-dependent functions to investigate their effects on the model; and a reflux system can be added to the numerical model to generate the complete vaporisation-condensation cycle of methanol. This numerical model could serve as a basis for optimizing the esterification of biodiesel under the microwave effect where the influence of other parameters (e.g. sample location, reactor design, waveguide position, and types and volume of alcohol) on the heating distribution could be studied as well by means of numerical simulation. Nonetheless, the numerical model poses a limitation as the reaction modelling of the PFAD esterification was simplified to a one-way esterification reaction. The reaction modelling could be more detailed by including a reversible esterification reaction as well as the three transesterification reaction steps for triglycerides which are minor constituents in PFAD feedstock. This also indirectly opens up an extra beneficial advantage to be able to include a wider range of feedstocks for the model simulation.

In addition, the PFAD biodiesel with improved cold flow properties can be analysed in future work to determine the fuel performance via compression ignition diesel engine test. Since a large portion of the saturated methyl palmitate which can improve the oxidative stability of biodiesel was removed during the vacuum fractionation process, the oxidative stability of the distilled PFAD biodiesel should be investigated as well. Conducting an optimization study which could balance the oxidative stability and low temperature

operability of PFAD biodiesel is also favourable. As the yield of distilled biodiesel via vacuum distillation was about 50 – 60% as observed in this study, the life cycle cost analysis of export grade biodiesel production from PFAD feedstock could be assessed in the future to evaluate its economic feasibility. Apart from that, it is also recommended to investigate microwave-assisted reactive distillation which combines both biodiesel production and separation process together in a single column. The biodiesel produced from the reactive distillation column can be used directly as the feed for the vacuum fractional distillation column, which eliminate the need of the time-consuming downstream processing (e.g. water washing and drying) that is still practiced in the industry. This may give rise to the birth of a new product line to produce PFAD biodiesel with improved cold flow characteristics which can be extended into the existing palm oil refinery facilities by integrating both technologies.

REFERENCES

Abdul Kapor, N. Z., Maniam, G. P., Rahim, M. H. A., & Yusoff, M. M. (2017). Palm fatty acid distillate as a potential source for biodiesel production-a review. *Journal of Cleaner Production, 143*, 1-9. doi:10.1016/j.jclepro.2016.12.163

Abdullah, B., Syed Muhammad, S. A. F. a., Shokravi, Z., Ismail, S., Kassim, K. A., Mahmood, A. N., & Aziz, M. M. A. (2019). Fourth generation biofuel: A review on risks and mitigation strategies. *Renewable and Sustainable Energy Reviews, 107*, 37-50. doi:10.1016/j.rser.2019.02.018

Abdurakhman, Y., Putra, Z., & Bilad, M. (2017). *Aspen HYSYS simulation for biodiesel production from waste cooking oil using membrane reactor.* Paper presented at the IOP Conference Series: Materials Science and Engineering.

Adebowale, K., & Adedire, C. (2006). Chemical composition and insecticidal properties of the underutilized Jatropha curcas seed oil. *African Journal of Biotechnology, 5*(10), 901.

Adewale, P., Vithanage, L. N., & Christopher, L. (2017). Optimization of enzyme-catalyzed biodiesel production from crude tall oil using Taguchi method. *Energy Conversion and Management, 154*, 81-91. doi:10.1016/j.enconman.2017.10.045

Al-Shanableh, F., Evcil, A., & Savaş, M. A. (2016). Prediction of Cold Flow Properties of Biodiesel Fuel Using Artificial Neural Network. *Procedia Computer Science, 102*, 273-280. doi:10.1016/j.procs.2016.09.401

Alalwan, H. A., Alminshid, A. H., & Aljaafari, H. A. S. (2019). Promising evolution of biofuel generations. Subject review. *Renewable Energy Focus, 28*, 127-139. doi:10.1016/j.ref.2018.12.006

Alam, M. S., Ashokkumar, B., & Mohammed Siddiq, A. (2018). The density, dynamic viscosity and kinematic viscosity of protic polar solvents (pure and mixed systems) studies: A theoretical insight of thermophysical properties. *Journal of Molecular Liquids, 251*, 458-469. doi:10.1016/j.molliq.2017.12.089

Alamu, O., Waheed, M., Jekayinfa, S., & Akintola, T. (2007). Optimal transesterification duration for biodiesel production from Nigerian palm kernel oil. *Agricultural Engineering International: CIGR Journal*.

Altaie, M. A. H., Janius, R. B., Rashid, U., Taufiq Yap, Y. H., Yunus, R., & Zakaria, R. (2015). Cold flow and fuel properties of methyl oleate and palm-oil methyl ester blends. *Fuel, 160*, 238-244. doi:10.1016/j.fuel.2015.07.084

Aranda, D. A. G., Santos, R. T. P., Tapanes, N. C. O., Ramos, A. L. D., & Antunes, O. A. C. (2008). Acid-Catalyzed Homogeneous Esterification Reaction for Biodiesel Production from Palm Fatty Acids. *Catalysis Letters, 122*(1-2), 20-25. doi:10.1007/s10562-007-9318-z

Ardebili, M. S. S., Hashjin, T. T., Ghobadian, B., & Najafi, G. (2014). Castor Oil Biodiesel Production by Ultrasonic-cum-Microwave. *Middle East Applied Science and Technology, 5*(6), 149-155.

Ardebili, M. S. S., Hashjin, T. T., Ghobadian, B., Najafi, G., Mantegna, S., & Cravotto, G. (2015). Optimization of biodiesel synthesis under simultaneous ultrasound-microwave irradiation using response surface methodology (RSM). *Green Processing and Synthesis, 4*(4), 259-267.

Aro, E.-M. (2016). From first generation biofuels to advanced solar biofuels. *Ambio, 45*(1), 24-31. doi:10.1007/s13280-015-0730-0

Asada, M., Kanazawa, Y., Asakuma, Y., Honda, I., & Phan, C. (2015). Surface tension and oscillation of water droplet under microwave radiation. *Chemical Engineering Research and Design, 101*, 107-112. doi:10.1016/j.cherd.2015.05.019

ASTM. (2010). D6371-05(2010): Standard Test Method for Cold Filter Plugging Point of Diesel and Heating Fuels. West Conshohocken, PA: ASTM International.

ASTM. (2011). D2500-11: Standard Test Method for Cloud Point of Petroleum Products. West Conshohocken, PA: ASTM International.

ASTM. (2015). D97-15: Standard Test Method for Pour Point of Petroleum Products. West Conshohocken, PA: ASTM International.

Atabani, A. E., Silitonga, A. S., Badruddin, I. A., Mahlia, T. M. I., Masjuki, H. H., & Mekhilef, S. (2012). A comprehensive review on biodiesel as an alternative energy resource and its characteristics. *Renewable and Sustainable Energy Reviews, 16*(4), 2070-2093. doi:10.1016/j.rser.2012.01.003

Atadashi, I., Aroua, M., & Aziz, A. A. (2011). Biodiesel separation and purification: a review. *Renewable Energy, 36*(2), 437-443.

Balat, M., & Balat, H. (2010). Progress in biodiesel processing. *Applied Energy, 87*(6), 1815-1835. doi:10.1016/j.apenergy.2010.01.012

Banavali, R., Schultz, A. K., Topp, K. D., & Vandersall, M. T. (2010). Ion Exchange Resins in Biodiesel Processing *The Biodiesel Handbook* (pp. 85).

Basso, R. C., Meirelles, A. J. d. A., & Batista, E. A. C. (2017). Experimental data, thermodynamic modeling and sensitivity analyses for the purification steps of ethyl biodiesel from fodder radish oil production. *Brazilian Journal of Chemical Engineering, 34*, 341-353.

Benson, S. W., & Dobis, O. (1998). Existence of negative activation energies in simple bimolecular metathesis reactions and some observations on too-fast reactions. *The Journal of Physical Chemistry A, 102*(27), 5175-5181.

Boffito, D., Galli, F., Pirola, C., Bianchi, C., & Patience, G. (2014). Ultrasonic free fatty acids esterification in tobacco and canola oil. *Ultrasonics Sonochemistry, 21*(6), 1969-1975.

Bonhorst, C. W., Althouse, P. M., & Triebold, H. O. (1948). Esters of Naturally Occurring Fatty Acids - Physical Properties of Methyl, Propyl, and Isopropyl Esters of C6 to C18 Saturated Fatty Acids. *Industrial & Engineering Chemistry, 40*(12), 2379-2384. doi:10.1021/ie50468a031

Bouaid, A., Vázquez, R., Martinez, M., & Aracil, J. (2016). Effect of free fatty acids contents on biodiesel quality. Pilot plant studies. *Fuel, 174*, 54-62. doi:10.1016/j.fuel.2016.01.018

British Standards Institution. (2011). BS EN 14103: 2011 *Fat and oil derivatives-Fatty acid methyl esters (FAME)-determination of ester and linolenic acid methyl ester contents.* .

British Standards Institution. (2014). BS EN 14214:2012+A1:2014 *Liquid petroleum products - Fatty acid methyl esters (FAME) for use in diesel engines and heating applications - Requirements and test methods*: BSI Standards Limited 2014.

Buszewski, B. (2000). SOLVENTS: DISTILLATION. In I. D. Wilson (Ed.), *Encyclopedia of Separation Science* (pp. 4199-4204). Oxford: Academic Press.

Campañone, L. A., & Zaritzky, N. E. (2010). Mathematical modeling and simulation of microwave thawing of large solid foods under different operating conditions. *Food and Bioprocess Technology, 3*(6), 813-825.

Canakci, M., & Van Gerpen, J. (2001). Biodiesel production from oils and fats with high free fatty acids. *Transactions-American Society of Agricultural Engineers, 44*(6), 1429-1436.

Capuano, L. (2018). *International Energy Outlook 2018 (IEO 2018)*. Retrieved from https://www.eia.gov/pressroom/presentations/capuano_07242018.pdf

Carwile, L. C., & Hoge, H. J. (1966). *Thermal conductivity of pyrex glass: Selected values*. Retrieved from

Central, T.-F. (2010). Thermophysical Properties: Methanol. Retrieved from http://www.thermalfluidscentral.org/encyclopedia/index.php/Thermophysical_Properties:_Methanol

Cermak, S. C., Kenar, J. A., & Evangelista, R. L. (2012). *Distillation of natural fatty acids and their chemical derivatives*: InTech.

Chabukswar, D. D., Heer, P. K. K., & Gaikar, V. G. (2013). Esterification of Palm Fatty Acid Distillate Using Heterogeneous Sulfonated Microcrystalline Cellulose Catalyst and Its Comparison with H2SO4 Catalyzed Reaction. *Industrial & Engineering Chemistry Research, 52*(22), 7316-7326.

Cheah, K. Y., Toh, T. S., & Koh, P. M. (2010). Palm fatty acid distillate biodiesel: Next-generation palm biodiesel. *May 2010 Inform*.

Chemat, F., & Esveld, E. (2001). Microwave Super‐Heated Boiling of Organic Liquids: Origin, Effect and Application. *Chemical Engineering & Technology, 24*(7), 735-744.

Chempro. Top-notch Technology in Production of Oils and Fats. Retrieved from https://www.chempro.in/palmoilproperties.htm

Chen, X., Qian, W.-W., Lu, X.-P., & Han, P.-F. (2012). Preparation of biodiesel catalysed by KF/CaO with ultrasound. *Natural Product Research, 26*(13), 1249-1256. doi:10.1080/14786419.2011.564581

Chipurici, P., Vlaicu, A., Calinescu, I., Vinatoru, M., Vasilescu, M., Ignat, N. D., & Mason, T. J. (2019). Ultrasonic, hydrodynamic and microwave biodiesel synthesis – A comparative study for continuous process. *Ultrasonics Sonochemistry, 57*, 38-47. doi:10.1016/j.ultsonch.2019.05.011

Cho, H. J., Kim, S. H., Hong, S. W., & Yeo, Y.-K. (2012). A single step non-catalytic esterification of palm fatty acid distillate (PFAD) for biodiesel production. *Fuel, 93*, 373-380. doi:10.1016/j.fuel.2011.08.063

Choi, J. H., Kim, S.-S., & Woo, H. C. (2017). Characteristics of vacuum fractional distillation from pyrolytic macroalgae (Saccharina japonica) bio-oil. *Journal of Industrial and Engineering Chemistry, 51*, 206-215. doi:10.1016/j.jiec.2017.03.002

Chongkhong, S., Tongurai, C., Chetpattananondh, P., & Bunyakan, C. (2007). Biodiesel production by esterification of palm fatty acid distillate. *Biomass and Bioenergy, 31*(8), 563-568.

Choo, Y. M., Lau, H. L. N., & Yung, C. L. (2008). Recommendation and Lessons Learned on the Use of Biodiesel for Future Practice. Retrieved from http://goo.gl/kgoqKU

Choo, Y. M., Puah, C. W., & Mohd Basri, W. (2007). Outlook of Palm Biodiesel in Malaysia - CSAM. Retrieved from http://un-csam.org/Activities%20Files/A0801/0202.pdf

Chuah, L. F., Klemeš, J. J., Yusup, S., Bokhari, A., & Akbar, M. M. (2017). A review of cleaner intensification technologies in biodiesel production. *Journal of Cleaner Production, 146*, 181-193. doi:10.1016/j.jclepro.2016.05.017

COMSOL Inc. (2012). *COMSOL Multiphysics Reference Manual, version 4.3* Retrieved from http://www.lmn.pub.ro/~daniel/ElectromagneticModelingDoctoral/Books/COMSOL4.3/mph/COMSOLMultiphysicsReferenceGuide.pdf

Conti, R., Gallitto, A. A., & Fiordilino, E. (2014). Measurement of the convective heat-transfer coefficient. *The Physics Teacher, 52*(2), 109-111.

Cravotto, G., & Cintas, P. (2007). The Combined Use of Microwaves and Ultrasound: Improved Tools in Process Chemistry and Organic Synthesis. *Chemistry – A European Journal, 13*(7), 1902-1909. doi:10.1002/chem.200601845

Derlacki, Z., Easteal, A., Edge, A., Woolf, L., & Roksandic, Z. (1985). Diffusion coefficients of methanol and water and the mutual diffusion coefficient in methanol-water solutions at 278 and 298 K. *The Journal of Physical Chemistry, 89*(24), 5318-5322.

Deshmane, V. G., Gogate, P. R., & Pandit, A. B. (2008). Ultrasound-assisted synthesis of biodiesel from palm fatty acid distillate. *Industrial & Engineering Chemistry Research, 48*(17), 7923-7927. doi:10.1021/ie800981v

Deutsches Museum. (2019). The First Diesel Engine, 1897. Retrieved from http://www.deutsches-museum.de/en/collections/machines/power-engines/combustion-engines/diesel-engines/the-first-diesel-engine-1897/

Díaz-Ortiz, Á., Prieto, P., & de la Hoz, A. (2019). A Critical Overview on the Effect of Microwave Irradiation in Organic Synthesis. *The Chemical Record, 19*(1), 85-97. doi:10.1002/tcr.201800059

Dindar, E. (2016). An overview of the application of hydrodinamic cavitation for the intensification of wastewater treatment applications: a review. *Innovative Energy & Research, 5*(137), 1-7.

Dortmund Data Bank. (2018). Saturated Vapor Pressure - Calculation by Antoine Equation. Retrieved from http://ddbonline.ddbst.com/AntoineCalculation/AntoineCalculationCGI.exe

Dunn, R. O. (2009). Effects of minor constituents on cold flow properties and performance of biodiesel. *Progress in Energy and Combustion Science, 35*(6), 481-489. doi:10.1016/j.pecs.2009.07.002

Dunn, R. O. (2018). Correlating the Cloud Point of Biodiesel to the Concentration and Melting Properties of the Component Fatty Acid Methyl Esters. *Energy & Fuels, 32*(1), 455-464. doi:10.1021/acs.energyfuels.7b02935

Dunn, R. O., & Bagby, M. O. (1995). Low-temperature properties of triglyceride-based diesel fuels: Transesterified methyl esters and petroleum middle distillate/ester blends. *Journal of the American Oil Chemists' Society, 72*(8), 895-904. doi:10.1007/BF02542067

Dunn, R. O., & Moser, B. R. (2010). Cold Weather Properties and Performance of Biodiesel. *The Biodiesel Handbook* (2nd ed.).

Dunn, R. O., Shockley, M. W., & Bagby, M. O. (1996). Improving the low-temperature properties of alternative diesel fuels: Vegetable oil-derived methyl esters. *Journal of the American Oil Chemists' Society, 73*(12), 1719-1728. doi:10.1007/bf02517978

Duz, M. Z., Saydut, A., & Ozturk, G. (2011). Alkali catalyzed transesterification of safflower seed oil assisted by microwave irradiation. *Fuel Processing Technology, 92*(3), 308-313. doi:10.1016/j.fuproc.2010.09.020

Edith, O., Janius, R. B., & Yunus, R. (2012). Factors affecting the cold flow behaviour of biodiesel and methods for improvement—a review. *Pertanika J. Sci. Technol, 20*, 1-14.

Eduljee, H. E. (1959). Design of sieve-type distillation plates. *British Chemical Engineering, 54*(320).

Edwards, J. E. (2008). *Design and Rating - Shell and Tube Heat Exchangers* (pp. 30). Retrieved from https://www.chemstations.com/content/documents/Technical_Articles/shell.pdf

Eevera, T., Rajendran, K., & Saradha, S. (2009). Biodiesel production process optimization and characterization to assess the suitability of the product for varied environmental conditions. *Renewable Energy, 34*(3), 762-765. doi:10.1016/j.renene.2008.04.006

El Sherbiny, S. A., Refaat, A. A., & El Sheltawy, S. T. (2010). Production of biodiesel using the microwave technique. *Journal of Advanced Research, 1*(4), 309-314. doi:10.1016/j.jare.2010.07.003

Elias, R. C., Senra, M., & Soh, L. (2016). Cold Flow Properties of Fatty Acid Methyl Ester Blends with and without Triacetin. *Energy & Fuels, 30*(9), 7400-7409. doi:10.1021/acs.energyfuels.6b01334

Encinar, J. M., González, J. F., Rodríguez, J. J., & Tejedor, A. (2002). Biodiesel Fuels from Vegetable Oils: Transesterification of Cynara cardunculus L. Oils with Ethanol. *Energy & Fuels, 16*(2), 443-450. doi:10.1021/ef010174h

Engineering ToolBox. (2003). Water - Thermophysical Properties. Retrieved from https://www.engineeringtoolbox.com/water-thermal-properties-d_162.html

Engineering ToolBox. (2008). Methanol - Thermophysical Properties. Retrieved from https://www.engineeringtoolbox.com/methanol-properties-d_1209.html

Engineering ToolBox. (2018). Water - Thermal Conductivity. Retrieved from https://www.engineeringtoolbox.com/water-liquid-gas-thermal-conductivity-temperature-pressure-d_2012.html

Fair, J. R. (1963). Tray hydraulics: Perforated trays *Design of Equilibrium Stage Progresses* (pp. 539-569): McGraw-Hill, New York.

Fernández, Y., Arenillas, A., & Menéndez, J. Á. (2011). *Microwave heating applied to pyrolysis, Advances in Induction and Microwave Heating of Mineral and Organic Materials*: Intech Open.

Fidkowski, Z. (2013). *Comparison of Batch and Continuous Industrial Distillation.* Paper presented at the AIChE Spring Meeting and Global Congress on Process Safety, San Antonio, TX.

Filho, E. G. T., Dall'Oglio, E. L., de Sousa Jr, P. T., de Vasconcelos, L. G., & Kuhnen, C. A. (2016). Dielectric Behavior of Reaction Mixture during Acid-Catalyzed Transesterification Reactions in Biodiesel Production. *Energy & Fuels, 30*(6), 4806-4819.

Fokaides, P. A., & Christoforou, E. (2016). 3 - Life cycle sustainability assessment of biofuels. In R. Luque, C. S. K. Lin, K. Wilson, & J. Clark (Eds.), *Handbook of Biofuels Production (Second Edition)* (pp. 41-60): Woodhead Publishing.

Franck, E. U., & Deul, R. (1978). Dielectric behaviour of methanol and related polar fluids at high pressures and temperatures. *Faraday Discussions of the Chemical Society, 66*(0), 191-198. doi:10.1039/DC9786600191

Freedman, B., Pryde, E. H., & Mounts, T. L. (1984). Variables affecting the yields of fatty esters from transesterified vegetable oils. *Journal of the American Oil Chemists Society, 61*(10), 1638-1643. doi:10.1007/BF02541649

Gadzama, S. W., Ufomba, E. C., Okeugo, C. A., Nwachukwu, O. I., Christina, A.-B., Ugwueze, O. S., & Uchechi, R. I. (2016). Computer Aided Design of a Multi-Component Distillation Column-Using the Fenske-Underwood-Gilliland Short-Cut Method. *Science Innovation, 4*(3-1), 24-33. doi:10.11648/j.si.s.2016040301.14

Gedye, R., Smith, F., Westaway, K., Ali, H., Baldisera, L., Laberge, L., & Rousell, J. (1986). The use of microwave ovens for rapid organic synthesis. *Tetrahedron Letters, 27*(3), 279-282. doi:10.1016/S0040-4039(00)83996-9

Gogate, P. R. (2008). Cavitational reactors for process intensification of chemical processing applications: A critical review. *Chemical Engineering and Processing: Process Intensification, 47*(4), 515-527. doi:10.1016/j.cep.2007.09.014

Gole, V. L., & Gogate, P. R. (2013). Intensification of synthesis of biodiesel from non-edible oil using sequential combination of microwave and ultrasound. *Fuel Processing Technology, 106*, 62-69.

Gole, V. L., Naveen, K. R., & Gogate, P. R. (2013). Hydrodynamic cavitation as an efficient approach for intensification of synthesis of methyl esters from sustainable feedstock. *Chemical Engineering and Processing: Process Intensification, 71*, 70-76. doi:10.1016/j.cep.2012.10.006

Gude, V. G. (2015). Synergism of microwaves and ultrasound for advanced biorefineries. *Resource-Efficient Technologies, 1*(2), 116-125. doi:10.1016/j.reffit.2015.10.001

Gude, V. G., Patil, P., Martinez-Guerra, E., Deng, S., & Nirmalakhandan, N. (2013). Microwave energy potential for biodiesel production. *Sustainable Chemical Processes, 1*(5), 1-31. doi:10.1186/2043-7129-1-5

Gui, M. M., Lee, K. T., & Bhatia, S. (2008). Feasibility of edible oil vs. non-edible oil vs. waste edible oil as biodiesel feedstock. *Energy, 33*(11), 1646-1653. doi:10.1016/j.energy.2008.06.002

Gunstone, F. D., Harwood, J. L., & Dijkstra, A. J. (2007). *The lipid handbook with CD-ROM*: CRC Press.

Han, H., Cao, W., & Zhang, J. (2005). Preparation of biodiesel from soybean oil using supercritical methanol and CO2 as co-solvent. *Process Biochemistry, 40*(9), 3148-3151. doi:10.1016/j.procbio.2005.03.014

Hiwot, T. (2017). Determination of oil and biodiesel content, physicochemical properties of the oil extracted from avocado seed (Persea Americana) grown in Wonago and Dilla (gedeo zone), southern Ethiopia. *Chem. Int., 3*, 311-319.

Ho, W. W. S., Ng, H. K., Gan, S., & Chan, W. L. (2015). Ultrasound-assisted transesterification of refined and crude palm oils using heterogeneous palm oil mill fly ash supported calcium oxide catalyst. *Energy Science & Engineering, 3*(3), 257-269. doi:10.1002/ese3.56

Hong, S. W., Cho, H. J., Kim, S. H., & Yeo, Y. K. (2012). Modeling of the non-catalytic semi-batch esterification of palm fatty acid distillate (PFAD). *Korean Journal of Chemical Engineering, 29*(1), 18-24. doi:10.1007/s11814-011-0132-3

Hsiao, M.-C., Lin, C.-C., Chang, Y.-H., & Chen, L.-C. (2010). Ultrasonic mixing and closed microwave irradiation-assisted transesterification of soybean oil. *Fuel, 89*(12), 3618-3622. doi:10.1016/j.fuel.2010.07.044

Hunt, C. D. A., Hanson, D. N., & Wilke, C. R. (1955). Capacity factors in the performance of perforated-plate columns. *AIChE Journal, 1*(4), 441-451. doi:10.1002/aic.690010410

Iakovlieva, A., Boichenko, S., Lejda, K., Vovk, O., & Shkilniuk, I. (2017). Vacuum Distillation of Rapeseed Oil Esters for Production of Jet Fuel Bio-Additives. *Procedia Engineering, 187*, 363-370. doi:10.1016/j.proeng.2017.04.387

ICARUS Corporation. (1998). Towers, Columns. ICARUS Reference (pp. 18). United States of America. Retrieved from https://instruct.uwo.ca/engin-sc/cbe497/Doc/Icarus/ir08.pdf.

Imahara, H., Minami, E., Hari, S., & Saka, S. (2008). Thermal stability of biodiesel in supercritical methanol. *Fuel, 87*(1), 1-6. doi:10.1016/j.fuel.2007.04.003

Imahara, H., Minami, E., & Saka, S. (2006). Thermodynamic study on cloud point of biodiesel with its fatty acid composition. *Fuel, 85*(12), 1666-1670. doi:10.1016/j.fuel.2006.03.003

Jaimes, W., Acevedo, P., & Kafarov, V. (2010). Exergy analysis of palm oil biodiesel production. *Chem Eng, 21*, 1345-1350.

Jermolovicius, L. A., Cantagesso, L. C. M., do Nascimento, R. B., de Castro, E. R., dos S. Pouzada, E. V., & Senise, J. T. (2017). Microwave fast-tracking biodiesel production. *Chemical Engineering and Processing: Process Intensification, 122*, 380-388. doi:10.1016/j.cep.2017.03.010

Johari, A., Nyakuma, B. B., Mohd Nor, S. H., Mat, R., Hashim, H., Ahmad, A., . . . Tuan Abdullah, T. A. (2015). The challenges and prospects of palm oil based biodiesel in Malaysia. *Energy, 81*, 255-261. doi:10.1016/j.energy.2014.12.037

Jones, D. S., & Pujadó, P. P. (2006). *Handbook of petroleum processing*: Springer Science & Business Media.

Joshi, S., Gogate, P. R., Moreira, P. F., & Giudici, R. (2017). Intensification of biodiesel production from soybean oil and waste cooking oil in the presence of heterogeneous catalyst using high speed homogenizer. *Ultrasonics Sonochemistry, 39*, 645-653. doi:10.1016/j.ultsonch.2017.05.029

Kalva, A., Sivasankar, T., & Moholkar, V. S. (2008). Physical mechanism of ultrasound-assisted synthesis of biodiesel. *Industrial & Engineering Chemistry Research, 48*(1), 534-544.

Karacan, S., & Karacan, F. (2015). Steady-state optimization for biodiesel production in a reactive distillation column. *Clean Technologies and Environmental Policy*, 1-9.

Kelkar, M. A., Gogate, P. R., & Pandit, A. B. (2008). Intensification of esterification of acids for synthesis of biodiesel using acoustic and hydrodynamic cavitation. *Ultrasonics Sonochemistry, 15*(3), 188-194. doi:10.1016/j.ultsonch.2007.04.003

Kesbi, O. M., Rajabipour, A., Omid, M., & Goldansaz, S. H. (2018). Determination of electric field intensity during microwave heating of selected vegetables and fruits. *Journal of Microwave Power and Electromagnetic Energy, 52*(4), 276-286. doi:10.1080/08327823.2018.1534054

Kim, D., Choi, J., Kim, G.-J., Seol, S. K., & Jung, S. (2011). Accelerated esterification of free fatty acid using pulsed microwaves. *Bioresource Technology, 102*(14), 7229-7231.

Kister, H. (1992). *Distillation design*: McGraw-Hill Professional.

Komarov, V., Wang, S., & Tang, J. (2005). Permittivity and measurements. *Encyclopedia of RF and microwave engineering*.

Kumar, D., Kumar, G., Poonam, & Singh, C. P. (2010). Ultrasonic-assisted transesterification of Jatropha curcus oil using solid catalyst, Na/SiO2. *Ultrasonics Sonochemistry, 17*(5), 839-844. doi:10.1016/j.ultsonch.2010.03.001

Lam, M. K., Lee, K. T., & Mohamed, A. R. (2009). Life cycle assessment for the production of biodiesel: A case study in Malaysia for palm oil versus jatropha oil. *Biofuels, Bioproducts and Biorefining, 3*(6), 601-612. doi:10.1002/bbb.182

Law, M. C., Chang, J. S. L., Chan, Y. S., Pui, D. Y., & You, K. Y. (2018). Experimental characterization and modeling of microwave heating of oil palm kernels, mesocarps, and empty fruit bunches. *Drying Technology*, 1-23. doi:10.1080/07373937.2018.1439057

Law, M. C., Liew, E. L., Chang, S. L., Chan, Y. S., & Leo, C. P. (2016). Modelling microwave heating of discrete samples of oil palm kernels. *Applied Thermal Engineering, 98*, 702-726. doi:10.1016/j.applthermaleng.2016.01.009

Lee, G. L., Law, M. C., & Lee, V. C. C. (2020). Numerical modelling of liquid heating and boiling phenomena under microwave irradiation using OpenFOAM. *International Journal of Heat and Mass Transfer, 148*, 119096. doi:10.1016/j.ijheatmasstransfer.2019.119096

Lee, R. A., & Lavoie, J.-M. (2013). From first- to third-generation biofuels: Challenges of producing a commodity from a biomass of increasing complexity. *Animal Frontiers, 3*(2), 6-11. doi:10.2527/af.2013-0010

Lee, S., & Shah, Y. T. (2012). *Biofuels and bioenergy: processes and technologies*: CRC Press.

Leonelli, C., & Veronesi, P. (2015). Microwave Reactors for Chemical Synthesis and Biofuels Preparation. In Z. Fang, J. R. L. Smith, & X. Qi (Eds.), *Production of Biofuels and Chemicals with Microwave* (Vol. 3, pp. 17-40): Springer Netherlands.

Leong, W. (1992). The refining and fractionation of palm oil. *Palm Oil Mill Engineers-Executives Training Course 14th Semester, 1*, 1-6.

Leung, D. Y. C., Wu, X., & Leung, M. K. H. (2010). A review on biodiesel production using catalyzed transesterification. *Applied Energy, 87*(4), 1083-1095. doi:10.1016/j.apenergy.2009.10.006

Li, Y., Ye, B., Shen, J., Tian, Z., Wang, L., Zhu, L., . . . Qiu, F. (2013). Optimization of biodiesel production process from soybean oil using the sodium potassium tartrate doped zirconia catalyst under Microwave Chemical Reactor. *Bioresource Technology, 137*, 220-225. doi:10.1016/j.biortech.2013.03.126

Li, Z.-H., Lin, P.-H., Wu, J. C. S., Huang, Y.-T., Lin, K.-S., & Wu, K. C. W. (2013). A stirring packed-bed reactor to enhance the esterification–transesterification in biodiesel production by lowering mass-transfer resistance. *Chemical Engineering Journal, 234*, 9-15. doi:10.1016/j.cej.2013.08.053

Liao, X., Raghavan, G. S. V., & Yaylayan, V. A. (2001). Dielectric properties of alcohols (C1-C5) at 2450 MHz and 915 MHz. *Journal of Molecular Liquids, 94*(1), 51-60. doi:10.1016/S0167-7322(01)00241-0

Lieu, T., Yusup, S., & Moniruzzaman, M. (2016). Kinetic study on microwave-assisted esterification of free fatty acids derived from Ceiba pentandra Seed Oil. *Bioresource Technology, 211*, 248-256. doi:10.1016/j.biortech.2016.03.105

Lim, S., & Teong, L. K. (2010). Recent trends, opportunities and challenges of biodiesel in Malaysia: An overview. *Renewable and Sustainable Energy Reviews, 14*(3), 938-954. doi:10.1016/j.rser.2009.10.027

Lin, L., Cunshan, Z., Vittayapadung, S., Xiangqian, S., & Mingdong, D. (2011). Opportunities and challenges for biodiesel fuel. *Applied Energy, 88*(4), 1020-1031. doi:10.1016/j.apenergy.2010.09.029

Liu, X., He, H., Wang, Y., Zhu, S., & Piao, X. (2008). Transesterification of soybean oil to biodiesel using CaO as a solid base catalyst. *Fuel, 87*(2), 216-221. doi:10.1016/j.fuel.2007.04.013

Lockett, M. J. (1986). *Distillation tray fundamentals*. Cambridge, England: Cambridge University Press.

Lokman, I. M., Rashid, U., & Taufiq-Yap, Y. H. (2015). Microwave-Assisted Methyl Ester Production from Palm Fatty Acid Distillate over a Heterogeneous Carbon-Based Solid Acid Catalyst. *Chemical Engineering & Technology, 38*(10), 1837-1844. doi:10.1002/ceat.201500265

Lokman, I. M., Rashid, U., Taufiq-Yap, Y. H., & Yunus, R. (2015). Methyl ester production from palm fatty acid distillate using sulfonated glucose-derived acid catalyst. *Renewable Energy, 81*, 347-354. doi:10.1016/j.renene.2015.03.045

Lokman, I. M., Rashid, U., Zainal, Z., Yunus, R., & Taufiq-Yap, Y. H. (2014). Microwave-assisted Biodiesel Production by Esterification of Palm Fatty Acid Distillate. *Journal of oleo science, 63*(9), 849-855.

Lopes, J. C. A., Boros, L., Krähenbühl, M. A., Meirelles, A. J. A., Daridon, J. L., Pauly, J., . . . Coutinho, J. A. P. (2008). Prediction of Cloud Points of Biodiesel. *Energy & Fuels, 22*(2), 747-752. doi:10.1021/ef700436d

Lü, J., Sheahan, C., & Fu, P. (2011). Metabolic engineering of algae for fourth generation biofuels production. *Energy & Environmental Science, 4*(7), 2451-2466. doi:10.1039/C0EE00593B

Lv, P., Cheng, Y., Yang, L., Yuan, Z., Li, H., & Luo, W. (2013). Improving the low temperature flow properties of palm oil biodiesel: Addition of cold flow improver. *Fuel Processing Technology, 110*, 61-64. doi:10.1016/j.fuproc.2012.12.014

Ma, F., Clements, L., & Hanna, M. (1998). The effects of catalyst, free fatty acids, and water on transesterification of beef tallow. *Transactions of the ASAE, 41*(5), 1261.

Ma, F., & Hanna, M. A. (1999). Biodiesel production: a review. *Bioresource Technology, 70*(1), 1-15. doi:10.1016/S0960-8524(99)00025-5

Ma, G., Hu, W., Pei, H., Jiang, L., Song, M., & Mu, R. (2015). In situ heterogeneous transesterification of microalgae using combined ultrasound and microwave irradiation. *Energy Conversion and Management, 90*, 41-46. doi:10.1016/j.enconman.2014.10.061

Maçaira, J., Santana, A., Recasens, F., & Angeles Larrayoz, M. (2011). Biodiesel production using supercritical methanol/carbon dioxide mixtures in a continuous reactor. *Fuel, 90*(6), 2280-2288. doi:10.1016/j.fuel.2011.02.017

Maddikeri, G. L., Gogate, P. R., & Pandit, A. B. (2014). Intensified synthesis of biodiesel using hydrodynamic cavitation reactors based on the interesterification of waste cooking oil. *Fuel, 137*, 285-292. doi:10.1016/j.fuel.2014.08.013

Maeda, Y., Vinatoru, M., Stavarach, C. E., Iwai, K., & Oshige, H. (2005). Method for producing fatty acid alcohol ester: Google Patents.

Mahlia, T. M. I., Syazmi, Z. A. H. S., Mofijur, M., Abas, A. E. P., Bilad, M. R., Ong, H. C., & Silitonga, A. S. (2020). Patent landscape review on biodiesel production: Technology updates. *Renewable and Sustainable Energy Reviews, 118*, 109526. doi:10.1016/j.rser.2019.109526

Martín, M. M. (2016). Chapter 2 - Chemical processes. In M. M. Martín (Ed.), *Industrial Chemical Process Analysis and Design* (pp. 13-60). Boston: Elsevier.

Martinez-Guerra, E., & Gude, V. G. (2014a). Synergistic effect of simultaneous microwave and ultrasound irradiations on transesterification of waste vegetable oil. *Fuel, 137*, 100-108.

Martinez-Guerra, E., & Gude, V. G. (2014b). Transesterification of used vegetable oil catalyzed by barium oxide under simultaneous microwave and ultrasound irradiations. *Energy Conversion and Management, 88*, 633-640. doi:10.1016/j.enconman.2014.08.060

Mazubert, A., Taylor, C., Aubin, J., & Poux, M. (2014). Key role of temperature monitoring in interpretation of microwave effect on transesterification and esterification reactions for biodiesel production. *Bioresource Technology, 161*, 270-279. doi:10.1016/j.biortech.2014.03.011

McCabe, W. L., Smith, J. C., & Harriott, P. (2005). *Unit operations of chemical engineering* (7th ed.): McGraw-Hill New York.

Mehdizadeh, M. (2015). Chapter 1 - The impact of fields on materials at microwave and radio frequencies *Microwave/RF Applicators and Probes (Second Edition)* (pp. 1-33). Boston: William Andrew Publishing.

Mekhilef, S., Siga, S., & Saidur, R. (2011). A review on palm oil biodiesel as a source of renewable fuel. *Renewable and Sustainable Energy Reviews, 15*(4), 1937-1949. doi:10.1016/j.rser.2010.12.012

Metre, A. V., & Nath, K. (2015). Super phosphoric acid catalyzed esterification of Palm Fatty Acid Distillate for biodiesel production: physicochemical parameters and kinetics. *Polish Journal of Chemical Technology, 17*(1), 88-96. doi:10.1515/pjct-2015-0013

Mofijur, M., Masjuki, H. H., Kalam, M. A., Hazrat, M. A., Liaquat, A. M., Shahabuddin, M., & Varman, M. (2012). Prospects of biodiesel from Jatropha in Malaysia. *Renewable and Sustainable Energy Reviews, 16*(7), 5007-5020. doi:10.1016/j.rser.2012.05.010

Mohammad Fauzi, A. H., Amin, N. A. S., & Mat, R. (2014). Esterification of oleic acid to biodiesel using magnetic ionic liquid: Multi-objective optimization and kinetic study. *Applied Energy, 114*, 809-818. doi:10.1016/j.apenergy.2013.10.011

Moser, B. R. (2009). Biodiesel production, properties, and feedstocks. *In Vitro Cellular & Developmental Biology - Plant, 45*(3), 229-266. doi:10.1007/s11627-009-9204-z

Motasemi, F., & Ani, F. N. (2011). The production of biodiesel from waste cooking oil using microwave irradiation. *Jurnal Mekanikal, 32*, 61-72.

Motasemi, F., & Ani, F. N. (2012). A review on microwave-assisted production of biodiesel. *Renewable and Sustainable Energy Reviews, 16*(7), 4719-4733. doi:10.1016/j.rser.2012.03.069

Muley, P. D., & Boldor, D. (2013). Investigation of microwave dielectric properties of biodiesel components. *Bioresource Technology, 127*, 165-174. doi:10.1016/j.biortech.2012.10.008

Murugesan, A., Umarani, C., Chinnusamy, T., Krishnan, M., Subramanian, R., & Neduzchezhain, N. (2009). Production and analysis of bio-diesel from non-edible oils—a review. *Renewable and Sustainable Energy Reviews, 13*(4), 825-834.

Nakamura, T., Shimizu, M., Kimura, H., & Sato, R. (2005). Effective permittivity of amorphous mixed materials. *Electronics and Communications in Japan (Part I: Communications), 88*(10), 1-9.

Nam, H., Choi, J., & Capareda, S. C. (2016). Comparative study of vacuum and fractional distillation using pyrolytic microalgae (Nannochloropsis oculata) bio-oil. *Algal Research, 17*, 87-96. doi:10.1016/j.algal.2016.04.020

Narvaes-Garcia, A., Zavala-Loria, J., Vilchiz-Bravo, L., & Rocha-Uribe, J. (2015). Performance Indices To Design A Multicomponent Batch Distillation Column Using A Shortcut Method. *Brazilian Journal of Chemical Engineering, 32*(2), 595-608.

National Center for Biotechnology Information. (2004, 22 September, 2018). Methanol. Retrieved from https://pubchem.ncbi.nlm.nih.gov/compound/methanol

Navarrete, A., Mato, R. B., & Cocero, M. J. (2012). A predictive approach in modeling and simulation of heat and mass transfer during microwave heating. Application to SFME of essential oil of Lavandin Super. *Chemical Engineering Science, 68*(1), 192-201. doi:10.1016/j.ces.2011.09.026

Navarro, M. C., Díaz-Ortiz, A., Prieto, P., & de la Hoz, A. (2019). A spectral numerical model and an experimental investigation on radial microwave irradiation of water and ethanol in a cylindrical vessel. *Applied Mathematical Modelling, 66*, 680-694. doi:10.1016/j.apm.2018.09.035

Nisar, N., Mehmood, S., Nisar, H., Jamil, S., Ahmad, Z., Ghani, N., . . . Abbas, M. (2018). Brassicaceae family oil methyl esters blended with ultra-low sulphur diesel fuel (ULSD): Comparison of fuel properties with fuel standards. *Renewable Energy, 117*, 393-403. doi:10.1016/j.renene.2017.10.087

Niza, N. M., Tan, K. T., Ahmad, Z., & Lee, K. T. (2011). Comparison and optimisation of biodiesel production from Jatropha curcas oil using supercritical methyl acetate and methanol. *Chemical Papers, 65*(5), 721-729. doi:10.2478/s11696-011-0063-9

Niza, N. M., Tan, K. T., Lee, K. T., & Ahmad, Z. (2013). Biodiesel production by non-catalytic supercritical methyl acetate: Thermal stability study. *Applied Energy, 101*, 198-202. doi:10.1016/j.apenergy.2012.03.033

Nomanbhay, S., & Ong, M. Y. (2017). A Review of Microwave-Assisted Reactions for Biodiesel Production. *Bioengineering, 4*(2), 57.

Oliveira, P. A., Baesso, R. M., Moraes, G. C., Alvarenga, A. V., & Costa-Félix, R. P. (2018). Ultrasound Methods for Biodiesel Production and Analysis. *Biofuels: State of Development*, 121.

Pal, A., Verma, A., Kachhwaha, S. S., & Maji, S. (2010). Biodiesel production through hydrodynamic cavitation and performance testing. *Renewable Energy, 35*(3), 619-624. doi:10.1016/j.renene.2009.08.027

Park, J.-Y., Kim, D.-K., Lee, J.-P., Park, S.-C., Kim, Y.-J., & Lee, J.-S. (2008). Blending effects of biodiesels on oxidation stability and low temperature flow properties. *Bioresource Technology, 99*(5), 1196-1203. doi:10.1016/j.biortech.2007.02.017

Parkar, P. A., Choudhary, H. A., & Moholkar, V. S. (2012). Mechanistic and kinetic investigations in ultrasound assisted acid catalyzed biodiesel synthesis. *Chemical Engineering Journal, 187*, 248-260.

Patil, P. D., Gude, V. G., Camacho, L. M., & Deng, S. (2010). Microwave-Assisted Catalytic Transesterification of Camelina Sativa Oil. *Energy & Fuels, 24*(2), 1298-1304. doi:10.1021/ef9010065

Patil, P. D., Gude, V. G., Reddy, H. K., Muppaneni, T., & Deng, S. (2012). Biodiesel production from waste cooking oil using sulfuric acid and microwave irradiation processes. *Journal of Environmental Protection, 2012*. doi:10.4236/jep.2012.31013

Patil, P. D., Reddy, H., Muppaneni, T., Ponnusamy, S., Cooke, P., Schuab, T., & Deng, S. (2013). Microwave-mediated non-catalytic transesterification of algal biomass under supercritical ethanol conditions. *The Journal of Supercritical Fluids, 79*, 67-72. doi:10.1016/j.supflu.2012.11.023

Patil, P. D., Reddy, H., Muppaneni, T., Schaub, T., Holguin, F. O., Cooke, P., . . . Deng, S. (2013). In situ ethyl ester production from wet algal biomass under microwave-mediated supercritical ethanol conditions. *Bioresource Technology, 139*, 308-315. doi:10.1016/j.biortech.2013.04.045

Perego, C., & Ricci, M. (2012). Diesel fuel from biomass. *Catalysis Science & Technology, 2*(9), 1776-1786. doi:10.1039/C2CY20326J

Perreux, L., & Loupy, A. (2001). A tentative rationalization of microwave effects in organic synthesis according to the reaction medium, and mechanistic considerations. *Tetrahedron, 57*(45), 9199-9223.

Peters, M. S., Timmerhaus, K. D., & West, R. E. (2004). *Plant design and economics for chemical engineers*. Boston: McGraw-Hill.

Phoo, Z. W. M. M., Razon, L. F., Knothe, G., Ilham, Z., Goembira, F., Madrazo, C. F., . . . Saka, S. (2014). Evaluation of Indian milkweed (Calotropis gigantea) seed oil as alternative feedstock for biodiesel. *Industrial Crops and Products, 54*, 226-232. doi:10.1016/j.indcrop.2014.01.029

Pratas, M. J., Freitas, S., Oliveira, M. B., Monteiro, S. C., Lima, A. S., & Coutinho, J. A. P. (2010). Densities and Viscosities of Fatty Acid Methyl and Ethyl Esters. *Journal of Chemical & Engineering Data, 55*(9), 3983-3990. doi:10.1021/je100042c

Price, R. M. (2003). Distillation. Retrieved from http://facstaff.cbu.edu/rprice/lectures/distill7.html

Qiu, Z., Zhao, L., & Weatherley, L. (2010). Process intensification technologies in continuous biodiesel production. *Chemical Engineering and Processing: Process Intensification, 49*(4), 323-330. doi:10.1016/j.cep.2010.03.005

Ramadhas, A. S., Jayaraj, S., & Muraleedharan, C. (2004). Use of vegetable oils as I.C. engine fuels — A review. *Renewable Energy, 29*(5), 727-742. doi:10.1016/j.renene.2003.09.008

Rana, K. K., & Rana, S. (2014). Microwave reactors: a brief review on its fundamental aspects and applications. *Open Access Library Journal, 1*(6), 1-20.

Ratanadecho, P., Aoki, K., & Akahori, M. (2002). A numerical and experimental investigation of the modeling of microwave heating for liquid layers using a rectangular wave guide (effects of natural convection and dielectric properties). *Applied Mathematical Modelling, 26*(3), 449-472. doi:10.1016/S0307-904X(01)00046-4

Rodríguez, A. M., Prieto, P., de la Hoz, A., Díaz-Ortiz, Á., Martín, D. R., & García, J. I. (2015). Influence of Polarity and Activation Energy in Microwave-Assisted Organic Synthesis (MAOS). *ChemistryOpen, 4*(3), 308-317. doi:10.1002/open.201402123

Román-Figueroa, C., Olivares-Carrillo, P., Paneque, M., Palacios-Nereo, F. J., & Quesada-Medina, J. (2016). High-yield production of biodiesel by non-catalytic supercritical methanol transesterification of crude castor oil (Ricinus communis). *Energy, 107*, 165-171. doi:10.1016/j.energy.2016.03.136

Roy, P. K., Datta, S., Nandi, S., & Al Basir, F. (2014). Effect of mass transfer kinetics for maximum production of biodiesel from Jatropha Curcas oil: A mathematical approach. *Fuel, 134*, 39-44. doi:10.1016/j.fuel.2014.05.021

Rudan-Tasic, D., & Klofutar, C. (1999). Characteristics of vegetable oils of some Slovene manufacturers. *Acta Chim Slov, 46*(4), 511-521.

Sabliov, C. M., Salvi, D. A., & Boldor, D. (2007). High frequency electromagnetism, heat transfer and fluid flow coupling in ANSYS multiphysics. *Journal of Microwave Power and Electromagnetic Energy, 41*(4), 5-17.

Saeed, R. M., Schlegel, J. P., Castano, C., Sawafta, R., & Kuturu, V. (2017). Preparation and thermal performance of methyl palmitate and lauric acid eutectic mixture as phase change material (PCM). *Journal of Energy Storage, 13*, 418-424. doi:10.1016/j.est.2017.08.005

Saimon, N. N., Jusoh, M., Ngadi, N., & Zakaria, Z. Y. (2020). Kinetic Study of Esterification of Palm Fatty Acid Distillate Using Sulfonated Glucose Prepared via Microwave-Assisted Heating Method. *Chemical Engineering Transactions, 78*, 403-408.

Salvi, D., Boldor, D., Aita, G. M., & Sabliov, C. M. (2011). COMSOL Multiphysics model for continuous flow microwave heating of liquids. *Journal of Food Engineering, 104*(3), 422-429. doi:10.1016/j.jfoodeng.2011.01.005

Sarin, A., Arora, R., Singh, N. P., Sarin, R., Malhotra, R. K., & Kundu, K. (2009). Effect of blends of Palm-Jatropha-Pongamia biodiesels on cloud point and pour point. *Energy, 34*(11), 2016-2021. doi:10.1016/j.energy.2009.08.017

Sarin, A., Arora, R., Singh, N. P., Sarin, R., Malhotra, R. K., & Sarin, S. (2010). Blends of Biodiesels Synthesized from Non-edible and Edible Oils: Effects on the Cold Filter Plugging Point. *Energy & Fuels, 24*(3), 1996-2001. doi:10.1021/ef901131m

Scott, T. A., Macmillan, D., & Melvin, E. H. (1952). Vapor pressures and distillation of methyl esters of some fatty acids. *Industrial & Engineering Chemistry, 44*(1), 172-175.

Selemani, A. (2018). Thermal chemical enhancement and influence of fluid flow in transesterification of palm oil. *Energy Sources, Part A: Recovery, Utilization, and Environmental Effects, 40*(1), 81-87. doi:10.1080/15567036.2017.1405113

Shah, Y. T., Pandit, A. B., & Moholkar, V. S. (1999). Cavitation Reactors. In Y. T. Shah, A. B. Pandit, & V. S. Moholkar (Eds.), *Cavitation Reaction Engineering* (pp. 193-245). Boston, MA: Springer US.

Shahbazi, M. R., Khoshandam, B., Nasiri, M., & Ghazvini, M. (2012). Biodiesel production via alkali-catalyzed transesterification of Malaysian RBD palm oil – Characterization, kinetics model. *Journal of the Taiwan Institute of Chemical Engineers, 43*(4), 504-510. doi:10.1016/j.jtice.2012.01.009

Sharma, A., Kodgire, P., & Kachhwaha, S. S. (2019). Biodiesel production from waste cotton-seed cooking oil using microwave-assisted transesterification: Optimization and kinetic modeling. *Renewable and Sustainable Energy Reviews, 116*, 109394. doi:10.1016/j.rser.2019.109394

Shin, H.-Y., Lim, S.-M., Kang, S. C., & Bae, S.-Y. (2012). Statistical optimization for biodiesel production from rapeseed oil via transesterificaion in supercritical methanol. *Fuel Processing Technology, 98*, 1-5. doi:10.1016/j.fuproc.2012.01.025

Sikarwar, V. S., Zhao, M., Fennell, P. S., Shah, N., & Anthony, E. J. (2017). Progress in biofuel production from gasification. *Progress in Energy and Combustion Science, 61*, 189-248. doi:10.1016/j.pecs.2017.04.001

Silitonga, A., Atabani, A., Mahlia, T., Masjuki, H., Badruddin, I. A., & Mekhilef, S. (2011). A review on prospect of Jatropha curcas for biodiesel in Indonesia. *Renewable and Sustainable Energy Reviews, 15*(8), 3733-3756.

Singh, A. (2010). *Optimization of microwave-assisted extraction of antioxidants from potato peels.* McGill University Library.

Singh, D., Sharma, D., Soni, S. L., Sharma, S., Kumar Sharma, P., & Jhalani, A. (2020). A review on feedstocks, production processes, and yield for different generations of biodiesel. *Fuel, 262*, 116553. doi:10.1016/j.fuel.2019.116553

Soltani, S., Rashid, U., Yunus, R., & Taufiq-Yap, Y. H. (2016). Biodiesel production in the presence of sulfonated mesoporous ZnAl2O4 catalyst via esterification of palm fatty acid distillate (PFAD). *Fuel, 178*, 253-262. doi:10.1016/j.fuel.2016.03.059

Sroynak, R., Srikalong, P., & Raviyan, P. (2013). Radical scavenging capacity and antioxidant activity of the vitamin E extracted from palm fatty acid distillate by sequential cooling hexane. *Journal of Agricultural Science, 5*(4), 224.

Stankiewicz, A. I., & Moulijn, J. A. (2000). Process intensification: transforming chemical engineering. *Chemical engineering progress, 96*(1), 22-34.

Stauffer, E., Dolan, J. A., & Newman, R. (2008). CHAPTER 7 - Flammable and Combustible Liquids. In E. Stauffer, J. A. Dolan, & R. Newman (Eds.), *Fire Debris Analysis* (pp. 199-233). Burlington: Academic Press.

Stavarache, C., Vinatoru, M., Maeda, Y., & Bandow, H. (2007). Ultrasonically driven continuous process for vegetable oil transesterification. *Ultrasonics Sonochemistry, 14*(4), 413-417. doi:10.1016/j.ultsonch.2006.09.014

Stavarache, C., Vinatoru, M., Nishimura, R., & Maeda, Y. (2003). Conversion of vegetable oil to biodiesel using ultrasonic irradiation. *Chemistry Letters, 32*(8), 716-717. doi:10.1002/chin.200350242

Stavarache, C., Vinatoru, M., Nishimura, R., & Maeda, Y. (2005). Fatty acids methyl esters from vegetable oil by means of ultrasonic energy. *Ultrasonics Sonochemistry, 12*(5), 367-372. doi:10.1016/j.ultsonch.2004.04.001

Su, Y.-C., Liu, Y. A., Diaz Tovar, C. A., & Gani, R. (2011). Selection of Prediction Methods for Thermophysical Properties for Process Modeling and Product Design of Biodiesel Manufacturing. *Industrial & Engineering Chemistry Research, 50*(11), 6809-6836. doi:10.1021/ie102441u

Tabatabaei, M., Aghbashlo, M., Dehhaghi, M., Panahi, H. K. S., Mollahosseini, A., Hosseini, M., & Soufiyan, M. M. (2019). Reactor technologies for biodiesel production and processing: A review. *Progress in Energy and Combustion Science, 74*, 239-303. doi:10.1016/j.pecs.2019.06.001

Talebian-Kiakalaieh, A., Amin, N. A. S., Zarei, A., & Noshadi, I. (2013). Transesterification of waste cooking oil by heteropoly acid (HPA) catalyst: optimization and kinetic model. *Applied Energy, 102*, 283-292.

Tan, K. T., Gui, M. M., Lee, K. T., & Mohamed, A. R. (2010). An optimized study of methanol and ethanol in supercritical alcohol technology for biodiesel production.

The Journal of Supercritical Fluids, 53(1), 82-87. doi:10.1016/j.supflu.2009.12.017

Tan, K. T., Lee, K. T., & Mohamed, A. R. (2009). Production of FAME by palm oil transesterification via supercritical methanol technology. *Biomass and Bioenergy, 33*(8), 1096-1099. doi:10.1016/j.biombioe.2009.04.003

Terigar, B. G., Balasubramanian, S., & Boldor, D. (2010). An analysis of the microwave dielectric properties of solvent-oil feedstock mixtures at 300–3000MHz. *Bioresource Technology, 101*(16), 6510-6516. doi:10.1016/j.biortech.2010.01.097

Thidé, B. (2004). *Electromagnetic field theory*: Upsilon Books Uppsala, Sweden.

Tiwari, A. K., Kumar, A., & Raheman, H. (2007). Biodiesel production from jatropha oil (Jatropha curcas) with high free fatty acids: an optimized process. *Biomass and Bioenergy, 31*(8), 569-575.

Towler, G., & Sinnott, R. (2013). *Chemical Engineering Design: Principles, Practice and Economics of Plant and Process Design* (2nd ed. Vol. 5). USA.

Verma, P., Sharma, M. P., & Dwivedi, G. (2016). Evaluation and enhancement of cold flow properties of palm oil and its biodiesel. *Energy Reports, 2*, 8-13. doi:10.1016/j.egyr.2015.12.001

Wei, C.-Y., Huang, T.-C., & Chen, H.-H. (2013). Biodiesel production using supercritical methanol with carbon dioxide and acetic acid. *Journal of Chemistry, 2013*.

Wright, L., Boundy, B., Badger, P. C., Perlack, B., & Davis, S. (2009). *Biomass Energy Data Book* Retrieved from https://info.ornl.gov/sites/publications/files/Pub15016.pdf

Wu, L., Zhu, H., & Huang, K. (2013). Thermal analysis on the process of microwave-assisted biodiesel production. *Bioresource Technology, 133*, 279-284. doi:10.1016/j.biortech.2013.01.009

Yadav, P. K., Singh, O., & Singh, R. (2010). Palm fatty acid biodiesel: process optimization and study of reaction kinetics. *Journal of oleo science, 59*(11), 575-580.

Ye, J., Zhu, H., Yang, Y., Huang, K., & Vijaya Raghavan, G. S. (2019). Dynamic analysis of a continuous-flow microwave-assisted screw propeller system for biodiesel production. *Chemical Engineering Science, 202*, 146-156. doi:10.1016/j.ces.2019.03.022

Ye, W., Gao, Y., Ding, H., Liu, M., Liu, S., Han, X., & Qi, J. (2016). Kinetics of transesterification of palm oil under conventional heating and microwave irradiation, using CaO as heterogeneous catalyst. *Fuel, 180*, 574-579.

Yeong, S. P., Law, M. C., Chan, Y. S., & Lee, V. C. C. (2017). Modelling batch microwave heating of water. *IOP Conference Series: Materials Science and Engineering, 217*(1), 012035. doi:10.1088/1757-899X/217/1/012035

Yeong, S. P., Law, M. C., You, K. Y., Chan, Y. S., & Lee, V. C. C. (2019). A coupled electromagnetic-thermal-fluid-kinetic model for microwave-assisted production of Palm Fatty Acid Distillate biodiesel. *Applied Energy, 237*, 457-475. doi:10.1016/j.apenergy.2019.01.052

Zahan, K. A., & Kano, M. (2018). Biodiesel production from palm oil, its by-products, and mill effluent: a review. *Energies, 11*(8), 2132.

Zhang, H., Ding, J., & Zhao, Z. (2012). Microwave assisted esterification of acidified oil from waste cooking oil by CERP/PES catalytic membrane for biodiesel production. *Bioresource Technology, 123*, 72-77. doi:10.1016/j.biortech.2012.06.082

Zhang, H., Li, H., Pan, H., Wang, A., Souzanchi, S., Xu, C., & Yang, S. (2018). Magnetically recyclable acidic polymeric ionic liquids decorated with hydrophobic regulators as highly efficient and stable catalysts for biodiesel production. *Applied Energy, 223*, 416-429. doi:10.1016/j.apenergy.2018.04.061

Zhou, H., Lu, H., & Liang, B. (2006). Solubility of Multicomponent Systems in the Biodiesel Production by Transesterification of Jatropha curcas L. Oil with Methanol. *Journal of Chemical & Engineering Data, 51*(3), 1130-1135. doi:10.1021/je0600294

APPENDICES

Appendix A: Images for experiment setups

Images for the experiment setups in this work are shown here.

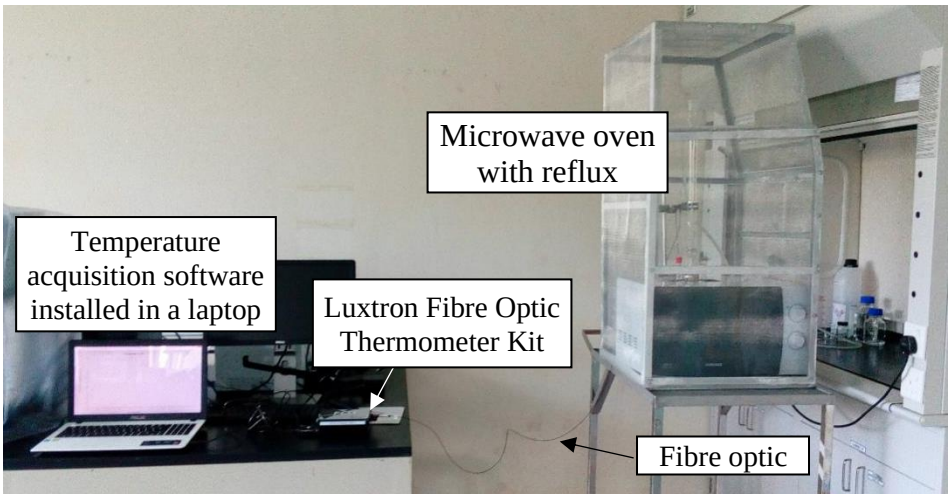

Plate 1 Actual microwave-assisted esterification setup

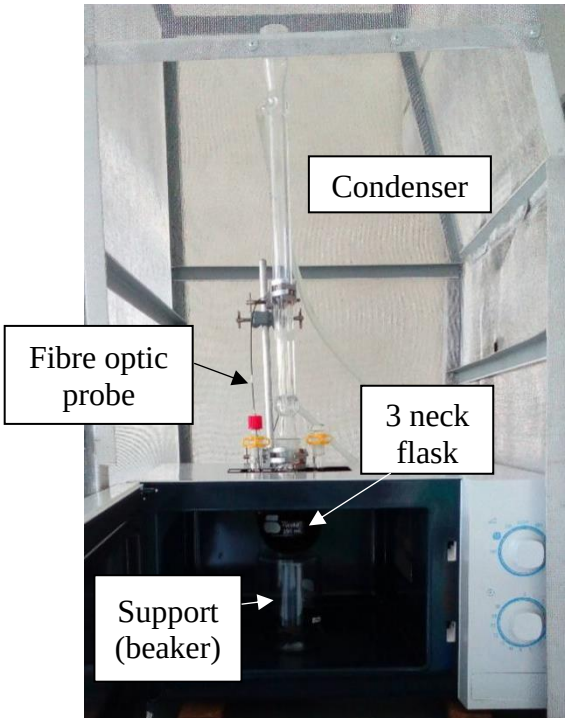

Plate 2 Closer view of the microwave oven with reflux system

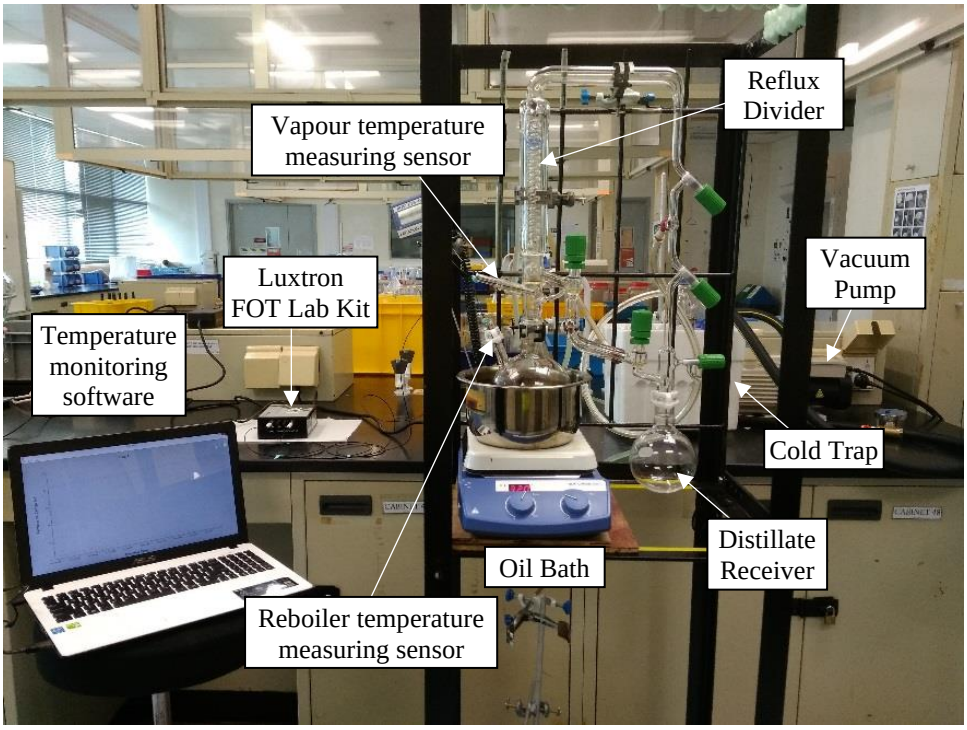

Plate 3 Lab scale vacuum distillation setup (actual)

Appendix B: Experimental data and design calculations

Table B-1 Actual Biodiesel Yield (%) of PFAD esterification under microwave irradiation

Microwave	**Microwave Irradiation Time (s)**			
Power (W)	**300**	**600**	**900**	**1200**
100	83.35 ± 1.78	84.58 ± 2.81	86.09 ± 2.26	89.02 ± 0.86
240	82.75 ± 0.41	85.13 ± 0.47	88.63 ± 0.67	92.12 ± 0.66
300	84.72 ± 2.44	86.44 ± 1.06	91.88 ± 0.86	92.39 ± 0.28

Table B-2 Yield and final acid value of biodiesel samples under 300W microwave irradiation from 60 s to 1200 s

Time (s)	**Acid Value (mg KOH/g)**	**Actual Yield (%)**
0	209.27	-
60	59.87	60.70 ± 1.88
120	38.79	70.74 ± 1.37
180	29.63	76.84 ± 1.40
240	24.81	82.04 ± 1.24
300	24.56	84.72 ± 2.44
600	22.75	86.44 ± 1.06
900	11.41	91.88 ± 0.86
1200	9.26	92.39 ± 0.28

Table B-3 Energy consumption at various microwave power levels

Microwave Power (W)	**Irradiation Time (s)**	**Specific Energy Consumed (J/ml)**	**Specific Energy Consumed (kJ/g)**	**Actual Biodiesel Yield (%)**
100	300	423.01	1.59	83.35 ± 1.78
	600	846.02	6.35	84.58 ± 2.81
	900	1269.04	14.28	86.09 ± 2.26
	1200	1692.05	25.38	89.02 ± 0.86
240	300	1015.23	3.81	82.75 ± 0.41
	600	2030.46	15.23	85.13 ± 0.47
	900	3045.69	34.26	88.63 ± 0.67

Microwave Power (W)	Irradiation Time (s)	Specific Energy Consumed (J/ml)	Specific Energy Consumed (kJ/g)	Actual Biodiesel Yield (%)
300	1200	4060.91	60.91	92.12 ± 0.66
	300	1269.04	4.76	84.72 ± 2.44
	600	2538.07	19.04	86.44 ± 1.06
	900	3807.11	42.83	91.88 ± 0.86
	1200	5076.14	76.14	92.39 ± 0.28

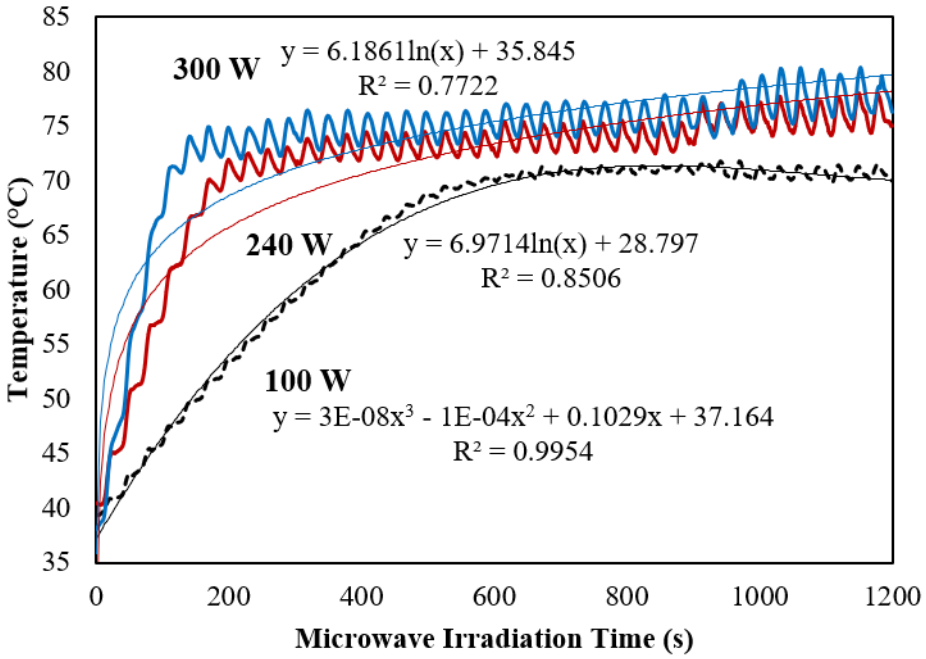

Plate 4 Comparison between experimental and simulated temperature profile

Table B-4 Mass fraction of the four major ester compositions in distillate samples determined via GC-FID analysis

Distillation Time (min)	C16:0	C18:0	C18:1	C18:2
10	68.60%	2.08%	19.17%	4.85%
20	68.51%	2.18%	20.01%	5.21%
30	67.07%	2.46%	22.31%	5.51%
40	66.21%	2.62%	23.58%	5.84%
50	61.44%	3.18%	28.14%	6.92%
60	60.80%	3.27%	28.44%	6.94%
70	60.29%	3.33%	28.93%	7.10%

Distillation Time (min)	C16:0	C18:0	C18:1	C18:2
80	59.62%	3.40%	29.41%	7.29%
90	61.58%	3.14%	28.11%	6.88%
100	61.73%	3.24%	27.85%	6.82%

Table B-5 Design calculations for column and tray design

1. Determine relative volatility of esters

Operating pressure: 1 kPa
Operating temperature: 186 °C
Feed flow rate: 13.23 kmol/h

$$K_i = \frac{P_{i,sat}}{P_i}$$ Equation (2.11)

$$\alpha_i = \frac{K_i}{K_{HK}}$$ Equation (2.12)

Using Hysys database, the $P_{i,sat}$ for each esters at operating temperature 459.15K are determined. At P_i = 1 kPa,

Ester	$P_{i,sat}$ (kPa)	K_i	α_i
C16:0	1.40	1.398	2.319
C18:0	0.54	0.538	0.892
C18:1	0.60	0.603	1.000
C18:2	0.34	0.344	0.570

The light key (LK), heavy key (HK), and heavy non-key (HNK) are identified. It is assumed that HNK exit in the bottoms.
LK: C16:0
HK: C18:1
HNK: C18:0, C18:2

2. Calculate Number of Stages and Reflux Ratio

i. Minimum Number of Stages, $N_{\min}$

Fenske equation is used to determine the number of stages at total reflux.

$$N_{\min} = \frac{\log\left[\left(\frac{X_{D,LK}}{X_{D,HK}}\right)\left(\frac{X_{B,HK}}{X_{B,LK}}\right)\right]}{\log \alpha_{avg}} \qquad \text{Equation (2.13)}$$

$$= \frac{\log\left[\left(\frac{0.95}{0.03}\right)\left(\frac{0.97}{0.05}\right)\right]}{\log 2.319} = 7.635 \approx 8$$

ii. Estimate distillate and bottom composition

The distillate and bottom composition is estimated using Geddes-Hengstebeck equation.

$$\log\left(\frac{X_{D,i}}{X_{B,i}}\right) = \log\left(\frac{X_{D,HK}}{X_{B,HK}}\alpha^{-N_{\min}}\right) + N_{\min}\log\alpha_i \qquad \text{Equation (2.14)}$$

$$\log\left(\frac{X_{D,HK}}{X_{B,HK}}\alpha^{-N_{\min}}\right) = \log\left(\frac{0.03}{0.97}(1)^{-7.635}\right) = -1.510$$

Distillate composition:

Ester	F_i (mole fraction)	$\log\left(\frac{X_{D,i}}{X_{B,i}}\right)$	$\frac{X_{D,i}}{X_{B,i}}$	$D_i = \frac{F_i}{1+\frac{X_{B,i}}{X_{D,i}}}$	$X_{D,i} = \frac{D_i}{\sum D_i}$
C16:0 (LK)	0.4963	1.28	19.000	0.4715	**0.9758**
C18:1 (HK)	0.3677	-1.51	0.0309	0.0110	**0.0228**
C18:0 (NHK)	0.0476	-1.89	0.0130	0.0006	**0.0013**
C18:2 (NHK)	0.0884	-3.37	0.0004	0.0000	**0.0001**
			$\sum D_i$	0.4832	

$$B_i = F_i - D_i \qquad \text{Equation (2.16)}$$

Bottom composition:

Ester	$B_i = F_i - D_i$	$X_{B,i} = \frac{B_i}{\sum B_i}$
C16:0 (LK)	0.0248	**0.0480**
C18:1 (HK)	0.3567	**0.6902**
C18:0 (NHK)	0.0470	**0.0909**
C18:2 (NHK)	0.0883	**0.1709**
$\sum B_i$	0.5168	

iii. Minimum Reflux Ratio, R_m and operating reflux ratio, R

Since the feed is saturated liquid, q = 1 and 1 - q = 0.

$$\sum \frac{\alpha_i X_F}{\alpha_i - \theta} = 1 - q \qquad \text{Equation (2.17)}$$

By using Excel solver, the θ is found to be 1.354.

$$\sum \frac{\alpha_i X_{D,i}}{\alpha_i - \theta} = R_m + 1 \qquad \text{Equation (2.18)}$$

With the known θ, $R_m + 1$ is determined to be 2.280.

Minimum reflux ratio, R_m = 1.280

Operating reflux ratio, $R = 1.3\, R_m$ = 1.664

iv. Theoretical number of stage

The number of equilibrium stages required at the operating reflux ratio is determined using Regressed equation from Gilliland graphical method

$$\psi = \frac{R - R_m}{R + 1} = \frac{1.664 - 1.280}{1.664 + 1} = 0.144 \qquad \text{Equation (2.20)}$$

$$\frac{N - N_{\min}}{N + 1} = 1 - \exp\left[\left(\frac{1 + 54.4\psi}{11 + 117.2\psi}\right)\left(\frac{\psi - 1}{\psi^{0.5}}\right)\right]$$

$$= 1 - \exp\left[\left(\frac{1 + 54.4(0.144)}{11 + 117.2(0.144)}\right)\left(\frac{(0.144) - 1}{0.144^{0.5}}\right)\right] \qquad \text{Equation (2.19)}$$

$$= 0.5106$$

Number of stages, N = 16.64 ≈ 17 (16 stages + 1 reboiler)

v. Feed tray location

The feed tray location of the distillation column can be estimated by solving Kirkbride correlation.

$$\log\left(\frac{N_r}{N_s}\right) = 0.206 \log\left[\left(\frac{B}{D}\right)\left(\frac{X_{F,HK}}{X_{F,LK}}\right)\left(\frac{X_{B,LK}}{X_{D,HK}}\right)^2\right]$$

$$= 0.206 \log\left[\left(\frac{0.5168}{0.4832}\right)\left(\frac{0.3677}{0.4963}\right)\left(\frac{0.05}{0.03}\right)^2\right] = 0.07 \qquad \text{Equation (2.21)}$$

N_r / N_s =1.18

$N_r + N_s = N = 16$ (remove reboiler)

Number of trays in rectifying section, $N_r = 8.649$

Number of trays in stripping section, $N_s = 7.351$

Feed tray location = 9th tray from the top

3. Calculate Column Diameter for both Rectifying and Stripping Section

i. Column Diameter Calculation for Rectifying Section

The diameter of the column is directly affected by its vapour flow rate. Having suitable column diameter can avoid the occurrence of entrainment or high pressure drop.

Liquid rate at rectifying section, L= RD = 16.0493 kmol/hr

Vapour rate at rectifying section, V = (R+1)D = 25.6953 kmol/hr

Liquid Vapour Flow Factor, F_{LV}

$$F_{LV} = \frac{L}{V}\sqrt{\frac{\rho_v}{\rho_L}}$$

Equation (2.23)

$$= \frac{16.0493}{25.6953}\sqrt{\frac{0.0722}{750.433}} = 0.0061 \approx 0.01$$

Souders and Brown factor, C_{sb}

At F_{LV} = 0.01, the C_{sb} can be obtained from Figure 15.5 (Peters et al., 2004).

At tray spacing = 0.46 m, C_{sb} = 0.09 m/s.

Net Vapour Velocity at Flooding Conditions, u_f

$$u_f = C_{sb}\left(\frac{\sigma_s}{0.02}\right)^{0.2}\sqrt{\frac{\rho_L - \rho_v}{\rho_v}}$$

Equation (2.22)

$$= 0.09\left(\frac{0.2}{0.02}\right)^{0.2}\sqrt{\frac{750.433 - 0.0722}{0.0722}} = 14.5436 \text{ m/s}$$

Actual Vapour Velocity, u_n

Considering 80% of flooding as safety margin,

$u_n = 0.8u_f = 0.8(14.5436) = 11.6348$ m/s

Net Column Area available for Vapour-Liquid Disengagement, A_n

$$A_n = \frac{Q}{u_n} = \frac{V}{\rho_v u_n} = \frac{1.9363}{0.0722(11.6348)} = 2.305 \text{ m}^2$$

Equation (2.25)

Cross sectional area of column, A_c

Assuming 15% of the cross-sectional area of the column is occupied by downcomer,

$$A_c = \frac{A_n}{0.85} = \frac{2.305}{0.85} = 2.71 \text{ m}^2$$

Diameter of Column, D_c

$$A_c = \frac{\pi}{4} D_c^2$$

Equation (2.26)

$$D_c = \sqrt{\frac{4A_c}{\pi}} = \sqrt{\frac{4(2.71)}{\pi}} = 1.86 \text{ m}$$

ii. <u>Column Diameter Calculation for Stripping Section</u>

Liquid rate at stripping section, L'= F+L = 29.2773 kmol/hr
Vapor rate at stripping section, V' = V = 25.6953 kmol/hr

Similar steps are performed for stripping section. The results obtained are:
$F_{LV} = 0.0115$, $C_{sb} = 0.089$ m/s, $u_f = 13.79$ m/s, $u_n = 11.03$ m/s,
$Q = 27.886 \text{ m}^3/\text{s}$, $A_n = 2.53 \text{ m}^2$, $A_c = 2.97 \text{ m}^2$, $D_c = 1.95$ m

It is more economical to use uniform column diameter. Hence, the larger column diameter (1.95 m) is chosen.

4. Determine Overall Tray Efficiency and Number of Actual Stages

Overall Tray Efficiency, E_o

$$E_o = 0.492\left[\mu_L \left(\alpha_{LK/HK}\right)_{av}\right]^{-0.245}$$

Equation (2.27)

$$= 0.492\left[0.4136\left(2.3185\right)\right]^{-0.245} = 49.71\%$$

Number of actual stages, N_{act}

$$N_{act} = \frac{N}{E_o} = \frac{16.64}{0.4971} = 33.48 \approx 34 \text{ trays}$$

5. Selection of Tray Spacing

By using trial and error approach, the tray spacing of 0.46 m (18 inch) is selected. The suitability of the trial tray spacing is justified through the calculation shown below.

6. Determination of Column Height

Column Height, H_c

$$H_c = (N_{act} - 1)l_t + \Delta H = \left(\frac{N}{E_o} - 1\right)l_t + 0.1\left(\frac{N}{E_o}\right)l_t \qquad \text{Equation (2.28)}$$

$$= (34-1)0.46 + 0.1(34-1)0.46 = 16.74 \text{ m}$$

Column Height-to-Diameter ratio = $\frac{16.74}{1.95} = 8.605$

The estimation for the column height and diameter is acceptable as the ratio of height-to-diameter falls within the range of 3 – 20 (ICARUS Corporation, 1998).

7. Decide Liquid Flow Arrangement

Maximum volumetric flow rate

$$L_{\max} = \frac{L_m' M_L}{3600\rho_L} = \frac{29.2773(295.029)}{3600(738.4874)} = 0.0032 \text{ m/s} \qquad \text{Equation (2.29)}$$

From Figure 17.35 (Towler & Sinnott, 2013), the suitable liquid flow arrangement is single pass cross flow plate.

8. Provision Plate Design

Assume 15% of the cross-sectional area of the column is occupied by downcomer, **downcomer area**, A_d

$$A_d = 0.15A_c = 0.4461 \text{ m}^2$$

For single-pass plates, **active area**, A_a

$$A_a = A_c - 2A_d = 2.9738 - 2(0.4461) = 2.0816 \text{ m}^2$$

Assume 13% of the active area are active holes, the **hole area** A_h

$$A_h = 0.13(2.0816) = 0.2914 \text{ m}^2$$

According to Figure 17.39 and 17.40 (Towler & Sinnott, 2013), when $\frac{A_d}{A_c} = 15\%$, $\frac{l_w}{D_c} = 0.81$ and $\frac{w_{dc}}{D_c} = 0.21$

Weir length, $l_w = 0.81D_c = 1576$ mm

Weir width (weir chord height), $w_{dc} = 0.21D_c = 408.63$ mm

The recommended **weir height** for vacuum operation is 6 – 12mm. In this design, let $h_w = 8$ mm .

The recommended **plate thickness**, t_p for stainless steel is 3 mm.

Let the diameter of a single hole on the plate, $d_h = 5$ mm.

9. Checking for Design Verification

i. Check Weeping

Minimum design vapour velocity, u_h

From Figure 17.37 (Towler & Sinnott, 2013), $K_2 = 27.8$

$$u_h = \frac{\left[K_2 - 0.90\left(25.4 - d_h\right)\right]}{\left(\rho_v\right)^{0.5}} \qquad \text{Equation (2.30)}$$

$$= \frac{\left[27.8 - 0.90\left(25.4 - 5\right)\right]}{\left(0.0755\right)^{0.5}} = 34.35 \text{ m/s}$$

Actual minimum vapour velocity, u_{act}

$$u_{act} = 0.7\frac{Q}{A_h} = 0.7\left(\frac{27.886}{0.2914}\right) = 66.98 \text{ m/s}$$

Design is acceptable as the actual minimum vapour velocity is well above the minimum design vapour velocity at the weep point.

Maximum liquid rate, $L_m' = L_w = 2.3994$ kg/s

Minimum liquid rate at 70% turn down = $0.7(2.3994) = 1.6795$ kg/s

Height of liquid crest over the weir, h_{ow}

$$h_{ow} = 750\left[\frac{L_w}{\rho_L l_w}\right]^{2/3} \qquad \text{Equation (2.31)}$$

$$\text{Maximum } h_{ow} = 750\left[\frac{2.3994}{738.49(1.5761)}\right]^{2/3} = 12.15 \text{ mm liquid}$$

$$\text{Minimum } h_{ow} = 750\left[\frac{1.6795}{738.49(1.5761)}\right]^{2/3} = 9.58 \text{ mm liquid}$$

Thus, at minimum rate, $h_w + h_{ow} = 8 + 9.58 = 17.58$ mm liquid

ii. Check Plate Pressure Drop

Orifice coefficient C_o

$$\frac{A_h}{A_a} = \frac{0.2914}{2.0816} = 0.14 \qquad \frac{t_p}{d_h} = \frac{3}{5} = 0.6$$

From Figure 2.13, $C_o = 0.77$

Maximum vapour velocity through holes, u_h

$$u_h = \frac{Q}{A_h} = \frac{27.886}{0.2914} = 95.6863 \text{ m/s}$$

Dry plate drop h_d

$$h_d = 51\left[\frac{u_h}{C_0}\right]^2 \frac{\rho_v}{\rho_L} \qquad \text{Equation (2.32)}$$

$$= 51\left[\frac{95.6863}{0.77}\right]^2 \frac{0.0755}{738.4874} = 80.53 \text{ mm liquid}$$

Residual loss, h_r

$$h_r = \frac{12.5\times10^3}{\rho_L} = \frac{12.5\times10^3}{738.4874} = 16.93 \text{ mm liquid} \qquad \text{Equation (2.33)}$$

Total plate pressure drop, h_t

$$h_t = h_d + h_w + h_{ow} + h_r$$

$$= 80.53 + 17.58 + 16.93 = 115.04 \text{ mm liquid}$$

iii. <u>Check Downcomer Liquid Backup</u>

Height of bottom edge of apron above the plate, $h_{ap} = h_w - 5 = 3$ mm

$$A_{ap} = h_{ap} l_w \qquad \text{Equation (2.36)}$$

$$= 0.003(1.5761) = 0.0047 \text{ m}^2$$

Since A_{ap} is less than $A_d = 0.4461 \text{ m}^2$, use A_{ap} as A_m.

$$h_{dc} = 166\left[\frac{L_{wd}}{\rho_L A_m}\right]^2 \qquad \text{Equation (2.35)}$$

$$= 166\left[\frac{2.3994}{738.4874(0.0047)}\right]^2 = 78.37 \text{ mm liquid}$$

$$h_b = \left(h_w + h_{ow}\right) + h_t + h_{dc} \qquad \text{Equation (2.34)}$$

$$= 17.58 + 115.04 + 78.37 = 210.99 \text{ mm liquid}$$

For safety purpose, downcomer liquid backup should not exceed half of the tray spacing in order to avoid flooding.

$$h_b \le \frac{1}{2}\left(l_t + h_w\right) \qquad \text{Equation (2.37)}$$

$$\frac{1}{2}\left(l_t + h_w\right) = \frac{1}{2}\left(460 + 8\right) = 234 \text{ mm liquid}$$

The tray spacing used is acceptable as the downcomer backup is less than 234 mm liquid.

iv. Downcomer Liquid Velocity

$$u_d = \frac{L_{\max}}{A_d} = \frac{0.0032}{0.4461} = 0.0073 \text{ m/s}$$

The velocity does not exceed the limit of 0.1 m/s, which is satisfactory.

v. Downcomer Residence Time

$$t_r = \frac{A_d h_b \rho_L}{L_{wd}}$$

Equation (2.38)

$$= \frac{0.4461 \times 0.211 \times 738.4874}{2.3994} = 28.97 \text{ s}$$

Since the downcomer residence time is > 3s, it is acceptable.

10. Recalculate Percentage of Flooding

The percentage of flooding can be calculated as shown below:

$$\textbf{Percentage of flooding} = \frac{u_n}{u_f} \times 100\% = \frac{10.61}{13.79} \times 100\% = 76.94\%$$

The distillation column can work well without flooding problem as the percentage of flooding is below 100%.

11. Check Entrainment

From Figure 17.36 (Towler & Sinnott, 2013), when F_{LV} = 0.0115, the entrainment, $\psi = 0.11$ at 76.94% flooding. It is slightly above the guideline of 0.1, indicating that the plate efficiency might be slightly affected.

12. Calculate Perforated Area & Number of Holes

For $\frac{l_w}{D_c} = 0.81$,

Angle subtended by chord, $\theta_c = 109°$

Angle subtended at plate edge by unperforated edge strips,
$\theta_{st} = (180 - 109)° = 71°$

Width of unperforated edge strips, $w_{us} = 50$ mm

Mean length, unperforated edge strips, l_{us}

$$l_{us} = (D_c - w_{us})\pi \times \frac{\theta_c}{180}$$

$$= (1.95 - 0.05)\pi \times \frac{109}{180} = 3.6067 \text{ m}$$

Area of unperforated edge strips, A_{us}

$A_{us} = w_{us} l_{us} = 0.05(3.6067) = 0.1803 \text{ m}^2$

Width of calming zone, $w_{cz} = 100 \text{ mm}$

Mean length of calming zone, l_{cz}

$l_{cz} = D_c + w_{us} = 1.95 + 0.05 = 2.00 \text{ m}$

Area of calming zone, A_{cz}

$A_{cz} = 2 l_{cz} w_{cz} = 2(2.00)(0.1) = 0.4 \text{ m}^2$

Total area for perforations, A_p

$A_p = A_a - A_{us} - A_{cz}$

$= 2.0816 - 0.1803 - 0.4 = 1.5 \text{ m}^2$ Equation (2.39)

$\frac{A_h}{A_p} = \frac{0.2914}{1.5} = 0.1940$

From Figure 17.4, at $\frac{A_h}{A_p} = 0.1940$, hole pitch $\frac{l_p}{d_h} = 2.15$

This is acceptable since it is within the range of 2.5 to 4.0.

Hole pitch, $l_p = 2.15(0.005) = 10.75 \text{ mm}$

Area of a single hole, A_h'

$A_h' = \frac{\pi d_h^{\,2}}{4} = \frac{\pi (0.005)^2}{4} = 1.9635 \times 10^{-5} \text{ m}^2$

Number of Holes, N_h

$N_h = \frac{A_h}{A_h'} = \frac{0.2914}{1.9635 \times 10^{-5}} = 14842 \text{ holes}$ Equation (2.46)

Table B-6 Design calculations for condenser

1. True temperature difference

Logarithmic mean temperature difference, ΔT_{lm}

$$\Delta T_{lm} = \frac{(T_1 - t_2) - (T_2 - t_1)}{\ln\left[\frac{(T_1 - t_2)}{(T_2 - t_1)}\right]} = \frac{(186 - 60) - (178.77 - 20)}{\ln\left[\frac{(186 - 60)}{(178.77 - 20)}\right]} = 141.76 \text{ °C}$$

Temperature correction factor, F_t

For horizontal condenser with one shell four tube passes,

$$R = \frac{T_1 - T_2}{t_2 - t_1} = 0.1806$$

$$S = \frac{t_2 - t_1}{T_1 - t_1} = 0.2410$$

$$F_t = \frac{\sqrt{(R^2+1)}\ln\left(\frac{1-S}{1-RS}\right)}{(R-1)\ln\left[\frac{2-S\left(R+1-\sqrt{(R^2+1)}\right)}{2-S\left(R+1+\sqrt{(R^2+1)}\right)}\right]} = 0.9976$$

True temperature difference, ΔT_m

$$\Delta T_m = F_t \Delta T_{lm} = 0.9976(141.76) = 141.42\ ^\circ\text{C}$$

2. Define heat transfer rate and mass flow rate of cooling water

The heat load is retrieved from Aspen Hysys simulation, q = 1243.36 kW

Cooling water flow rate, $\dot{m}_t = \frac{q}{c_p(t_2 - t_1)} = \frac{1243.36}{4.227(60-20)} = 7.354$ kg/s

3. Assume overall heat transfer coefficient

According to Table 19.1 (Towler & Sinnott, 2013), the overall heat transfer coefficient for vacuum condenser with cooling water should be within the range of 200 – 500. Thus, use 300 W/m^2.°C for the first trial U_o calculation.

4. Heat Transfer Area

Heat transfer area, A_o that is required:

$$A_o = \frac{q}{U_o \Delta T_m} = \frac{1243360}{300(141.42)} = 29.31\ \text{m}^2$$

5. Layout and Tube Size

Square pitch is used. The standard tube dimension for tubes made from stainless steel 304 steel that is used are:

Tube outer diameter, D_o = 25.4 mm

Tube inner diameter, D_i = 17.018 mm

Tube wall thickness, t_w = 4.191 mm

Tube length, L = 4.88 m (16ft)

Modified tube length after wall thickness, $L_m = L - t_w = 4.876$ m

6. Number of Tubes

Surface area of one tube, $A_{st} = \pi D_o L_m = 0.3891 \text{ m}^2$

Number of tubes required, $N = \frac{A_o}{A_{st}} = \frac{29.31}{0.3891} = 75.33 \approx 76 \text{ tubes}$

Number of tubes per pass, $N_t = \frac{N}{\text{number of pass}} = \frac{76}{4} = 19$

Tube cross-sectional area, $A_{tcs} = \frac{\pi D_i^2}{4} = \frac{\pi (0.017018)^2}{4} = 0.00023 \text{ m}^2$

Tube area per pass, $A_t = 19 \times 0.00023 = 0.00432 \text{ m}^2$

7. Bundle and Shell Diameter

To calculate the diameter of shell, the bundle diameter D_b has to be determined. The constant K_1 and n_1 for 4 tube passes with square pitch are 0.158 and 2.263 respectively.

Bundle diameter, D_b

$$D_b = D_o \left(\frac{N}{K_1} \right)^{\frac{1}{n_1}} = 25.4 \left(\frac{76}{0.158} \right)^{\frac{1}{2.263}} = 389.09 \text{ mm}$$

From Figure 19.12 (Towler & Sinnott, 2013), the **bundle diameter clearance** for heat exchanger with a split-ring floating head type is 53 mm.

Shell inside diameter, $D_s = D_b + \text{bundle diameter clearance} = 442.09 \text{ mm}$

For the U-tube exchanger, number of tubes in centre row, N_r

$$N_r = \frac{D_s}{p_t} = \frac{D_s}{1.25 D_o} = \frac{442.09}{1.25(25.4)} = 13.92 \approx 14$$

8. Heat Transfer Coefficient of Shell Side

Choose baffle spacing, $l_B = \frac{D_s}{5} = \frac{442.09}{5} = 88.42 \text{ mm}$

Tube pitch $p_t = 1.25 D_o = 31.75 \text{ mm}$

The **cross-flow area for the tubes at the shell equator**, A_s

$$A_s = \frac{(p_t - d_o) D_s l_B}{p_t}$$

$$= \frac{(31.75 - 25.4) 442.09 \times 88.42}{31.75} \times 10^{-6} = 0.00782 \text{ m}^2$$

Shell-side mass flow velocity $G_s = \frac{W_s}{A_s} = \frac{0.485}{0.00782} = 61.986 \text{ kg/m}^2\text{.s}$

For a square pitch arrangement, the **shell-side equivalent diameter**, d_e

$$d_e = \frac{1.27}{d_o}\left(p_t^{\,2} - 0.785 d_o^{\,2}\right)$$

$$= \frac{1.27}{25.4}\left((31.75)^2 - 0.785(25.4)^2\right) = 25.08 \text{ mm}$$

The **shell-side Reynolds number**, Re

$$\text{Re} = \frac{G_s d_e}{\mu} = \frac{61.986(25.08\times10^{-3})}{0.4382} = 3547.81$$

Taking 25% baffle cuts, from Figure 19.29 (Towler & Sinnott, 2013),
The heat transfer factor, $j_h = 0.018$

Shell-side heat transfer coefficient, h_o
Neglecting the viscosity correction term,

$$h_o = j_h \,\text{Re}\,\text{Pr}^{0.33} \times \frac{k_f}{d_e}$$

$$= 0.018(3547.81)\left(\frac{2.4125\times0.4382}{0.0845}\right)^{0.33} \times \frac{0.0845}{(25.08\times10^{-3})} = 499.45 \text{ W/m}^2.^\circ\text{C}$$

9. Heat Transfer Coefficient of Tube Side

Thermal conductivity of tube fluid (cooling water), $k_f = 0.6315$ W/m.°C

Fluid (cooling water) velocity, $u_t = \frac{\dot{m}_t}{\rho A_t} = \frac{7.354}{996\times0.00432} = 1.708$ m/s

Tube-side Reynolds number,

$$\text{Re} = \frac{\rho u_t D_i}{\mu} = \frac{996\times1.708\times0.017018}{0.65\times10^{-3}} = 44453.47 (\text{turbulent})$$

Prandtl number, $\text{Pr} = \frac{c_p \mu}{k_f} = \frac{4.227\times0.65}{0.6315} = 4.36$

$$\frac{L}{D_i} = \frac{4.88}{0.017018} = 286.76$$

From Figure 19.23 (Towler & Sinnott, 2013), at L/D_i=286.76, the **heat transfer factor**, $j_h = 0.0022$.

Neglecting viscosity correction, **Nusselt number**, Nu

$$\text{Nu} = j_h \,\text{Re}\,\text{Pr}^{0.33}$$

$$= 0.0022\times44453.57\times4.36^{0.33} = 158.99$$

Tube-side heat transfer coefficient, h_i

$$h_i = \frac{\text{Nu}\, k_f}{D_i} = \frac{158.99 \times 0.6315}{0.017018} = 5899.71 \text{ W/m}^2.^\circ\text{C}$$

10. Overall Heat Transfer Coefficient and its Percentage Error

From Table 19.6 (Towler & Sinnott, 2013), the thermal conductivity of stainless steel, k_w = 16 W/m.°C.

Fouling coefficients for organic esters, h_{od} = 5000 W/m^2.°C

Fouling coefficients for cooling water, h_{id} = 3000 W/m^2.°C

$$\frac{1}{U_{o,calc}} = \frac{1}{h_o} + \frac{1}{h_{od}} + \frac{d_o \ln\left(\frac{d_o}{d_i}\right)}{2k_w} + \frac{d_o}{d_i} \times \frac{1}{h_{id}} + \frac{d_o}{d_i} \times \frac{1}{h_i}$$

$$\frac{1}{U_{o,calc}} = \frac{1}{499.45} + \frac{1}{5000} + \frac{0.0254 \ln\left(\frac{0.0254}{0.0170}\right)}{2(16)} + \frac{0.0254}{0.0170} \times \frac{1}{3000} + \frac{0.0254}{0.0170} \times \frac{1}{5899.71}$$

$$= 0.003271 \text{ m}^2.\text{癈/W}$$

The overall heat transfer coefficient based on the outside area of the tube,

$$U_{o,calc} = \frac{1}{0.003271} = 305.75 \text{ W/m}^2\,^\circ\text{C}$$

$$\% \text{ error} = \frac{U_{o,calc} - U_o}{U_o} = \frac{305.75 - 300}{300} = 1.92\%$$

The predicted overall heat transfer coefficient is satisfactory as its percentage error is well below 30%.

11. Pressure Drop

Shell-side pressure drop

From Figure 19.30 (Towler & Sinnott, 2013), the shell-side friction factor j_f = 0.055.

Shell-side linear velocity $u_s = \frac{G_s}{\rho} = \frac{61.986}{750.43} = 0.0826$ m/s

Neglecting the viscosity correction term, **shell-side pressure drop** ΔP_s

$$\Delta P_s = 8 j_f \left(\frac{D_s}{d_e}\right)\left(\frac{L}{l_B}\right)\left(\frac{\rho u_s^{\,2}}{2}\right)$$

$$= 8(0.055)\left(\frac{442.09}{25.08}\right)\left(\frac{4880}{88.42}\right)\left(\frac{750.43 \times 0.0826^2}{2}\right) = 1.096 \text{ kPa}$$

Tube-side pressure drop, ΔP_t

$$\Delta P_t = N_p \left[8 j_f \left(\frac{L}{D_i} \right) + 2.5 \right] \frac{\rho u_t^{\,2}}{2}$$

$$= 4 \left[8(0.0022) \left(\frac{4.88}{0.017018} \right) + 2.5 \right] \frac{996(1.708)^2}{2} = 43.88 \text{ kPa}$$

Table B-7 Design calculations for reboiler

1. Mean temperature difference

For a pure saturated vapour at a fixed temperature and constant pressure,

Mean temperature difference, ΔT_{lm}

$$\Delta T_{lm} = \frac{(T_2 - T_1)}{\ln \left[\frac{(T_{sat} - T_1)}{(T_{sat} - T_2)} \right]} = \frac{(196.77 - 186)}{\ln \left[\frac{(220 - 186)}{(220 - 196.77)} \right]} = 28.27 \text{ °C}$$

No correction factor is required for multiple passes.

2. Define heat transfer rate and heat transfer area

Total heat load, q

$$q = \dot{m} \left[c_p (T_2 - T_1) + \Delta H_{vap} \right]$$

$$= 0.5571 \left[2.485 (196.77 - 186) + 252.62 \right] = 155.64 \text{ kW}$$

Adding 5% for heat losses:

Maximum heat load = $1.05q$ = 163.42 kW

From Table 19.1 (Towler & Sinnott, 2013), for heaters with hot steam and light oils, the typical overall heat transfer coefficient is 300 – 900 W/m^2.°C

Using a trial value of 600 W/m^2.°C for U_o ,

The heat transfer area required

$$A_o = \frac{q}{U_o \Delta T_{lm}} = \frac{163420}{600(28.27)} = 9.17 \text{ m}^2$$

3. Number of Tubes

Tube outer diameter, D_o = 30 mm

Tube inner diameter, D_i = 25 mm

Tube length, L = 4.8 m

Number of tubes required, $N_t = \frac{4A_o}{\pi D_i^2} = \frac{4(9.17)}{\pi(0.03)^2} = 20.28 \approx 21$

4. Overall Heat Transfer Coefficient and its Percentage Error

Based on the estimated heat transfer area, actual heat flux, q

$$q = \frac{\text{max. heat load}}{A_o} = 17.81 \text{ kW/m}^2$$

Liquid (biodiesel) critical pressure, $P_c = 11.63$ bar

Operating pressure = 0.01 bar

To estimate pool boiling equation, use Mostinski's equation,

$$h_o = h_{nb} = 0.104 P_c^{0.69} q^{0.7} \left[1.8\left(\frac{P}{P_c}\right)^{0.17} + 4\left(\frac{P}{P_c}\right)^{1.2} + 10\left(\frac{P}{P_c}\right)^{10} \right]$$

$$= 746.31 \text{ W/m}^2.^\circ\text{C}$$

Steam condensing coefficient, $h_i = 8500$ W/m^2.°C

Steam fouling coefficient, $h_{id} = 5000$ W/m^2.°C

Biodiesel fouling coefficient, $h_{od} = 5000$ W/m^2.°C

Thermal conductivity of plain carbon steel tube, $k_w = 55$ W/m.°C

$$\frac{1}{U_{o,calc}} = \frac{1}{h_o} + \frac{1}{h_{od}} + \frac{D_o \ln\left(\frac{D_o}{D_i}\right)}{2k_w} + \frac{D_o}{D_i} \times \frac{1}{h_{id}} + \frac{D_o}{D_i} \times \frac{1}{h_i}$$

$$\frac{1}{U_{o,calc}} = \frac{1}{746.31} + \frac{1}{5000} + \frac{0.03 \ln\left(\frac{0.03}{0.025}\right)}{2(55)} + \frac{0.03}{0.025} \times \frac{1}{5000} + \frac{0.03}{0.025} \times \frac{1}{8500}$$

$$= 0.001971 \text{ m}^2.\text{癈/W}$$

The overall heat transfer coefficient based on the outside area of the tube,

$$U_{o,calc} = \frac{1}{0.001971} = 507.40 \text{ W/m}^2\text{°C}$$

$$\% \text{ error} = \frac{U_{o,calc} - U_o}{U_o} = \frac{507.40 - 600}{600} = 15.43\%$$

The predicted overall heat transfer coefficient is satisfactory as its percentage error is well below 30%.

5. Pressure Drop

Tube cross-section area, $A_{tcs} = \frac{\pi D_i^2}{4} = 0.000491 \text{ m}^2$

Surface area of one tube, $A_t = \pi D_o L = 0.4524 \text{ m}^2$

Number of tubes required, $N_t = \frac{A_o}{A_t} = \frac{9.17}{0.4524} = 20.28 \approx 21$

For one tube pass, total flow area $A_T = A_{tcs} N = 0.00995 \text{ m}^2$

Mass flow rate of high pressure steam, $\dot{m}_t = 2.029 \text{ kg/s}$

Mass flow rate per unit flow area, $u_f = \frac{\dot{m}_t}{A_T} = \frac{2.029}{0.00995} = 203.87 \text{ kg/s.m}^2$

Tube side velocity, $u_t = \frac{u_f}{\rho_t} = \frac{203.87}{10.18} = 20.017 \text{ m/s}$

Reynolds number, $\text{Re} = \frac{\rho_t u_t D_i}{\mu_t} = \frac{20.017 \times 10.18 \times 0.025}{0.000016} = 311846$

From Figure 19.24 (Towler & Sinnott, 2013), friction factor $j_f = 0.00024$

Tube-side pressure drop, ΔP_t

$$\Delta P_t = N_p \left[8 j_f \left(\frac{L}{D_i} \right) + 2.5 \right] \frac{\rho u_t^2}{2}$$

$$= 1 \left[8(0.0024) \left(\frac{4.8}{0.025} \right) + 2.5 \right] \frac{20.017(10.18)^2}{2} = 12.62 \text{ kPa}$$

Shell-side pressure drop

The shell side pressure drop may be considered negligible for liquid level that is not too high above the tube bundle. The hydrostatic head for the flow of liquid from the column to reboiler can be considered negligible.

6. Layout

To calculate the diameter of shell, the bundle diameter has to be determined. For square pitch, the constant K_1 and n_1 for one U-tube pass is 0.215 and 2.207 respectively. From tube sheet layout,

$$D_b = D_o \left(\frac{N}{K_1} \right)^{\frac{1}{n_1}} = 0.03 \left(\frac{20.28}{0.215} \right)^{\frac{1}{2.207}} = 235.41 \text{ mm}$$

Shell inside diameter, $D_s = 2.5 D_b = 589 \text{ mm}$

The freeboard between the liquid level and shell should be > 0.25m.
Take liquid level as 300 mm from base, freeboard = 0.289 m (satisfactory).

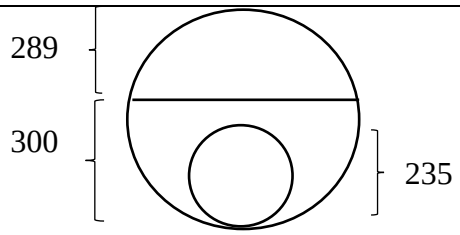

From the sketch (as shown above), width at liquid level = 0.589 m
Surface area of liquid = 0.589 × 4.8/2 = 1.414 m^2

$$\text{Vapour velocity at surface} = \frac{m_{in}}{\text{surface area of liquid} \times \rho_v}$$

$$= \frac{0.5571}{1.414 \times 0.0755} = 5.22 \text{ m/s}$$

Maximum allowable velocity, u_v

$$\hat{u}_v = 0.2\sqrt{\frac{738.49 - 0.0755}{0.0755}} = 19.78 \text{ m/s}$$

The design is satisfactory as the actual velocity (5.22 m/s) is well below the maximum allowable velocity.

Appendix C: Reprinted Permission Statements

1) Reprinted permission from the author of Rana and Rana (2014)

SIEW PING YEONG <yeong.siew.ping@postgrad.curtin.edu.my> Tue, 9 Jun, 13:02
to kalyankrana

Dear Dr Kalyan Rana,

I would like to request permission to use the figures (Figure 2 - Figure 4) of your journal paper in my thesis.
Paper Title: Microwave Reactors: A Brief Review on Its Fundamental Aspects and Applications
DOI: 10.4236/oalib.1100686

May I have your approval please?
Thank you very much and have a nice day.

Regards,
Yeong Siew Ping

Dr. Kalyan Kumar Rana Tue, 9 Jun, 14:10
to me

Dear *Yeong Siew Ping*,
We are happily giving you the permission to use Figures of our publication.
We expect after publication of your paper, you will send us the link so that we can have a chance to read you publication.
Thanking you
Dr. Kalyan Kumar Rana

2) Reprinted Permission from Mazubert et al. (2014), with permission from Elsevier

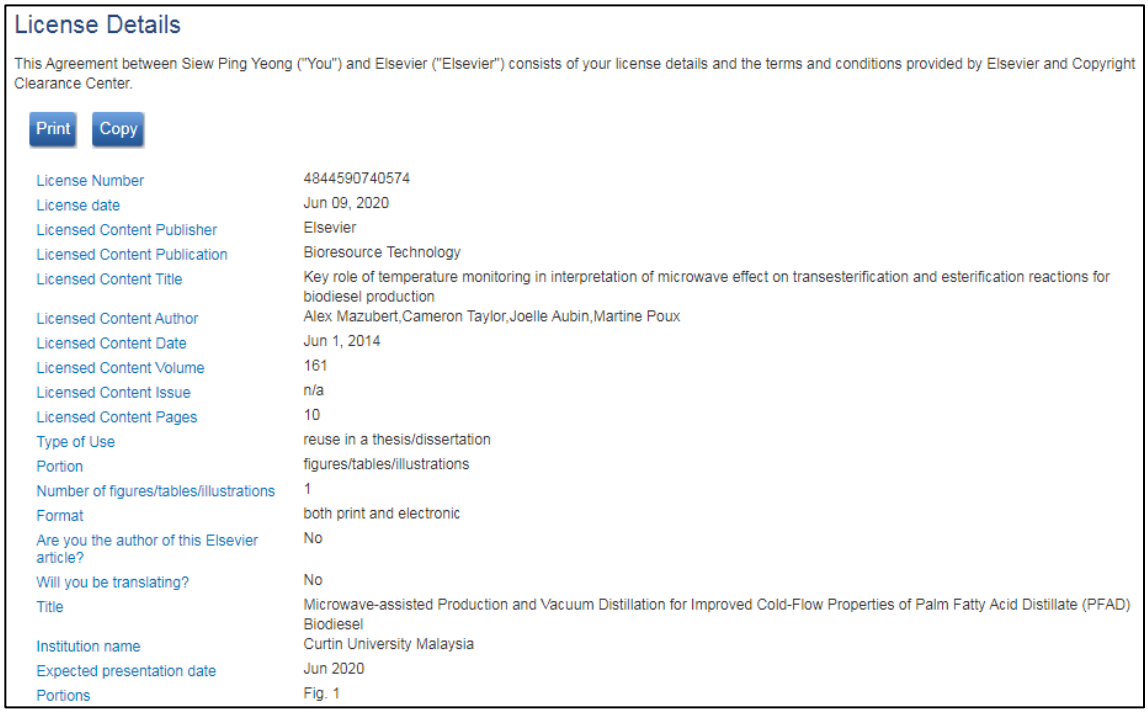

License Details

This Agreement between Siew Ping Yeong ("You") and Elsevier ("Elsevier") consists of your license details and the terms and conditions provided by Elsevier and Copyright Clearance Center.

Print Copy

License Number	4844590740574
License date	Jun 09, 2020
Licensed Content Publisher	Elsevier
Licensed Content Publication	Bioresource Technology
Licensed Content Title	Key role of temperature monitoring in interpretation of microwave effect on transesterification and esterification reactions for biodiesel production
Licensed Content Author	Alex Mazubert,Cameron Taylor,Joelle Aubin,Martine Poux
Licensed Content Date	Jun 1, 2014
Licensed Content Volume	161
Licensed Content Issue	n/a
Licensed Content Pages	10
Type of Use	reuse in a thesis/dissertation
Portion	figures/tables/illustrations
Number of figures/tables/illustrations	1
Format	both print and electronic
Are you the author of this Elsevier article?	No
Will you be translating?	No
Title	Microwave-assisted Production and Vacuum Distillation for Improved Cold-Flow Properties of Palm Fatty Acid Distillate (PFAD) Biodiesel
Institution name	Curtin University Malaysia
Expected presentation date	Jun 2020
Portions	Fig. 1

3) Reprinted permission from Martinez-Guerra and Gude (2014a), with permission from Elsevier

License Details

This Agreement between Siew Ping Yeong ("You") and Elsevier ("Elsevier") consists of your license details and the terms and conditions provided by Elsevier and Copyright Clearance Center.

Print Copy

License Number	4843960125364
License date	Jun 07, 2020
Licensed Content Publisher	Elsevier
Licensed Content Publication	Fuel
Licensed Content Title	Synergistic effect of simultaneous microwave and ultrasound irradiations on transesterification of waste vegetable oil
Licensed Content Author	Edith Martinez-Guerra,Veera Gnaneswar Gude
Licensed Content Date	Dec 1, 2014
Licensed Content Volume	137
Licensed Content Issue	n/a
Licensed Content Pages	9
Type of Use	reuse in a thesis/dissertation
Portion	figures/tables/illustrations
Number of figures/tables/illustrations	1
Format	both print and electronic
Are you the author of this Elsevier article?	No
Will you be translating?	No
Title	Microwave-assisted Production and Vacuum Distillation for Improved Cold-Flow Properties of Palm Fatty Acid Distillate (PFAD) Biodiesel
Institution name	Curtin University Malaysia
Expected presentation date	Jun 2020
Portions	in Graphical abstract

4) Reprinted permission from G. Ma et al. (2015), with permission from Elsevier

License Details

This Agreement between Siew Ping Yeong ("You") and Elsevier ("Elsevier") consists of your license details and the terms and conditions provided by Elsevier and Copyright Clearance Center.

Print Copy

License Number	4843960906723
License date	Jun 07, 2020
Licensed Content Publisher	Elsevier
Licensed Content Publication	Energy Conversion and Management
Licensed Content Title	In situ heterogeneous transesterification of microalgae using combined ultrasound and microwave irradiation
Licensed Content Author	Guixia Ma,Wenrong Hu,Haiyan Pei,Liqun Jiang,Mingming Song,Ruimin Mu
Licensed Content Date	Jan 15, 2015
Licensed Content Volume	90
Licensed Content Issue	n/a
Licensed Content Pages	6
Type of Use	reuse in a thesis/dissertation
Portion	figures/tables/illustrations
Number of figures/tables/illustrations	1
Format	both print and electronic
Are you the author of this Elsevier article?	No
Will you be translating?	No
Title	Microwave-assisted Production and Vacuum Distillation for Improved Cold-Flow Properties of Palm Fatty Acid Distillate (PFAD) Biodiesel
Institution name	Curtin University Malaysia
Expected presentation date	Jun 2020
Portions	Fig. 1

5) Reprinted permission from J. Ye et al. (2019), with permission from Elsevier

License Details

This Agreement between Siew Ping Yeong ("You") and Elsevier ("Elsevier") consists of your license details and the terms and conditions provided by Elsevier and Copyright Clearance Center.

Print Copy

License Number	4850781442485
License date	Jun 16, 2020
Licensed Content Publisher	Elsevier
Licensed Content Publication	Chemical Engineering Science
Licensed Content Title	Dynamic analysis of a continuous-flow microwave-assisted screw propeller system for biodiesel production
Licensed Content Author	Jinghua Ye,Huacheng Zhu,Yang Yang,Kama Huang,G.S. Vijaya Raghavan
Licensed Content Date	Jul 20, 2019
Licensed Content Volume	202
Licensed Content Issue	n/a
Licensed Content Pages	11
Type of Use	reuse in a thesis/dissertation
Portion	figures/tables/illustrations
Number of figures/tables/illustrations	1
Format	both print and electronic
Are you the author of this Elsevier article?	No
Will you be translating?	No
Title	Microwave-assisted Production and Vacuum Distillation for Improved Cold-Flow Properties of Palm Fatty Acid Distillate (PFAD) Biodiesel
Institution name	Curtin University Malaysia
Expected presentation date	Jun 2020
Portions	Fig. 4